

# **Thermomechanical processing of 34CrNiMo6 steel for Large Scale Forging**

**Nasar Abdlssalam Ali**



The  
University  
Of  
Sheffield.

**Department of Materials Science and  
Engineering**

*This dissertation is submitted in fulfilment of the degree of  
Doctor of Philosophy*

**2014  
Sheffield, UK**

## Summary

This work simulated the thermo-mechanical processing of large-scale forging product made of 34CrNiMo6 steel to evaluate the effect of different processing condition parameters and cooling rates on the variation of microstructure and the final mechanical properties. Through this investigation we tried to achieve the required mechanical properties for deep sea applications, which were a minimum Charpy impact value of 38J at temperature of -20 °C according to ABS specifications and a minimum surface hardness of 302 HB according to First Subsea specification design.

Initially, a series of single and multi-hit plane strain compression tests were performed to evaluate the hot-deformed microstructure in thermo-mechanical processing, with particular attention paid to the effect of austenitising temperature and deformation conditions of temperature, strain and strain rate. The hot working process conditions were: austenitising temperatures of 1260 °C and 1100 °C; deformation temperature range of 1260 °C – 900 °C; strain rates of 0.1, 0.5 and 1 s<sup>-1</sup>; to a total strain of 0.8 were used in order to understand and optimize the hot deformation process parameters. Furthermore, an austenitising temperature of 1260 °C and deformation temperature of 1000 °C with strains of 0.4, 0.6, and 0.8 and strain rates of 0.1, 0.5, and 1 s<sup>-1</sup> with each strain were also investigated. The flow stress constitutive equations of the work hardening/dynamic recovery (DRV) curves and dynamical recrystallisation (DRX) curves were also established for 34CrNiMo6 steel.

The exponential law, power law and hyperbolic sine law types of Zener–Hollomon equations were utilised to calculate the hot activation energy of deformation ( $Q_{def}$ ). In addition the constitutive equations were used for modelling and generalising the DRV and DRX flow curves of 34CrNiMo6 steel, using the method proposed by Avrami. Secondly, a heat treatment process using different austenitising temperatures and different cooling rates was also investigated to achieve the required aims, in which many tests were performed through controlling the temperatures, soaking times, and cooling rates to study the effect of the heat treatment parameters on the grain size and transformation behaviour of austenite.

Additionally, to attempt to refine the austenite grain size and to increase the austenite phase percentage within the microstructure, multiple heat treatment paths were also used. A double normalizing, double quenching, and single tempered process were used in all possible combinations to investigate their influence on the final microstructure in an attempt to identify the most effective heat treatment cycle with an effective sequence for the heat treatment operations. According to the obtained results, a microstructural characterization of the studied material was conducted using techniques such as optical microscopy (e.g. Polyvar) and scanning electron microscopy (SEM). Moreover, some mechanical tests such as Charpy impact and hardness testing were performed. The linear intercept method was used to calculate grain size diameter.

The obtained results of the hot deformation simulation with the PSC tests showed that there are many parameters which need to be controlled throughout the process. Understanding the microstructure variation at different temperatures and cooling rates is the best way to achieve the required mechanical properties. Using an austenitising temperature of 1100 °C gives better equiaxed grains and higher recrystallisation percentages than using an austenitising temperature of 1260 °C. Moreover, the smallest grain sizes were obtained at an austenitising temperature of 1100 °C and strain rate of 0.5 s<sup>-1</sup> with all tested deformation temperatures. Also, the results showed that reducing the austenitising temperature has an effect on the mechanical properties, especially fracture toughness, accordingly starting with a small austenite grain size before heat treatment will help to obtain the required mechanical properties. On the other hand, the presence of banding in almost all optical deformed microstructures, represented by dark lines parallel to the direction of deformation, and also the existence of some types of non-metallic inclusions had a negative effect on these required properties.

Generally, in the case of using very low cooling rates with these deformation conditions the toughness requirements will not be achieved. First, this may be attributed to the presence of non-uniform microstructures resulting from the variation in grain size distributions (i.e. bimodal distribution), which usually causes scattering in the measured data, especially when one test sample is used. Second, it may also be attributed to the lower hardenability of 34CrNiMo6 steel, as we could not get a high percentage of martensite within the microstructure of the tested samples. The results of the tests show that to

achieve a higher percentage of martensite in the sampling position, the cooling rate should be higher than 1.2 °C/s for a large section billet with diameter of 480 mm. However, using a multiple heat treatment process consisting of double normalizing, double quenching and single tempering in different orders gave values of high toughness and good hardness within the required specifications. Moreover, the obtained microstructures were more uniform with less variation in grain size distributions (i.e. unimodal distribution) compared to the single heat treatment, which usually helps to reduce the scattering in data.

## Contents

Summary .....	I
Acknowledgments.....	XI
Nomenclature .....	XII
1. Chapter 1 Introduction.....	1
1.1 Background of the work.....	1
1.2 Definition of the Problem .....	3
3.1 Mechanical properties and specifications of 34CrNiMo6 steel.....	4
1.3 Thesis overview .....	5
2. Chapter 2 Literature Review .....	7
2.1 Introduction .....	7
2.1.1 Austenite .....	7
2.1.2 Austenite decomposition .....	8
2.1.3 Eutectoid transformations of austenite.....	8
2.2 Bainite reaction .....	11
2.2.1 Upper bainite .....	12
2.2.2 Lower bainite .....	14
2.3 Martensite.....	17
2.3.1. Martensite transformation characteristic .....	17
2.3.2 Morphology of martensite.....	19
2.3.3 Retained austenite .....	20
2.4 Metallurgy of hot working .....	22
2.4.1 The flow stress curve .....	23
2.4.2 Recrystallisation .....	27
2.4.2.1 Dynamic recrystallisation.....	27
2.4.2.2 Static recrystallisation.....	32
2.5 Isothermal and Continuous Cooling Transformation .....	36
2.5.1 Isothermal Transformation Diagram .....	36
2.5.2 Continuous Cooling Transformation Diagram .....	39
2.5.2.1 Microstructure evolution.....	41
2.5.2.2 Impact of tempering .....	45
2.6 Non-metallic inclusions.....	48

2.6.1	Non-metallic inclusions parameters .....	50
2.6.1.1	Inclusion morphologies.....	50
2.6.1.2	Critical size of inclusions .....	51
2.6.1.3	Distribution and clusters.....	51
2.6.2	Influence of inclusions on mechanical properties of steel .....	52
2.7	Effects of microstructure variability on scatter of properties data of materials.....	55
2.8	Mechanical properties .....	57
2.8.1	Strength.....	58
2.8.2	Fracture toughness and impact testing .....	59
2.8.3	Effect of austenite grain size on mechanical properties .....	60
2.9	Forging.....	64
2.9.1	Large scale forging .....	65
2.10	Heat treatment .....	66
2.10.1	Annealing and Homogenizing .....	67
2.10.2	Normalizing .....	68
2.10.3	Hardening (quenching) .....	69
2.10.4	Tempering .....	70
2.10.4.1	Tempering temperature .....	71
2.10.4.2	Holding time of tempering process .....	72
2.10.4.3	Tempering of martensite .....	73
2.10.4.3.1	Stages of tempering martensite .....	75
2.10.4.4	Tempering of bainite.....	77
2.10.5	Tempering embrittlement .....	78
2.10.5.1	Introduction .....	78
2.10.5.2	Cr-Mo Steel .....	80
2.10.5.3	Effect of Mn and Si.....	80
2.10.5.4	Effect of sulphur.....	81
2.10.5.5	Effect of Ni .....	81
2.10.6	Multiple heat treatment .....	81
2.10.6.1	Double normalizing.....	82
2.10.6.2	Double quenching.....	82
2.10.6.3	Double tempering.....	83

2.11 Hardenability.....	84
2.11.1 Hardenability for small and large scale sections .....	85
2.11.2 Calculation of ideal diameter from the chemical composition .....	86
2.11.3 Methods to improve hardenability using alloying elements .....	87
2.11.3.1 Use of Vanadium (v).....	90
2.11.3.2 Use of niobium (Nb).....	92
2.11.3.3 Use of Boron (b) .....	93
2.12 Summary .....	95
2.13 Research Objectives .....	95
3. Chapter 3 Experimental Procedure.....	97
3.1 Introduction .....	97
3.2 As received material.....	98
3.2.1 CCT diagrams for 34CrNiMo6 steel.....	100
3.2.2 Dimensions and weight of the casting Ingot .....	101
3.2.3 Macro-segregation through the billet .....	101
3.2.4 Forged dimensions and sampling location .....	102
3.2.5 Effects of variations in structure and segregation on the test samples .....	103
3.3 The forging and heat treatment processes for the real product.....	105
3.3.1 The forging process.....	107
3.3.2 The heat treatment process.....	107
3.4 Plane strain compression (PSC) testing.....	108
3.4.1 The thermo-mechanical compression test machine .....	109
3.5 Deformation Process.....	111
3.5.1 Isothermal Deformation Process (single hit) .....	112
3.5.2 Non-isothermal Deformation Process (Multi hit).....	113
3.5.2.1 Four hits .....	113
3.5.2.2 Three hits .....	114
3.6 Heat Treatment.....	115
3.6.1 Create initial conditions to simulate the real heat treatment process .....	115
3.6.2 Thermocouple position .....	118
3.6.3 The effect of normalizing process on the deformed austenite grain size .....	119
3.6.4 Quenching process.....	120

3.6.4.1	Quenching process using different austenitising temperatures and cooling rate of 0.6 °C/sec .....	121
3.6.5	Tempering process.....	122
3.6.5.1	The comparison between tempering temperatures of 630 °C and 640 °C. ....	123
3.6.6	Multiple heat treatment processes .....	124
3.6.6.1	Cycle 1 (Double normalizing + Quenching + Tempering) .....	125
3.6.6.2	Cycle 2 (Double normalizing + Double quenching + Tempering) .....	126
3.6.6.3	Cycle 3 (Normalizing + Quenching + Normalizing + Quenching + Tempering) .....	127
3.6.6.4	Cycle 4 (Normalizing + Double quenching + Tempering) .....	127
3.7	Metallographic specimen preparation .....	128
3.7.1	Sectioning.....	128
3.7.2	Grinding, polishing and etching .....	129
3.7.3	Optical microscope .....	130
3.8	Grain Size Measurement.....	130
3.9	Scanning electron microscope (SEM).....	131
3.10	Energy dispersive X-ray spectroscopy (EDX).....	132
3.11	Mechanical testing .....	132
3.11.1	Hardness test .....	132
3.11.2	Ultimate tensile strength (UTS) calculation:.....	133
3.11.3	Charpy impact test.....	133
4.	Chapter 4 Results of isothermal deformation processes (single hit) in terms of flow behaviour and modelling.....	134
4.1	The austenite grain sizes at different holding times.....	134
4.2	Flow curves at austenitising temperatures of 1100 °C and 1260 °C.....	135
4.3	Flow curves at different strains .....	137
4.4	Activation energy and flow stress constitutive equations.....	137
4.4.1	Flow stress constitutive equations .....	138
4.4.2	Calculation of activation energy of deformation.....	141
4.4.3	The Zener–Hollomon Parameter (Z) as a function of stress.....	142
4.5	The relation between grain size diameter and the Zener-Hollomon parameter .....	144
4.6	Modelling equations of isothermal stress-strain curves .....	145



4.6.1	Verification of the constitutive modelling equation:.....	148
5.	Chapter 5 Results of isothermal deformation processes (single hit) in terms of microstructures.....	150
5.1	Austenite grain sizes at different holding times .....	150
5.2	The optical microstructure at austenitising temperatures of 1260 °C and 1100 °C..	151
5.3	The relation between grain size diameter and deformation temperatures .....	154
5.4	The optical microstructure at different strains.....	155
6.	Chapter 6 Results of non-isothermal deformation processes (multi hit).....	156
6.1	Non-isothermal deformation (Four hits) .....	156
6.2	Non-isothermal deformation (Three hits) .....	157
6.3	Summary of grain size results .....	159
6.4	The oxide scale .....	160
6.5	Non-metallic inclusion .....	162
7.	Chapter 7 Results of heat treatment .....	164
7.1	The effect of normalising process on the deformed austenite grain size .....	164
7.2	Quenching and tempering processes .....	169
7.2.1	Using different cooling rates.....	169
7.2.1.1	With austenitising temperature of 840 °C and tempering temperature of 520 °C	169
7.2.1.2	With austenitising temperature of 960 °C and tempering temperature of 630 °C	173
7.2.1.3	Grain size and mechanical properties results.....	177
7.2.2	Using different austenitising temperatures.....	182
7.2.2.1	With tempering temperatures of 520 °C and 630 °C and cooling rate of 0.6 °C/sec	182
7.2.2.2	Grain size and mechanical properties results.....	184
7.2.3	Comparison between tempering temperatures of 630 °C and 640 °C.....	188
7.3	Multiple heat treatment processes .....	192
7.3.1	Cycle 1 (Double normalizing + Quenching + Tempering) .....	192
7.3.2	Cycle 2 (Double normalizing + Double quenching + Tempering) .....	193
7.3.3	Cycle 3 (Normalizing + Quenching + Normalizing + Quenching + Tempering) ...	194
7.3.4	Cycle 4 (Normalizing + Double quenching + Tempering).....	195

7.4	Fracture surfaces of the some impact tested (Charpy) samples showing the facet sizes	201
8.	Chapter 8 Discussion	203
8.1	Isothermal deformation processes (single hit)	203
8.1.1	Austenitising temperatures and holding time	203
8.1.2	Flow curves and optical microstructure at both austenitising temperatures of 1260 °C and 1100 °C	205
8.1.3	The relation between grain size diameter and deformation temperatures	210
8.1.4	Calculation of activation energy of deformation	210
8.1.5	The Zener–Hollomon Parameter (Z) as a function of stress	213
8.1.6	The relation between grain size diameter and the Zener-Hollomon parameter	214
8.1.7	Modelling equations of isothermal stress-strain curves	216
8.1.8	Verification of the constitutive modelling equation	216
8.1.9	Flow curves and optical microstructure at different strains:	217
8.2	Non-isothermal deformation processes (multi hit)	218
8.3	The oxide scale	221
8.4	Non-metallic inclusions	222
8.5	Heat treatment	223
8.5.1	The effect of normalizing process on the deformed austenite grain size	223
8.6	Quenching and tempering processes	226
8.6.1	Using different cooling rates	226
8.6.2	Using different austenitising temperatures	229
8.6.3	Comparison between tempering temperatures of 630 °C and 640 °C	232
8.7	Multiple heat treatment processes	233
8.8	Fracture Surface Facets	235
9.	Chapter 9 Conclusions	237
-	Isothermal deformation processes (single hit)	237
-	Non-isothermal deformation processes (multi hit)	239
-	Heat treatment	240
-	Multiple heat treatment processes	242
10.	Chapter 10 Suggestion for the future	244

10.1 Study the possibility of increasing the cooling rate .....	244
10.1.1 Use near net-shape forging.....	244
10.1.2 Study the performance improvement of Somers Forge quenching tank.....	244
10.2 Modifying the chemical composition of the 34CrNiMo6 alloy steel .....	245
10.2.1 The addition of niobium (Nb) instead of vanadium (V) in the chemical composition of 34CrNiMo6 steel .....	246
10.3 Bimodal grain size distribution and its effect on scatter in toughness results .....	246
10.4 The effect of microstructural banding on mechanical properties and fracture behaviour .....	246
10.5 The effect of non-metallic inclusions on fracture toughness properties .....	247
10.6 The effect of oxide scales on interfacial heat transfer and friction during hot forging 247	
10.7 Optimization of the austenitising temperature before deformation .....	248
10.8 Verification of double normalizing and double quenching results in the heat treatment process.....	248
Appendix A: PSC Test Data and calculations.....	249
Appendix B: Grain size measurement: Linear intercept method .....	253
Appendix C: Charpy specimens results sheets .....	255
Appendix D - 1: Certificate of conformity for chemical composition of 34CrNiMo6 steel ...	258
Appendix E: Examples of equivalent grades of 34CrNiMo6 steel .....	260
References .....	261

## **Acknowledgments**

I would like to thank my superiors Dr. Bradley P Wynne, Dr. Richard Thackray for their guidance and discussions during the course of my search, and I would also like to thank all the post graduate students and staff in the Institute for Microstructural and Mechanical Process Engineering: The University of Sheffield (IMMPETUS).

I am indebted to my country which is Libyan government, and I wish to sincere thank her for their financial support for this research project.

I would like to express my gratitude to the technical staff of the Materials Science and Engineering Department, whose knowledge and practical skills have been very important for this research and a sincere thanks to the staff in Sorby Centre of Electron Microscopy for their technical assistance with everything related to microscopy.

Special thanks to my colleagues in D1, for the friendly and enjoyable atmosphere, and help me to overcome some of the difficulties when I need to that. And for all my friends who shared with me these years in Sheffield.

Finally, I would like to express my sincere gratitude to my family, especially my parents who were the cause of my existence in this life for their encouragement and support me to complete this thesis. And also to my wife for making sure that I put all my time and energy in my work, and to my sons and my daughters, who were the reason of my happiness.

## Nomenclature

M	Martensite
P	Pearlite
TMC	Thermo-mechanical compression
HV	Vickers hardness
HB	Brinell hardness
PSC	Plane strain compression
UTS	Ultimate tensile strength (MPa)
FTTU	Fast thermal treatment unit
IMMPETUS	Institute for microstructural and mechanical process engineering: The University of Sheffield.
SEM	Scanning electron microscopy
EDX	Energy dispersive X-ray spectroscopy
$\varepsilon$	True strain
$\varepsilon_c$	Critical strain
$\dot{\varepsilon}$	Strain rate ( $s^{-1}$ )
$\sigma$	True stress (MPa)
$\sigma_{0.1}$	True stress at 0.1 true strain
$\sigma_{ss}$	Steady state flow stress for dynamic recrystallisation (MPa)
$\sigma_e$	Onset of steady state for dynamic recovery (MPa)
$\sigma_0$	Maximum stress when $\varepsilon = 0$
$\sigma_p$	Peak stress (MPa)
$\varepsilon_p$	Peak strain
Z	Zener–Hollomon parameter
d	Grain size diameter ( $\mu m$ )
$Q_{def}$	Activation energy of deformation ( $KJ mol^{-1}$ )

R	Universal gas constant ( $\text{J K}^{-1} \text{mol}^{-1}$ )
T	Deformation temperature ( $^{\circ}\text{C}$ )
WQ	Water quench
$n, \beta, n'$	Hot deformation constants
$A, A', A'', n, n', \beta, \alpha$	Material constants
$m'$	Avrami coefficient
FC	Furnace cooling
K	Work hardening constant
s	time (sec)
DBTT	Ductile-brittle transition temperature
DRV	Dynamic recovery
DRX	Dynamic recrystallisation
FCC	Face-centred cubic
BCC	Body-centred cubic
$\gamma$	Face centred cubic phase (austenite)
$\alpha$	BCC phase (ferrite) transformed from $\gamma$ phase
$\delta$	BCC phase (delta ferrite) formed on solidification
WF	Widmanstätten ferrite
$M_s$	Martensite start temperature
$M_f$	Martensite finish temperature
CCT	Continuous cooling transformation
TTT	Time-temperature transformation
AARE	Average absolute relative error (%)
$A_1$	Lower critical temperature
$A_3$	Upper critical temperature (hypoeutectoid steel)
$A_{cm}$	Upper critical temperature (hypereutectoid steel)

TE	Temper embrittlement
FATT	Fracture appearance transition temperature
BCT	Body centred tetragonal
$\bar{L}$	Mean linear intercept grain size
N	Number of segments in Scheil analysis
$\bar{N}_L$	Number of grains per unit length

# Chapter 1 Introduction

## 1.1 Background of the work

Forging iron to a specific shape can be dated back to the 12<sup>th</sup> century[1]. Typically this was done by a blacksmith making simple iron forgings by hammering hot small parts to make wrought products. Today forging is used to produce many types of products for various applications, ranging from small simple components to eventual complicated structural components; for instance, companies that work in offshore oil and gas industries use large sections. Furthermore, these industries require materials for their products that are totally reliable and can resist the most aggressive environments. In general metal forming processes, such as forging of steels, aim to produce a near-net shape product with good material properties; these properties are a direct result of the final microstructure, which in turn is determined by a series of deformation steps and heat treatments within a process route. One of the major issues in the microstructure of large scale forging is strain penetration, which becomes less inside large scale forgings. This means the penetration of plastic deformation will be different from the surface to the core of the metal, which causes differences in grain size between the central and surface zones. Moreover, a large variation in cooling rates between the surface and centre leads to large variation in microstructure, which in turn produces a large variation in transformed microstructure and the properties leading to a complicated design strategy.

34CrNiMo6 steel[2] is a heat treated low alloy engineering steel with high strength (See Tables 1.1 and 1.2) and hardenability, containing nickel, chromium and molybdenum. It also has good toughness properties with CVN (Charpy V-notch) at a very low temperature. According to a number of international standards organizations (e.g., Standard of steel SR EN 10083) the AISI 4340 steel is considered one of the 34CrNiMo6 steel grades when the steel is classified by their composition (See Appendix E). Knowing that materials grade comparison usually be to the nearest available grade and might sometimes have slight variations in actual chemistry. Compared with the AISI 4340 steel, the 34CrNiMo6 steel has additional elements of 0.004 %Al, 0.07 %V, 0.13 %Cu and 0.01 %Sn. A typical heat treatment for this steel involves two stages, quenching and tempering.



The steel usually obtains its high strength by quenching to a full martensitic microstructure and the tempering process is used to improve ductility and toughness. This steel, which is used in subsea oil and gas, nuclear, renewable energy and aerospace applications, is subjected to extreme environmental conditions and complex dynamic loading cycles. The supply of materials with properties within the specifications has depended on experience and an intelligent supply chain. These days, even the most adept suppliers are struggling to produce efficient, cost-effective materials that meet all market demands within increasing specifications at an ever increasing size. The First Subsea Company works in partnership with Somers Forge Ltd which undertakes the process of forging and heat treatment of cast material supplied by Sheffield Forgemasters. A mooring system, which is one of the First Subsea company products, was used to anchor an offshore platform in the Gulf of Mexico. A failure in a seabed mooring shackle in this system led to the company client base becoming very worried about the quality of manufacture of long-term mooring systems. Forged and cast steel subsea mooring system components and accessories are required to meet the relevant chain specifications, but these are limited when dealing with large scale products. Unfortunately, these specifications do not provide a consistent and accurate representation of toughness throughout larger geometry parts, which has led to a re-examination of the metallurgical test criteria demanded by end customers according to standard chain specifications. These mooring components need to exhibit high levels of strength and toughness over an extended period. Accordingly, many tests were carried out to verify the mechanical properties according to standard specifications, but the results obtained were not consistent throughout the forging, and often did not confirm these required specifications. The failure of the as forged material to achieve the required specification of mechanical properties, especially toughness and ultimate tensile strength, has an effect on company business in issues such as company reputation, product quality and an increase in production cost. Consequently, this project proposes to treat these issues through testing and investigation in an attempt to improve the forging and heat treatment routes. This will be done through determining the most important parameters that define the metallurgical uniformity of large scale forging products. These parameters lead to understanding, optimisation, and control of the microstructure throughout the whole process chain. All of these proposed investigations will potentially provide the company with technical support and a good knowledge of best practice in the manufacturing process.

## 1.2 Definition of the Problem

One of the most important issues for the producing company is to supply their customers with products which conform to certified specifications, because any failure to meet the specification would be dangerous, costly, and affect the company's reputation. 34CrNiMo6 low alloy steel was used to produce a large scale forging of offshore mooring connectors (diameter  $\geq 485$  mm) for use in deep seas. A number of incidents happened with these products, leading to the company becoming very concerned about the quality of products supplied for use in special applications which should be subject to standard specifications. Several tests were carried out to verify the standard specifications for these products and as a result of these tests many billets were rejected.

The problem, according to the company database which represents the whole production of large scale forged and heat treated billets for several years, is shown in Figure 1.1. From a total of 37 billets that were tested just 19 billets were accepted after the heat treatment process, which represents a percentage of 51.4 %, while the other 18 billets were rejected, a percentage of 48.6 %. This means nearly 50 % of the total production was rejected. Moreover, according to the company data, the main mechanical properties which caused the rejection of billets as shown in Figure 1.2 were toughness, UTS, and a mixture of both. As illustrated in the Pareto diagram, toughness is the main cause of rejection with a percentage of 55.6 %, whilst the UTS came second with 27.7 %. Presence of both problems was represented as a percentage of 16.7 % of the rejected billets.

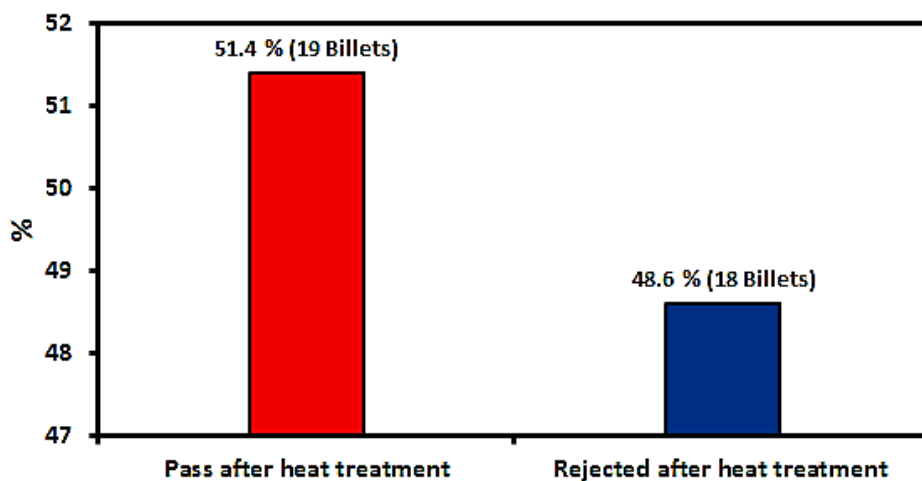


**Figure 1-1** Quantity and percentage of billets accepted and rejected after heat treatment process.

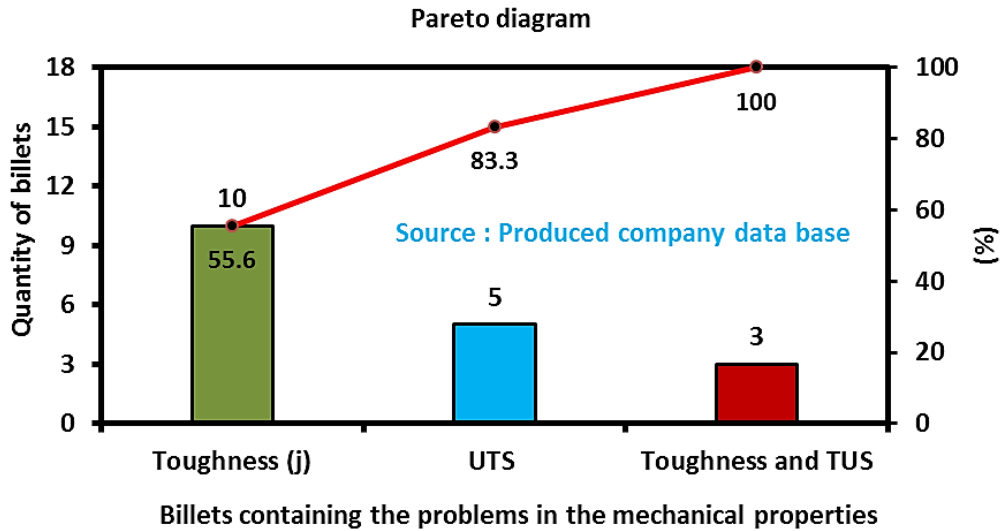


**Figure 1-2** Main mechanical properties which caused rejection after heat treatment.

### 3.1 Mechanical properties and specifications of 34CrNiMo6 steel

According to the specification design of the producing company, the maximum surface hardness of the material must be > 302 HB. Tables 1.1 and 1.2 illustrate the mechanical properties required according to ABS certification for offshore Mooring Chain and accessories, and DNV OS-E302 Rules. The manufacture of the producer company component (mooring connectors- Series 1, 2 and 3) requires steel that satisfies Grade R4.

**Table 1-1** Mechanical properties described in the ABS specification.

Grade	Min Yield Stress (N/mm <sup>2</sup> )	Min Tensile Strength (N/mm <sup>2</sup> )	Min Elongation (%)	Min Reduction of Area (%)	Min. Charpy V-notch Energy (J)				
					Temp (°C)	Base		Weld	
						Average Energy (J)	Single Energy (J)	Average Energy (J)	Single Energy (J)
R4	580	860	12	50	-20	50	38	36	27

**Table 1-2** Mechanical properties described in the DNV OS-E302 specification.

Grade	Min Yield Strength (N/mm <sup>2</sup> )	Min Tensile Strength (N/mm <sup>2</sup> )	Min Elongation (%)	Min Reduction of Area (%)	Charpy V-Notch impact tests Energy (J) Min Average		
					Temp (°C)	Average for Base Metal	Average at Flash Weld
R4	580	860	12	50	-20	50	36

### 1.3 Thesis overview

Literature which provides the details of the necessary background to this project is reviewed in Chapter 2. Included in this overview are: phase transformation characteristics accruing at high temperature, selected required mechanical properties and various heat treatment processes with influencing factors. The need to understand the thermo-mechanical process and the factors influencing it such as strain, strain rate, holding time and temperature, effects on material microstructure evolution and constitutive behaviour under hot working conditions and some of the experimental techniques used are explained in Chapter 3 to characterize the microstructures and mechanical properties of 34CrNiMo6 steel. In addition, this chapter will also briefly describe specimen preparation, the techniques used to characterize the processed microstructures using different analytical techniques such as optical microscopy (Polyvar) and scanning electron microscopy (SEM), and some mechanical properties tests required to verify the results.

In Chapter 4 the experimental results of isothermal deformation processes (single-hit) in terms of flow behaviour of the 34CrNiMo6 steel obtained from a plane compression testing simulator machine are presented. Furthermore, the flow stress constitutive equations of the work hardening dynamical recovery (DRV) curves as well as dynamical recrystallisation (DRX) curves are established for 34CrNiMo6 steel and the exponential, power law and hyperbolic sine law types of Zener–Hollomon equations used to calculate the hot activation energy of deformation ( $Q_{def}$ ). In addition the constitutive equations are used for modelling and generalised the dynamic recovery (DRV) and dynamic recrystallisation (DRX) of these flow curves. In Chapter 5 the experimental results of plane strain compression (PSC) testing (single-hit) in terms of microstructure evolution are presented. Those microstructures were investigated over a temperature range of 1260 °C – 900 °C, strain rates of 0.1, 0.5 and 1 s<sup>-1</sup>, and strains of 0.4, 0.6 and 0.8 in order to understand and optimize the hot deformation process parameters that determine microstructure parameters and thus the final mechanical properties. For a more realistic appraisal, non-isothermal deformation processes (multi-hit) were performed in the same range of real deformation temperatures to try to simulate the real forging process. The results of these experiments in terms of microstructures and stress strain curves are presented in Chapter 6.

The experimental results of heat treatment processes, including normalizing, hardening, and tempering processes with different temperatures and cooling rates, are presented in Chapter 7. Chapter 8 analyses and discusses the major results provided in Chapters 4, 5, 6 and 7. Summaries of the principal observations, some conclusions of this project, and suggestions for future work are presented in Chapters 9 and 10.

## Chapter 2 Literature Review

### 2.1 Introduction

Some industries such as offshore oil and gas industry requires materials that can withstand the most aggressive environments and are totally reliable. These materials should meet strict yield strength, tensile strength, and hardness specifications without losing toughness. The key factors in providing higher strength and toughness of such steels, may be obtained by the addition of alloying elements, thermo--mechanically controlling austenite grain diameter, accelerated cooling, and usually a careful combination of these factors.

This chapter covers an assessment of the theoretical aspects of this working including a review of the physical metallurgy of steels, bainite and martensite reactions, and a general overview of the metallurgy of hot working including follow stress, recrystallisation and typical forging conditions. Some related heat treatments of steel, isothermal and continuous cooling transformation also is given in this chapter, followed by theoretical aspects of hardenability.

#### 2.1.1 Austenite

Austenite is a solid solution of carbon in iron called gamma ( $\gamma$ ) which has a face-centre cubic (FCC) crystal structure. Austenite has a high solubility for carbon, where the maximum solubility reaches 2.1 % at temperature of 1148 °C. In plain carbon steel, austenite phases usually exist above the eutectoid temperature of 727 °C. Steels are classified according to their carbon content and the amount of alloying additions, where most of the carbon steels contain less than 1 % C[3]. Figure 2.1 shows the formation of austenite in pearlite as a function of time, where not all of the cementite is dissolved as the austenite grows into the pearlite. The cementite continues in the form of spheroidized particles, and dissolves only with longer holding times at temperature[4].

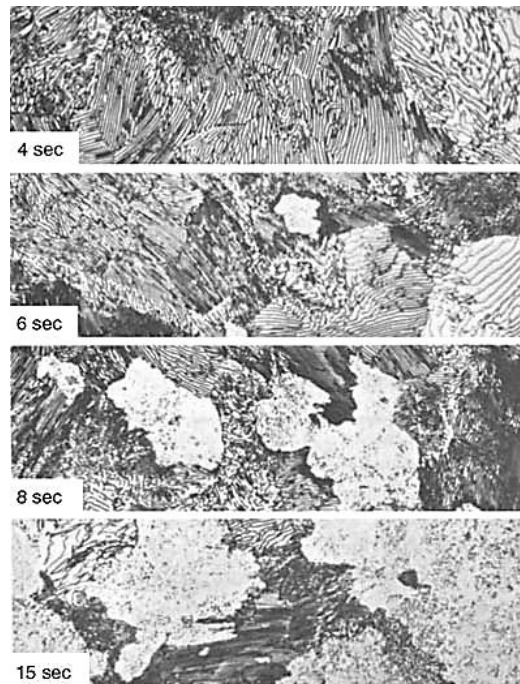


**Figure 2-1** Formation of austenite (light patches) in pearlite as a function of time. Light micrographs[5].

### 2.1.2 Austenite decomposition

The austenite starts to decompose during cooling to room temperature, where it disappears to form a particular microstructure. There are several factors affecting austenite decomposition such as chemical composition, austenite grain size, and cooling path[6]. The decomposition of austenite according to the carbon content and very slow cooling rates will be explained in the following.

### 2.1.3 Eutectoid transformations of austenite

There are three types of microstructure which can be obtained from austenite when cooled very slowly from the austenite zone, depending on the carbon content. As illustrated in Figure 2.2, the entire microstructure will transform to proeutectoid ferrite and pearlite if the carbon content is less than 0.76 %, to pearlite alone if the carbon percentage is equal 0.76 %, or to proeutectoid cementite and pearlite if the carbon content is more than 0.76 %.

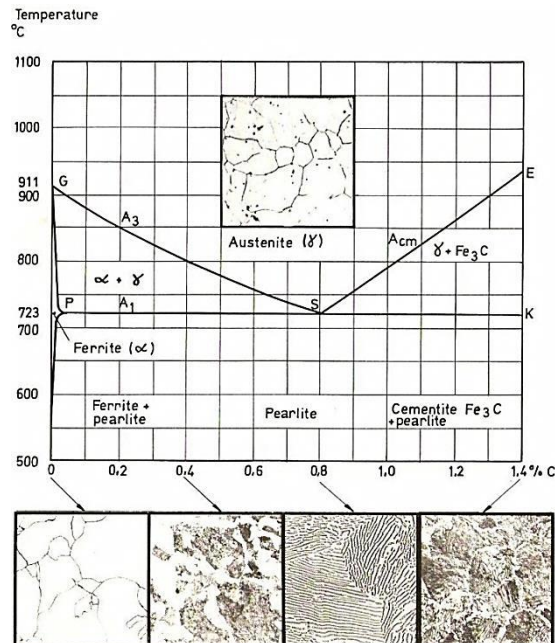


**Figure 2-2** The lower left-hand part of the iron-carbon equilibrium diagram[7].

The most common of these microstructures is proeutectoid ferrite and pearlite, especially widespread in medium carbon steel products. Nucleation of proeutectoid pearlite is initiated at either the austenite grain boundaries or within coarse austenite grains at inclusions. Sometimes the nucleation of proeutectoid pearlite increases at inclusions at the expense of nucleation at grain boundaries. That occurs when the austenite grain size increases, thus the total austenite surface area will decrease which results in a decrease in the number of nucleation sites at the austenite grain boundaries[8]. According to Dubé and Aaronson later, the resulting morphologies based on optical microscopy when austenite transforms to ferrite in plain carbon steel are classified to four morphologies[9].

**Allotriomorphic** is the term used when the shape which is crystalline in internal structure is not reflected in the form of microstructural appearance. Allotriomorphic ferrite as seen in Figure 2.3 is nucleated heterogeneously at the austenite grain boundary where at least two austenite grains are in contact. The orientation between allotriomorphic and contact austenite grains will be random with one grain but more coherent with the other[10].

**Idiomorphic ferrite** is equiaxed morphology nucleated intragranularly at non-metallic inclusions such as precipitates of vanadium nitride(VN), manganese sulphide (MnS), as well as titanium oxide[11, 12].



**Widmanstätten ferrite (WF)** is shaped as elongated laths or plates divided into two types, primary Widmanstätten ferrite, which nucleates directly from the austenite grain boundaries and grows towards the centre of the grains, and secondary Widmanstätten ferrite which grows from allotriomorphic ferrite formed in austenite grain boundaries.

**Acicular ferrite** takes the shape of fine plates when viewed in three dimensions nucleated entirely within the austenite grains from inclusions such as oxide, or silicate particles. These plates usually form at a temperature a bit higher than that used for upper bainite. Acicular ferrite has a chaotic ordering and interlocking structure that contributes to improving strength and toughness[13].

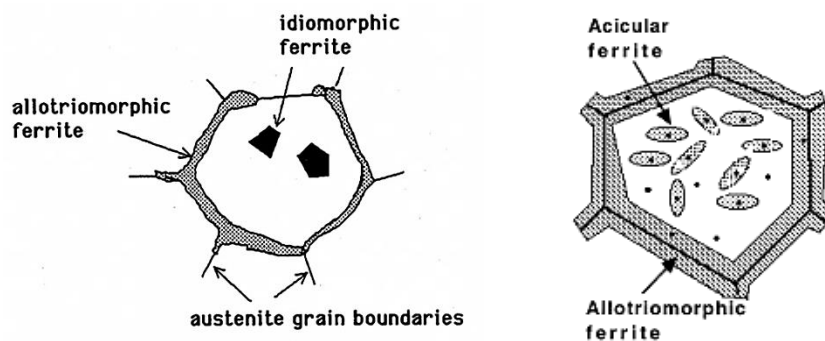


**Figure 2-3** Schematic illustration of the Grain boundary allotriomorphic ferrite, idiomorphic ferrite as well as acicular ferrite [14, 15].

The austenite normal orientation relationship with ferrite is represented with Kurdjumov–Sachs relationship. Where, normally the nucleate has a random orientation relationship with two neighbouring austenite grains as below[9]:

$$\{111\}_\gamma \parallel \{110\}_\alpha$$

$$\langle 110 \rangle_\gamma \parallel \langle 111 \rangle_\alpha$$

Where  $\{110\}$  is a plane of ferrite phase and  $\{111\}$  is a plane of austenite phase, these planes are habit planes. The boundaries between the planes are aligned according to the Kurdjumov-Sachs relation. While the  $\langle 111 \rangle$  is a ferrite nucleus direction and  $\langle 110 \rangle$  is an austenite nucleus direction in the habit plane. Movement of curved austenite/ferrite grain boundaries decreases at low deformation temperature, thus the interfaces become more coherent[16]. Figure 2.4 shows the composition of alternating an immobile  $(0\ 1\ 1)_\alpha \parallel (1\ 1\ 1)_\gamma$  terrace plane and a mobile lateral ledge.

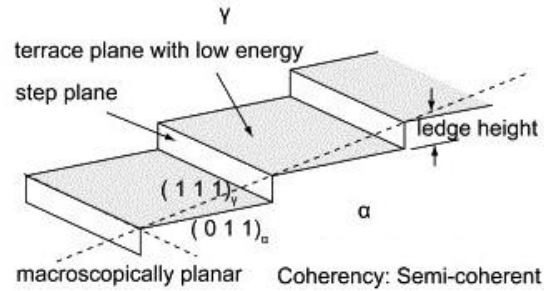


**Figure 2-4** The ledge structure of a partially coherent  $\alpha/\gamma$  interface connecting ferrite and austenite by Kurdjumov–Sachs (K–S) orientation relationship[17].

## 2.2 Bainite reaction

When the steel is cooled from the austenite zone, bainite will be one of the microstructures that is produced from decomposition of austenite, and that occurs when the diffusion rate is faster than the rate required for the formation of pearlite, but slower than the rate required to form martensite. In general, bainite is a mixture of ferrite and cementite and the bainitic transformation occurs either isothermally or during continuous cooling. The bainite formation temperature range for an iron carbon alloy of eutectoid composition is between about 215 °C - 540 °C which is usually located below the pearlite reaction temperature range of about 540 °C - 727 °C and above the martensite start temperature. As seen in Figure 2.5, bainite begins to form first from the austenite grain boundaries toward the centre by the lengthening of sub-units and sheaves.

Bainite microstructure consists of two main phases; ferrite and cementite forms as plates or needles depending on the transformation temperature[18]. If a portion of steel alloy has transformed to bainite it is not possible to transform it to pearlite without reheating back to austenite, and vice versa. The structure of bainite changes as the transformation temperature is changed. According to that, bainite occurs in two main morphologies or forms, upper bainite and lower bainite. Figure 2.6 illustrates the difference in morphology between upper and lower bainite in respect to the precipitation of carbides particles[19]. It is believed that the transition between lower and upper bainite happens over a narrow range of temperatures. The difference in structure between upper and lower bainite can be interpreted in terms of the rate at which carbides can precipitate from ferrite and the speed of carbide precipitation from supersaturated ferrite into austenite[20].

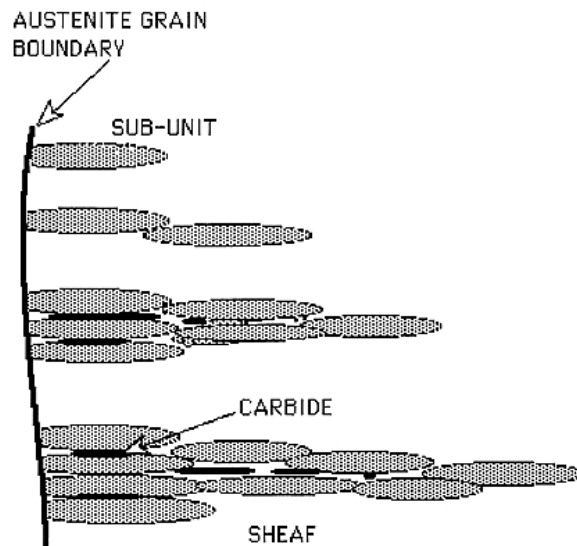


**Figure 2-5** The microstructural features pertinent in the kinetic explanation of a bainitic microstructure [21].

### 2.2.1 Upper bainite

Upper bainite is formed just below the temperature required for pearlite formation in the range of 540 °C-400 °C[22]. The morphology of upper bainite, which is consisted of long ferrite laths, is close to Widmanstatten ferrite at high temperature. The bainitic ferrite laths for both (upper bainite and Widmanstatten ferrite) are represented in the Kurdjumov-Sachs relationship with the parent austenite, but this relationship becomes less accurate as the temperature decreases[23]. Moreover, the density of dislocation in the upper bainite is higher than in the Widmanstatten ferrite specially at low deformation temperature where it increases (dislocation) with decreasing deformation temperature[24]. Upper bainite consists of ferrite plates or laths and is usually separated by the cementite (carbide) precipitated between them. These carbides precipitate from austenite which is enriched in carbon. The platelets of ferrite in the upper bainite structure, which is usually nucleation at the austenite grain boundaries, grow in clusters called sheaves adjacent to each other in almost the same crystallographic orientation.

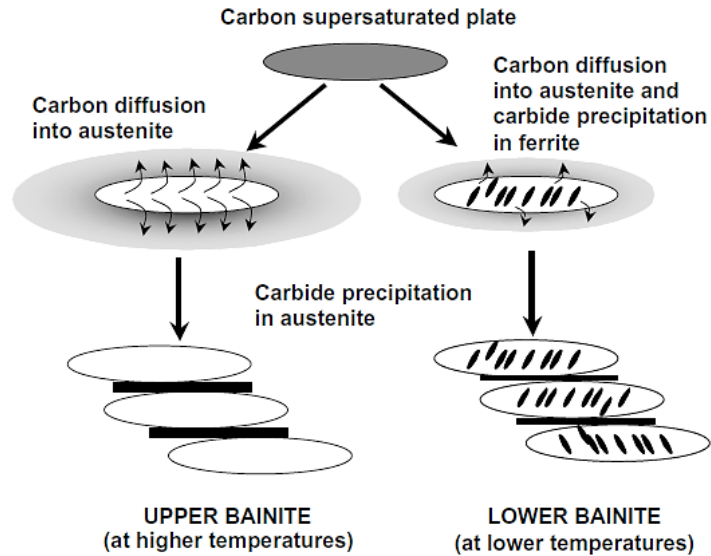


**Figure 2-6** Schematic representation of upper and lower bainite formation mechanism[25].

Upper bainite ferrite has a carbon concentration of less than 0.03 % which is much lower than the carbon in parent austenite, therefore when the upper bainite plates grow the remaining austenite becomes enriched with carbon. The partition between ferrite and austenite occurs due to carbon diffusivity which is high enough at the upper bainite formation temperature (540 °C-400 °C); carbon precipitation occurs at the lath boundaries of the austenite when a critical carbon concentration is reached, not within the laths themselves[26]. In addition, the concentration of carbon in the residual austenite will be reduced because of precipitation of the carbide particles between upper bainite which stimulates the formation of a further quantity of ferrite[27].

There are two types of heterogeneous phase transformations for steel microstructure that can be categorized into two major types; reconstructive and displacive transformation[28]. Reconstructive transformation involves breakdown of bonds and rearrangement of the lattice via diffusion which is relatively sluggish; an example for this transformation is the allotropic ferrite and pearlite transformation[29]. This type of transformation minimises the strain energy caused by partition produced during transformation. Displacive transformation involves the movement of the atoms in a disciplined manner to deform the lattice in order to change the crystal structure and no diffusion takes place. The rate of this transformation is usually rapid. The bainite phase transformation is intermediate between

pearlite and martensite phase transformations so, according to the above, upper bainite exhibits transition features of both reconstructive pearlite and displacive martensite transformations[30]. Moreover, Bhadeshia mentioned that in the absence of incoherence interface on grain boundaries to start the process of transformation, there is a low probability that this secondary ferrite is formed by reconstructive transformation[27].

The amount of cementite formed between lath boundaries is usually based on the amount of carbon concentration in the steel. For low carbon steels, the carbide is typically presented as intermittent stringers or small particle of cementite between lath boundaries, whereas in steels with high carbon contents these stringers become longer or continuous between adjacent laths[31]. To have a very good toughness and avoid brittle cementite within bainitic steel, silicon concentration to about 1.5 wt% should be added to prevent the precipitation of cementite from austenite, because silicon is insoluble in cementite[32]. Figure 2.7 shows two light microscope images for upper bainite formed after holding the 4360 steel at temperatures of 495 °C and 410 °C. As can be seen, the bainite appears dark because it has low reflectivity and the individual ferritic crystals have an acicular shape. The other light phase is martensite which appears as a result of uncompleted of bainitic transformation during the isothermal hold[33].

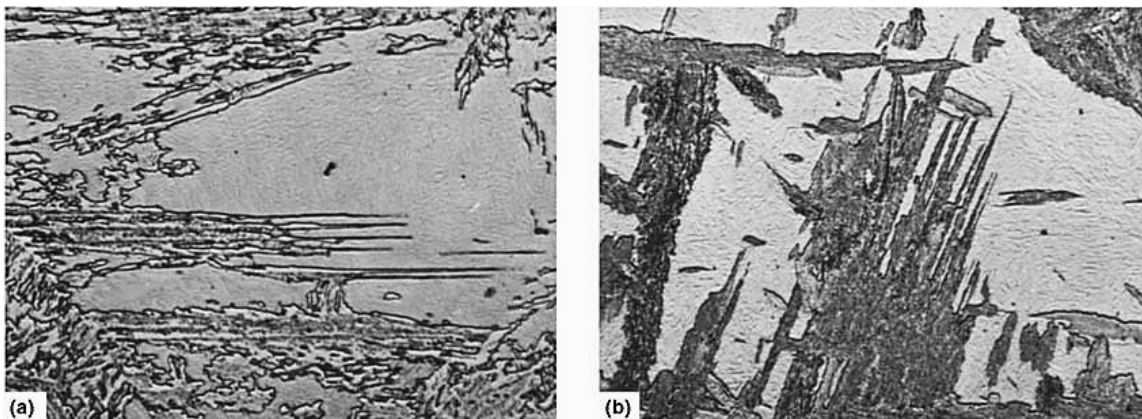


**Figure 2-7** Upper bainite in 4360 steel isothermally transformed after hold at (a) 495 °C and (b) 410 °C.[34]

### 2.2.2 Lower bainite

In carbon steels lower bainite usually forms just below the temperature required to form upper bainite and above the martensite start ( $M_s$ ) temperature. The microstructure as well as the crystallographic features of lower bainite are similar to those in upper bainite. The

main difference between these two structures is that in lower bainite the fine particles of cementite exist within the bainitic laths or plates and are also dispersed inside plates. These carbides exist inside plates rather than between bainite subunits (Fig. 2.6 and 2.8). The reason for that is attributed to the slower diffusion related to the transformation temperature reduction which gives a chance for part of the carbon content to precipitate within the supersaturated ferrite[20]. Furthermore, the microstructure of lower bainite is similar in appearance to that of tempered martensite; the major difference is tempered martensite shows many crystallographic variants of carbides, while only a single variant shows in lower bainite[26]. The plates or lathes of lower bainite have a higher dislocation density compared to upper bainite, but considerably less than a similar composition of martensite.

The carbides in ferrite plates or lathes of the lower bainite should appear dark after etching, but because it is very fine it cannot be resolved under a light microscope. In terms of mechanical properties, lower bainite has hardness and strength approaching that of martensite but with toughness often better than that which can be obtained in martensite[35]. Lower bainite, similar to upper bainite, consists of a non-lamellar aggregate of ferrite but differs in carbides, containing two types instead of one. These carbide particles which precipitate to form enriched austenite have two types; cementite (orthorhombic) or  $\epsilon$ -carbide (hexagonal), depending on the transformation temperature. Results of some studies suggest that in hypoeutectoid bainitic-steel the initial carbide is epsilon ( $\epsilon$ ) which is later substituted by cementite by holding at the constant transformation temperature. The  $\epsilon$ -carbide converts to cementite at a rate of increase depending on both the steel composition and the increase in temperature[36]. Some alloying elements such as silicon and nickel enhance the precipitation of  $\epsilon$ -carbide in lower bainite and retard the formation of cementite. Furthermore, during the process of tempering lower bainite the metastable  $\epsilon$ -carbide will be transformed to martensite.

The crystallography of the lower bainitic steel plates or lathes depends on the transformation temperature as well as on the carbon amount. Furthermore, the phenomenological theory used for martensite can be also used for the same situation occurring in lower bainite to provide an acceptable matching between both of theory and experiment. Some researchers, for example, Bowles and Kennon, showed that the habit

plane is affected by changing the transformation temperature, where the habit plane at low transformation temperature becomes closer to martensite transformation. As seen in Figure 2.9, at 400 °C the habit plane was near  $(111)_\alpha$  while at transformation temperature of 100 °C the habit plane was much closer to  $(110)_\alpha$ . Therefore, the martensite reaction at low temperature could be used for lower bainite[37].

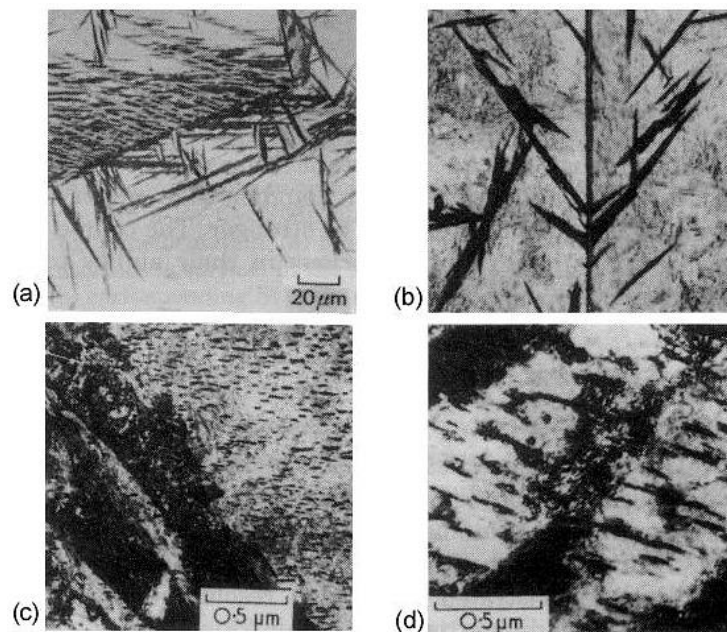


**Figure 2-8** Microstructure of lower bainite. (a) 0.8 % carbon steel transformed in 30 sec at 300 °C, (b) two surface composite micrograph, (c), and (d) Thin-foil EM showing the carbide precipitation.[38]

Chemical composition has a significant influence on the formation of upper and lower bainite. Some data was collected from other researchers via Harry Bhadeshia about the formation of microstructure in respect of both the formation temperature and the chemical composition. These data are important because they can be used to give an idea of the type of microstructure that can be obtained for the steel used in this study. With Fe, 7.9 %Cr, 1.1 %C alloy steel which has large carbon concentration, just lower bainite was found, whereas in a types of high purity of Fe, 0.16-0.81 %C alloy steels just upper bainite was found when  $C < 0.4$  %. Moreover, in a Fe, 2 %Si, 1 %Mn, 0.34 %C alloy steel upper bainite only was formed, while at a high carbon content ( $C > 0.59$  w%) both of upper and lower bainite phases can be found during examination[39]. In this research, the experiments that were done on 34CrNiMo6 steel at low cooling rate found only upper bainite.

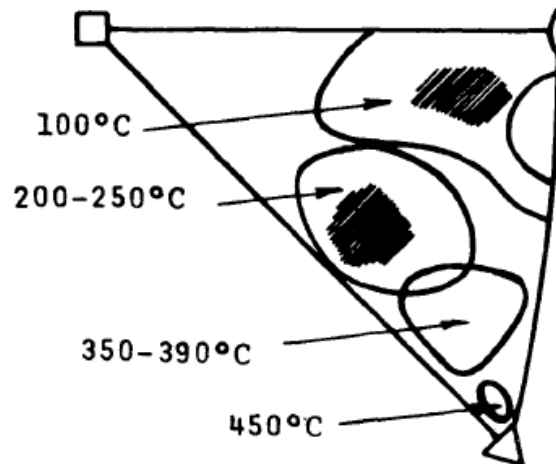


**Figure 2-9** Stereographic projection showing the change of bainite habit planes with temperature of formation for bainite. (Bowles and Kennon. J. Aust Inst Metals.vol5.1960)[40].

## 2.3 Martensite

Martensite in carbon steels is the diffusionless, shear type transformation of bcc structure formed when austenite is rapidly cooled to room temperature. Rapid cooling is used to avoid diffusion dependent transformations. Martensite is a very hard and brittle phase and is not commercial at this status, but when combined with other phases such as ferrite can be used in many industrial applications. Other applications of martensite include the large forging products made of 34CrNiMo6 steel which are produced from tempered martensite microstructure. The two major microstructural morphologies of the martensite formed in steel are lath and plate. Moreover, the main factors that influence the amount of martensite in the microstructure are carbon content, alloying, and austenitic grain size. martensite is only formed where austenite is present, but this transformation does not only happen in steel; it also occurs in many nonferrous systems such as Cu-Al and Au-Cd and in oxides such as SiO<sub>2</sub> and ZrO<sub>2</sub>[41, 42].

### 2.3.1. Martensite transformation characteristic

Martensite in steel is produced in the condition that the cooling rate used is fast sufficiently to make the majority of carbon atoms in solution in the FCC  $\gamma$ -Fe remain in solution in the BCC  $\alpha$ -Fe phase. Put simply, martensite is a supersaturated solid solution of interstitial carbon atoms in  $\alpha$ -iron. Martensite is a non-equilibrium phase, so it will not appear on the Fe-Fe<sub>3</sub>C equilibrium diagram, but the transformation from austenite to martensite phases is represented on the isothermal transformation diagram. Martensite starts to form when the



quenched steel reaches the required temperature for the transformation which is represented by a horizontal line in the TTT diagram designated  $M_s$ , and the percentage of martensite transformation increases as the temperature drops in the direction of the room temperature. Moreover, the transformation ends at martensite finish temperature, designated  $M_f$ , which is also called  $M_{90\%}$  because the transformation of martensite in practice is not 100 % below  $M_f$  temperature as some retained austenite will be left[43, 44].

The  $M_s$  temperature changes depending on the steel composition and the transformation of an austenitic microstructure in most commercial steels takes places continuously with decreasing temperature during uninterrupted cooling. Krauss[45] indicates in his book that the retained austenite content in Fe-C alloys containing 1.2 -1.4 % of carbon is reached up to 30- 40 %, where this percentage was measured by using x-ray diffraction techniques at room temperature. Even in alloys containing as little as 0.3-0.4 % carbon, some small amount of austenite is retained. Furthermore, austenite stabiliser elements increase the amount of retained austenite at any given carbon level and temperature.

Martensite transformation also is named as an athermal transformation. This means in practice that martensite formation is started virtually as soon as  $M_s$  temperature is reached and if the cooling is stopped at a particular temperature before the whole transformation is complete, no further transformation to martensite will occur. That is because martensite transformation is independent of time and the driving force for the reaction is temperature change[46, 47], unlike isothermal transformation which is variable in time, e.g. pearlite formation occurs continuously when the austenite is held at a constant temperature below  $A_1$ . However, in some Fe-Ni alloys the martensite isothermal growth characteristic is exhibited. Porter[43] indicated that a good treatment for martensite transformation was given by Christian and Nishiyama. They mention that the formation of martensite is a random process (see Fig. 2.10), and the martensite is commonly shaped like a lens. Observations showed that the initial ferrite lens spans an entire grain diameter and then these martensite lenses form a coherent interface with the surrounding austenite. The velocity of the transformation of martensite is really fast where the grain may form within a time of  $10^{-7}$  s.

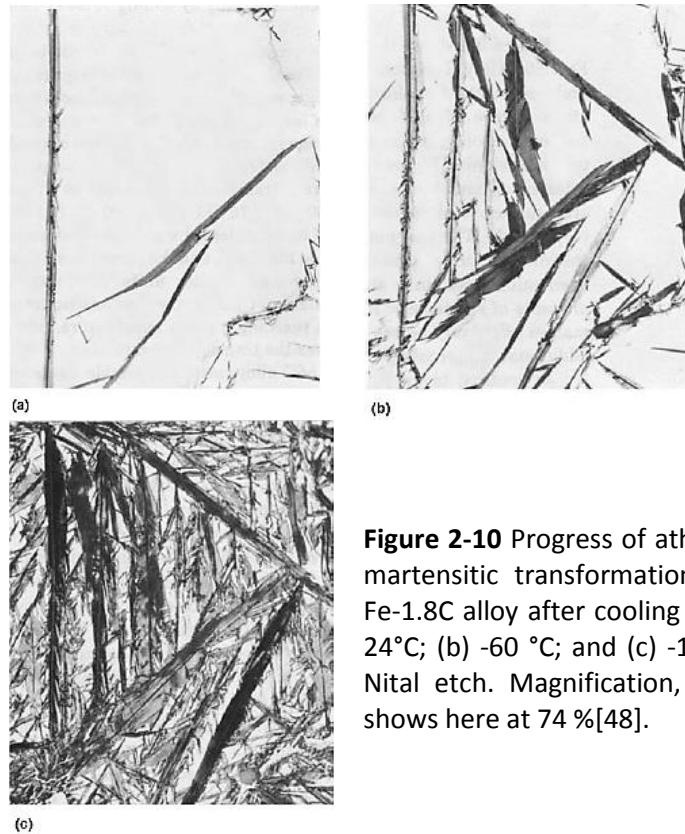


**Figure 2-10** Progress of athermal martensitic transformation in a Fe-1.8C alloy after cooling to: (a) 24°C; (b) -60 °C; and (c) -100 °C. Nital etch. Magnification, 500X, shows here at 74 %[48].

### 2.3.2 Morphology of martensite

According to the major morphologies, martensite is divided into two main types, lath and plate. The names of these two morphologies originally come from the three dimensional shapes of the individual units of martensite. Besides shape, these types of martensite are different in common arrangement of crystals, substructure, and habit planes. Plate martensite, which has needle-shaped crystals or a thin lenticular, is usually found in high-carbon steels and carbon-free iron alloys. These neighbouring plates, as can be seen in Figure 2.11, are not parallel to each another. Lath martensite is usually massive and has nearly the same orientation, and the crystal with a shape like interconnected plates can be found in low and medium carbon steels[49]. In respect to the carbon content, the lath martensites have great industrial significance, because the most hardenable steels have low or medium carbon content. Plate martensite is important in some heat treated applications such as tool steels and the high carbon case structures of carburized steels. The plate dimensions are limited by the dimension of the austenite grain, which means that small martensite grains will give a fine plate needles structure. This structure is called

structureless martensite and is the most desirable microstructure[50]. Figure 2.12 shows a TEM of lath martensite in a Fe-0.2 %C alloy.



**Figure 2-11** Plate martensite formed in an austenitic single crystal of a Fe-33.5Ni alloy by cooling to -196 °C. Plates are visible only because of surface relief generated by martensitic transformation[51].

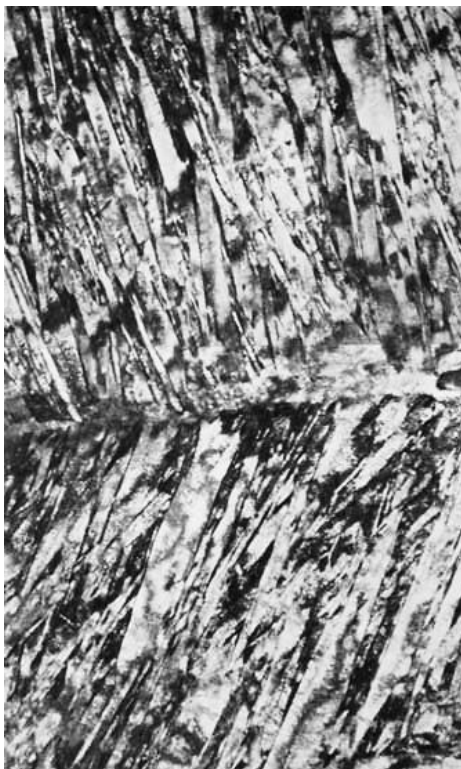


**Figure 2-12** Lath martensite in a Fe-0.2 C alloy. Two packets, each with two variants of laths, are shown. Transmission electron micrograph[52].

### 2.3.3 Retained austenite

During quenching eutectoid steel to room temperature to produce martensitic microstructure through transforming the austenite to martensite, a small amount of the untransformed part is termed retained austenite. The transformation of austenite occurs

after the temperature falls below the martensite start temperature ( $M_s$ ), and should be finished when the temperature goes below martensite finish temperature ( $M_f$ ). The quantity or amount of retained austenite obtained in quenched steel is affected by austenite chemical composition, especially the carbon content, as seen in Figure 2.13. By increasing the percentage of carbon, the amount of retained austenite will be increased[53]. The effect will be more significant in hypereutectoid steels than hypoeutectoid steels where the carbon content is less than 0.76 %. The reason for that is due to the strong effect of austenite chemical composition on the variation of  $M_s$  temperature. The most alloying elements which exist as solid solution in austenite, such as austenite stabilizer and ferrite stabilizer, decrease the martensite start temperature and therefore the percentage of retained austenite at room temperature will increase when the  $M_s$  temperature is reduced.

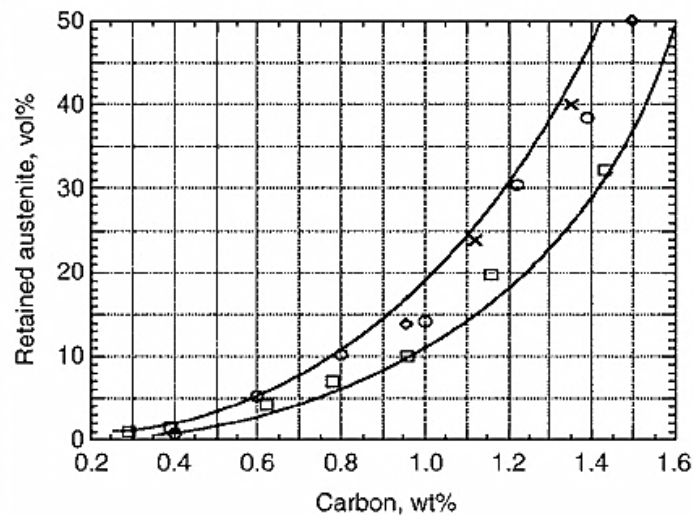


**Figure 2-13** Influence of carbon content of the austenite on the volume percent of retained austenite in plain carbon steels quenched to room temperature[54].

Furthermore, the austenitising temperature and thus the austenite grain size also has an influence on the amount of retained austenite[55], it is known that increasing the austenitising temperature leads up to increase in the austenite grain size. According to new experimental data published by Hong-Seok and Bhadeshia[56], where the Fisher model based on the geometrical partition was used, a relationship between the  $M_s$  temperature and the grain size of austenite was proved. They reported that the cube of the austenite grain size is proportional to the percentage of martensite content that was formed in the initial stage of the transformation. Figure 2.14 displays the variation of  $M_s$  temperature as a function of the austenite grain size for steel with composition in weight percentage (0.125

%C, 5.02 %Ni, 2.27 %Mn). The smaller austenite grain size leads to a decrease in the martensite start ( $M_s$ ) temperature, thus a higher percentage of retained austenite is obtained. Either by tempering or by subzero treatment which include cooling the steel below a temperature of  $-70\text{ }^\circ\text{C}$ , the retained austenite is transformed to martensite, where in the former bainite or martensite is formed depending on tempering temperature and holding time at that temperature[57].

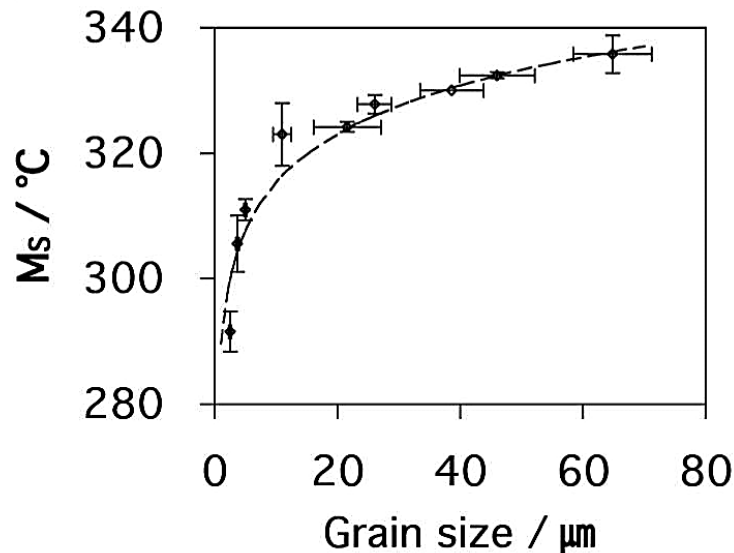


**Figure 2-14** Variation of  $M_s$  as a function of the austenite grain size for the steel with chemical content in wt% ( 0.125 %C, 5.0 2%Ni, 2.27 %Mn)[56].

## 2.4 Metallurgy of hot working

Hot working refers to processes where metals are plastically deformed above their recrystallisation temperature, which according to some references is  $\sim 0.6 T_m$ , where  $T_m$  is the melting point in K[58]. Work is carried out in this temperature range so that large deformations are possible at relatively high strain rates, which can be successively duplicated considering that the metal remains soft and ductile[59]. Under the correct conditions, recrystallisation will occur, either during or after deformation, with resultant differences in the final microstructure and properties. Furthermore, occurrence of recrystallisation during metal deformation is important because recrystallisation prevents the materials from strain hardening, which ultimately keeps the hardness and strength low and ductility high [60].

### 2.4.1 The flow stress curve

The response of a metal to hot deformation is described well by the flow stress curve. Flow stress is described as the instant value of yield stress or true stress needed to preserve plastic deformation at a certain strain to keep the metal flowing. The data used to draw flow stress curves are usually calculated from load-displacement data recorded during experiments, using Equations 2.1 for true stress and 2.2 for true strain:

$$\sigma = \frac{P}{A} \quad 2-1$$

where P is the instantaneous load (N) and A is the instantaneous cross sectional area (m<sup>2</sup>) over which the load is acting;

$$\varepsilon = \ln \frac{L}{L_0} \quad 2-2$$

where L is the instantaneous length and L<sub>0</sub> is the initial length. Equation 2.2 can also be expressed in terms of the instantaneous and initial areas[61]. The flow stress is a function of two main related factors; material factors such as composition, microstructure, and grain size, and process factors including strain rate, deformation temperature as well as strain. Hot working behaviour of alloys, which is generally reflected in flow curves, can be expressed under dynamic recrystallisation (DRX) as well as dynamic recovery (DRV) as illustrated in Figure 2.15.

The flow stress curve starts with work hardening, where a significant increase in stress with increasing strain can be observed. After that the curve shows a small decrease in the rate of work hardening, as indicated by the change in gradient up to the maximum peak value of stress. Once a maximum value of stress has been achieved it is then followed by either a constant steady state flow stress (DRV), or a reduction in flow stress, to a steady state value (DRX). These two distinct types of behaviour in this region depend on the material, temperature as well as strain rate, and could be attributed to different dynamic mechanisms[58]. Furthermore, Jonas[62] and his co-workers mentioned in their study that in at low strains value in all studied metals there was evidence of dynamic recovery. In some metals like  $\alpha$ -Fe and Al (high stacking fault energy materials), the dominant restorative process, which balances work hardening and maintains a constant steady state flow stress,

is dynamic recovery at large strains. Nevertheless, in metals like  $\gamma$ - Fe, Ni and Cu, which usually has low or medium stacking fault energy materials dynamic recrystallisation is the proven mechanism. In another study Luton and Sellars[63] explain that the flow curves of a dynamically recrystallised materials might be characterised by single or multiple peaks (i.e. several oscillations).

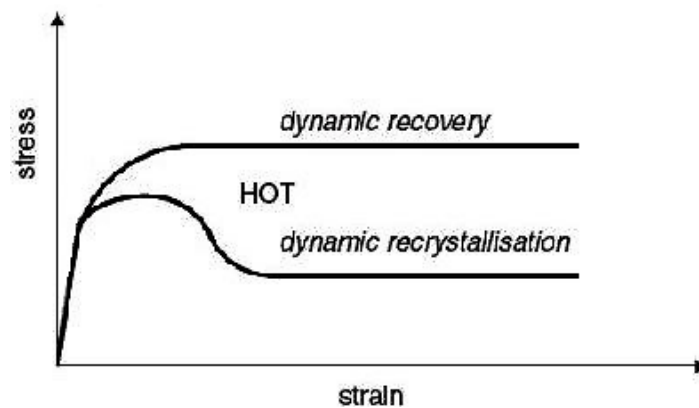


**Figure 2-15** Typical flow curves during hot deformation.

Stress is also a function of the Zener-Hollomon parameter ( $Z$ ), which is also known as the temperature compensated strain rate parameter. This parameter, which is represented by Equation 2.3, is usually used to describe creep strain at elevated temperature for metals like steel.

$$Z = \dot{\epsilon} \exp\left(\frac{Q_{\text{def}}}{RT}\right) \quad 2-3$$

where  $T$  is the absolute temperature,  $\dot{\epsilon}$  is the strain rate,  $Q_{\text{def}}$  is the activation energy for plastic flow and  $R$  is the universal gas constant ( $8.314 \text{ JK}^{-1}\text{mol}^{-1}$ ). A study was done by Yang and his co-workers[64] investigating the Zener-Hollomon parameter in the hot deformation behaviour of 20CrMnTi steel. They mentioned that the peak flow stress increased with decreased deforming temperature, while with increasing deformation temperature as well as decreasing strain rate, flow stress decreases. Furthermore, the higher temperature and lower strain rate facilitated recrystallisation. They also concluded that the three factors of equivalent strain rate, temperature and equivalent strain are all significant influencing factors, with the order of influence being equivalent strain rate > deformation temperature > equivalent strain. In other words, the strain rate as well as deformation temperature are the most sensitive and main factors for technical control.

Majid and et al.[65], and Mirzadeh et al.[66] studied the behaviour of a medium carbon microalloyed steel by hot compression test, using two different chemical compositions. However, both materials were tested under almost the same conditions of the deformation temperature and strain rate ranges. The majority of the flow curves for the studied steels at a high Z exhibited typical dynamic recrystallization behaviour with a single peak stress, whereas, at a low Z (very low strain rates  $0.0001 - 0.01 \text{ s}^{-1}$ ), multi peak dynamic recrystallization behaviour was observed. Excluded from that, in the Mirzadeh study some samples showed typical dynamic recovery behaviour at a deformation temperature of  $850^\circ\text{C}$ . Moreover, Sajadifar and his co-workers[67] studied dynamic recrystallization behaviour and hot deformation characteristics in 4340 steel. Axisymmetric compression tests were conducted under conditions of the temperature range of  $900 - 1200^\circ\text{C}$  and strain rate range of  $0.01 - 1 \text{ s}^{-1}$  to strain of 0.9. The results show that all the flow curves exhibited typical dynamic recrystallization behaviour with a single peak stress before reaching a steady state. The peak stress decreases with decrease in Z value (increase in deformation temperature and decrease in strain rate). Moreover the study proposed that the development of dynamic recrystallization grain structures could be associated by an extensive migration of grain boundaries.

Grain size also affects the flow behaviour of a material; the grain boundaries are obstacles to dislocation movement and so act as a strengthening mechanism. Consequently a fine-grained material will have a higher flow stress than a coarse-grained material. This relationship has been quantified by the Hall-petch equation:

$$\sigma_y = \sigma_i + \frac{k}{\sqrt{D}} \quad 2-4$$

where  $\sigma_y$  is the yield stress,  $\sigma_i$  is the friction stress, k is the strengthening coefficient and D is the average grain diameter[68]. The coefficient k is equal to the slope of a plot of  $\sigma_y$  versus  $(D)^{-1/2}$ , and  $\sigma_i$  is the intercept of this slope, i.e. the yield stress when no additional strengthening mechanisms are active, and is a function of temperature and strain[69]. Equation 2.4 can also be expressed in terms of the dislocation density. The strengthening arises from stress intensification at the grain boundary due to the elastic interaction between dislocations in the pile up, leading to increased stress in the adjacent grain[70]. There is a relationship between flow stress behaviour and both the initial grain size and



deformation conditions (Z). When the temperature increases, Z becomes low (Eq. 2.3), a reduction in flow stress occurs which facilitates dynamic softening and the grain size will increase. When strain rate increases, Z becomes higher and the flow stress will decrease, which facilitates work hardening, and the grain size will decrease. For a constant temperature, the flow stress of a material increases with increasing strain rate. This relationship can be expressed by the general equation proposed by Sellars & Tegart[71]:

$$\dot{\epsilon} = A[\sinh(\alpha\sigma)]^{n'} \exp\left(-\frac{Q}{RT}\right) \quad 2-5$$

which abbreviates to Equation 2.5 at low stresses ( $\alpha\sigma < 0.8$ ) and to Equation 2.6 at high stresses ( $\alpha\sigma > 1.2$ ) as follows:

$$\dot{\epsilon} = A'\sigma^n \exp\left(-\frac{Q}{RT}\right) \quad 2-6$$

$$\dot{\epsilon} = A'' \exp(\beta \sigma) \exp\left(-\frac{Q}{RT}\right) \quad 2-7$$

where A, A', A'', n, n',  $\alpha$  and  $\beta$  are all temperature-independent constants, and Q is the activation energy. The constants n',  $\alpha$  and  $\beta$  are related by  $\alpha = \beta/n'$ , and  $\beta$  and n' can be determined from experimental data. These equations allow the activation energies of dynamic restorative processes to be determined, and confirm that dynamic recovery is dominant in aluminium whilst dynamic recrystallisation occurs in metals such as copper, at high strains[72].

There are other factors such as alloy content and the formation of precipitates which can influence dislocation mobility and hence affect the flow behaviour of a material. Solid solution strengthening can arise due to the formation of substitutional or interstitial solid solutions. This leads to changes in the yield stress and flow stress with changes in alloy composition[73]. Precipitation strengthening can be due to particle coherence or due to dispersion hardening, both of which lead to an increase in the flow stress. Coherent particles lead to strains in the matrix around them, hindering dislocation movement. Dispersion hardening results from the presence of a distribution of fine undeformable and incoherent particles. Each dislocation when passing a particle will form a loop (Orowan looping) around this particle, leading to a back stress to the dislocation source, and strain hardening[74].

## 2.4.2 Recrystallisation

The improvement of microstructure during thermomechanical processing is actually depends upon recrystallization. The energy that is stored within the metals during deformation in the form of different crystalline defects, such as dislocations, boundaries and deformation bands, will release through recovery, recrystallisation and grain growth. Accordingly, recrystallisation can be defined as the formation of new strain-free grains within some areas of the sample and the next growth driven by the stored energy of deformation. Recrystallisation may occur during deformation, which is termed dynamic, or after deformation (e.g. during cooling or a subsequent heat treatment), which is termed static. The former takes place when the stacking fault energy is low for recovery and adequate stored energy residues to nucleate recrystallisation during deformation, while the latter takes place on holding a deformed structure at temperature for a period of time. Generally, recrystallization is usually accompanied by a decrease in hardness and strength and at the same time an increase in ductility.

### 2.4.2.1 Dynamic recrystallisation

In metals that recover slowly, generally those with low stacking fault energy (SFE), dynamic recrystallisation might occurs as soon as a critical deformation condition is achieved[75], as summarised in Figure 2.16.

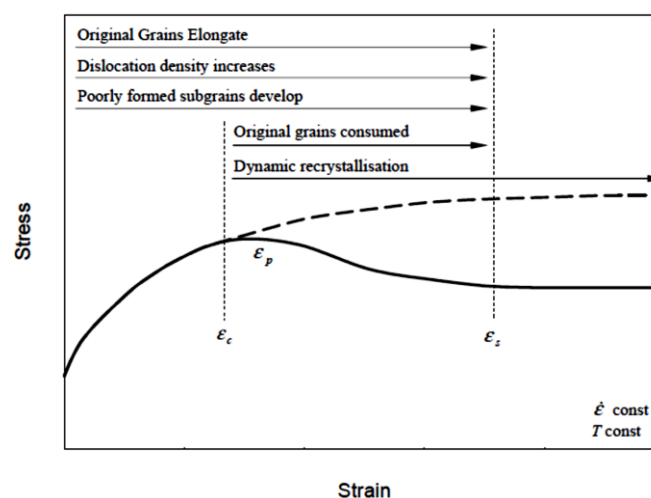


**Figure 2-16** The flow curves for steel in the austenitic condition, with work hardening, slow dynamic recovery and dynamic recrystallisation, adapted from Sellars[75].

The new dynamically recrystallised grains generally start nucleation at the ancient grain boundaries, and new grains are subsequently nucleated within the boundaries of the growing grains. This process continues like so until a thickening band of recrystallised grains is formed. Moreover, nucleation usually occurs at high angle grain boundaries, as demonstrated in Figure 2.17. In contrast to dynamic recovery, in hot working of steels in the austenitic condition, the flow curves for a dynamically recrystallising material generally can be recognized by a broad peak due to the softening effect of recrystallisation[76].

Another study on an interstitial free (IF) steel, by Tsuji et al.[77] concluded that dynamic recrystallisation was difficult to distinguish from the stress-strain curves alone, because there was no obvious drop, as in the flow stress during the dynamic recrystallisation of austenite. Sandstrom and Lagneborg[78] showed the dynamically recrystallised grain size to be a function of initial grain size as well as strain rate. The effect of different ratios of initial grain size to recrystallised grain size is shown in Figure 2.17. A comparatively large initial grain size will result in a necklace structure, with layers of recrystallised grains forming on the boundary, while a fine initial grain size will lead to the structure as shown in Figure 2.17e.

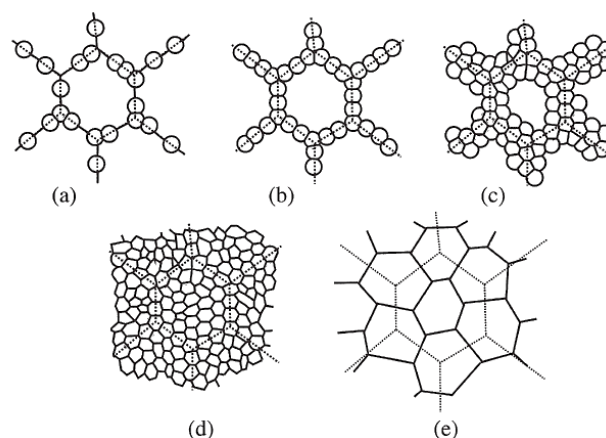


**Figure 2-17** Schematic representation showing, the progress of dynamic recrystallisation in a material with initial grain sizes (a)-(d) large (e) small[79].

As dynamic recrystallization take place new grains will initiate within the previous grain boundaries, and as the process of deformation is continuous this leads the dislocation density in the new recrystallised grains to increase, as a result the driving force for grain growth will be reduced. Furthermore, the nucleation of new grains will also help to halt the growth of recrystallising grains. In other meaning, dynamic recrystallisation spreads by a

process of repeated nucleation and limited growth. The two curves shown schematically in Figure 2.18 illustrate the two different types of dynamic recrystallisation behaviour. Weiss et al. [80] mention in their study that this can be due to differences in the initial grain size for constant values of  $Z$ , or a function of  $Z$  for a fixed initial grain size. Figure 2.19 illustrates the two mechanisms in two distinct ranges of operating conditions. As can be seen from the figure, high values of  $Z$  or a relatively fine initial grain size will result in a single peak, whereas low values of  $Z$  or a relatively coarse initial grain size will result in stress oscillation. Moreover, both the peak stress and the steady state stress are functions of the strain rate [78].

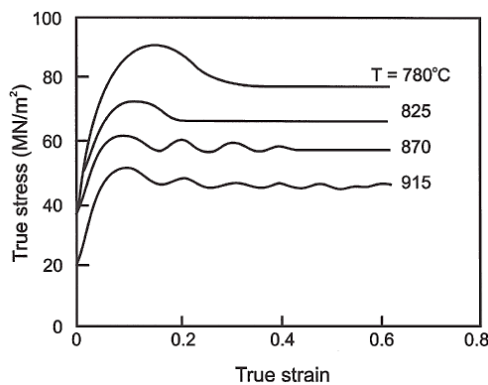


**Figure 2-18** The influence of temperature on the stress-strain curves for 0.68%C steel, deformed in axisymmetric compression,  $\dot{\epsilon}=1.3 \times 10^{-3} \text{ s}^{-1}$ , (Petkovic et al. 1975)[76].

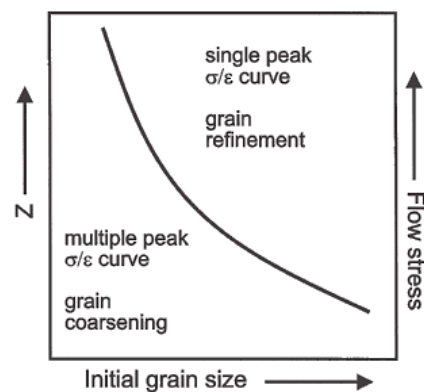


**Figure 2-19** The conditions for single and multiple peak dynamic recrystallisation, (after Sakai et al. 1983)[81].

In hot working temperature and strain are considered to be the main parameters that control the microstructure. However, the initial structure, which is represented in segregation of chemical composition and grain size inhomogeneity, also has influence on dynamic recrystallisation. During, the casting of large ingots, which are used as forged material for large scale products, the structure usually consists of undesirable characteristics. The microstructure, precipitation and segregation that develop during casting have a direct effect on the final microstructure. In general segregation defined as a process where solidified alloy has non-uniformity of composition and concentrations of elements are not equal in the entire alloy. This usually occurs because of partition of solutes in alloys between solid and liquid during freezing. Moreover, the effects of microscopic segregation become apparent in the forging in the region of individual grains and grain boundaries [82].

The final grain size usually could be justified through the parameters that affect the nucleation and growth processes. Many factors including a fine initial grain size as well as a high strain will result to a small grain size within the final microstructure. Moreover, the initial grain size has a significant effect on the kinetics of recrystallisation as a result of the change that usually happen within the grain boundary surface area, which is considered the main place of nucleation[83]. In some cases, such as in large scale products, the grain size usually does not be consistent within a whole billet. As the different grain sizes within the billet recrystallize at various rates, the shape as well as size of final grains inside sample might also be various[84]. Furthermore, the growth rate during recrystallisation is not constant through the microstructure. The variation in driving force is thought to be the prime reason with regard to this variation in growth rate, where the driving force might vary throughout the metals because of microstructural inhomogeneity[85].

Figure 2.20 illustrates a microstructure where the deformed grains, have variation of stored energy in different grains. Even if supposed that the nucleation will be relatively uniform, growth will take place rapidly within the high-stored energy grains, which will lead the microstructure in Figure 2.20a to become as presented in Figure 2.20b. However, the growth rate of the grains will decreases during recrystallisation by way of consuming the higher stored energy areas as well as by collision of new recrystallised grains with their neighbours inside the original grains[86].

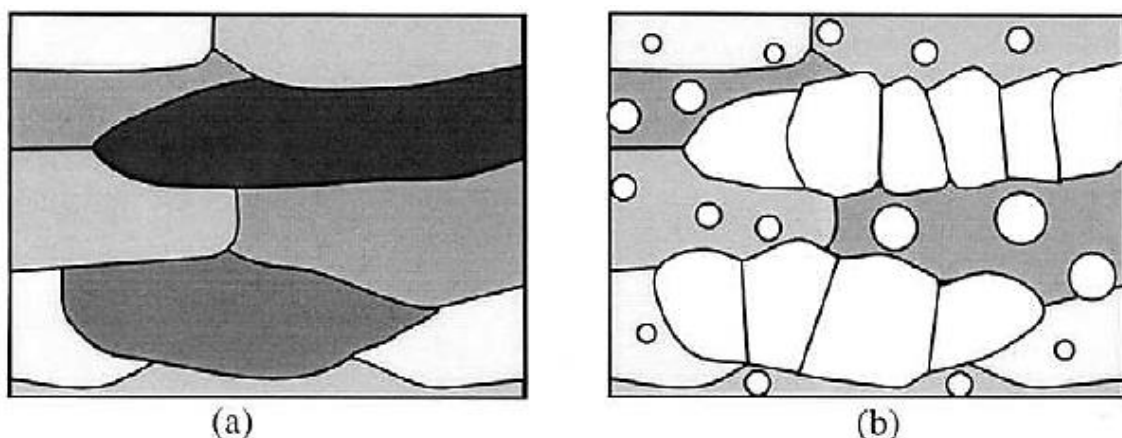


**Figure 2-20** showing in (a) the variation of stored energy in different grains (areas of higher stored energy appeared darker), (b) inhomogeneous grain growth results during recrystallisation[86].

P. Wray[87] studied the influence of chemical content as well as the initial grain size on the dynamic recrystallisation of austenite within some different base carbon steels. The results of this work indicated that the rate of recrystallization will increase in presence of fine grain structure. He reasoned that was probably as a result of existence of a larger number of grain corners, edges, as well as surfaces per unit volume. However, in some studied steels the impeding influence of grain growth at temperatures over 1200°C overcomes the normal temperature reliance of the recrystallisation rate, where the rate of dynamic crystallization decreased above this temperature. He suspected that the reason for this is due to the impeditive precipitate. In the situation of coarse grain structure the opposite influence will be obtained, where recrystallization rate become slower as the grain size increased.

Furthermore, the outcomes of the research on the effect of composition on dynamic recrystallisation indicated that the beginning of dynamic recrystallisation is delayed and the rate of recrystallisation decreases with increasing solute content. For instance, Figure 2.21 illustrates the effect of Mn amount on the dynamic recrystallisation behaviour of a 0.05 %C, 0.25 %Si based alloy. As can be seen from the figure, the solute addition (Mn) delays the beginning as well as impedes the rate of recrystallisation. The study also showed that the delaying influence of manganese increases with increasing strain rate. Generally, the rate of dynamic recrystallisation is reduced by the addition of solutes in an arrangement of increasing effectiveness of Carbon, Nickel, Manganese, Silicon, and Phosphorus. Nevertheless, P has the strongest influence probably due to grain boundary segregation. Whereas, in the case of austenite the delay of beginning of dynamic recrystallisation, the solute additions in arrangement of increasing effectiveness is Nickel, Manganese, Silicon, and Phosphorus. In addition, the effectiveness of addition of any of these solutes individually also depends upon the base content. Figure 2.22 presents the Influence of two different Si amounts on the dynamic recrystallisation behaviour of 0.05 %C, 0.8 - 1.4 %Mn steel. In the case of Mn, increased Si amount delays the beginning as well as impedes the rate of recrystallisation, but the influence of Si is stronger at a low Mn content than at high level, which means that the effectiveness of Si may depend on the amount of Mn.

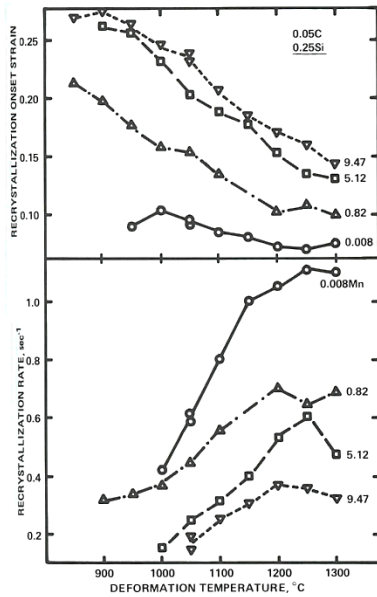


**Figure 2-21** The delay in beginning as well as the retardation of rate of dynamic recrystallisation as a result of the addition of Mn to 0.05 %C, 0.25 %Si steels, C, E, V, and W [87].

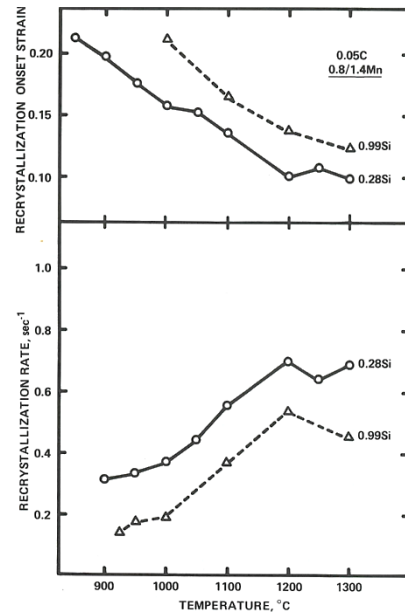


**Figure 2-22** Influence of increased Si percentage amount on recrystallisation in 0.05 %C, 0.8-1.4 %Mn steels E and U [87].

#### 2.4.2.2 Static recrystallisation

Static recrystallisation is triggered by the stored energy that was present in the material after deformation. It occurs after deformation, or during intervals between deformations. The process of static recrystallisation comprises two parts, namely a nucleation and growth process of new free dislocation density grains from previously deformed grains. Nucleation can occur at a number of different inhomogeneities within the structure, depending primarily on the material characteristics. Grain boundaries, the deformation zones around hard particles and features of the deformation structure such as transition bands or shear bands, which are good sources of stored energy, and areas of high misorientation are the most significant nucleation sites[88]. Nucleation is followed by growth of the grains to impingement with their neighbours; any further growth is coarsening of the recrystallised structure. The rate of grain growth is a function of boundary mobility and the driving pressure, which is in turn a function of the stored energy (dislocation density). Hence, the rate of growth is related to the amount of recovery prior to recrystallisation. Recent work by Lauridsen[89] about kinetics of individual grains during recrystallisation has shown that the growth rate varies from grain to grain, probably due to the inhomogeneous distribution of dislocations within the recrystallising structure.

One characteristic of static recrystallisation is the minimal amount of strain (critical strain), which is needed before the static recrystallisation occurs. For instance, the critical strain required to initiate static recrystallisation in C-Mn steel is 7% or less over the temperature range 900 - 1000 °C[90]. Moreover, the newly evolved grain diameter is directly related to the amount of deformation, deformation temperature, original austenite grain diameter, and the kinetics of static recrystallisation. Static recrystallisation occurs after the dislocations are rearranged and nucleation sites provided for recrystallisation slowly progress, then grain growth of statically recrystallised grains can occur within a very short period time. For static recrystallisation, the fraction recrystallised,  $f$ , at any given time, between deformation intervals is expressed by the Avrami Equation[91, 92]:

$$f = 1 - \exp\left[-c \left(\frac{t}{t_x}\right)^k\right] \quad 2-8$$

where  $t$  is the time from leaving the deformation tool,  $t_x$  is the time for some specified fraction of recrystallisation,  $k$  is Avrami coefficient, generally found to have a value of approximately 2, and the constant  $c = \ln(1 - f_x)$  under the condition of  $t/t_x=1$  where  $f_x$  is the time fraction recrystallisation at  $t_x$ . By substituting these values in the Avrami Equation 2.8 gives:

$$f = 1 - \exp\left[-0.693 \left(\frac{t}{t_{50}}\right)^2\right] \quad 2-9$$

where  $t_{50}$  is the time required for 50% recrystallisation, i.e.  $f_x=0.5$ . This equation is used to describe the form of the recrystallisation curve.

Some authors, including T. Gladman[93], summarized the factors which control the rate of static recrystallisation as following:

- The level of strain and the initial grain size strongly influence the recrystallisation kinetics. Work by Barraclough & Sellars[94] showed that an increase in strain or a decrease in initial grain size both lead to shorter recrystallisation times (see Figures 2.23 and 2.24) and a decrease in the recrystallised grain size. This is to be expected, as greater strains result in a higher driving force for recrystallisation, due to the increase in stored energy. Consequently, the number of nuclei and the nucleation and growth rates will increase, which means in other words increasing the rate of recrystallisation. Furthermore, a reduction in the initial



grain size increases the grain boundary area per unit volume, thus enhancing the number of possible nucleation sites. Humphreys & Hatherly[95] also mentioned that for a specific level of strain, the stored energy in a fine grained material will be greater than that of a coarser grained material, for low strains ( $\epsilon < 0.5$ ). This leads to the same previous result of increase in the number of nuclei and increase in the nucleation rates.

- Furthermore, the temperature also has an effect on static recrystallisation, where both the nucleation and growth stages are thermally activated processes. In general, a higher temperature results in a faster recrystallisation rate.
- The temperature compensated strain rate ( $Z$ ) value also has some bearing on the rate of static recrystallisation and on the recrystallised grain size. Jonas and his colleagues[58] concluded that an increase in  $Z$ , by decreasing deformation temperature and increasing strain rate, gives a higher level of stored energy. As a result, the recrystallised grain size will be reduced and recrystallisation will accelerate. However, Barraclough & Sellars[94] concluded that such changes in strain rate and deformation temperature ( $Z$ ) have a relatively small influence compared to alterations to strain magnitude and initial grain size.
- Humphreys & Hatherly[96] also mentioned the influence of solutes, both deliberate additions and impurities, on recrystallization kinetics. Elements in solution can retard the movement of subgrain boundaries by the mechanism of solute drag, affecting the rate of recrystallisation. This occurs due to atoms within grains having a different energy to those in the region of a boundary. Consequently, solute atoms can be attracted to a grain boundary, so forming an area of enrichment. The solute atoms will cause a reduction the mobility of the grain boundary, and this reduction becomes greater with the presence of higher concentrations. If the concentration of solutes at the boundary became low enough, the boundary can break away and return to the expected velocity. Furthermore, they mention that the solute drag at high temperatures becomes less effective. The concentration of solute atoms may also have a substantial influence on recrystallisation temperature; e.g. 0.004% Fe in high purity aluminium may increases the recrystallisation temperature by around 100 °C[97].

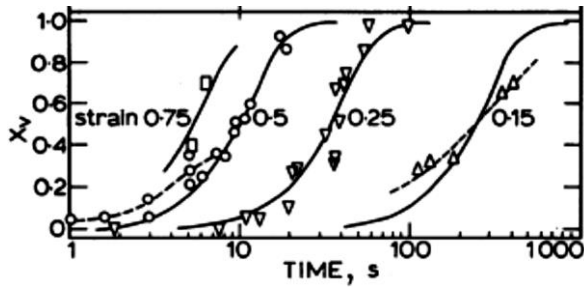


**Figure 2-23** Effect of strain on static recrystallisation curves for specimens of original grain size 160  $\mu\text{m}$  deformed at 1050°C and 1  $\text{s}^{-1}$ [94].

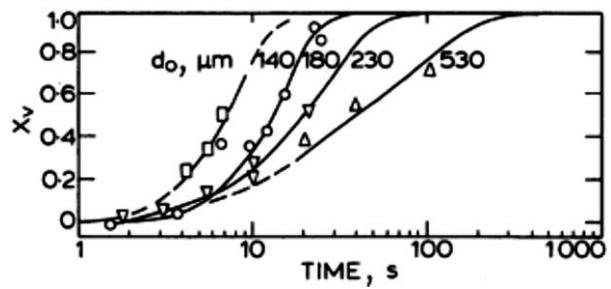


**Figure 2-24** Influence of original grain size on static recrystallisation curves for samples deformed under conditions of an equivalent strain of 0.5 at 1050°C and strain rate of 1  $\text{s}^{-1}$ [94].

These factors which enhance the rate of recrystallisation have been incorporated into a general equation. Sellars and Whiteman[90] (using results from a number of different authors) stated that the kinetics of static recrystallisation depend on variations in dislocation density, which produce the driving force, as well as on grain size ( $d_0$ ) and subgrain size since nucleation take place preferentially at grain boundaries. Moreover, the dislocation structures in turn depend on temperature-compensated strain rate ( $Z$ ) and strain. Accordingly, they found that the effects of these variables on the time to 95% recrystallisation  $t_{0.95}$  can be expressed as below when  $\epsilon < \epsilon_c$ :

$$t_x = A' Z^{-3/8} \epsilon^{-4} d_0^2 \exp\left(\frac{Q_{rex}}{RT}\right) \quad 2-10$$

where  $A'$  is a constant,  $Q_{rex}$  is the activation energy for recrystallisation and independent of strain. The recrystallised volume fraction for any isothermal holding after any deformation condition can be determined, and when full recrystallisation is achieved, the grain diameter can be calculated.

From similar considerations, they proposed the following equation for the recrystallised grain size  $d_{rex}$  as following:

$$d_{rex} = A'' \left(\frac{1}{\beta} \ln \frac{Z}{A}\right)^{-2/3} \epsilon^{-1} d_0^{1/2} \quad 2-11$$

for strains  $<$  the critical strain. The values of the constants such as  $A''$  and  $\beta$  vary for different grades of steel, and were evaluated for a range of microalloyed steels[98].

## 2.5 Isothermal and Continuous Cooling Transformation

Both types of transformation diagram - isothermal transformation (IT) and continuous cooling transformation (CCT) - are useful, and help in selecting the optimum steels which have the desirable microstructure and in designing a suitable heat treatment route to reach the required final properties. By using these diagrams, microstructures such as ferrite and pearlite can be produced, or the production of hardened microstructures such as martensitic microstructure avoided[99].

### 2.5.1 Isothermal Transformation Diagram

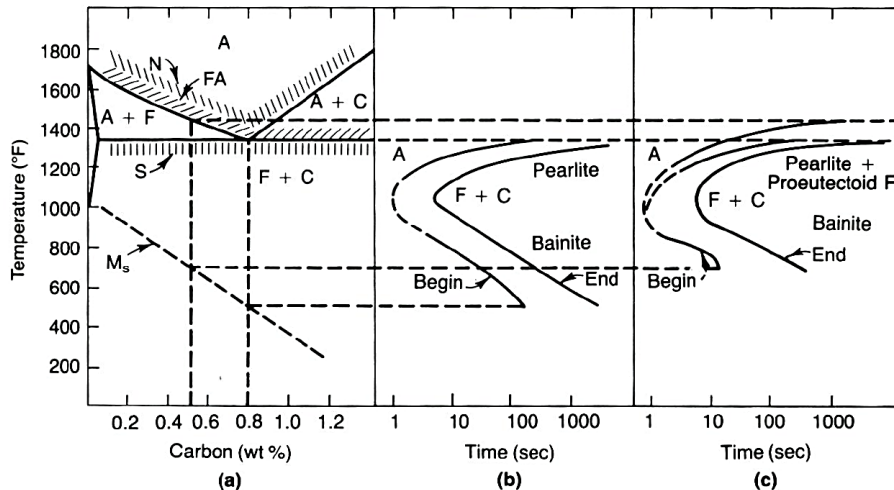
The isothermal transformation (IT) diagram, or as it is called time temperature transformation diagram, represents the kinetics of transformation of austenite as a function of time and at a constant temperature. This diagram is used to determine the beginning and completion of isothermal transformations of alloyed steels when cooled rapidly from austenite zone to a required temperature, which is lower than the eutectoid temperature, and then left it to transform isothermally. Moreover it is used to determine what percentage of the phase transformation could be achieved at a constant temperature. A large series of experiments, where the specimens are held for various times at various temperatures, should be performed to build up a complete TTT diagram. The samples are placed in the furnace and austenitised to a temperature higher than the eutectoid temperature. As soon as the austenitising is complete, the samples are rapidly cooled by quenching in a liquid salt bath to a given temperature below the eutectoid temperature.

The samples are held for different time intervals before quenching in water to room temperature. The microstructure after each transformation is examined in order to quantify the percentage of microstructure changes of the new phases[100]. As a result of transformation, the austenite, if held for a short time and cooled rapidly, will change completely to martensite, while if held for a long period of time the microstructure will transform to ferrite, cementite, pearlite, or bainite according to both of cooling rate and composition of the steel. A fine grained microstructure such as fine pearlite can be obtained at lower temperature compared to coarse pearlite, because the transformation which is controlled by the rate of nucleation occurs sooner and the grain growth is reduced.

Pearlite forms at a higher temperature than bainite, which forms at low temperature. Each type of steel with specific chemical composition has its own diagram. The main important factors affecting TTT diagrams are the composition of steel, austenite grain size, and heterogeneity of austenite grains. For instance, increasing carbon wt% and alloying elements will cause a decrease in the A3 line which means that the incubation period for transforming the austenite to pearlite will increase, thus the C curve of the TTT diagram will move to the right[101]. Figure 2.25 represents Fe-Fe<sub>3</sub>C metastable equilibrium diagram and TTT diagrams for hypoeutectoid steel containing 0.5 %C, and eutectoid steel (0.8 %C) with different phases at different temperatures and soaking times.

The presence of a proeutectoid ferrite phase coexisting with the pearlite is one of the differences between hypoeutectoid steel and eutectoid steel in the TTT diagram, which means that there will be another curve for proeutectoid transformation to be added. Also, there is a difference in A3 and Ms temperature lines, where A3 and Ms are higher in the case of hypoeutectoid steel because of lower carbon content. Another difference, as shown in Figure 2.25 (b, c), is the distance between the nose curve and the vertical temperature line, where the nose in the case of the hypoeutectoid steel is more closed which mean less time for transformation in comparison with the eutectoid steel.

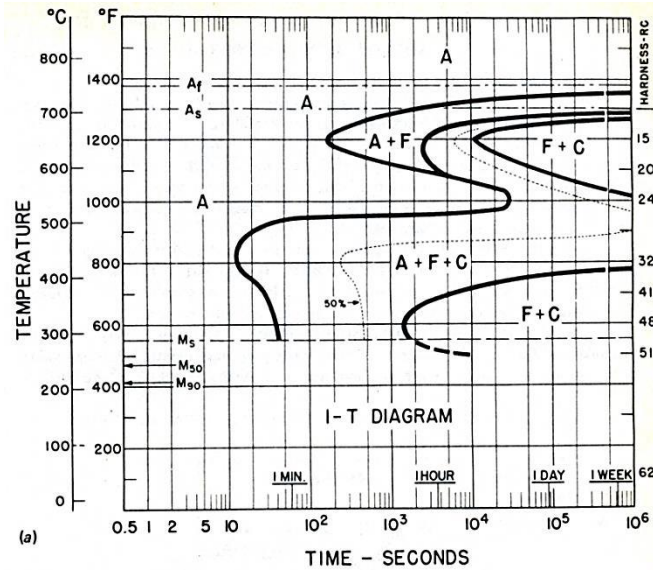
Moreover, several studies [56, 102, 103] have documented a clear effect of prior austenite grain size on the Ms temperature in ferrous systems. The types of steels with different chemical compositions that have been tested proved a large dependence on Ms as a function of the austenite grain size. A smaller austenite grain size, which results from decreased austenitising temperature, leads to a reduction in the martensite start ( $M_s$ ) temperature. In contrast, a slight increase in the austenite grain size will result in higher  $M_s$  values (See Fig. 2.14).



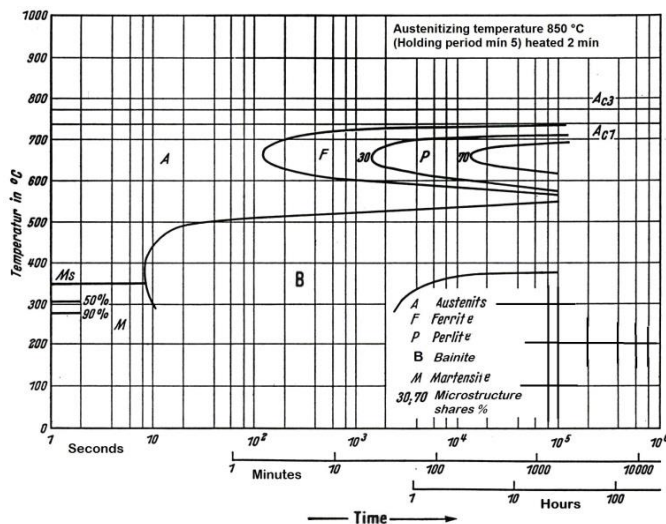
**Figure 2-25** Relationship to (a) Fe-C diagram, (b) Isothermal transformation diagram of eutectoid steel, and (c) Isothermal transformation diagram of steel containing 0.5 % carbon [104]. N = normalising, FA = full annealing, and S = spheroidizing heat treatments

Figure 2.26 represents the isothermal transformation diagram of AISI 4340 steel, which is closed grade to the 34CrNiMo6 steel with slight variations in actual chemical composition (See section 1.1) and indicates the transformation phases for different temperatures and different times[105]. As can be seen from the diagram the addition of alloying elements such as Ni, Cr and Mo to this steel which contains 0.04 %C produced a significant change to the IT diagram that was shown in Figure 2.25. The rates of transformation now have two curves with two maximum noses: one is the pearlite nose at temperature of about 650°C and the other is bainite nose at about 440°C. These two curves are separated by a bay at about 540°C, where the transformation is extremely delayed. The transformation over the entire temperature range between  $A_3$  and  $M_s$  is delayed by pushing the whole diagram to the right and decreasing  $M_s$ , and as consequence, the hardenability is increased[106].

Another example IT diagram, which is also close to the 34CrNiMo6 steel is 28NiCrMo7 steel[107] with chemical composition of 0.30%C, 0.46%Mn, 0.241% Si, 2.06%Ni, 1.44%Cr, 0.37%Mo, 0.03%P, 0.20%Cu, 0.025%S, <0.01V is shown in figure 2.27. Comparing the IT curves for the 4340 and 28NiCrMo7 steels, in general the two curves are considered similar in terms of shape. However, it can be seen that the 4340 steel IT curve is pushed a little more to the right than the 28NiCrMo7 steel IT curve. Moreover, the whole IT curve of 4340 steel was also moved down, causing a decrease in the  $A_1$ ,  $A_3$ ,  $M_s$  and  $M_f$  compared to the 28NiCrMo7 steel IT curve. This may be due to the high percentage of carbon (0.42%) in 4340 steel, which is one of the most important elements affecting the IT curves.



**Figure 2-26** Isothermal transformation diagram of AISI 4340 steel (0.42 %C, 0.78 %Mn, 1.79 %Ni, 0.80 %Cr, 0.33 %Mo). Grain size 7-8. Austenitised at 843°C [108].



**Figure 2-27** IT diagram of 28 NiCrMo 7 steel (0.30 %C, 0.46 %Mn, 0.241 %Si, 2.06 %Ni, 1.44 %Cr, 0.37 %Mo, 0.03 %P, 0.20 %Cu, 0.025 %S, <0.01V) Austenitised at 850°C[107].

### 2.5.2 Continuous Cooling Transformation Diagram

As mentioned in the previous section, the isothermal transformation diagram represents the kinetics of transformation of austenite as a function of time at a constant temperature where an alloy must be rapidly cooled from a temperature higher than eutectoid temperature and kept at an elevated temperature for some time to complete the transformation. This is impractical in real applications, especially with large scale products where the temperature within the part being heat treated will vary from the surface to the centre, and from the middle to the sides. The continuous cooling transformation (CCT)

diagram, which represents the transformation process of austenite phase during continuous cooling from the austenite zone to room temperature with various cooling rates where the temperature is constantly changing, is usually used for most industrial heat treatment[109]. In this research all heat treatment tests were done by continuous cooling transformation. Figure 2.28 shows the relationship of continuous cooling transformation and isothermal transformation diagrams with end-quench hardenability test (Jominy specimen) data and four cooling rates for eutectoid carbon steel[110]. As indicated, the TTT diagram was modified to be valid for the constantly changing transformation temperature that occurs in the CCT diagram by shifting the curves to longer times and lower temperatures[111]. The main difference when the TTT and CCT diagrams are interpreted is that the TTT diagram is read from left to right at a constant temperature whereas the CCT diagram is read along the cooling curves from the top left to the bottom right[112].

The bottom part of Figure 2.28 shows the Jominy end-quench test specimen which is used to calculate or measure hardenability i.e. the ability of the steel to transform partly or entirely to martensite. The maximum cooling rate will be in the quenched end of the specimen as represented by curve A (100% martensite), and the cooling rate will decrease at given distances from the end as represented by curves B, C, and D. In other words, with decreasing cooling rate or increasing distance from the quenching end of the Jominy specimen, the austenite transforms to microstructures containing increasingly greater quantities of bainite, ferrite and pearlite. Moreover, the hardness decreases as the cooling rate decreases where the martensite is also replaced with pearlite or bainite, and vice versa. Through a comparison between the TTT and the CCT diagrams there are a several features in the CCT diagram which have no counterpart in the TTT diagrams especially in alloy steels. These features include the following [112]:

- A depression of the  $M_s$  temperature at slow cooling rates.
- The tempering of martensite that takes place on cooling from the  $M_s$  temperature to about 200°C.
- A great variety of microstructures.

The reason for reduction of the  $M_s$  temperature when the cooling rate decreases in alloy steel is due to the rejection of carbon into austenite during the transformation of the microstructure to ferrite or bainite, where the untransformed enriched austenite with

carbon has a lower  $M_s$  temperature. However, the tempering of martensite on cooling is referred to as autotempering especially in low carbon steels with high  $M_s$  temperatures, where in this range of temperatures ( $M_s$  to  $200^\circ\text{C}$ ) carbon has adequate mobility to form the carbides characteristic of tempered martensite. The variety of microstructures refers to the increase in fineness and intermixing of the austenite transformation products as transformation progresses at sequentially lower temperatures on cooling[104].

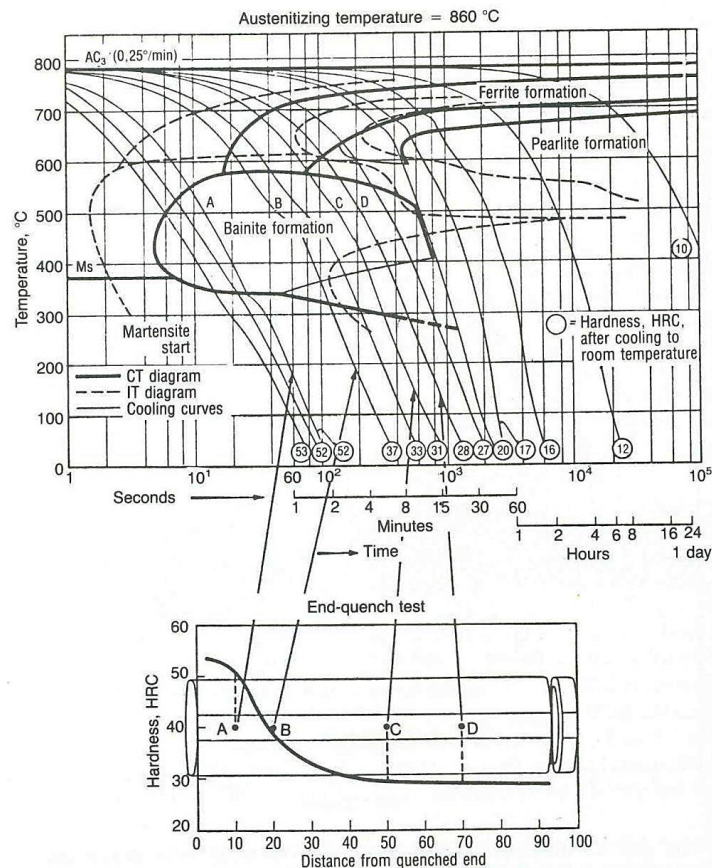


**Figure 2-28** CT diagram (continuous line) for steel with German designation 42CrMo4 (0.38%C, 0.99%Cr and 0.16%Mo). IT diagram is also shown (dashed line)[113].

When using the CCT diagram for practical heat treatments, the cooling curves will not be linear but will depend on the heat transfer emitted from the specimen to cooling media and the rate of emission of latent heat during transformation [112].

### 2.5.2.1 Microstructure evolution

Using different cooling rates gives various combinations of phases. For instance, by using a very slow cooling rate (e.g., furnace cooling), as in the process of full annealing, coarse pearlite will be result, while by using a faster cooling rate, which can be obtained by cooling



in air as in the normalising process, the result will be finer pearlite. By further reducing the cooling rate (e.g., oil quenching) a combination of bainite and martensite can be obtained. If the cooling rate was more than the martensite critical cooling rate (e.g., water quenching), the microstructure will become fully martensite. As can be seen in the medium carbon steel, the critical cooling rate is reduced even by the presence of carbon. The alloying elements that are mainly effective in rendering steels heat-treatable are Cr, Ni, Mo, Mn, Si, and W. These elements must be in solid solution with the austenite at the time of quenching[114].

Figure 2.29[115] indicates several cooling curves superimposed on the CCT diagram of 4340 (~ 34CrNiMo6) alloy steel; these curves represent transformation behaviour and how various cooling rates such as quenching, normalizing, and full annealing can produce different final microstructures. For this type of steel the critical cooling rate is 8.3 °C/sec; higher than this cooling rate all the austenite microstructure will transform to martensite at room temperature. Quenched martensite is extremely hard as well as strong but it is also very brittle, so it will break under stresses. Moreover, it has almost no ductility, and its hardness is dependent on the percentage of carbon content. The highest hardness of martensite in some cases can achieve up to 700 HB. For eutectoid steel, some austenite, called retained austenite, will remain in the microstructure and this amount increases with increased carbon content. The strength of the martensite is also reduced as the amount of retained austenite increases. The tempering process is typically used to address this weakness, where the tempering process helps to increase ductility and toughness.

At intermediate rates of cooling, besides the martensite, the diagram shows the dominance of bainite formation. From the figure this intermediate rate will be in the range of less than 8.3°C/sec and more than 0.3°C/sec. By decreasing the cooling rate, the percentage of bainite will increase and martensite percentage will decrease in the microstructure[114]. Generally, the structure of bainite, like pearlite, consists of dislocation-rich ferrite and cementite. However, bainitic steels are commonly harder compared to the pearlitic ones, because the bainitic structure is a finer structure. bainite microstructure usually exhibits a desirable combination of strength and ductility compared with pearlite. Davenport and Bain[116] originally described the bainite microstructure as being similar in appearance to tempered martensite. As can be seen in Figure 2.30[117] bainite is an intermediate of pearlite and martensite in terms of hardness. By further reducing the

cooling rate in Figure 2.29 to less than 0.3°C/sec, besides the martensite and bainite phases, some austenite also will begin to transform to ferrite and pearlite, which results in a greater decrease in hardness. Pearlite consists of cementite (Fe<sub>3</sub>C) and ferrite ( $\alpha$ ), where the Fe<sub>3</sub>C is harder as well as more brittle compared to  $\alpha$ . Consequently, increasing the amount of cementite within a steel alloy will lead to obtain a stronger and harder microstructure, when other microstructural elements remain constant. The strength (tensile and yield) as well as the hardness increases with increasing carbon concentration (or equivalently as the percentage of cementite). In contrast, both the ductility and toughness will decrease by increasing the cementite content; this is due to the brittleness of cementite. The thickness of  $\alpha$  and Fe<sub>3</sub>C also has an effect on the mechanical behaviour of the metals. The microstructure that consists of fine pearlite is always harder as well as stronger than that with coarse pearlite, whereas coarse pearlite is more ductile.

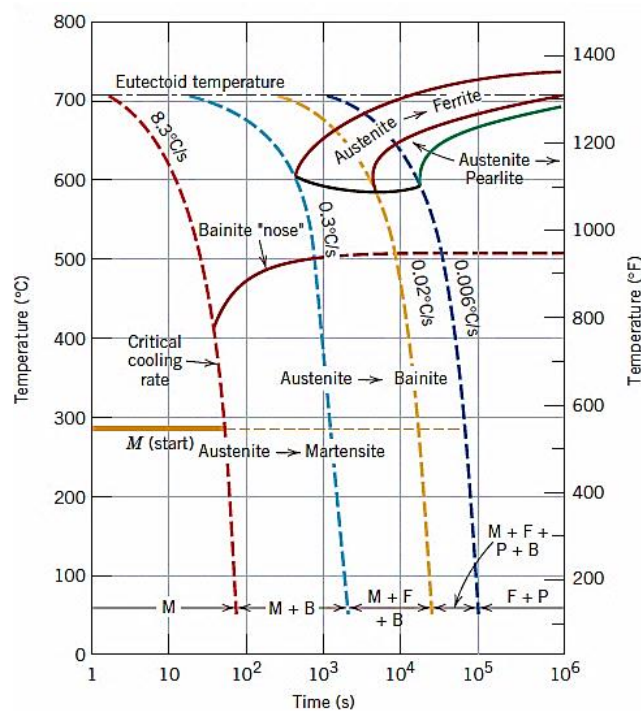


**Figure 2-29** CCT diagram for 4340 medium carbon steel with several cooling curves representing the final microstructure and its dependency on the transformations that take place during of cooling (Adapted from H. E. McGannon [118])[115].

Figure 2.30[117] presents the CCT chart of the 34CrNiMo6 steel with chemical composition 0.35%C, 0.55%Mn, 0.25%Si, 1.55%Ni, 1.55%Cr, 0.20%Mo, 0.025%P, and 0.015%S. Moreover, several cooling curves showing the phases ratios for each one and the hardness values of the microstructures produced by those cooling rates are also illustrated

in the figure. Popescu et al.[117] mention that the main heat treatment features of 34CrNiMo6 steel are low quenching temperature, high bainitic hardenability and good temperability, due to the high proportions of martensite and bainite in the quenched structure. Furthermore the results showed that the greater the distance from the quenched end, the lower the proportion of martensite (simultaneously the higher the proportion of bainite) and the lower the hardness.

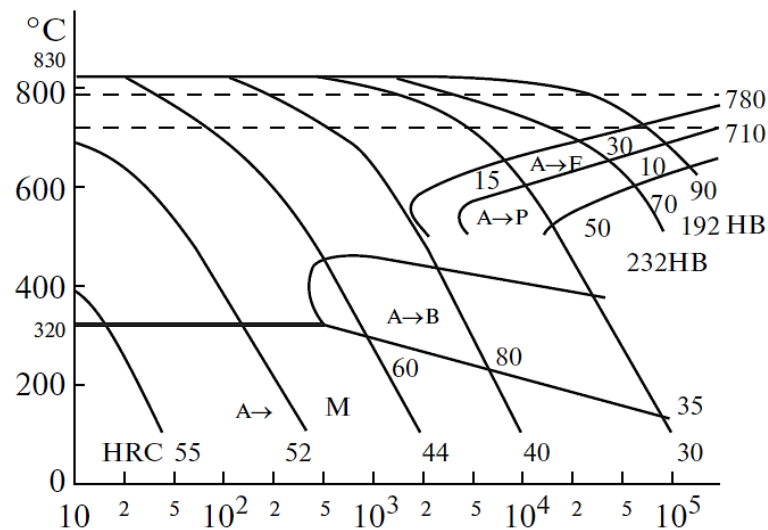


**Figure 2-30** CCT diagram of 34CrNiMo6 steel (0.35 %C, 0.55 %Mn, 0.25 %Si, 1.55 %Ni, 1.55 %Cr, 0.20 %Mo, 0.025 %P, 0.015 %S) Austenitised at 830°C for 15 mins[117].

Furthermore, Figure 2.31 [119] illustrates the CCT diagram for steel VCNMO150, which also, according to standard designations, is one of the 34CrNiMo6 steel grads (See appendix E) with a chemical composition of 0.34%C, 0.4%Si, 0.65%Mn, 1.5%Cr, 0.23%Mo, 1.5%Ni. The curve represents the austenite transformation continuously as a function of cooling rates and hardness. Another example of a CCT curve for medium carbon steel, to compare with 4340 steel, is steel VCNMO150. The critical cooling rates for all the phases are less in steel VCNMO150 due to differences in the percentages of the elements, which in turn affect the CCT curve. For this kind of steel (steel VCNMO150) the critical cooling rate, where the austenite will transform to martensite, is higher than 2.5°C/sec, while the bainite transformation will be in the range between 2.5°C/sec and 0.15°C/sec. These ranges of cooling rates for transformation are approximately close to the ranges that were obtained in our experiments. By decreasing the cooling rate to less than 0.15°C/sec, the ferrite and pearlite phases will start to appear in the microstructure at the expense of martensite and bainite.

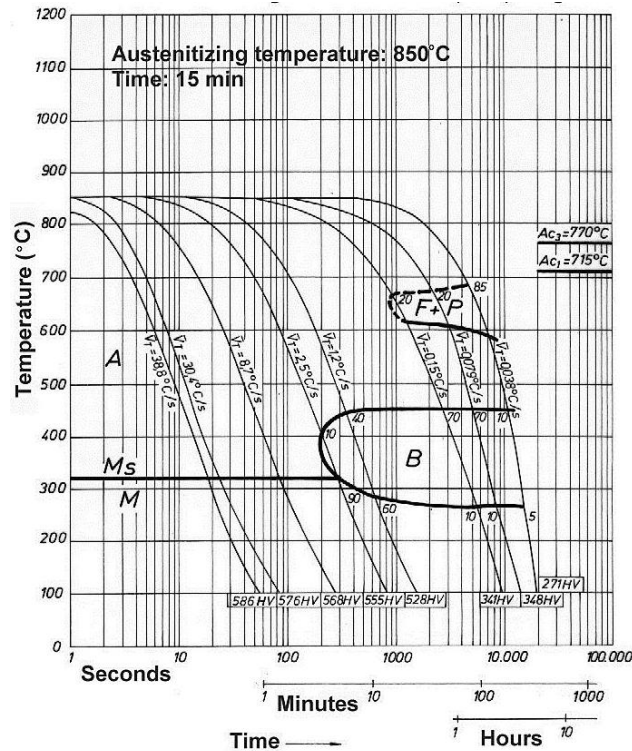


**Figure 2-31** shows the CCT diagram for steel VCNMO150 (0.34 %C, 0.4 %Si, 0.65 %Mn, 1.5 %Cr, 0.23 %Mo, 1.5% Ni)[119].

### 2.5.2.2 Impact of tempering

By tempering hard quenched plain carbon steels, which have poor ductility, the hardness is decreased and the ductility increased. During tempering the martensite decomposes to ferrite and a metastable phase of  $\epsilon$ -carbide. On further heating, stable carbide (cementite) is formed and eventually the ferrite matrix recrystallizes. Moreover, the retained austenite, if it is present after quenching, will decompose during tempering to give a carbide and ferrite. The final stage of tempering is the growth of the ferrite grains. The tempered martensite is not quite as hard, but becomes tougher, i.e., less likely to break and more malleable, and thus more suitable for engineering applications[120].

The effect of alloying elements added to steel usually depends upon the affinity of those elements for carbon. With the addition of elements such as Si, Ni, and Mn, which have a relatively weak affinity for carbon, the microstructural changes that occur on tempering are similar to those found in plain carbon steels. Nevertheless, these elements may affect the kinetics of the tempering reactions. If alloying elements like Cr, Mo, Ti, V, and Ni, which have a relatively strong affinity for carbon, are added to steel, they may significantly modify the tempering process. In this case the formation of  $\epsilon$ -carbide and cementite are retarded and

may even be prevented. Other alloy carbides, e.g.  $\text{Mo}_2\text{C}$ ,  $\text{Cr}_7\text{C}_3$ ,  $\text{V}_4\text{C}_3$ ,  $\text{TiC}$ , and  $\text{NbC}$ , are then formed at the expense of cementite, where in the end complex carbides of the type  $\text{M}_{23}\text{C}_6$  and  $\text{M}_6\text{C}$  may replace the simple alloy carbides. Tempering alloy steels that contain strong carbide formers may increase the hardness, for the reason that the alloy carbides are initially precipitated in a very fine coherent dispersion. This phenomenon is known as secondary hardening, which is a form of precipitation hardening[121].

Xue and Baker[122] have studied the mechanical properties of Fe-0.1C-1.5Mn-0.05V steels with varying Al contents in the tempered condition. The steels were solution treated at  $1200^\circ\text{C}$  for 2h, quenched into water and tempered at 600 or  $650^\circ\text{C}$  for 1h. Tempered martensite was observed in all samples after tempering. The study showed that the precipitation of VC was at a minimum in the steel containing 0.13% Al. They also suggested that the precipitation of VC or V (C, N) was retarded at level of 0.1-0.15% Al. Moreover, at this level of Al (0.1-0.15%), the tensile strength and ductile-brittle transition temperature decreased to their minimum values and also the hardness become lower. However, they considered that a smaller amount of VC or V(C, N) precipitation gives benefits of increased toughness.

Bainitic ferrite usually contains only slight excesses of carbon in solid solution and the carbon in transformed sample usually exists as cementite particles ( $\text{M}_3\text{C}$ ). In the case of martensite the strength falls dramatically as a result of precipitation of the carbon during tempering process, due to the effectiveness of carbon in solid solution strengthening. However, this does not occur in the case of tempering of bainite where the carbon amount is mainly existent as coarse carbides, which causes a slightly effect to strength. Consequently, the tempering response of bainite is expected to be somewhat insensitive to the overall carbon concentration. The most important changes within strength usually happen when the bainitic microstructure coarsens or even recrystallisation occurs, forming equiaxed grains of ferrite. During tempering the actual change or transition from  $\text{Fe}_3\text{C}$  to the equilibrium carbide might happen through some of other transition carbides. As illustrated in Figure 2.32, Baker and Nutting[123] concluded that during the tempering of bainite in the Fe-2.12 %Cr, 0.94 %Mo, 0.15 %C alloy steel, the  $\text{M}_2\text{C}$  carbide particles, which usually has a needle shape, were the first alloy carbide formed, which precipitate independently of the cementite.

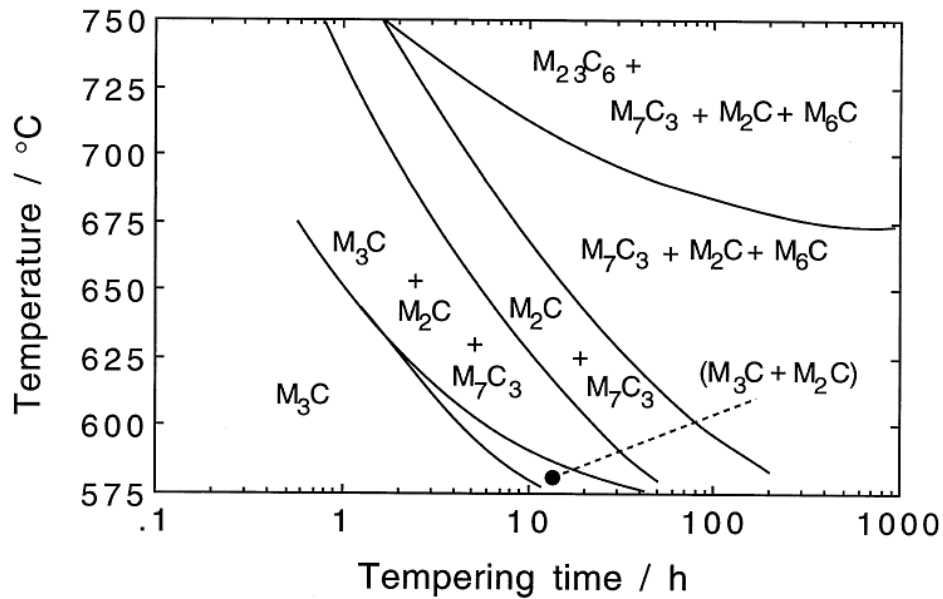


**Figure 2-32** Shows an updated classic version for the carbide stability diagram by Baker-Nutting for 2.25 Cr and 1 Mo steel (after Nutting, 1998)[124].

A study was done by T. Okuno[125] about the influence of microstructure on the toughness of AISI H13, H10, and H19 steels. The study investigated the microstructural contributions to the toughness of hot work tool steels, which tempered after quenching at various cooling rates. The CCT diagram of H 13 is shown in Figure 2.33. The martensite microstructure was produced by oil quenching, while the upper bainite structure occurred at the cooling rate of 15 min. The study found that toughness can be improved by refinement of the laths of martensite and bainite and the effective grain size. This can be achieved by reduction of the volume fraction as well as the size of retained carbides, suppression of the dense dispersion of fine carbides like MC and  $M_2C$  in matrix, and retardation of the preferential precipitation of carbides along grain boundaries of prior austenite and bainite.

Furthermore, he concluded that decreasing the quenching rate leads to gradual increase in the width of bainite laths as well as leading to modification of the morphology of bainite from lath to granular type together with increase in volume fraction of upper bainite. Decreasing the cooling rate also results in deterioration of toughness.

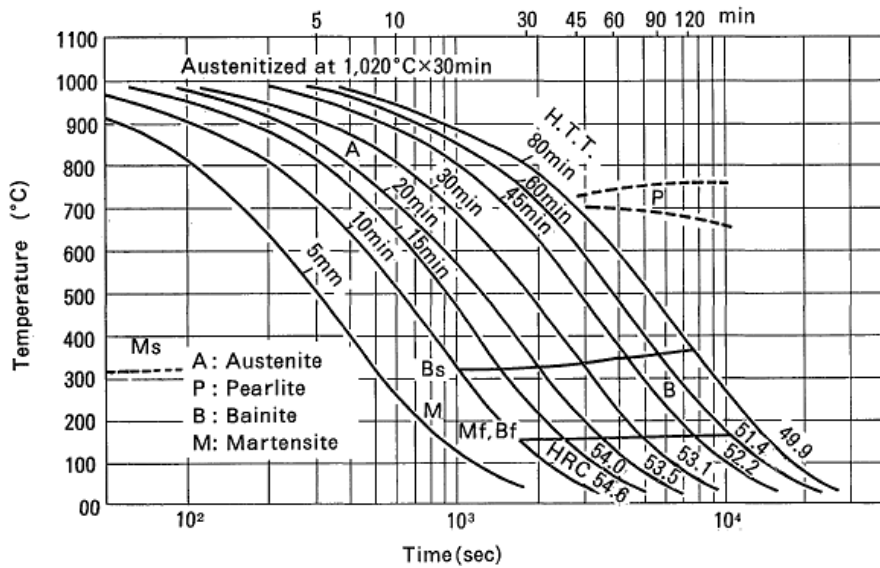


Figure 2-33 Continuous cooling transformation diagram of H13 steel[125].

## 2.6 Non-metallic inclusions

Clean steel is demanded by all customers, which means producing high quality steel with a desirable composition. One of the main issues during steel making is the presence of non-metallic inclusions, which should be eliminated or at least minimized to a desirable amount. Non-metallic inclusions significantly influence the ingot structure, which is the raw material for thermomechanical processes such as forging; hence they subsequently influence the final mechanical properties. Non-metallic inclusions are defined as chemical compounds, both metallic elements like manganese or aluminium and non-metals like oxygen or sulphur. Non-metallic inclusions found in steel are oxides, e.g.,  $Al_2O_3$ , sulphides, e.g.  $MnS$ , nitrides, e.g.  $VN$ , carbides, e.g.  $VC$ , and sometimes complexes of these, e.g.  $Al_2O_3 \cdot CaS$ [126]. They are formed at several different stages of the steel making process, i.e. melting, deoxidation, solidification and cooling.

The old method classifies sources of inclusions into exogenous inclusions and indigenous inclusions. Exogenous inclusions are particles entering a steel ingot during interaction with external sources like refractory or mould material, or oxidized material from the atmosphere. These inclusions are not too dangerous because they can be minimised by techniques such as using a vacuum furnace and good housekeeping[127]. Indigenous inclusions are usually formed because or as a result of chemical reactions between some added elements within steel, for example,  $Al_2O_3$ ,  $SiO_2$ , or  $MnO$  being made during de-

oxidation, depending on the deoxidizing material, or MnS, CaS, or MgS during desulphurisation, depending on the desulphurising material[128].

According to Kiessling and Nordberg[129] this classification is an oversimplification of the situation because many inclusions are the result of endogenous precipitation of different oxides and sulphides on exogenous nuclei; instead, they suggest that inclusions should be classified according to their compositions. Moreover, Matsushima et al.[130] have suggested that a convenient way of classifying inclusions is according to their ductility, divided into ductile and non-ductile inclusions. This is sensible because their influence on properties of steel differs significantly. Accordingly, ductile inclusions are generally sulphide and silicate inclusions which undergo plastic deformation during deformation. Non-ductile inclusions are divided into:

- a) Inclusions of granular oxides, usually oval in shape, which are hardly deformed and which are rather irregularly scattered, such as  $\text{Al}_2\text{O}_3$ ,  $\text{TiO}_2$ .
- b) Globular inclusions, which are also scarcely deformed during deformation, such as CaO- $\text{Al}_2\text{O}_3$ .
- c) Silicate type inclusions enriched with  $\text{SiO}_2$ , which are plastically deformed to some degree through deformation, usually existing in a steel ingot with a globular shape.

The behaviour of hard non-ductile inclusions of the type globular silicate, crystalline high alumina calcium aluminate and  $\text{Al}_2\text{O}_3$  cluster during deformation is illustrated in Figure 2.34[131]. The small particles generally agglomerate to form large inclusions. The merge between inclusions becomes easier when they collide if the inclusion has higher surface energy.



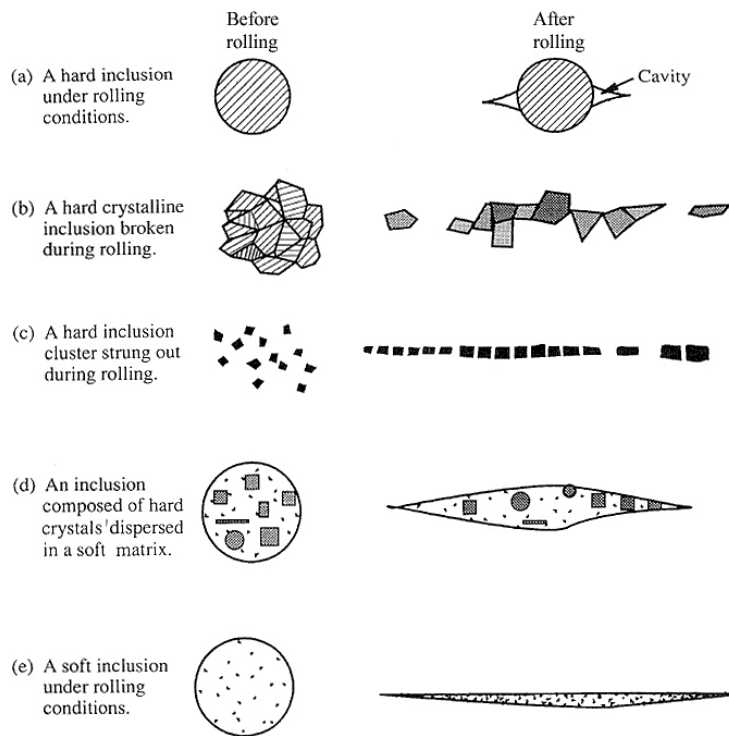


**Figure 2-34** Schematic representation of inclusion shapes before and after deformation[131].

## 2.6.1 Non-metallic inclusions parameters

The main important parameters of non-metallic inclusions are size, shape, quantity, distribution, interfacial strength, and chemical composition [132].

### 2.6.1.1 Inclusion morphologies

The shape of inclusions during solidification is significant in casting steel ingots, where the shape can be controlled during steel processing by controlling their mechanical behaviour. Therefore hard or un-deformable inclusions like pure alumina should be eliminated, compared with soft inclusions like manganese sulphide (MnS). The most common inclusion shapes are spherical, platelet, dendrite, and polyhedral. Spherical inclusions are more desirable than other inclusions because they have a medium effect on the mechanical properties of ingot steel. Some of these spherical inclusions form during solidification in interdendritic space[133]. The platelet shape is a thin plate from manganese sulphides and oxy-sulphides formed during aluminium killed steel, usually located through steel grain boundaries. This kind of inclusion is undesirable, because it causes weakness of the grain boundary and affects the properties of the steel, especially in hot state[134]. Similarly, the dendrite shape of inclusions is also undesirable, because internal stress may concentrate in

the sharp edges of this shape. This type of inclusion is also very hard because the melting temperature of steel is lower than inclusions. Furthermore, polyhedral-shaped inclusions have a moderate impact on the properties of steel compared to the dendrite shape, because the polyhedral shape somewhat resembles a spherical shape[133].

#### **2.6.1.2 Critical size of inclusions**

Critical inclusion size is the size above which the inclusion can be harmful to a particular property of steel. Generally, inclusions of a very small size are inescapable and are usually not dangerous, but if the size is large, inclusions will be very dangerous. Kiessling and Nordberg[129] have tried to estimate this critical defect size by using  $K_{1C}$  values in fracture mechanics. They have concluded that the critical defect size when calculated this way gives a measure of the critical inclusion size if the inclusion has a smaller thermal expansion than the matrix. However, for inclusions with larger expansion coefficients, the critical size is larger than those calculated. Pomey and Trentini[135] provided an explanation for the difference in critical inclusion size according to difference in the thermal expansion coefficients. During cooling, the inclusions with smaller expansion coefficients than the matrix develop thermal stresses, while those with higher expansion coefficients develop voids or parting of the matrix and inclusions. The thermal stresses promoted reduce the fatigue resistance of the steel considerably.

#### **2.6.1.3 Distribution and clusters**

The distribution of non-metallic inclusions inside a steel ingot is also one of the important parameters that influence the mechanical properties. Sometimes the distribution can change the metal forming results, such as anisotropy of properties. Homogeneous distribution of small particles of inclusions is good and desirable. This type of distribution is sometimes used to increase the strength of steel, by homogeneous distribution of carbide particles within the steel. On the other hand, inclusions located along the grain boundaries which cause weakness of the metal are undesirable. Moreover, clusters of inclusions are also undesirable; these usually result from breaking large inclusions, which leads to decrease in mechanical properties of steel. Some kinds of clusters - coral-like, dendritic and plate-like structures - are shown in Figure 2.35.

Deformation processes (e.g., forging process) also affect the distribution of inclusions inside the deformed steel ingot. During forging, the inclusions re-form and are distributed according to the direction of metal flow. If the inclusions are hard they may break into chains of fragments and be distributed in the metal during forging, but if they are soft like MnS, they will extend in the direction of forging[136].

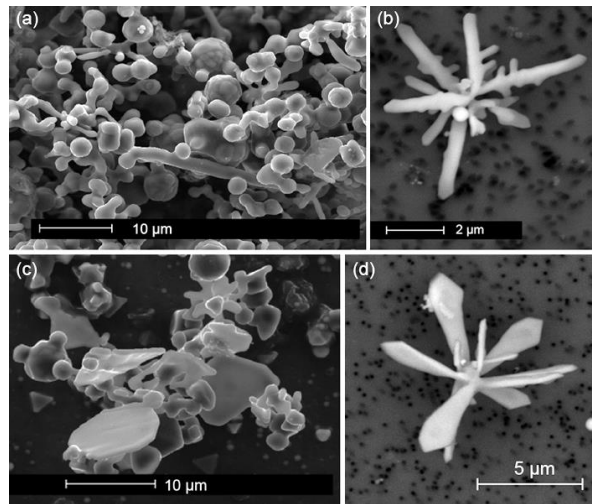


**Figure 2-35** Clusters may occur with (a)coral-like, (b)dendritic, or (c) and (d) plate-like structure [137, 138].

## 2.6.2 Influence of inclusions on mechanical properties of steel

Inclusions have a deleterious influence on the properties of steel. Their presence becomes advantageous only in a few cases, like the improvement of machinability obtained with inclusions of MnS. The influence of inclusions on the properties of steel depends very much on their composition, shape, size, and distribution, in addition to the stress system imposed during deformation. Moreover, the influence of non-metallic inclusions also depends on the applications of steel products[139]. For instance, if steel were produced to work under dynamic loading, such as in gears or crankshafts, the main focus would be on the effect of the inclusions on fatigue strength.

Characteristics of the inclusions cause a reduction in fatigue strength. Brittle and hard non-metallic inclusions, such as Al<sub>2</sub>O<sub>3</sub>, have the greatest influence on fatigue strength; in contrast more deformable inclusions, such as MnS have less effect. During deformation the stress concentrated between hard inclusions and steel matrix produces voids. Coalescence of these voids nucleated around the hard particles of non-metallic inclusions will cause ductile fracture. Figure 2.36 shows an example of such a surface, where cavities are formed

at inclusions[132]. Generally, if the inclusion particles is actually rigid, has low internal fracture strength or even has a low cohesion with the matrix, all that makes the nucleation of voids becomes easier[140].



**Figure 2-36** A ductile rupture surface of a low carbon, 1.2 Mn steel showing some cavities formed by inclusions[132].

Sellers and Tegart[141] mention that the fracture that originate by the side of inclusions is mainly depend on the deformation characteristics of the inclusion (soft or hard) comparative to the metal matrix, which means that the poorer the ductility of the inclusion, the worse its effect on the steel. Therefore, hot working should be performed within the temperature range where inclusions become soft and could deform plastically to preserve continuity with the metal matrix. Figure 2.37 gives the variation of the index of deformability of different types of inclusions with temperature in steel. Moreover, Sellers and Tegart in the same paper concluded that increasing the quantity or amount of inclusions contributes to lower ductility.

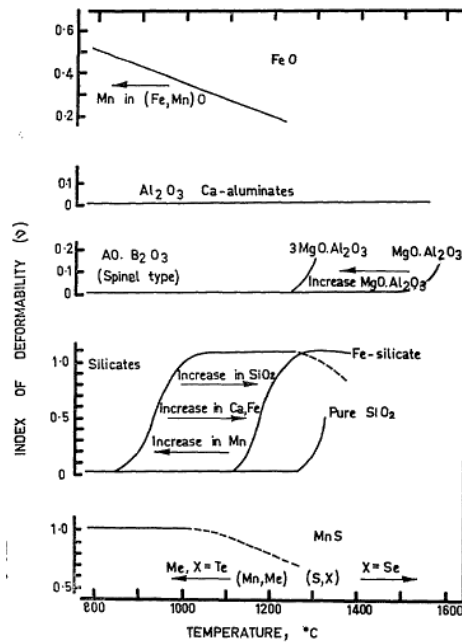


**Figure 2-37** Effect of temperature on the plastic deformation of various kinds of inclusion, in comparison with steel[141].

In the three stages of the ductile fracture process of initiation, growth, and coalescence of microvoids, inclusions played a main role, serving as hard particles for void initiation. Therefore, they significantly affect the upper shelf energies during Charpy V-notch (CVN) testing. Coarse inclusion particles also serve as fatigue initiation sites and may initiate cleavage fracture[139]. Elongated inclusions may become harmful to ductility because of their anisotropy behaviour and their orientation relative to the deformation direction. Consequently, the presence of ductile (soft) inclusions, particularly sulphides e.g. MnS, can be detrimental to impact and fracture toughness. These inclusions, as shown in figure 2.34 types (d) and (e), deform with the steel matrix because of their high plasticity[131].

In another study, Ray and Paul[142] revealed that the inclusion morphology has a very strong influence on both of Charpy shelf energy as well as impact transition temperature (ITT) in studied steels even if the grain sizes were similar. Furthermore, significantly high shelf energies, low ITT, as well as minimum anisotropy of impact properties were obtained when the inclusions shape were modified from longitudinal stringer (sulphides) to small lenticular or globular (oxysulphides). Moreover, Pacyna and Mazur[143] through using the hot working tool steel they discovered that the effect of non-metallic inclusions on toughness property is linked to the distribution of inclusion as well as to the hardness value of the steel. The fracture toughness will not be seriously affected if the distribution of

inclusions was uniform within the steel. As for the effect of hardness of the steel, they mention that, at a high hardness level, inclusions which have a little plastic strain area might be considered as obstacles to prevent the crack propagation. Atkinson et al.[144] concluded that, in fatigue-related states, failure usually initiates from big oxides instead of sulphides. However, in the case of fracture toughness the sulphide inclusions, which considered very significant for the anisotropic behaviour of steel, are important than others. Furthermore, majority of the failures that usually occurs in high strength steels was as a result of oxide inclusions instead of sulphide inclusions.

## **2.7 Effects of microstructure variability on scatter of properties data of materials**

During the experiments that are usually performed to test or verify some of the mechanical properties there will be some scatter or variability in the results of the samples even if there is a highly controlled test procedure. There are some factors that lead to scatter in measured data of the material properties. Many authors[145, 146] summarised these factors as test method, variation in specimen fabrication procedure, operator bias, apparatus calibration, and material inhomogeneities and/or compositional differences. Nevertheless, appropriate measures must be taken to minimise the possibility of errors, and also to mitigate those factors that lead to data variability. In many cases it is desirable to specify a typical value and degree of scattering for some measured properties; this is usually performed by taking the average and the standard deviation, respectively[146]. To minimise experiment errors, three specimens are often required to test at each test condition. The average value of these three tests is used as a result for the test. If a minimum test value is specified for a material property acceptance, not more than one test result of the three should fall below that value [147].

In other cases, repeat testing is required because, if the steel shows scatter in its some tested properties, a single poor result may well force the downgrading of the entire batch. Moreover, the presence of defects in metals such as minute cavities, inclusion particles and grain boundary segregates also has an effect on the results of some mechanical properties. These defects have a serious effect on the material impact properties, but are likely to have a limited effect on tensile strength, and relatively none on hardness. These defects, especially under impact loading, will act as stress raisers through introducing points at which

a sudden concentration of stress accumulates. Consequently, for the same material, the results in the impact test on a single cast material will be much more scattered than in the tensile test, since a casting microstructure is expected to be much less homogeneous than a wrought material. However, even in wrought materials, the direction of fibre will have a more significant influence on impact toughness than on either tensile strength or ductility[148]. Furthermore, variation in chemical composition and average grain size during the production of steel is often unavoidable from one batch to another. This causes variation in results of some properties, e.g. hardenability. In such case the scattering in measured hardenability results are often plotted as a band indicating the maximum and minimum values that has to be expected for the specific alloy. Figure 2.38 is illustrate a plotted hardenability band for 8640 steel[149].

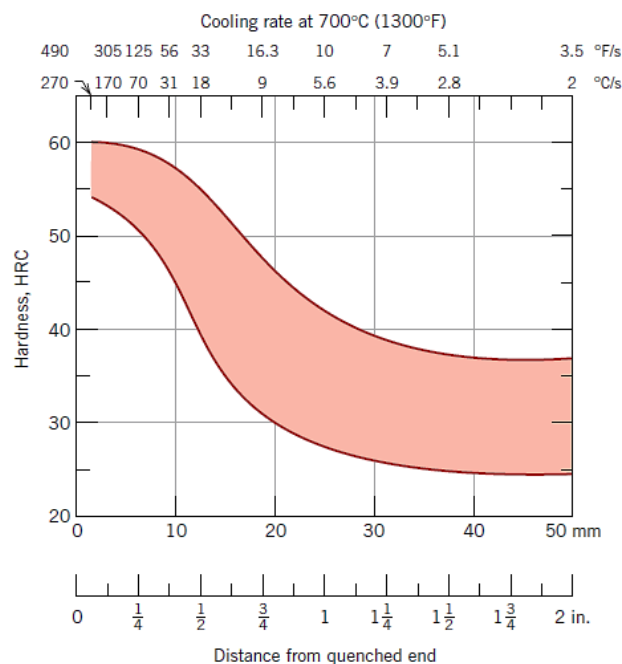


**Figure 2-38** The hardenability region for the 8640 steel showing the maximum and minimum limits [150]

A previous study was carried out by Chakrabarti et al. [151] to find out the influence of a bimodal ferrite grain size distribution on scattering of toughness data. This was done through using three types of microstructure of uniformly coarse grains, uniformly fine grains as well as bimodal grains and comparing them with the values of local fracture stress for heat treated microstructures. They mention that the variations within the notch root microstructure, which is considered to be the main factor for scatter in the toughness data, were associated to the distance between the coarse grain sized band and the notch root. If

the notch root is located close to this band, the cleavage fracture stress as well as impact energy is going to be lower, and vice versa. Moreover, in this study they concluded that the bimodal grain size has a significantly larger distribution microstructure in comparison to the unimodal grain distribution microstructures. This distribution (i.e., bimodal) was very high compared to the any kind of experimental error. The coarse or big grains, which is exist in adequate volume fraction within the microstructure, usually initiate the cleavage fracture. By increasing the percentage of these grains (i.e., coarse) in the microstructure, grain size bimodality increases the probability of presence of those grains at the cleavage initiated area and, thus, the scatter in fracture stress value also will increase.

Some others authors also found that cleavage fracture is easy to initiates in presence of coarse grains. Chen et al.[152] discovered that it is not necessary for the cleavage crack to initiate and extend at the point of the peak stress; instead, it usually happens on both sides and at a lesser or greater distance from it. Moreover, the scattering of a local fracture stress was caused by the distribution of grain sizes in group of largest grains. Wu and Davis[153] used the Niobium microalloyed steels to study the influence of grain size distribution of duplex ferrite on the local fracture stresses. They also mentioned that within the studied steels the scattering in fracture stress data can be defined by the distribution of coarse grains. In terms of hardness, they found that the microhardness of coarse grain areas is significantly lower than that of fine grain areas.

## **2.8 Mechanical properties**

The mechanical properties of materials is a term used to explain the behaviour of these materials under different factors such as temperature, load and environment. During applications these metals have different kinds of mechanical problems. These problems are sometimes studied or investigated individually, but also often in practice the combined effects of these properties must be assessed[154]. Furthermore, to study the failure to achieve these required mechanical properties, or to improve them, manufacturing processes e.g. thermo-mechanical and heat treatment processes through microstructure must be well understood.



### 2.8.1 Strength

Strength is one of the main mechanical properties of metals and alloys, and is a very important measure of a material's ability to perform the required applications. Strength is defined as the amount of stress that a material can withstand while being tensile or compressed, before failing or breaking. There are many factors affecting the strength of steel, some of which are related to the initial steel composition like alloying elements. The amount of carbon in the steel is one of the main elements affecting strength, as it often dictates the total hardness of steel. Both the yield strength and tensile strength increase with increased carbon content[155]. However, on the other hand, ductility drops as the carbon content increases, so other alloying elements should be added with carbon to steel to try to increase the strength while maintaining toughness. Alloying elements such as Al, V, Ti or Nb are also added to steel to obtain a fine grain size to increase the strength[156].

Moreover, some metals are modified by alloying elements and processing to promote their resistance to dislocation movement to increase strength. Grain boundaries are used to provide an obstacle to dislocation movements. Accordingly, by reducing the grain size there is a larger probability of decreasing dislocation motion, thus the strength of the metal typically increases[157]. Other factors used to improve strength are related to processes applied after creating the steel, such as metal forming and heat treatment processes. The microstructure, which is formed after deformation or after heat treatment, is significantly affected by the austenite grain size, where a small austenite grain size is preferred to improve some mechanical properties, including strength. Accordingly control of austenite grain size during the austenitising process is the first step in most heat treatment processes to help to enhance strength.

For instance, the strength and impact toughness of 17CrNiMo6 steel can be improved with refinement of the prior austenite grain size[158]. Furthermore, the refinement of martensitic structure can be obtained by reducing the quenching temperature from 1200 °C to 900 °C, and refine the grains of austenite can promote the refinement of martensitic packets and blocks, which results in enhanced yield strength and toughness simultaneously[159, 160]. Likewise, different levels of hardness and strength can be obtained during heat treatment by using different cooling rates (e.g. quenching) and

tempering temperatures (see Fig. 2.39) to control the grain size. In general, the faster a metal is cooled, the smaller the grain sizes will be.

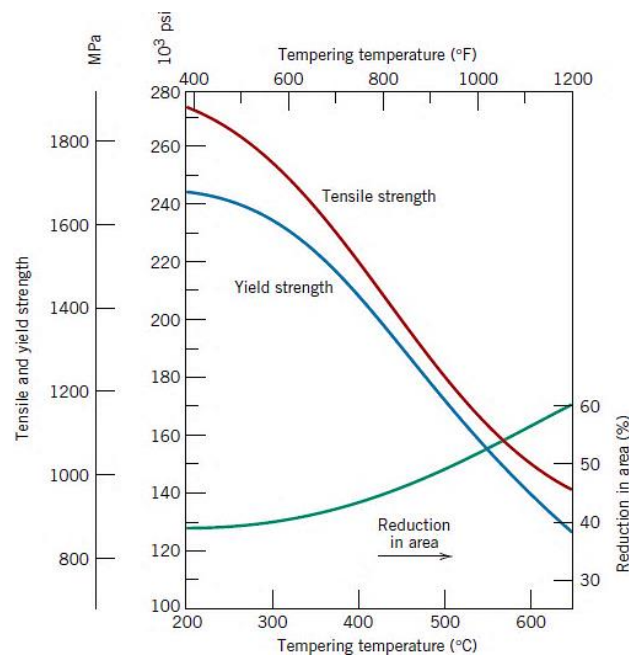


**Figure 2-39** Tensile strength, yield strength as well as ductility (RA%) (at room temperature) are plotted against the tempering temperature for 4340 alloy steel quenched in oil[161].

## 2.8.2 Fracture toughness and impact testing

Toughness is known as the capability of the metal to resistance the fracture by absorb impact energy and plastically deformed. Fracture toughness is used to characterize toughness. An impact test (Charpy impact test) is used to give an indication of fracture toughness through measuring the resistance of the material to impact load without fracture[162]. The absorbed energy is also used as a tool to evaluate the ductile-brittle transition temperature (DBTT). A schematic diagram of a standard impact testing machine is shown in Figure 2.40. If the material was ductile that does not mean it has a good toughness, because the toughness is a combination of strength and ductility. For instance, steel with high strength and high ductility has more toughness than steel with high ductility and low strength. Decrease or increase in toughness depends on its importance for the required specifications. Fully quenched steel is very brittle and has low toughness; therefore to improve toughness tempering is required as the following step[163]. There are several factors that help to improve toughness such as refined grain size and decreased carbon content. Minimizing the carbon content in steel can improve toughness, while increasing the

percentage of carbon will cause a loss of toughness. Also, to improve toughness inclusions must be eliminated because their presence is detrimental to toughness. Toughness can be improved through the microstructure as well, where using a microstructure of tempered martensite or lower bainite instead of upper bainite or ferrite-pearlite microstructure can improve the toughness[164]. Furthermore, chemical composition has an effect on toughness, where the addition of certain elements has an effect.

Nickel (Ni) and manganese (Mn) usually help to improve toughness as their addition can result in reduction of the ductile-brittle transition temperature. Sometimes this effect is related to production process parameters. For instance, rolling mill process using HSLA steel elements such as Ti, V, and Nb used for precipitation hardening when added to alloys has a different influence on toughness depending on the finishing temperature. If the temperature is high it may be detrimental to toughness. In contrast, if the finishing temperature is low it helps to refine the ferrite grain size, thus the toughness will improve[165].

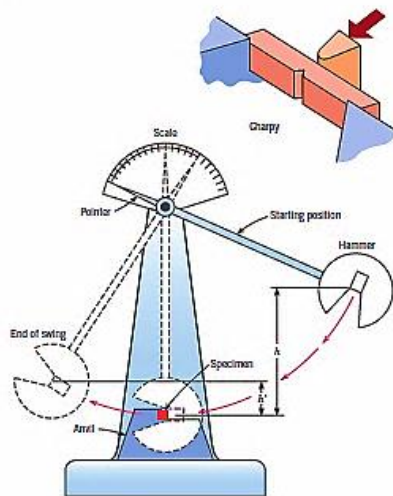


**Figure 2-40** Schematic diagram of a standard impact testing machine[166].

### **2.8.3 Effect of austenite grain size on mechanical properties**

Austenite grain size has a significant role in thermo-mechanical processing and is considered an important factor that needs to be taken into consideration when mechanical properties like strength and impact toughness need to be improved. In addition the microstructure, which is formed after deformation or after heat treatment, is significantly affected by the austenite grain size. For example:

- The hardenability (section 2.11) of the steel is affected by austenite grain size, where if the austenite grains become coarse fewer nucleation sites will be available, which leads to slowing the diffusion controlled transformation of the austenite. In other words, as shown in Fig. 2.41 deeper hardening, which means moving the nose of the CCT curve to the right, is caused by coarse austenitic grain size which is obtained by heating to higher temperatures[167].

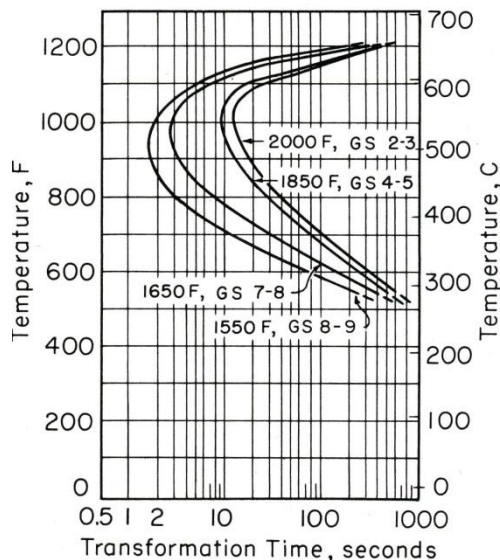


**Figure 2-41** Comparative time intervals for 50 % transformation in a single steel as heated to four different temperatures in the austenite range prior to transformation, with corresponding differences in austenite grain size (GS) (U. S. Steel)[168].

- In steel products consisting of ferrite and cementite, grain size of austenite considered an important factor in creating the conditions that help to make small grains of ferrite, pearlite, or combination ferrite pearlite structure that affect the mechanical properties. Production of small austenite grains is important but these austenite grains need to be considered carefully with the type of steel and the characteristics of the microstructure needed. A study was done by J. M. Hyzak and his co-workers[169] about the effect of pearlite inter-lamellar spacing, pearlite colony size and austenite grain size on mechanical properties of fully pearlitic microstructures in a steel with a percentage of 0.81 %C. One of the important results of this study is the inverse relationship between the inter-lamellar spacing and the austenite grain size diameter; the pearlite inter-lamellar spacing increases as the prior austenite grain diameter decreases, shown in Table 2.1. According to the mechanical properties the pearlite inter-lamellar spacing is considered as being the main microstructural parameter that through it the strength of pearlitic microstructures can be controlled. As well as yield strength, hardness is also dependent on pearlite inter-lamellar spacing, as shown in Figure 2.42. In addition the study shows

that in comparison to austenite grain size, inter-lamellar spacing has more effect on yield strength. Consistent with the relationship shown in Figure 2.43 between the Charpy transition temperature and austenite grain size, austenite grain size has a large effect on the impact toughness in pearlitic steel. Impact toughness, as measured by the Charpy transition temperature, increases with decreasing the austenite grain size; in other words, the finer the grain size the greater the toughness.

**Table 2-1** The influence of heat treatment on microstructure of eutectoid steel, adapted from Hyzak[169].

Heat treatment	Austenite grain size, $10^{-3}$ cm	Pearlite colony size, $10^{-4}$ cm	Pearlite spacing, $10^{-6}$ cm
1	1.43	4.78	14.10
2	1.43	4.57	15.35
3	1.43	5.26	19.50
4	2.52	5.38	13.00
5	2.52	4.75	13.75
6	2.52	6.58	15.16
7	2.52	6.09	17.50
8	2.52	6.34	27.00
9	3.51	6.04	12.10
10	3.51	5.33	14.00
11	3.51	4.29	14.10
12	3.51	5.15	16.35
13	4.02	5.56	11.93
14	4.02	5.76	13.75
15	14.73	5.67	13.62
16	16.65	5.70	11.57
17	13.0*	7.12	15.67

(The uncertainty in the values for grain size, colony size and pearlite spacing is of the order of 10 pct.). \*Estimated.

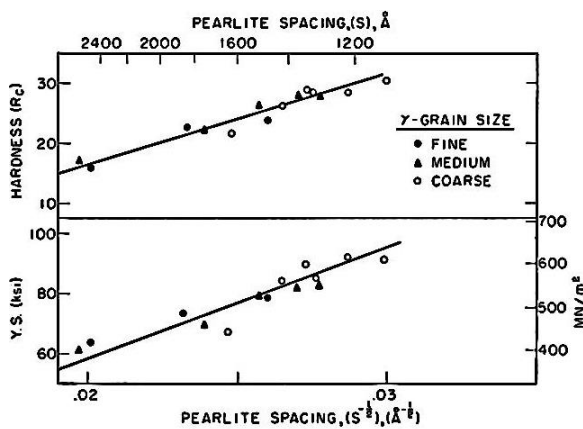


**Figure 2-42** Yield strength and hardness vs pearlite interlamellar spacing[169].

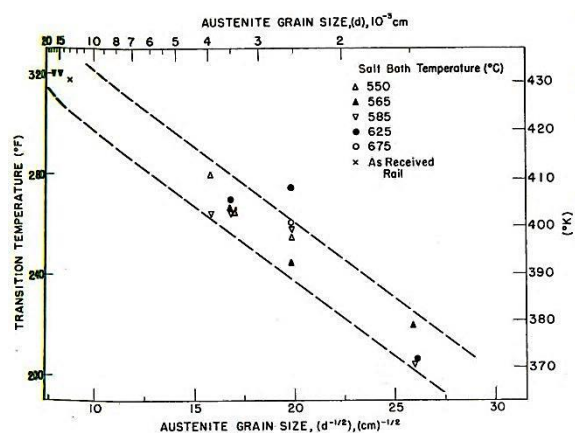


**Figure 2-43** Charpy transition temperature vs prior austenite grain size[169].

- When some of the mechanical properties such as strength and toughness are targeted for increase or improvement, the most important issue to focus on is the refinement of austenite grain size during deformation and heat treatment. Furthermore, the starting microstructure also has an effect on the austenite grain size. The mechanical properties usually increase at the expense of each other, which means that if one increases the other could decrease. Using multiphase structures is one of the ways to overcome this problem. A study was undertaken by Nack Kim[170] using dual phase steel with the chemical composition of Fe, 2 %Si, 0.1 %C and with and without 0.09% V. Two different types of heat treatment of intercritical annealing and intermediate quenching were used to produce microstructures with different characteristics.

As received pearlite-ferrite microstructure and as received microstructure after being held for one hour and quenched to produce martensitic microstructure were used in the study. Both microstructures were followed by two-phase annealing at a temperatures range of 850 - 950 °C to obtain a variety of volume fractions of martensite. According to this study, the intermediate quenching treatment produced a memory effect microstructure. The martensite laths that were produced prior to intercritical annealing have nearly the same crystallographic orientations as the final austenite which nucleated and grew at the lath boundaries of ferrite after intercritical annealing treatment. Table 2.2 shows the mechanical properties of dual phase steel for both heat treatments.

The microstructure produced by intermediate quenching has a much higher ductile to brittle transformation temperature than that produced by intercritical annealing. In other words, the intermediate quenching microstructure has low toughness which can only be controlled by austenite grain size because there is no resistance of crack propagation between the ferrite-martensite microstructure, whereas with the intercritical annealing treatment there is no memory effect, because the newly formed austenite does not have the same orientation as that of the parent austenite.

**Table 2-2** Mechanical properties of dual phase steel, adapted from Nack[170].

Heat treatment	Amount of martensite (vol %)	Strength (MPa)		Elongation (%)		DBTT (°C)	Energy absorbed at 25 °C(J)
		Yield strength	UTS	Uniform	Total		
Intermediate quenching	23	393	766	15	22	10	38
Intermediate quenching	40	413	871	10	15	11	33
Intercritical annealing	14	404	747	16	24	-28	42
Intercritical annealing	50	502	944	10	16	-26	32

- Generally, quenching and tempering processes are used with some types of steel to increase their strength and toughness. Martensitic structure is mainly produced by quenching, while tempering is used to precipitate the dispersion of fine carbides in the alloy. The microstructure is one of the major factors that affects the mechanical behaviour of the quenched and tempered steel.

## 2.9 Forging

Forging has been known for a long time. At first simple iron forgings were produced, where small pieces of hot iron were hammered to make wrought products. Over time the demand for more complicated forgings arose, which led to the start of significant progress in forging. Accordingly, metalworkers started to invent and design new die shapes, mechanical hammers, and presses. After that, a big development happened in forging machines in terms of increased power, capacity and size. Today forging is used to produce most kind of products for various applications, from small simple parts to large scale complicated shapes weighing hundreds of tons. In general, hot forging is a thermo-mechanical process where a metal ingot or billet is preheated and then mechanically shaped to the desired shape by tools or dies.

The forged material (stock) traditionally is a cast ingot, but in some cases it is useful to produce forgings directly from continuously cast steel. There are some main types of general forging, which are usually divided according to temperature or the production process: extrusion, open die, ring rolling, rotary, and closed die[171]. As can see in figure 2.44 by using forging we can create better and stronger parts, with good mechanical properties, than by machining or casting. This is because the metal during forging process is always forced to flow in a direction where the strength, resistance to impact and fatigue as

well as yield ductility should to be a maximum[172]. Furthermore the forging process causes refining of the metal structure, improved homogeneity of the cast ingot, and heals some defects such as voids. Moreover, from an economic aspect, the forging process can reduce the amount of machining required, if the size of the cast ingot is close to the shape of the final part.



**Figure 2-44** Differences between forged, cast and machined parts (a) Cast Bar (b) Machined Bar (c) Forged Bar[172].

### 2.9.1 Large scale forging

The worldwide demand for increased energy efficiency in power generation or for drilling for oil in deeper seas means there has been a requirement for bigger sections and components for these systems[173, 174]. This has led to a requirement to produce bigger and bigger components. There are many kinds of steel used to produce large scale forgings including 34CrNiMo6 steel. This structural steel is suitable for large heavy forgings with high tensile strength properties and impact toughness, and for mechanical components subjected to high stresses.

Open-die forging (fig. 2.45) is usually used to manufacture large scale forgings from heavy elongated ingots. Consequently the machine dimensions, machine power, and holding equipment are the main important factors in open-die forging because they limit the size of the forged ingot which in turn will determine the size of the forged product. Large hydraulic presses or power forging hammers are usually used with open die forging; however, large hydraulic presses are commonly used with large-scale forgings - the capacity of some presses is in excess of 10,000 tons[175]. As a result of the size and weight of hot raw material (e.g. ingot) when removed from the furnace, and the finished products after forging, special equipment is needed to handle it. Large mobile manipulators (e.g. powerful tongs) are used to move these parts forward, back, or rotated around the longitudinal axis.



These manipulators are free running or on a track; overhead travelling cranes and porter bars are also used[176].

The major issues of large scale forging on the microstructure are less strain inside the forged component, where the penetration of plastic deformation differs from the surface to the core of metal, causing a difference in grain size between the central and surface zones. Also, a bigger variation in cooling rate leads to a large variation in the microstructure which causes the appearance of fine grains on the surface of the metal compared with coarse grains within the centre. N. Switzner[177] Studied the influence of strain rate as well as deformation temperature during forging process on the mechanical properties of the stainless steel. Four different forging machines were used to impart four different strain rates, and three different deformation temperatures were used with each strain rate. The results showed that by using a lower strain rate less strengthening occurred as a result of longer deformation times. Additionally, by increasing the strain rate the hardness become less variation within the metal as well as the yield strength become less sensitivity to variations in temperature. On the other hand the average hardness decreases and the hardness variation within the metal increases with increasing the temperature of deformation.

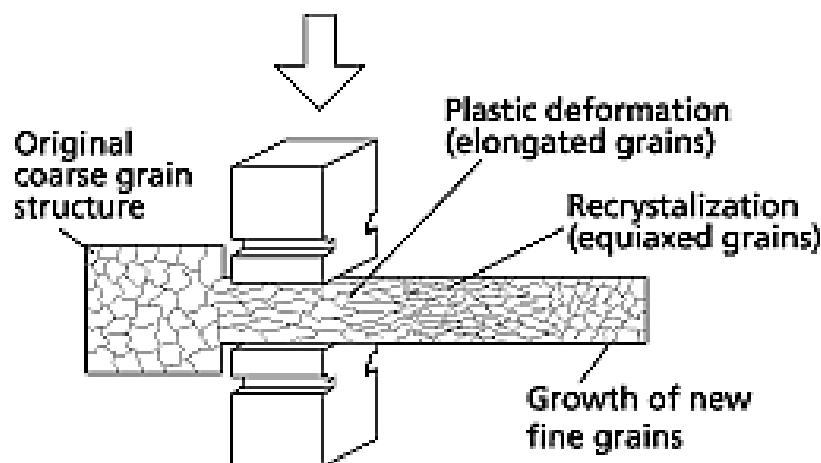


**Figure 2-45** The open die forging process and its resulting crystal structure[178].

## 2.10 Heat treatment

To achieve the desired purpose, steel parts or products made for use in various applications are usually subjected to a heat treatment process. During heat treatment a series of factors can be modified to produce steel with good and uniform mechanical properties. The

microstructure, thus the required mechanical properties, can be improved by modifying some parameters involving austenite grain size, dissolution of carbide particles, cooling rate, and composition of the steel. Generally the purpose of heat treatment is to soften the metal to improve or to increase toughness and ductility, but also to increase or reduce hardness and strength depending on the heating temperature and cooling rate. In heat treatment some properties are often improved at the expense of others. Moreover, heat treatment is used to reduce internal stresses when the metal has been exposed to high stress during deformation. In the case of large scale parts, the temperature differences between the outside and inside of the piece should be taken into consideration during heating and cooling. If the gradient is too big it can cause a difference in the microstructure which may lead to warping or cracking the piece. TTT and CCT diagrams are usually used in heat treatment to help determine suitable heat treatment conditions such as holding time and cooling rate. Some heat treatment processes include annealing, normalising, tempering and quenching.

### **2.10.1 Annealing and Homogenizing**

The annealing process is a generic term denoting a heat treatment in which steel is austenitised for a period of time at an elevated temperature above the  $A_3$  transformation temperature for hypoeutectoid steels and between  $A_1$  and  $A_{cm}$  transformation temperatures for hypereutectoid steels, followed by slow cooling, usually in a furnace[179]. If the hypereutectoid steel is heated above  $A_{cm}$ , proeutectoid cementite forms along the grain boundaries when the low cooling rate is used; these carbides helps cracks to propagate and render the steel brittle[180]. In full annealing slow cooling causes the transformation of austenite to coarse pearlite and ferrite or cementite. As can be seen in Fig. 2.47, the most important parameters are temperature and cooling rate to produce slightly fine or coarse microstructure in a full annealing process.

Generally, the annealing process aims to reduce internal stresses and produces a microstructure which provides good machinability, high softness, and moderate strength. Fig. 2.46 shows the different stages of the full annealing process, where it can be seen that in hypo-eutectoid steels the annealing temperature decreases with increased carbon content, while it is nearly constant below  $A_{cm}$  temperature for hypereutectoid steels.

However, the homogenising process is defined as annealing of as casting ingots at a high temperature of nearly at or above 1100 °C and holding it for enough time (sometimes extending to hours) to minimize or eliminate local differences of segregation or chemical concentration gradient by diffusion. Furnace cooling is used with this process[181].

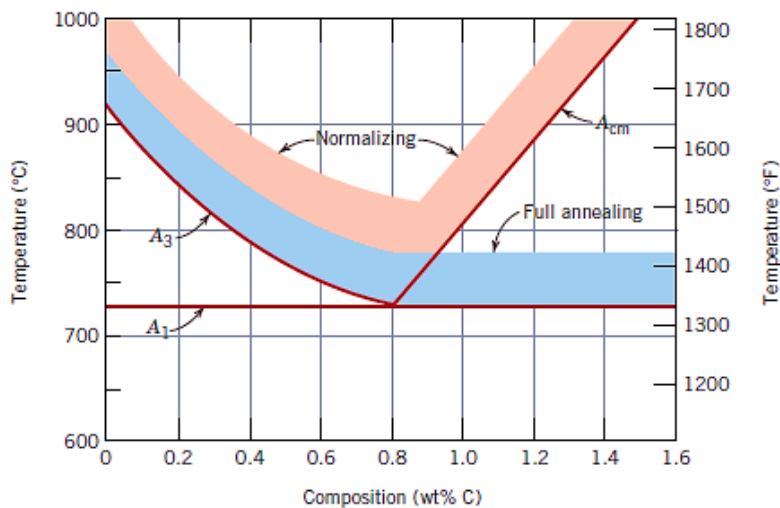


**Figure 2-46** A side of the Fe-C phase diagram representing the full annealing, as well as normalizing ranges temperature[182].

### 2.10.2 Normalizing

Normalizing is a heat treatment process consisting of heating the steel to an elevated temperature in the austenite zone, holding for a period of time sufficient to allow the alloy to completely transform to austenite, and then cooling slowly, usually in still air, to produce a uniform and fine ferrite-pearlite microstructure. As represented in Fig. 2.46, the normalizing temperature for hypoeutectoid steels is above the full annealing temperature zone which is about 30 - 80 °C above the  $A_3$  temperature. For hypereutectoid steels normalizing is usually performed only in special cases and the normalizing temperature is about 30 - 80 °C above the  $A_{cm}$  temperature[183]. The main differences between annealing and normalizing in regard to normalizing are the higher austenitising temperatures to ensure that most carbides are dissolved, and the faster cooling rate which means a finer ferrite and pearlite microstructure is produced. Moreover, normalized steel has a higher hardness and strength, and a lower ductility than annealed steel[184].

The main objectives of the normalizing process are production of a good uniformity in the austenitic structure and refining the grain size that usually become coarser after hot

deformation processes at high temperature, and in some cases is applied for better machinability of low carbon steels. For instance, after hot deformation the steel microstructure becomes non-uniform in the longitudinal and transverse directions and the grains become irregularly shaped and relatively large, thus this will cause a difference in mechanical properties between the two directions. To get the same mechanical properties in all directions the normalization process has to be applied.

Also, after hot forging, especially with large scale forgings with different cross sections, the micro structures will be heterogeneous because of different cooling rates. In such a case, the normalizing process will also help to make the microstructure uniform[185]. One of the main parameters of the normalizing process is the cooling rate, but in large scale products this parameter is not controlled, where the resulting microstructure structure is dependent on the thickness. Therefore the normalizing process is considered more effective for improving the mechanical properties of thin products[186].

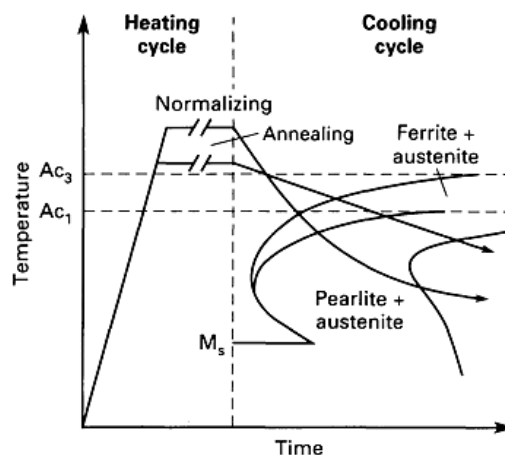


**Figure 2-47** Schematic time temperature cycles for normalizing and full annealing and the slow cooling results in higher temperature transformation to ferrite and pearlite and coarser microstructures than does normalizing (Courtesy of M.D. Geib, Colorado School of Mines)[187].

### 2.10.3 Hardening (quenching)

Conventional hardening is a heat treatment process involving heating the steel to temperature in the austenite zone, holding for a period of time sufficient to complete the transformation of the whole microstructure to austenite, and cooling at a very fast (rapid) rate to room temperature or in some cases below room temperature. The cooling rate, which is usually a function of a steel chemical content and the austenite grain size, is applied

rapidly to avoid the formation of ferrite, pearlite or bainite[188]. When a good hardenability steel is quenched in water the resulting microstructure will be martensite which is a very strong structure and, depending on the carbon content, this structure has a good hardness and strength but at the same time is very brittle.

Various cooling media are applied for different purposes with the steel and the most common media used are water, forced air, oil and brine. These different cooling media are selected according to the cooling power needed, to avoid or minimize the risk of quench cracks and distortion[189]. In large scale products, especially those with low hardenability, there is usually a difference in temperature between the surface and the centre during rapid cooling. This difference occurs when the surface is fully cooled while the core remains hot (unquenched). Therefore, special quenching tanks with good cooling regimes are used to reduce the difference to the minimum[190].

#### **2.10.4 Tempering**

After hardening with a rapid cooling rate steel usually becomes harder than is necessary, too brittle, and has severe internal stresses which make it difficult to use in most applications. Therefore the tempering process is used to relieve internal stresses, reduce brittleness, and produce a good tough microstructure. Tempering consists of heating the martensitic steel to a selected temperature which is below the lower transformation temperature ( $A_1$ ), holding for specified time period and then permitting the metal to cool to achieve the required combination of mechanical properties[191]. The most important variables related to tempering that affect the microstructure and thus the mechanical properties are tempering temperature, holding time at that temperature, and the steel chemical composition[192].

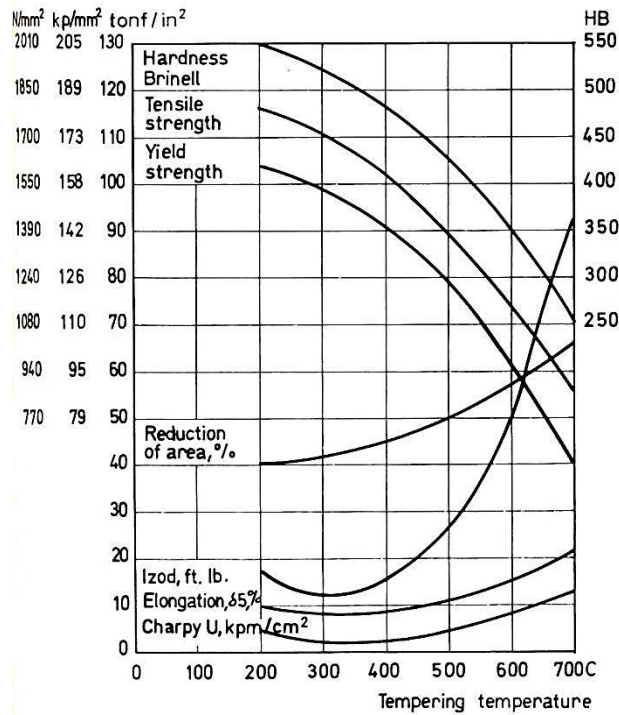


**Figure 2-48** Tempering diagram for SS 2541 (34 CrNiMo 6). Diagram applicable to bar stock 50 mm (2 in) in diameter, oil quenched from 850°C[193].

#### 2.10.4.1 Tempering temperature

The tempering process is usually performed directly or shortly after hardening. In some cases tempering is carried out as soon as the hardening temperature approaches 50 °C. The reason is that the steel may crack if it is cooled to room temperature before tempering. There are many ways to heat the steel to tempering temperature, including conventional muffle furnaces, convection type furnaces, gas flame or electric induction furnaces. The tempering temperature can be identified according to the superficial colour during heating, where the steel surface changes as the temperature increases, and this becomes easier to distinguish especially at high temperatures[194]. Larger product sizes require more time for heating to the tempering temperature. Moreover, with large and complicated products slow heating is preferable, because rapid heating can induce undesirable stresses on the surface according to increase of surface layers in volume, which leads to the occurrence of cracks. However, some investigations observed that the time required to heat pieces up to the tempering temperature is more or less independent of the temperature[195].

In the tempering process time and temperature are interdependent variables, where by finding the appropriate combination of length of holding time and tempering temperature a

range of mechanical properties can be achieved. However, in terms of effectiveness, tempering temperature has more influence than holding time, as minor changes in temperature have more effect than minor changes in time. In regards to the tempering time, several publications report an old rule called rule-of-thumb which says that the tempering time should be from 1-2 hours for each 25.4 mm of section thickness[195]. The one thing missing in this rule is that it does not say if the time is counted directly the work piece enters the furnace, or when it reaches the required temperature. Often the tempered parts are placed in the furnace at a temperature below tempering temperature which means a longer time is required to reach the tempering temperature, especially with large scale parts. Accordingly, the tempering time starts the moment the furnace reaches the required tempering temperature. As seen in Figure 2.48, at room temperature strength and hardness decrease with increased tempering temperature, while ductility, which is measured by either reduction of area and elongation, increases with increased tempering temperature[196].

#### **2.10.4.2 Holding time of tempering process**

The carbides formed during tempering because of the diffusion of carbon and alloying elements depend not only on the temperature, but also on the holding time at that temperature. Hollomon and Jaffe [197], among others have developed an empirical tempering parameter which links hardness, time, and temperature of tempering as follows:

$$P = T(k + \log t) \quad 2-12$$

Where P is a parameter linked to the tempering process (corresponding to a hardness value), T is temperature (kelvin), k is a constant, and t is time (hours). Extensive tests were performed to ensure the validity of this expression to be applied to all steels. The results showed good correlations especially with quenched and tempered low and medium alloy steels, with the exception of when big quantities of retained austenite are exist[198]. An example of the influence of tempering holding time on hardness (at room temperature) applied to 0.82 %C steel tempered at different temperatures is shown in Fig. 2.49. As we can see, the hardness decreases with increased holding time which is presented on a logarithmic scale.

In the first 10 seconds the change in hardness is clear and rapid. As these changes continue the effect becomes less and less with increased holding time, with smaller changes occurring between 1 and 2 hours. This effect becomes more important in high temperature than in low temperature. So, for consistency and to reduce the dependency on variations in holding time, or in case of absence of information, a tempering time of 1-2 hr is recommended[199].

In this study the tempering time for a large ingot of 34CrNiMo6 steel was 1 h for each 25.4 mm, calculated as twice the quenching time, which was 1/2 h for each 25.4 mm. The cooling rate from tempering temperature also has an impact on the microstructure and thus on the mechanical properties. Toughness, which is measured by notched bar impact testing, is the property most affected by cooling rate, and can be reduced if a slow cooling rate is used through specific temperature ranges. This phenomenon, called temper embrittlement, occurs more in steel that contains carbide forming elements[200].

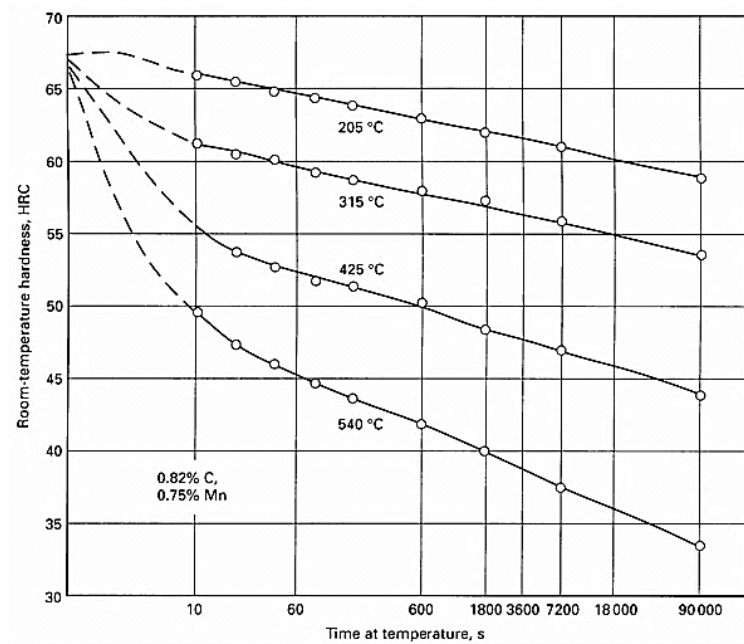


**Figure 2-49** Influence of time on room temperature hardness of quenched 0.82 %C steel at four different tempering temperatures[199].

#### 2.10.4.3 Tempering of martensite

The martensite formed during quenching is not an equilibrium microstructure, and thus its transformation to become a stable phase occurs only at room temperature and takes place



over a very long period of time. There are many stages for microstructure transformation that are passed during continuous rise of tempering temperature for carbon steel, where different temperature ranges will give different characteristics in terms of microstructure and mechanical properties.

Porter and his partners[201], summarized in Table 2.3 the transformation mechanisms during different tempering temperatures from as quenched martensite microstructure starting from room temperature. As can be seen from the table, there is a big overlap between the ranges of tempering temperatures, and also these given ranges are only approximate[202].

**Table 2-3** transformation occurring during tempering of ferrous martensite, adapted from Porter [201].

Temperature (°C)	Transformation	Remarks
25-100	Carbon segregation to dislocations and boundary; preprecipitation and ordering	Clustering predominant in high-carbon steels
100-200	Transition-carbides precipitation, diameter 2 nm (first stage of tempering)	Carbides may be $\eta(\text{Fe}_2\text{C})$ or $\epsilon(\text{Fe}_{2.4}\text{C})$
200-350	Retained austenite transforms to ferrite and cementite ( second stage)	Associated with tempered martensite embrittlement
250-350	Lath-like $\text{Fe}_3\text{C}$ precipitation (third stage)	
350-550	Segregation of impurity and alloying elements	Responsible for temper embrittlement
400-600	Recovery of dislocation substructure; Lath-like $\text{Fe}_3\text{C}$ agglomerates to form spheroidal $\text{Fe}_3\text{C}$	Lath structure maintained
500-700	Formation of alloy carbides (secondary hardening or fourth stage)	Occurs only in steels containing Ti, Cr, Mo, V, Nb, or W; $\text{Fe}_3\text{C}$ may dissolve
600-700	Recrystallisation and grain growth; coarsening of spheroidal $\text{Fe}_3\text{C}$	Recrystallisation inhibited in medium-carbon and high-carbon steels; equiaxed ferrite formed

#### **2.10.4.3.1 Stages of tempering martensite**

Several authors [203-206] have written about the stages of the mechanism of as quenched martensite during tempering, which is divided into four main stages. The transformations were almost the same, but the ranges of the tempering temperatures were a little different. The reason for that is these temperature ranges are approximate because they depend on tempering time. Furthermore, all the mentioned authors started the first stage from a tempering temperature of 100 °C, unlike Porter[201] in Table 2.3, in which the range of temperature started from 25 °C where the carbon atoms rearrange in martensite crystals and segregate to dislocations and boundaries.

##### **First stage 100-200 °C**

The transition carbides formed in this stage, which is a carbon rich phase, called epsilon ( $\epsilon$ ) or eta ( $\eta$ )-carbide, are precipitated in the martensite and are very small and metastable; their instability increases with increasing the tempering temperature. The precipitation of these carbides depends on the percentage of carbon in the steel. According to some kinetic researches the tempering process in this stage is depending on the diffusion of carbon through the martensite[207]. Although the carbon in martensite is reduced to approximately 0.25 %[203], the martensite is still supersaturated with carbon, which will be subject to further decomposition when heated to a higher temperature. In this stage of tempering the precipitation of carbides improves toughness, but also leads to a slight decrease in hardness compared to that of as quenched martensite. Therefore the high strength and hardness are kept nearly the same, because the low tempering temperature contributes to make the transition carbide particles very small in size and causes little change in the dislocation substructure of the as quenched microstructure[208].

##### **Second stage 200-350 °C**

In this stage the untransformed austenite during quenching is decomposed. The existence of retained austenite in the microstructure is rather difficult to observe directly especially if it exists in low concentrations. The percentage of retained austenite becomes significant only in high carbon steels. Many authors mention that the retained austenite during this stage transforms to ferrite and cementite, while others such as Thelning[203] state that the

retained austenite decomposes to bainite. Moreover, Bhadeshia suggests that in this stage the retained austenite decomposes to bainitic ferrite and cementite, but there is not much evidence available to confirm this[209].

Figure 2.50 shows that in the as quenched specimens of 4340 (~ 34CrNiMo6) and 4140 steels, the percentage of retained austenite was small and this amount decreases with increasing the tempering temperature. The transformation of retained austenite in these types of steels starts just above tempering temperature of 200 °C and is nearly completed at about 300 °C, and the cementite becomes more in the microstructure at a tempering temperature higher than 300 °C[210].

Impact toughness and fracture toughness (K<sub>ic</sub>) could be improved because of the presence of the retained austenite films between the martensite laths, but this improvement will be reflected, and toughness will decrease with increasing of tempering temperature due to an increase in decomposition of the retained austenite; this is called tempered martensite embrittlement[211]. Thomas[212] mentions that tempering martensite embrittlement can be retarded at a higher tempering temperature, if the precipitation of cementite during tempering can be delayed through adding some alloying elements. For example, by adding Mn and Ni the amount of retained austenite can be increased; consequently through using these elements, the precipitation of cementite can be accelerated or retarded.

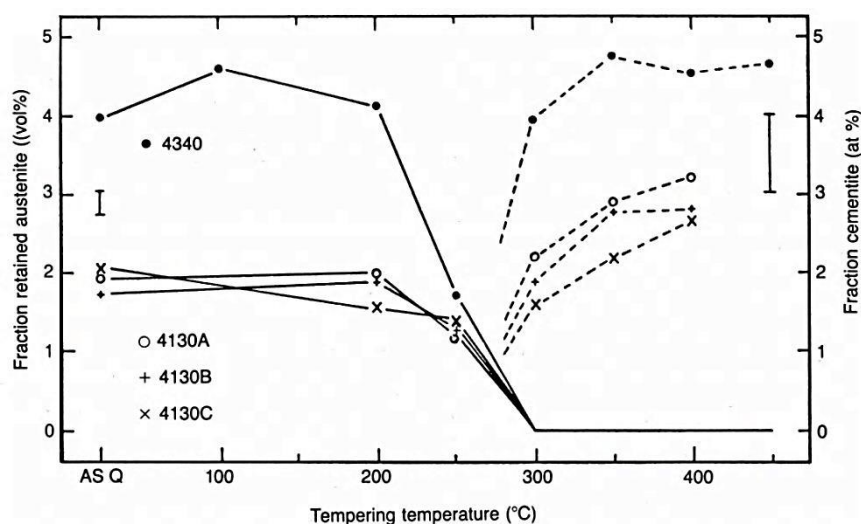


**Figure 2-50** Retained austenite and cementite as a function of tempering temperature in 4340 and 4140 type steels. The amounts of the phases were determined by Mössbauer spectroscopy[213].

### **Third stage 250-400 °C**

During this stage of tempering, more carbon combines with iron and transforms to very fine cementite particles ( $\text{Fe}_3\text{C}$ ). These small particles precipitate within the martensite and grow at the expense of the  $\epsilon$ -carbide. The cementite formed has an orthorhombic crystal structure and usually occurs as Widmanstätten plates. In high-carbon steels, the cementite precipitates along the twin boundaries of martensite and also nucleates at prior austenite grain boundaries or interlath boundaries[214]. Several researchers[212] found that toughness decreases sharply when secondary interlath and intralath cementite were precipitated during tempering[215].

These precipitated interlath or intralath carbides may create crack nucleation sites, thus producing a brittle fracture. Two fracture paths are produced: intergranular with regards to tempered martensite, as well as transgranular with regards to the prior austenite. This means the  $\text{Fe}_3\text{C}$  particles in this stage start with nucleation then extend dramatically through the austenite grains, which will become weak due to the segregation of residual elements such as phosphorous in the prior-austenite grains before quenching[216].

### **Fourth stage 400-700 °C**

In this temperature range the cementite particles continue to grow and coarsen and with increased tempering temperature these particles become spheroidized. Moreover, recrystallisation also happens at the end of this temperature range, where the martensite lath boundaries will gradually disappear after starts replace it by equiaxed ferrite grain boundaries. Consequently, the final microstructure will become coarse spheroidized particles of cementite and equiaxed grains of ferrite[217].

#### **2.10.4.4 Tempering of bainite**

There are several variations in behaviour between tempering bainite and tempering martensite, but one of the most important differences is the amount of carbon in the solid solution. Most of the carbon is precipitated or partitions during bainite reaction from ferrite which caused a reduction in the amount of carbon in solid solution, making it less sensitive to additional tempering heat treatment[218]. Furthermore, bainite exposes to autotempers

process during transformation, thus the tempering process usually performed much more gently. Moreover this carbon particles, which is in the cementite form is usually coarse compared with those produced during tempered martensite. Therefore, the influence of tempering heat treatment process with bainite will be less than the martensite when the same steel is used. Unlike martensitic steels, a small variation in the carbon content has little influence on the tempering of bainite. Carbon content usually has strong effect on solid solution strengthening when precipitates during tempering as in the case of tempered martensite. However, in the case of bainite, the presence of coarse carbides makes less contribution to strength, which means that the tempering process response is relatively insensitive to the big carbon concentration[219].

A hardness test could be used to quantify the softening process (tempering process). Before the tempering temperature reaches recrystallisation region, hardness is kept constant or has little variation during different tempering temperatures, while this steady behaviour is changed as soon as the tempering temperature reaches the recrystallisation region where the ferrite changes its morphology to equiaxed ferrite and the cementite spheroids coarsen considerably, so producing a more rapid softening.

## **2.10.5 Tempering embrittlement**

### **2.10.5.1 Introduction**

Temper embrittlement (TE) is characterized by the conspicuous reduction in impact toughness that occurs on tempering through a high specific temperature range. This usually happens through the ageing of low alloy steels within a critical temperature range (isothermally embrittled) or by slow cooling through the same temperature range. TE can be avoided in a simple way if possible by heating the steel above the critical temperature e.g. 600 °C and then quenching[220]. The components that may be affected of TE that are used at high temperature up to 550 °C such as steam turbine, some of vessel steels, and turbo-generator rotors, where the impact toughness dramatically drop according to reversible TE. The study of reversible TE usually revealed by the notched bar impact test, where the ductile-brittle transition temperature (DBTT) was raised and the energy become lower. Furthermore the trans-granular fracture mode will changed to an Intergranular

embrittlement below the DBTT[221]. Fig. 2.51 shows the effect of reverse temper embrittlement on the fracture appearance transition temperature (FATT) properties of low alloy steel. The FATT is basically a particular energy recorded at which the fracture is 50 % ductile and 50 % brittle. This FATT depends on the impurities segregation along the austenite grain size, hardness, and the prior austenite grain size[222].

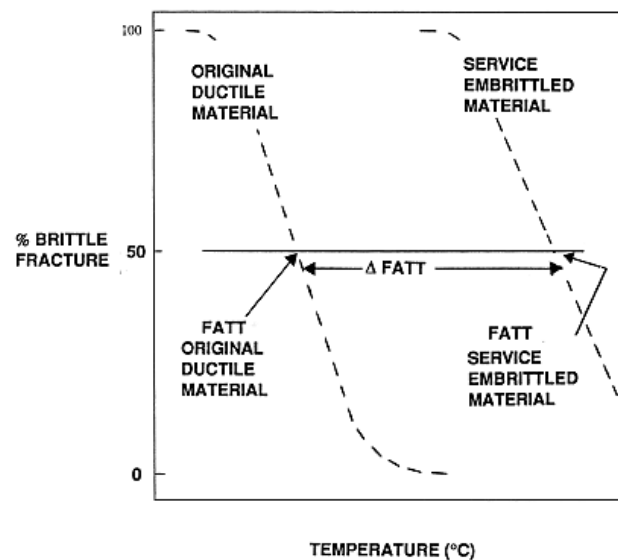


**Figure 2-51** Influence of reverse temper embrittlement on the fracture appearance transition temperature properties of low alloy steel[222].

Reversible TE has been studied for many decades and has only recently been clearly understood after surface analysis equipment, which has the capability to detect the grain boundary segregation on an atomic scale, became available. The effect of TE is increased with segregation of certain metalloid elements and impurities to grain boundaries, creating weak spots in the structure. The most detrimental impurities are phosphorus (P), tin (Sn), antimony (Sb), and arsenic (As) which reduce the intergranular cohesion of iron. Furthermore many of these impurities cause conspicuous reduction in the surface energy of iron which causes the grain boundary energy to lower, thus reducing cohesion. Cr-Ni steels are the most susceptible to TE in alloy steels, which is usually used to produce large scale products. In Cr-Ni steels the TE effect is attained by segregation of Sb, Sn and P and the segregation level of each impurity also grows with the Ni content [223]. Cr-Mn steels also have a high embrittling effect which is attained by segregation of P and Sb.

### **2.10.5.2 Cr-Mo Steel**

Temper embrittlement (TE) is a phenomenon that usually appears in alloy steels. Unfortunately the alloying elements most used with steel, such as Mn, Cr, and Ni, enhance temper embrittlement. These elements have a weaker effect when used separately than when combined. Moreover, the amount of the element also plays a big role in TE; for example, a small amount of Mo, between 0.2 % and 0.3 %, can reduce TE, while greater additions of Mo promote the effect of TE. The effect of Mo on delay of TE depends on interaction with other alloy elements such as Mn, Si, Cr and P. The role of Mo is basically to reduce susceptibility to TE and this is attributed to a positive interaction between molybdenum and phosphorus[224]. McMahon and Jr[225] pointed out that Mo will decrease its potential as phosphorus scavenger due to formation of carbide particles. Moreover Dumoulin and co-workers[226] found that if the amount of phosphorus in the steel is less than or equal to 0.02 %, the Mo which is located in solid solution will prevent this P from segregating to the grain boundary through binding with it to form Mo-phosphides. If the amount of P is more than 0.03 %, the Mo which is located in the grain boundaries will reduce the embrittling effect caused by the phosphorus atoms.

### **2.10.5.3 Effect of Mn and Si**

Mn and Si are alloying elements that can affect the mechanical properties of steel, where both Si and Mn are used as deoxidisers and improve strength and hardness, but this improvement is less with Si than with Mn. Moreover, Mn, as well as being one of the least expensive elements contributing to hardenability and used as a sulphur scavenger, also contributes to embrittlement. These two elements (Mn, Si) tend to promote susceptibility to temper embrittlement, but their segregation mechanisms are different. Mn co-segregates with P to grain boundaries whereas an interaction of Si and P accrues in Fe[227]. Phosphorus is the principal contributor to promote TE, especially when its amount increases to more than 0.015 %. Mn and Si each have an undesirable influence with this amount of P, together promoting P segregation very strongly[228]. Commercial steels such as Cr-Mo generally contain Mn and Si in certain amounts mainly because of the benefits mentioned above.

#### **2.10.5.4 Effect of sulphur**

Sulphur is an element that is usually combined with manganese to form manganese sulphide, one of the common non-metallic inclusions in steel. This non-metallic compound (MnS) contributes to impairing some of the mechanical properties of steel such as Charpy V-notch impact toughness, ductility and fracture toughness ( $K_{Ic}$ ) according to the sulphur content and the shape and the size of MnS[229]. Therefore the sulphur does not cause reversible temper embrittlement, but segregates to the grain boundaries, which reduces the cohesion strength and produces an intergranular fracture of iron[221]. The fracture energy decreases in proportion with both the amount of intergranular fracture and the energy necessary to fracture the grain boundaries depending on the segregation of the amount of impurities and other residual elements[225]. Moreover the sulphur content contributes to impair the notched toughness which is represented by increasing the transition temperature[229].

#### **2.10.5.5 Effect of Ni**

Nickel is used to produce alloy steels in combination with other elements to improve some mechanical properties; for example, with chromium to improve impact strength, toughness, hardenability, and corrosion resistance. Smaller amounts of nickel are added to alloy steels to increase toughness at low temperatures, while large amounts are added to produce high chromium stainless steel which has a high ability to resist corrosion and heat resistance[230]. The presence of Ni decreases the solubility of phosphorus in  $\alpha$ -Iron, and this solubility decreases even more with the presence of Cr. Moreover Cr is more effective than Ni in producing P segregation and embrittlement in steels[231]. Tin (Sn) is also one of the elements that induces severe embrittlement and co-segregates with Ni.

#### **2.10.6 Multiple heat treatment**

Double heat treatment processes in one heat treatment cycle are used in some cases to achieve or improve the desired mechanical properties of alloys, such as toughness or ultimate tensile strength. There are several types of heat treatment generally used with steel alloys. In our study normalizing, quenching, and tempering processes were used among those heat treatments when large-scale forgings are manufactured. Double



normalizing, double quenching, and double tempering processes are required in certain heat treatment cycles in different arrangements to confirm completion of these processes and to promote stability of the final microstructure.

#### **2.10.6.1 Double normalizing**

The main aim of the normalizing process is to reduce internal defects, produce a homogeneous microstructure, uniformly distribute carbides and refine austenite grain size before hardening. In some types of low alloyed steel, especially with casting and forgings of large dimensions, double normalizing is usually applied as a way to improve the mechanical properties. The first normalizing process is done at a temperature from 50 to 100 °C higher than that used for conventional normalizing, while the second normalizing process is done at conventional normalizing temperature[232]. Polushin and his co-workers[233] studied the influence of heat treatment on the structure and mechanical properties of steels with different amounts of chromium. They mentioned that, after using a double normalizing process followed by tempering process, a difference in grain size with the presence of coarse carbides together with their high dispersion was established. Furthermore, Jung[234] and his colleagues concluded that the microstructure and grain size of double normalized steel became equiaxed and fine due to homogenizing and recrystallisation through double heat treatment.

#### **2.10.6.2 Double quenching**

Quenching is commonly used to harden steel through producing a martensite phase within the microstructure. However, in some cases, this process is done twice in the same heat treatment cycle in an attempt to improve grain size refinement or to increase the percentage of martensite within the microstructure. A study was done by Lee and Hong[235] about the effect of double quenching on the grain refinement of bearing steels. A double quenching process was performed for heat treatment of high carbon chromium bearing steels for the purpose of improving the fatigue properties through refinement of the microstructure. The study concluded that when the double quenching process was used, the prior austenite grain size has been refined, thus leading to improvement in the tensile, impact, and high cycle fatigue strengths and the elongation.

Several studies have mentioned that the double quenching process is usually related to the carbon content in some heat treatments. For instance, in some kinds of steel that are adapted to the difference in carbon content between the case and core such as occurs in the carburised process, double quenching is not often used because of the resulting distortions that could be caused by two subsequent martensitic transformations[236]. Edward and Nisbett[237] mentioned that in such a situation the double quenching cycle is sometimes used consistent with the difference in carbon content between the case and core. So that, the first process is done at a higher temperature consistent with the core carbon content for grain refinement, while the second process is done at a lower temperature more consistent with the carbon content of the case, both the cycles being followed by oil quenching.

#### **2.10.6.3 Double tempering**

As is known, the tempering process is used after hardening to reduce brittleness and to increase the toughness of iron-based alloys through tempering the martensite. In some cases not all the austenite transforms to martensite after hardening, but remains as retained austenite. During the first tempering process and after a time the untransformed austenite does convert to martensite. This martensite is not tempered in the first cycle, therefore the second cycle of tempering will help to transfer this martensite and enhance stability of the resulting microstructure. Moreover, double tempering also helps to spheroidize and reduce the harm of inter-lath carbides formed by the transformation of retained austenite[238].

The double tempering process could be useful with some, but not all, types of alloy steels. For instance, it will be of benefit with alloy steels that have a high hardenability and high possibility for retained austenite after the first quenching and tempering processes, whereas in steels that are used to produce large scale products, such as heat treatable alloy steels that form bainite after tempering, or that already have a bainitic structure after hardening, tempering will not be needed more than once. After the initial tempering process, if the required hardness is reached, the second tempering process must be carried out at a temperature less than 10 to 30 °C below the first tempering temperature to maintain the hardness from reduction[239].

## 2.11 Hardenability

One of the aims of heat treatment of steel is very often to obtain a suitable degree of hardness, and this hardness should be high enough a certain depth from the surface; this phenomenon is called hardenability. Therefore, hardenability is known as the capability of a steel alloy to form a partial or complete martensite phase (i.e. Percentage) at a certain depth when quenched or cooled under some given conditions from a temperature above the upper critical temperature[240]. Worldwide demand for producing heavy sections, such as those used in power generation or for drilling for oil in deep seas that need to fulfil certain mechanical properties in their internal position, has increased. A large scale billet quenched in water or oil will cool more slowly than a small billet when the same treatment conditions are used, which means that the smaller diameter is more expected to become entirely martensitic, while a billet of large diameter will become partially martensitic[241]. Therefore the issue of the level of hardenability could be an important factor in design of these large scale products. Fig. 2.52 represents a plots of the depth below the steel surface versus hardness using three different test pieces with diameters of 25, 50, and 100 mm after oil quenching[242].

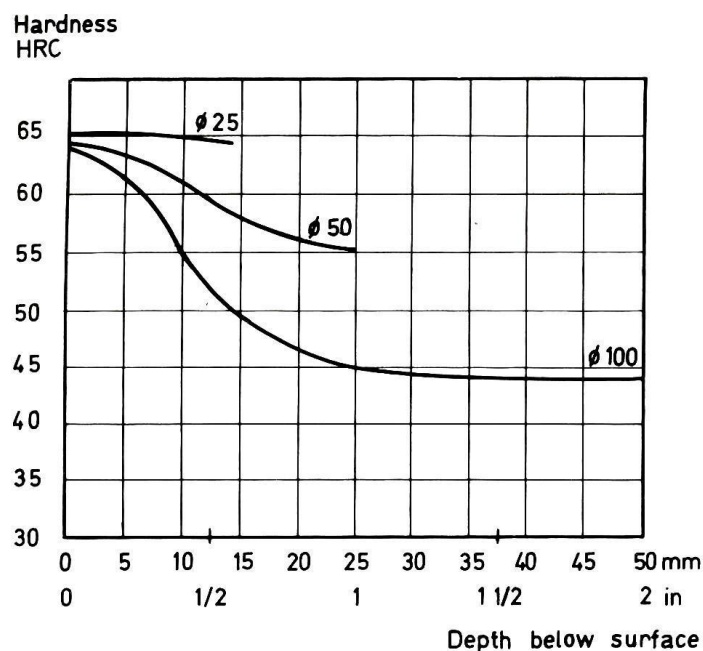


**Figure 2-52** Depth of hardening in different dimensions after oil quenching (AISI 01). Test piece 25 mm diameter hardened from 800 °C in oil. Test piece 50 mm diameter hardened from 820 °C in oil. Test piece 100 mm diameter hardened from 840 °C in oil[242].

### 2.11.1 Hardenability for small and large scale sections

The depth of hardening is important for many manufactured parts, and the hardness distribution along the cross section is related to factors such as quenching medium, quenching effectiveness, the cross section size and sometimes the oxidation layers that form on the surface[243]. These factors can affect the internal cooling rate, consequently, this effect will reflect on the microstructure and hardness as well. In other words, the heavier the section to be hardened the smaller the depth of hardness found, which means a lower cooling rate is used in the core[244]. Figure 2.53 shows the schematic for CCT diagram with two cooling curves for the outer surface as well as the core of an oil quenched bar. From this figure can be seen that the surface cooling curve which represents the high cooling rate passes in front of the ferrite and bainite noses where the resulting microstructure will be only martensite, whereas the core cooling curve which represents the low cooling rate passes through the bainite area and as a result some bainite will be expected in the core microstructure (See Fig. 2.29); thus the core hardness will be reduced[245]. In large scale forgings, if the hardenability is not high enough it results in significant variations in cooling rate leading to a large variation in microstructure, which causes the appearance of fine grains on the surface of the metal compared with coarse grains within the centre. In summary, high hardenability steel is the steel which can produce martensite microstructure even at a really low cooling rate.

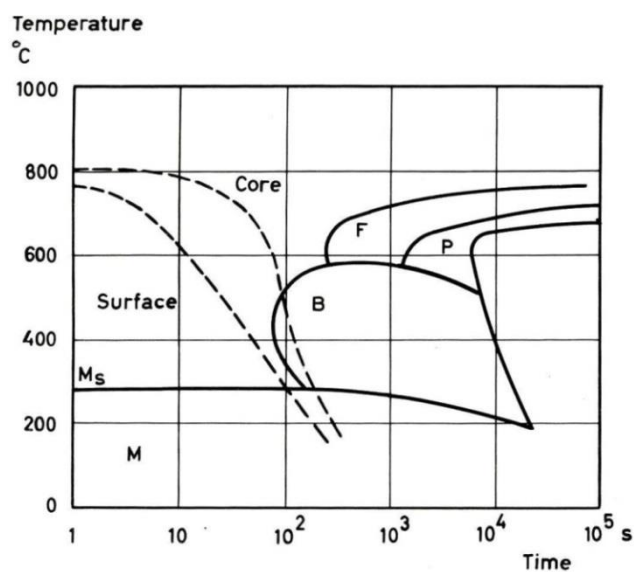


**Figure 2-53** Schematic illustration of the cooling curves for the surface and centre of an oil quenched bar with 95 mm diameter. The surface microstructure is wholly martensitic; the core contains some upper bainite[242].

### 2.11.2 Calculation of ideal diameter from the chemical composition

The hardenability of steel can be determined independently of the quenching medium. Grossmann and his co-workers[246] produced a method to calculate the ideal diameter ( $D_i$ ) by using the amount of each element in solid solution at austenitising temperature and the austenite grain size.  $D_i$  is the bar diameter of a given steel that yields a structure and produces 50 % martensite at the centre when the surface is cooled at an infinitely rapid rate ( $H=\infty$ ).  $H$  is a factor representing the coefficient of intensity of a quenching medium and this factor can have different values depending on the type of cooling and agitation[247]. Table 2.4 shows the  $H$  values for oil, water, and brine under various rates of agitation. As can be seen from the table, the agitation rate has a big effect on the  $H$  factor.

**Table 2-4** Shows the Grossmann quenching intensity factor  $H$  at different cooling media, adapted from Thelning[248].

Agitation	H Value (in. <sup>-1</sup> )		
	Oil	Water	Brine
None	0.25 - 0.30	0.9 - 1.0	2.0
Mild	0.30 - 0.35	1.0 - 1.1	2.0 - 2.2
Moderate	0.35 - 0.40	1.2 - 1.3	
Good	0.4 - 0.5	1.4 - 1.5	
Strong	0.5 - 0.8	1.6 - 2.0	
Violent	0.8 - 1.1	4.0	5.0

To determine the total  $D_i$  value, first the curve shown in Figure 2.54 should be used to calculate the hardenability of the steel as a function of carbon content and austenite grain size. Second, from the curve shown in Figure 2.55 hardenability of each alloying element present in the steel composition should be calculated according to the weight percentage[249]. Finally, the total hardenability of steel calculated by multiplied the two of previous hardenability values together as shown in the equation below[250] to get the  $D_i$  (inch) value.

$$D_i \text{ (in)} = f_{C\%} * f_{Mn\%} * f_{Cr\%} * f_{Mo\%} * f_{Si\%} * f_{Ni\%} * f_{Mn\%} \dots\dots$$

The critical diameter ( $D_{crit}$ ) is the diameter of a bar that has 50% martensite at its centre, and in practice the  $D_i$  value is used to determine the  $D_{crit}$  for various quenching media uses for that several converting charts represented the correlation between the  $D_i$  and  $D_{crit}$  for any given quenching severity  $H$ [248].

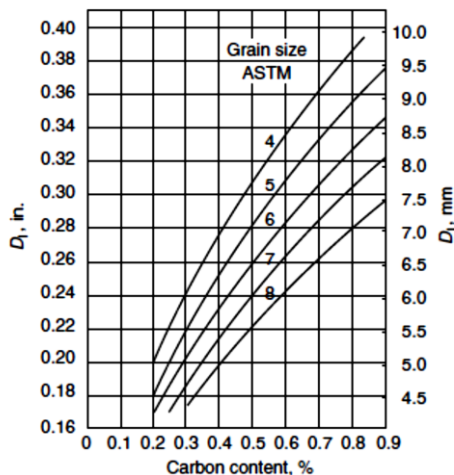


**Figure 2-54** The ideal critical diameter ( $D_i$ ) as a function of the carbon content and austenite grain size for plain carbon steels, according to Grossmann[251].

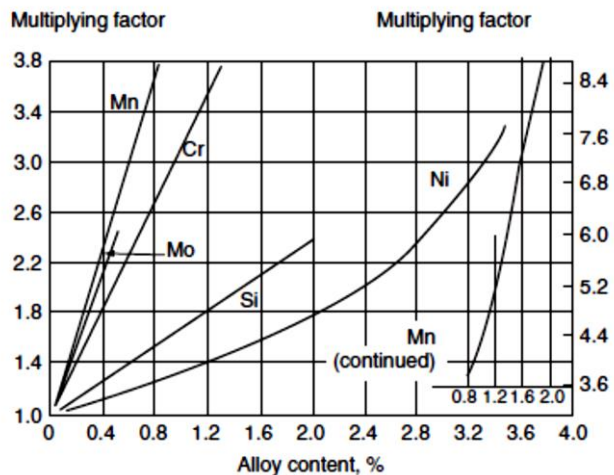


**Figure 2-55** Multiplying factors for different alloying elements when calculating hardenability as  $D_i$  value, according to AISI[252].

### 2.11.3 Methods to improve hardenability using alloying elements

Alloying elements have a big influence on depth of hardness; accordingly, the best way to improve or increase hardenability is by adding some alloying elements like Mn, Nb, Mo, V, Ni, Cr, Cu, and Si to steels. These elements basically delay the time required to form bainite and ferrite-pearlite microstructure, that is, produce martensite by using a slower cooling rate. The alloying elements can reduce the rate of austenite decomposition in two main ways, by retarding either the growth rate or the nucleation rate of ferrite-pearlite or bainite. According to effect these elements can be divided into two types; Ferrite stabilizers (V, Cr, Mo, Si) that increase the  $A_1$  temperature, and austenite stabilizers (Mn, Ni, Cu) that reduce  $A_1$  temperature[253].

Figure 2.56 shows the two different TTT diagrams for low alloy steels with various concentrations of chrome and molybdenum that were used in the first curve and chrome, molybdenum, and nickel that were used in the second curve. Comparing the two curves we can see that in the second curve, when the amount of Cr and Mo were modified and 1.8 % Ni was added to the steel, the curve shifted to the right and also tended to form two distinct

knees, one for pearlite formation and one for bainite formation. Therefore, alloying elements such as Cr, Mo, and Ni, which are usually added to steel improve hardenability by shifting the pearlite C nose in the TTT diagrams to the right which gives a longer time during cooling to form martensite[254].

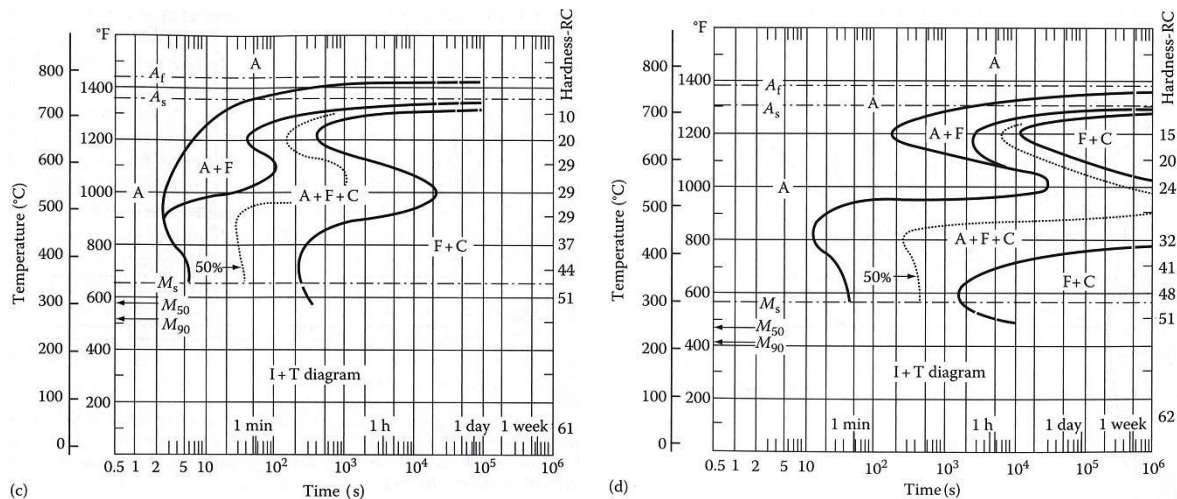


**Figure 2-56** TTT diagram for two commercial low alloy steels of which contain roughly 0.4 %C and 1 %Mn. In addition (c) contains 1.0 %Cr and 0.2 %Mo, and (d) contains 0.8 %Cr and 0.3 %Mo, and 1.8 %Ni[255].

During transformation of austenite partition will occur to form ferrite and pearlite. At equilibrium the alloying elements in pearlite will partition between ferrite and cementite in different concentrations through keeping or rejecting it during the process of nucleation and growth. Carbide forming elements such as Cr will concentrate in the cementite whereas elements such as Si will concentrate in the ferrite. However, in comparison with carbon that is form of interstitial solid solution, these elements are really slow to produce partition which therefore reduces the pearlite growth rate. The pearlite growth rate increases as fast as substitutional diffusion of alloying elements allows for partition to occur, which means in other words reducing the diffusivity of these elements retards the formation of ferrite, pearlite and bainite. The probable diffusion route for substitutional elements is through the  $\gamma/\alpha$  and  $\gamma/\text{cementite}$  interface[256].

Fig. 2.57 shows the partitioning of alloying elements in Fe-0.6 wt% C-0.85 % Cr-0.66 % Mn-0.26 % Si steel transformed at 597 °C for 2 mins[256]. As can be seen in this figure, when the variations of alloying elements are measured in this steel during the formation of pearlite, Si does not have solubility in carbide, thus partition is needed to reject Si into ferrite. In the case of Mn, the solubility in carbide is a bit higher but the partition of Mn can be attributed

to the same reason. The situation with the chromium is inverted where the Cr dissolves in the ferrite until the saturation state, then the excess Cr is rejected to the ferrite boundary, producing a partition and then precipitating as carbide.

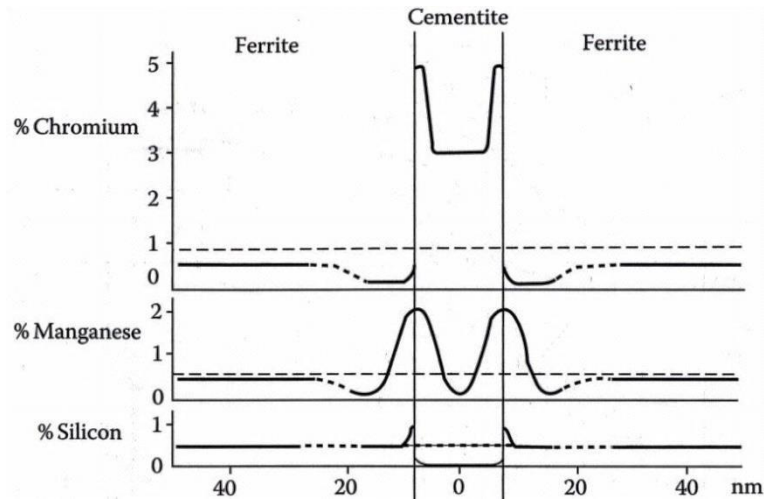


**Figure 2-57** Schematic diagram showing the measured variations of alloying elements in pearlite. These measurements were made using a time-of-flight atom probe[257].

Porter and his co-workers[253] also mentioned that the effect of austenite stabilizer elements such as Ni is different, where it is possible for pearlite to grow without partitioning under conditions of sufficiently high undercooling, which means that it (Ni) can be accepted either in ferrite and cementite without need for substitutional diffusion. However, the growth rate of pearlite will still be lower than in binary Fe-C steel because the concentration of Ni in the ferrite and cementite will raise their free energy, whereas with strong carbide forming elements such as Cr they suggest that these elements can reduce the growth rate of pearlite by a solute drag effect on the moving  $\gamma/\alpha$  interface.

Figure 2.58 shows the different hardenability curves for five alloy steels that have 0.40 %C and various contents of other alloying elements. From this figure we can see that all five alloys have nearly the same value of hardness at the end of the quenching where 100 % martensite is present, and this hardness is usually a function of the carbon amount only. As the Jominy distance increases towards the centre, the hardenability curves begin to change either by continuing or declining according to the cooling rate which is usually affected by existing alloying elements. In this figure the lowest and highest hardenability curves were 1040 and 4340 ( $\sim$  34CrNiMo6), respectively. For 1040 steel, the hardenability is low because the hardness falls sharply in a short time and the steel hardens just to a small depth



under the surface; according to that the steel microstructure will be mostly pearlitic with some proeutectoid ferrite. As for the 4340 steel, the hardenability is higher and the hardness will continue to a much greater depth; according to that the steel microstructures will consist mostly of a combination of martensite and bainite, and the amount of bainite increases with a decreasing the rate of cooling. This big difference in the hardenability for these two types of steel is, as explained previously, because of the existence of Ni, Cr, and Mo in the alloy steels[258].

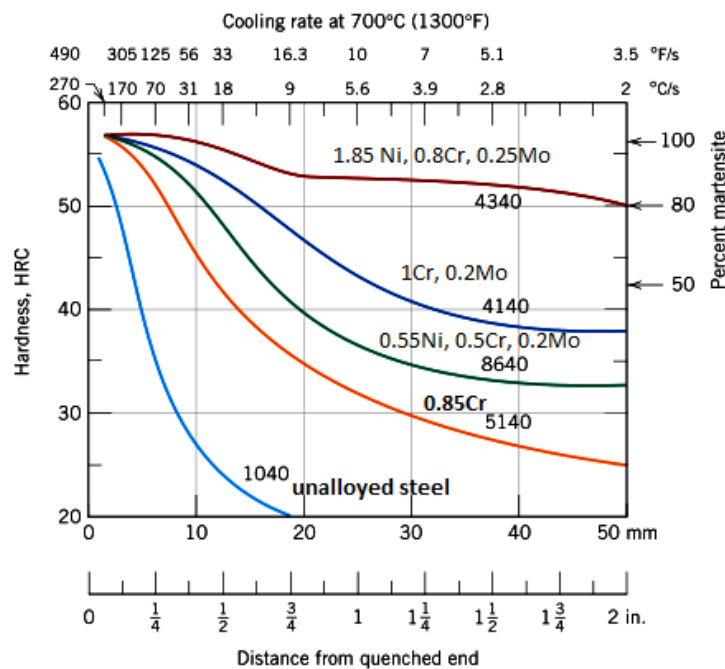


**Figure 2-58** Hardenability curves for five different steel alloys, each containing 0.4 %C (Approximate alloy contents as shown in the curve)[259].

### 2.11.3.1 Use of Vanadium (v)

Crafts and Lamont[260] discussed the effect of vanadium on hardenability and mentioned that the hardenability of steel will be improved in presence of the vanadium if this steel is austenised at a high enough temperature and for long enough to be sure the vanadium is in solution. This can happen under the condition that a small amount of vanadium is added, but opinions differ if a maximum amount of vanadium is added even if the effect of undissolved vanadium carbides, which can reduce hardenability, is avoided. Vanadium is usually added to constructional alloy steel for its ability to promote secondary hardening during tempering, but does not improve hardenability because of its sensitivity to austenite condition[261]. Furthermore, according to Odd Sandberg and co-workers[262], vanadium in solid solution also improves the hardenability of the steel with a mechanism similar to Nb.

This study also compared the hardenability of MoV steel with Ti and without Ti. The results show that the hardenability of MoVTi is better than MoV, where the value of hardness that was obtained for MoVTi was equal to three times that obtained for MoV at the same Jominy distance. This is basically due to the presence of vanadium as solid solution, where vanadium can work effectively by formation of VN during hardening, so the VN can be inhibited through the presence of a strong nitride former such as Ti. Another study by Mangonon[263] used different amounts of vanadium to improve hardenability of four grades of steels at several austenitising temperatures depending on carbon content. The first row of Table 2.9 shows the initial composition for the 4330 steel. Subsequently the V and Mo were modified until kept at about 0.15 %V-0 %Mo and 0.15 %V-0.05 %Mo in the composition.

The results showed that a good interaction of molybdenum and vanadium was found at normal austenitising temperature. Table 2.5 shows the chemical composition of 4330 and 4030 steels with a series of modification of Mo and V. All these modified combinations of molybdenum and vanadium at all temperatures indicate a higher hardenability than the standard grade, for instance the 4330 steels with modified of 0.10 %Mo and 0.10 %V showed a higher hardenability exceeding the standard composition with just 0.3 %Mo. Furthermore, the hardenability of vanadium modified steels increases and the austenite grain size coarsens as the austenitising temperature is raised. Fig. 2.59 shows the hardenability data of different modifications of Mo and V for 4330 steel.

**Table 2-5** Composition of alloy steels (wt. %), adapted from Mangonon[263]

Alloy	Heat No	C	Mn	P	S	Si	Ni	Cr	Mo	V	Al	N (ppm)
<b>STD 4330</b>	254	0.30	0.49	0.003	0.017	0.21	1.78	0.53	0.30	<.01	0.056	135
<b>Partial V-Substitution</b>	288	0.28	0.51	0.005	0.009	0.23	1.93	0.53	0.05	0.15	0.065	69
	289	0.28	0.49	0.004	0.016	0.20	1.94	0.53	0.10	0.10	0.057	81
<b>4330V</b>	255	0.30	0.48	0.001	0.014	0.22	1.76	0.53	0.10	0.16	0.063	117
<b>Total V-Substitution</b>	256	0.31	0.50	0.001	0.016	0.23	1.72	0.50	<.01	0.24	0.056	134
	271	0.29	0.52	0.003	0.017	0.21	1.75	0.53	<.01	0.15	0.053	82
<b>4330v</b>	291	0.28	0.50	0.004	0.011	0.21	1.94	0.52	<.01	0.10	0.058	48
	329	0.28	0.78	0.007	0.014	0.22	0.03	0.03	0.30	---	0.058	0.0116
	299	0.34	0.81	0.009	0.018	0.23	0.03	0.02	0.32	---	0.057	NA
	300	0.31	0.82	0.007	0.017	0.24	0.03	0.02	----	0.15	0.056	NA
	301	0.31	0.82	0.007	0.016	0.25	0.03	0.02	0.05	0.15	0.059	NA

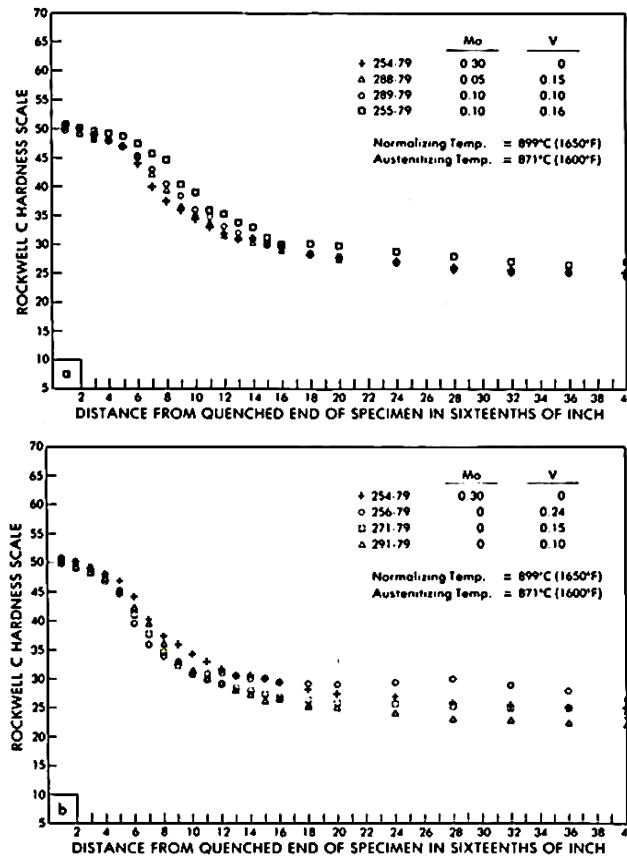


Figure 2-59 Hardenability data of 4330 steel after 871 °C austenitisation; (a) partially substituted alloys; (b) totally substituted alloys[263].

### 2.11.3.2 Use of niobium (Nb)

Niobium is an effective microalloying element, typically used in steel to refine the austenite grain through formation of niobium carbide and niobium nitride, and also used to improve strength and ductility within the structure[264]. A study done by C. Fossaert and H. Bhadeshia[265] investigated the influence of Nb on the hardenability of microalloyed austenite based on the critical cooling rate to get a martensite percentage of 0.95 % within the steel microstructure. Table 2.6 shows two similar compositions of steel (steel 1 with and steel 2 without Niobium) that were used in their study.

Table 2-6 Chemical cocontents (wt. %) of the experimental steels, adapted from Bhadeshia[265]

	C	Mn	Si	Nb	N
Steel 1	0.152	1.545	0.467	0.035	0.0053
Steel 2	0.178	1.527	0.023	---	0.0037

The authors in this research tried to explain the influence of Nb as solid solution on the hardenability with respect to the austenite grain size. As seen, Figures 2.60 and 2.61 illustrate the plots of the critical cooling rate versus both of austenite grain size and the calculated concentration of Nb in solution, respectively. According to Figure 2.60 austenite grain size is not the main dominant factor affecting the hardenability of steel 1, where the hardenability occurred over a very small range of grain growth. Fig. 2.61 indicates that the critical cooling rate to form martensite decreases as the Niobium increases in solid solution. From these two curves Forssaert and his co-workers concluded that the decomposition of austenite can be delayed through presence of a small amount of Nb in solid solution, while the transformation to bainite can be accelerated by Niobium carbide precipitate. They suggested the possible reason was due to segregation of Nb atoms within austenite grain boundaries, where a free energy of segregation and also interaction of the alloy elements through repulsion and attraction mechanism exists.

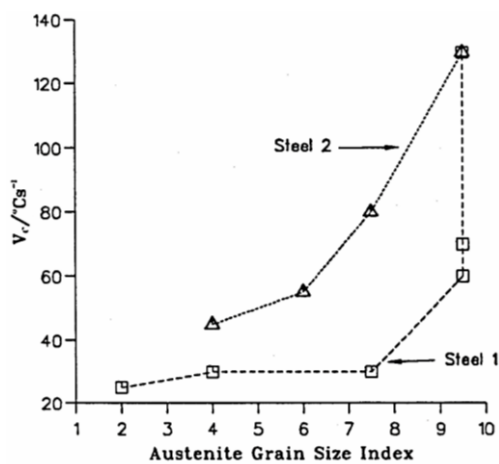


**Figure 2-60** The critical cooling rate required to get a percentage of 0.95 of martensite is plotted against the austenite grain size for both steels 1 and 2[265].

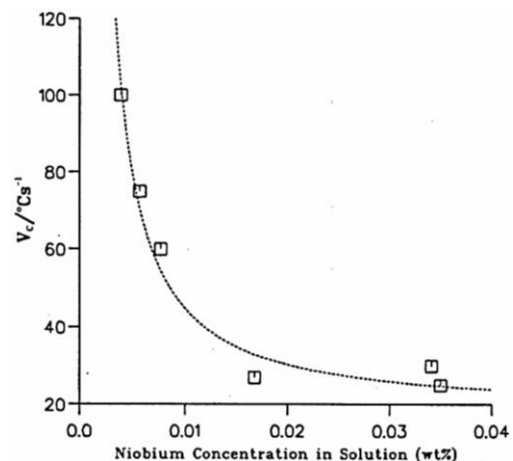


**Figure 2-61** Critical cooling rate is plotted against the calculated concentration of Ni within solid solution for steel 1[265].

### 2.11.3.3 Use of Boron (b)

Boron is one of the alloying elements used to raise or improve hardenability of structural steels with a smaller quantity than other alloying elements such as Cr, or Ni, where usually its amount in steel does not exceed 0.002-0.005 %. A higher amount of boron does not produce any further improvement in hardenability, but conversely boron can enhance formation of a boride eutectic that causes the reduction of both hot ductility and toughness of the steel at various temperatures. Boron is an interstitial element and has a very low

solubility in  $\alpha$ -solid solution which is less than 0.003 % and its effect on hardenability is relatively constant. The carbon content of the steel has an effect on the potency of boron, which becomes very effective at low carbon contents[266]. Furthermore, boron has good affinity for oxygen and nitrogen; therefore other elements should be added to steel with boron such as aluminium, titanium, or zirconium.

Consequently the effect of boron on hardenability can be improved if the steel is preliminarily well deoxidized and denitrified. Figure 2.62 shows hardenability curves of four different alloy steels without boron, and with boron and some other additives elements. As can be seen in the figure, with boron the extent of the martensite range becomes greater than that in steels without boron, but this range is extended much more if the steel contains other additives along with boron[267]. T. I. Titova and his co-workers[268] have studied the effect of boron (0.002-0.0035 %) microalloying on hardenability, and to provide a good strength ( $\sigma_{0.2} \geq 690$  MPa) and toughness of building steel alloyed with Cr, Mn, V, Ti and in the presence of about 0.5 %Mo. The result which they achieved was good, and with this amount of boron the hardenability of the steel can considerably improve.

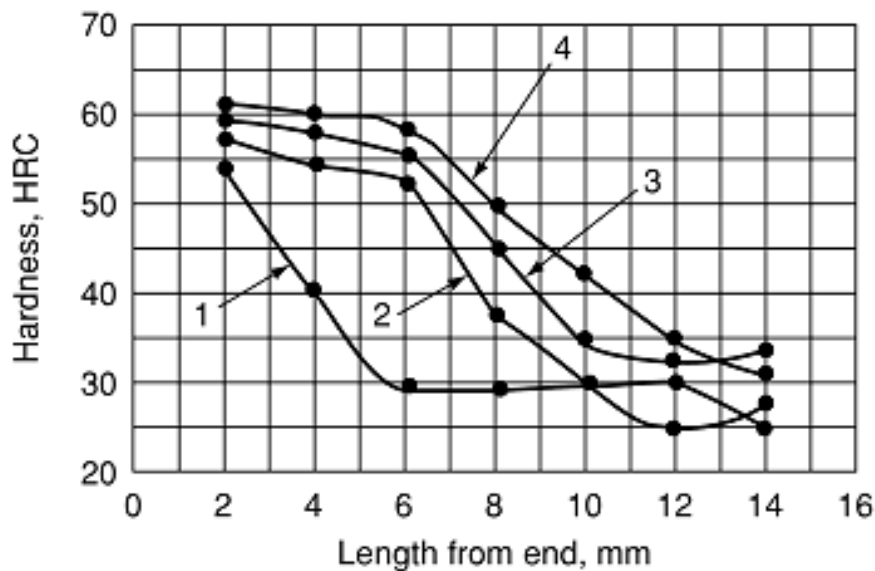


**Figure 2-62** Curves of hardenability for steels with 0.44–0.43 %C and various small amounts of additives. 1, Without boron; 2, with an addition of boron; 3, with boron and vanadium added; 4, with boron, vanadium, and titanium added[269].

## 2.12 Summary

In summary, steel is considered one of the most important materials and is widely used in a variety of industrial applications. Required mechanical properties can be achieved through the possibilities of adapting the microstructure of steel by using several different methods such as chemical composition, forming processes, and heat treatment. All of this has led to the presence of large amounts of data to cover all these areas. This chapter covers the most important knowledge related to this study, such as some physical metallurgy principles, some alloying elements affecting the microstructure, and others. Even with this vast amount of data about steel there are areas concerning large scale forging, especially thermomechanical and heat treatment with very low cooling rates and using multiple heat treatment cycles, that still that have not been covered in sufficient detail. Consequently, through this study we will try to cover thermomechanical processes and heat treatments of a large scale product made of 34CrNiMo6 steel with those conditions and try to investigate the processing parameters that help to improve the mechanical properties.

## 2.13 Research Objectives

The objective of this research is to investigate and simulate all process conditions such as temperature, cooling rate, strain, and strain rate experienced in the large scale forging of 34CrNiMo6 low alloy steel in order to understand and optimize the thermo-mechanical and heat treatment process parameters that determine microstructure parameters and thus the final mechanical properties. The strategy followed to meet this aim has several stages, as follows:

- Investigate the behaviour of isothermal hot working process over the deformation temperature range of 1260 °C – 900 °C, strain rates of 0.1, 0.5 and 1 s<sup>-1</sup>, and strains of 0.4, 0.6 and 0.8 on the austenite grain size refinement.
- Perform three and four hits of non-isothermal deformation process in different deformation temperatures to try to simulate the forging process and make it more realistic, and also to explore the difference in flow stress behaviour under non-isothermal process conditions.

- Investigate the influence of changes of austenitising temperature on the normalizing process and study the effects of increasing the holding time of normalizing process on variation grain size and the uniformity of microstructure.
- Study the entire heat treatment process of normalizing, hardening, and tempering to investigate the effect of the heat treatment parameters (temperature and cooling rate) on the grain size, amount, and transformation behaviour of austenite to try to improve toughness and ultimate tensile strength.
- Study the effect of double heat treatment of normalizing and quenching together with its effectiveness on the refinement of microstructure and grain size, which improves the mechanical properties and thus leads to achieving the same aim of improving toughness and ultimate tensile strength.

## Chapter 3 Experimental Procedure

### 3.1 Introduction

During the deformation and heat treatment processes a series of factors can be modified to produce steel with good and uniform mechanical properties. The microstructure and consequently the mechanical properties can be improved by modification of some parameters that involve austenite grain size, cooling rate and chemical composition. Austenite grain size is a really important factor that needs to be taken into consideration when mechanical properties such as strength and impact toughness need to be improved. The microstructure, which is formed after deformation or after heat treatment processes, is significantly affected by the size of austenite grains; small austenite grain size is preferred to improve impact toughness and strength. Many investigators have reported that the prior austenite grain size plays a significant role in controlling some mechanical properties of steels.

The first part of this chapter describes a series of plane strain compression (PSC) tests carried out on a Thermo-mechanical Compression Machine (TMC) to simulate the deformation process conditions experienced in large scale forging of 34CrNiMo6 low alloy steel over the temperature range of 900 °C – 1260 °C, strain rates of 0.1, 0.5 and 1 s<sup>-1</sup>, and strains of 0.4, 0.6 and 0.8, in order to understand and optimize the thermo-mechanical process parameters that determine microstructure parameters and thus the final mechanical properties.

In the second part we examine the effect of heat treatment process with different temperatures and cooling rates on the refinement of microstructure and grain size to improve mechanical properties, which are represented primarily by the toughness and the ultimate tensile stress. Heat treatment consists of three main processes: normalizing, quenching, and tempering. In addition, to study all heat treatment possibilities, a double normalizing, double quenching, and single tempering processes were used in different orders. A range of microscopy methods were used for microstructure analysis.



### 3.2 As received material

34CrNiMo6 low alloy steel is the material used in this study. This type of steel, which is used to produce company components, is generally characterized as quenched and tempered low alloy engineering steel with high hardenability, containing nickel, chromium and molybdenum. The steel usually develops its high strength by quenching to a full martensitic microstructure and the tempering process is used to improve ductility and toughness. The addition of Molybdenum prevents the steel from being susceptible to temper brittleness. Typical applications are for structural use, such as shafts of large dimensions, power transmission components, and some products for use in deep seas such as mooring connectors [270].

A full circle from the actual forged and heat treated large scale product made of 34CrNiMo6 steel, which represent the cross-section for the final product, was received from Somers Forge. All required thermo-mechanical operations of forging and heat treatment were carried out on this received part. The chemical composition of this steel is shown in Table 3.1. A small sample was cut from as received material that had been supplied as fully heat treated after hot forging to reveal the as received microstructure. Moreover, this microstructure was then able to be used later for comparison with the microstructure produced after experimentation. The microstructure at room temperature of as received metal, as can be seen in Figure 3.1 (A) consists of two different carbon region concentrations. The first, which is dark with high carbon concentration, while the second is light in colour with low carbon concentration, which is represents a higher volume fraction.

Furthermore, during the SEM imaging, the backscattered electrons are influenced by the atomic number, where elements with lowest atomic number during scattering will not reach the detector, which make it show up dark in the image. On the contrary, as the atomic number increases, the resultant area will appear lighter. In other meaning, the heavier atoms, such as iron, will show up darker, while the light atoms, like carbon, will show up light. According to that, the white small segments in Figure 3.1 (B) are cementite, which means that the structure may consists of upper or lower bainite. The average hardness of the as received material was approximately  $260 \pm 5$  HB, and the average austenite grain size ranged between 40~55  $\mu\text{m}$ .

**Table 3-1** Chemical composition (wt %) of 34CrNiMo6 alloy steel

Element	Acceptable range W%	Measured W%
C	0.33 - 0.35	0.33
Cr	1.45 - 1.7	1.52
Ni	1.6 - 1.7	1.66
Mo	0.2 - 0.3	0.23
Mn	0.4 - 0.7	0.51
Pmax	0.015	0.009
Si	0.15 - 0.35	0.22
Smax	0.01	0.01
Almax	0.01	0.004
V	0.05 - 0.12	0.07
Cumax	0.3	0.13
Snmax	0.05	0.01

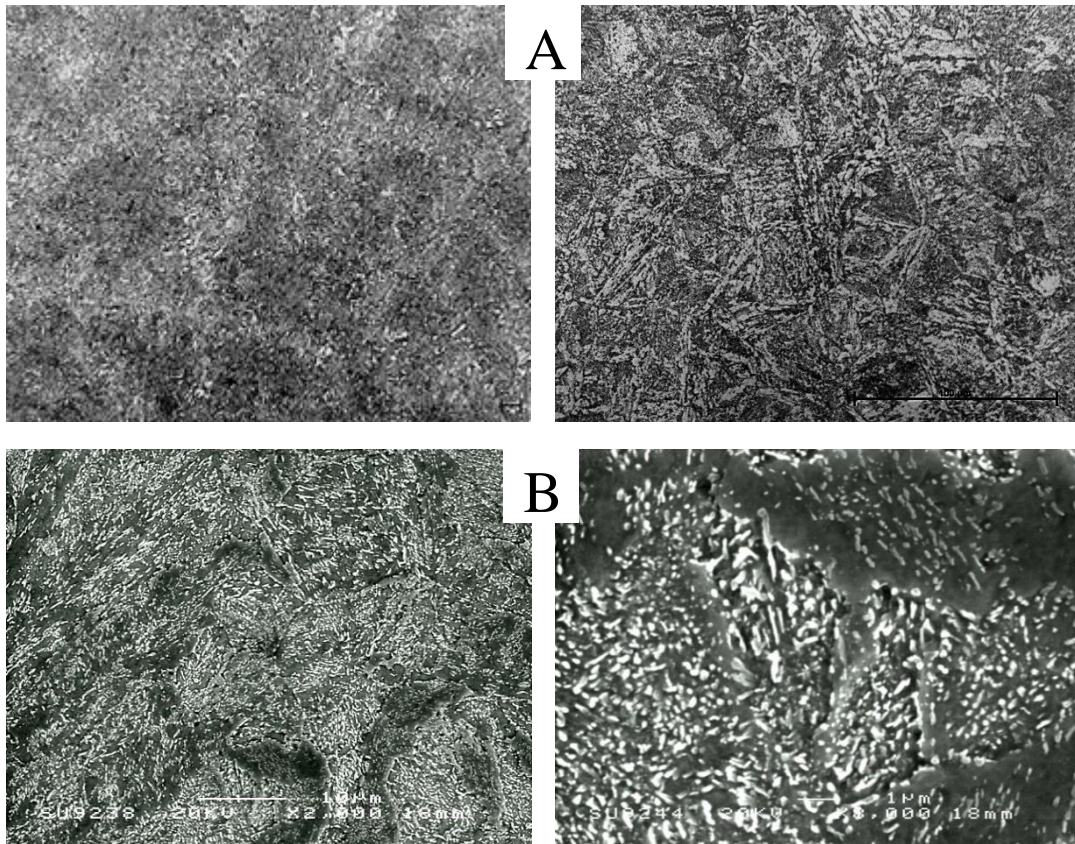


**Figure 3-1** Microstructure of as received material (A) Optical image, 5x and 50x (B) SEM image, 2000x and 8000x.

### 3.2.1 CCT diagrams for 34CrNiMo6 steel

In order to have indications on the nature and quantity of phases present after the transformation, a continuous cooling transformation (CCT) diagram containing several superimposed cooling rates curves is frequently used. The CCT diagram is applicable for a specific steel chemistry, prior austenite grain diameter, and cooling condition used[271]. In this work, CCT diagrams were constructed for 34CrNiMo6 steel using JMatPro software database with grain size of 40  $\mu\text{m}$  and 50  $\mu\text{m}$  at austenitizing temperature of 860  $^{\circ}\text{C}$  as shown in Figures 3.2 and 3.3 respectively.

As explained in the literature review in section 2.5.2 and according to these CCT diagrams it can be observed that the bainite and martensite microstructures are characteristic in the range of used cooling rates (0.3 to 1.2  $^{\circ}\text{C}/\text{sec}$ ). In addition, the amounts of martensite increases with increasing cooling rate, while the proportion of bainite decreases. Accordingly, the two phases in Figure 3.1 (A) are tempered bainite and martensite. The first phase which is dark fine grains is tempered martensite, while the second is a tempered bainite phase which is light in colour.

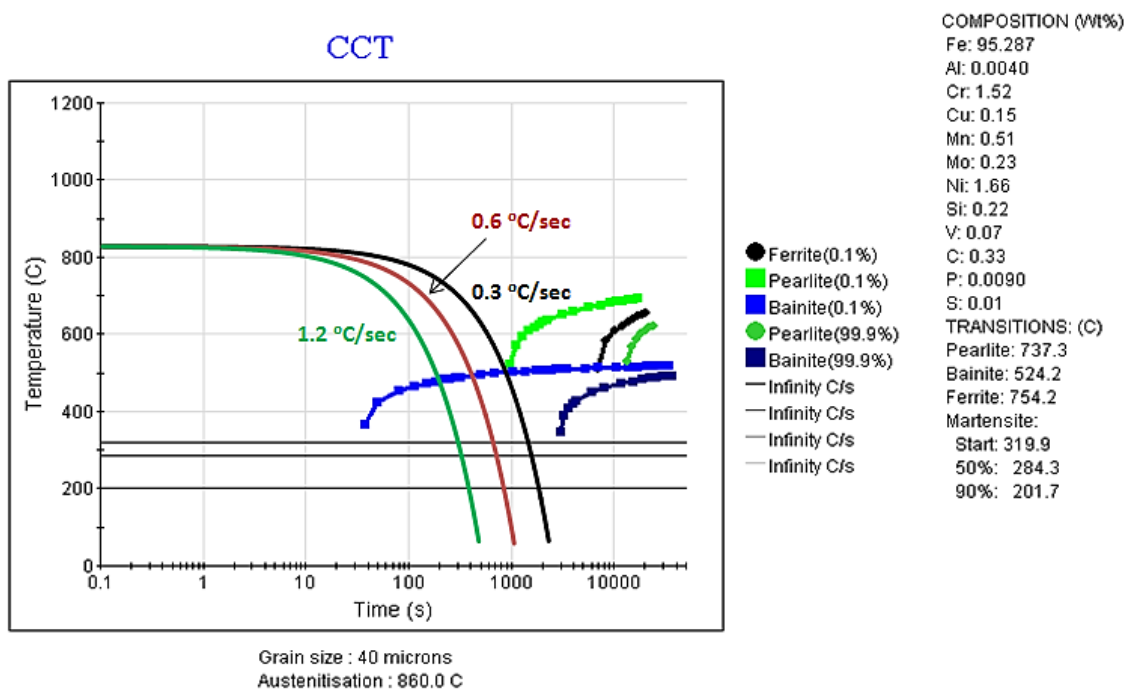


**Figure 3-2** CCT diagram for 34CrNiMo6 steel with grain size of 40 $\mu\text{m}$  at austenitizing temperature of 860  $^{\circ}\text{C}$  (JMatPro software).

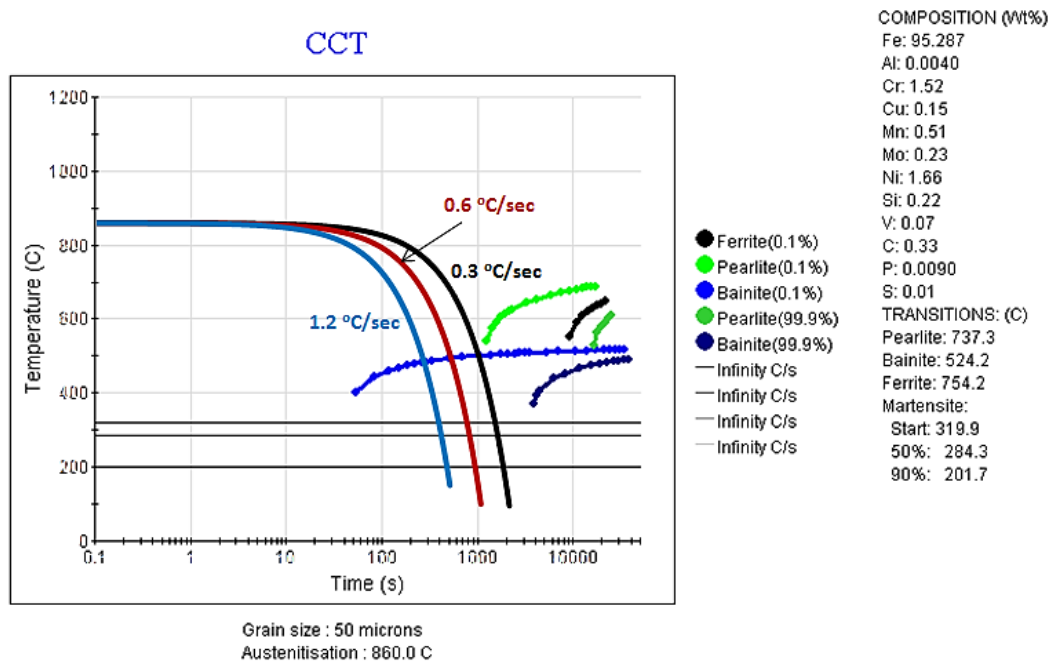


**Figure 3-3** CCT diagram for 34CrNiMo6 steel with grain size of 50 $\mu$ m at austenitizing temperature of 860 °C (JMatPro software).

### 3.2.2 Dimensions and weight of the casting Ingot

The size and weight of the cast ingots usually produced depend on the dimension and quantity of final forged product. In this project the casting process takes place in Sheffield Forge Master and the dimension and weight of the ingot that were used to largest forged billet size are:

- Top diameter : 1067 mm
- Bottom diameter : 965 mm
- Height : 2286 mm
- Mid-line area : 810835 mm<sup>2</sup>
- Weight : 17.24 Ton

### 3.2.3 Macro-segregation through the billet

The variations of chemical composition through the billet must be taken into account especially in the case of large scale products, where the variation in the composition is usually expected. Accordingly, the chemical composition analysis and toughness from 4 positions of the billet are tested, as shown in the appendix D-2 (According to company data base). Although, the toughness results for these samples were different, the chemical

analysis of these specimens shows that the composition is nearly consistent. From results in the appendix D-2 we can conclude that there is no macro-segregation along the length of the billet, and the small different of percentage of each element may not alter the mechanical properties of the steel.

### **3.2.4 Forged dimensions and sampling location**

According to First Subsea data base, the final dimensions of billet after the forging process were about 8000 mm long and 480mm diameter. Once, the desired dimension of the billet is reached after deformation, the billet is sent to the heat treatment plant to refine the microstructure and reach the mechanical properties. Generally, the prepared test pieces which are taken from the forged billet should be equivalent of cross section and be fully representative of the product. In our study all the PSC Specimens and Charpy V-Notch Specimens that were used to verify the specification of mechanical properties were taken from a position located at 1/3 of the radius from the surface. Moreover, the longitudinal direction of these specimens should be oriented in the forging direction of the billet, which is the forging direction.

Commonly for each test condition, three test samples (e.g., Charpy V-Notch) often required to repeat in each case. The average value of these three tests usually used as a result for the test to avoid or minimise the experiments error. Unfortunately in our study there was some problems that occurred during the experimental work, which made the number of tests at each condition is limited. For instance, the as received material was not enough to make adequate number of samples, besides that the number of PSC and Charpy specimens also were limited due to the condition of sampling position (1/3 from the surface). Furthermore, many samples also were lost during perform the tests on the TMC machine for many reasons, which means more samples to repeat these tests. Moreover, besides lots of users for TMC machine, the machine was broke down several times and for long periods during the study, which means it was available for a limited time to each user. For all these reasons, only one specimen for each test condition was performed, which makes the occurrence of error in the experimental results is possible. Fig. 3.4 shows a typical forging drawing with the sampling position, according to ABS guide for the certification of offshore mooring chain R4 and DNV OS-302 which also clients requirements.

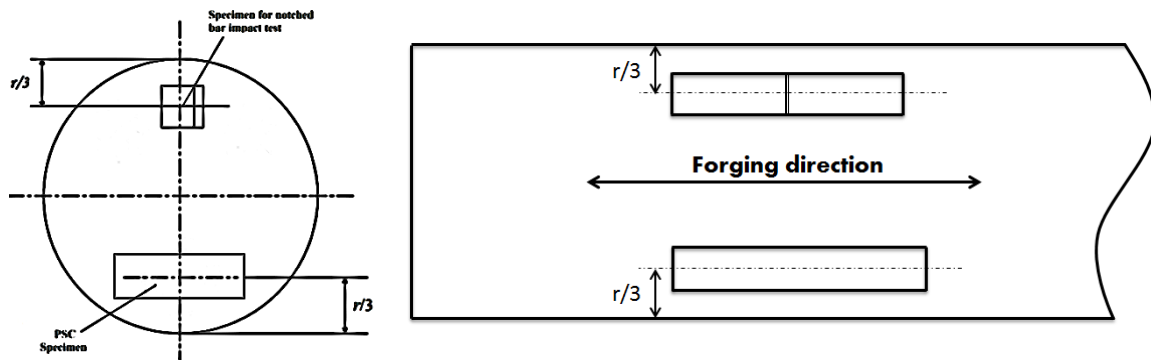


**Figure 3-4** Shows the position sampling for PSC Specimens and Charpy V-Notch Specimens on the forged Steels bar.

### 3.2.5 Effects of variations in structure and segregation on the test samples

Generally, consistency throughout the sampling position is very important issue, because if there was any variation in the samples composition that will leads to scatter in data results even under the same test conditions. The as received material also may have residual segregation or chemical concentration gradient that was produced during large ingot solidification. This issue should be taken in consideration when the sampling position is chosen, because this variation will effect on the test samples, consequently on the later results. This variation is usually distributed from the surface areas to the other areas towards the centre. Therefore, to reduce this effect all the samples were taken from the same position where the microstructure should be consistent. Accordingly, from as received cross section, all the test specimens were taken around the circumference of a circle that has a radius of  $2/3$  from the centre.

Furthermore, the mechanical properties of alloy steels usually depend both on the thermomechanical history and on its chemistry[272]. Therefore, the variations of structure, heat treatment or a combination of both through a forging may cause differences in some later results. The question is does multiple heat treatments modify the response of the alloy e.g., the austurity grain size, which also may affect later results. Krzyzanowski[273] et al. have reported that in thermo-mechanical processing, the thermal history of the workpiece has profound influence on the final properties of the product. However, the repeated heat treatment is used when the forged bar does not meet the required properties after first heat treatment.

Thus a second and even third heat treatment in some cases is needed in an attempt to approach or to achieve these properties. In our experimental results shows that repeated reheating has good effect on modify the response of the 34CrNiMo6 steel especially on toughness. Generally, before perform the simulation test; the conditions of the real case and the simulated test should be matched. Where later, these condition can be modified to test the extent of their impact on the properties. For instance, in this study before simulation the real tempering process, the initial conditions were created to try to simulate the similar structure that was produced through a forging (See section 3.6.1). The austenite grain size of the tested samples that was used for our experiment must match the average austenite grain size for samples that were taken from the real product before tempering. Hence, it is important to create a condition of temperature to match this austenite grain size. Moreover, the cooling rate that was used in this experiment must be equal to the real cooling rate and in the same place through the cross section required for testing.

### 3.3 The forging and heat treatment processes for the real product

$$\dot{\epsilon} = 10^{-2} - 10^{-1} \text{ s}^{-1}$$

$$\epsilon = 1$$

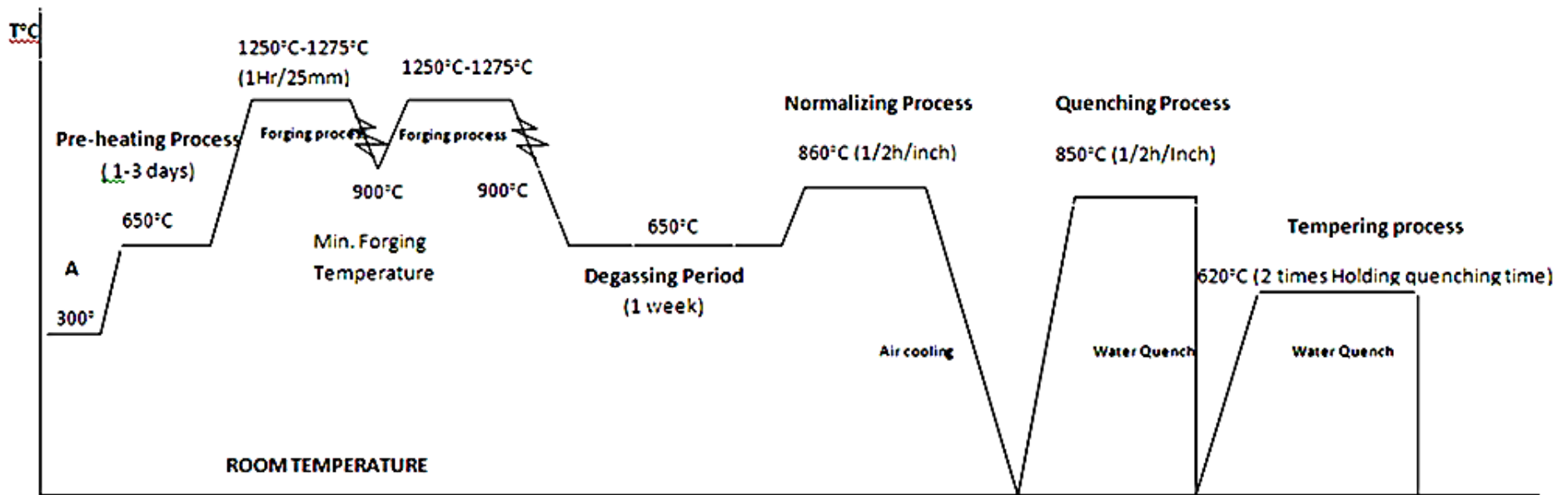


Figure 3-5 Scheme of forging process and Heat Treatment for the real company product.





**Figure 3-6** Shows the real forging process in Somers Forge Company (company archive).



**Figure 3-7** Quenching and tempering process (company archive).

### **3.3.1 The forging process**

The first stage in the manufacturing process of the company's real product started with heating the billet gradually to the temperature of 1260 °C, soaking for a period of time according to the ratio of 1 h/25 mm in a flame furnace. Then, the process of deformation took place at temperatures ranging between 1260 °C and 900 °C. At that time, when the deformation temperature became close to 900 °C, the billet was returned into the furnace to increase the austenitising temperature to continue the deformation process again. After that, the forged section was sited in a degassing furnace for a period of one week at temperature 650 °C in order to keep the hydrogen content values lower than 2 ppm, as shown in Figure 3.3. Moreover, images of the real forging process in Somers Forge Company are shown in Figure 3.6.

### **3.3.2 The heat treatment process**

The first stage in the heat treatment process of the real product began with a normalizing process. The process was performed by soaking the billet for a period of time according to the ratio of 1/2 hour/25 mm at a temperature of 860 °C, as shown in Figure 3.5. The objectives of a normalizing process are to refine the grain size that frequently become coarser after hot deformation at high temperature, and distribute uniformity in the austenitic microstructure. The second stage of heat treatment is the quenching process where the billet is sent back to the furnace and soaked at a temperature of 850 °C for a time according to the ratio of 1/2 h/25 mm followed by quenching in water. The benefit of this process is to obtain martensite throughout the cross section of the billet. The final stage of heat treatment is the tempering process. The process is carried out by holding the billet at 620 °C for a period of time that is double the quenching time, finally quenching the billet in water. This process is usually used to obtain desired mechanical properties such as hardness and toughness in the finished product. Images of the quenching and tempering heat treatment process that were done in Somers Forge Company for the real product are shown in Figure 3.7.

### 3.4 Plane strain compression (PSC) testing

Standard plane strain compression (PSC) specimens with dimensions of 10 x 30 x 60 mm, as shown in Figure 3.8 (a), were machined from the as received forged and heat treated material to be used in thermo-mechanical tests on a TMC machine. This kind of test is performed to simulate the conditions that are used in metal working operations and to obtain stress-strain curves that can be used to determine some material characteristics. All PSC specimens were cut to the preferential orientation which is 60 mm is the forging direction. The PSC tests were performed at the University of Sheffield on a modern (TMC) machine equipped with a computer system which allows it to control all the deformation conditions. As shown in Figure 3.9, the sample was placed between two flat dies, where a narrow band from the specimen length was compressed by these dies which are wider than strip. Deformation happens in the direction of die movement and in the direction normal to the length of the dies. The required data such as load, displacement, velocity and temperature from the tested specimen are recorded through the computer system to be used later for analysis and to draw stress-strain curves. Figure 3.8 (b) shows the PSC specimen before and after the deformation process.

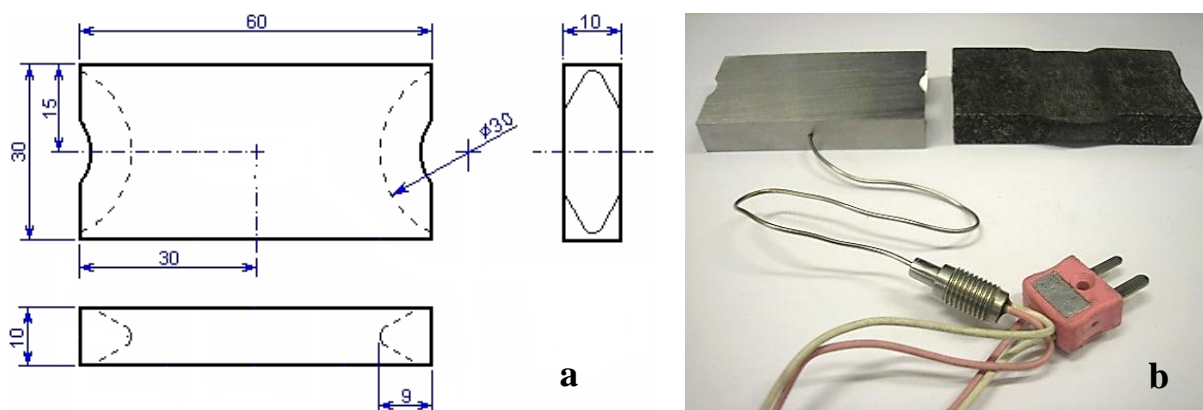


**Figure 3-8** Plane strain compression (a) specimen dimensions (b) specimens before and after TMCP test.

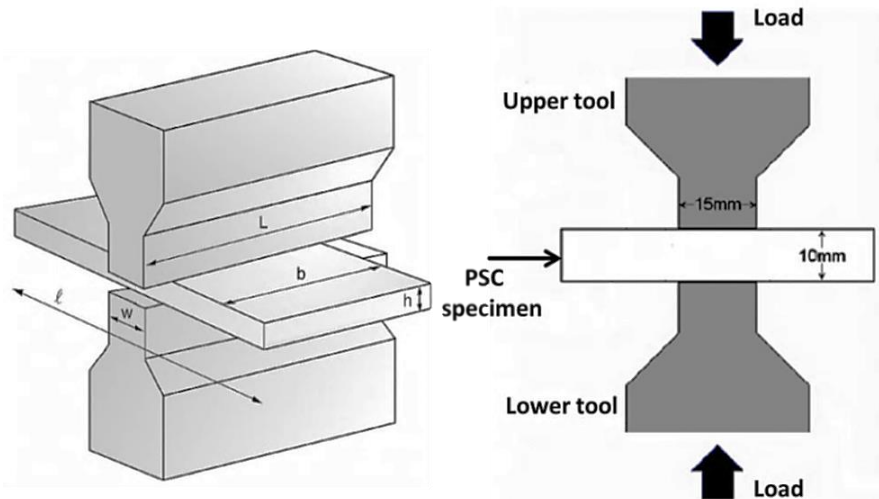


**Figure 3-9** Schematic of the Plane strain compression test.

### 3.4.1 The thermo-mechanical compression test machine

PSC tests were performed in the servo-hydraulic thermo-mechanical compression (TMC) machine, as shown in Figure 3.10. The main purpose of this machine is to simulate metal forming processes such as forging under different manufacturing conditions of temperature, strain, strain rate, and heating and cooling rates. Two types of deformation test can be performed in this machine, plane strain compression and axisymmetric compression tests. The TMC machine is designed for the computer system to control fully the deformation and heat treatment processes where the specimen handling is controlled by a robot arm, as shown in Figure 3.11. During the years that the TMC machine has been working several adjustments have been made to the machine and to the controlled software to attempt to improve the results obtained. The rig is designed to communicate with the actuators and recording instruments such as a transducer for detecting displacement, temperature, velocity and load of the deformation specimens at elevated temperatures and different strain rates. For heating and cooling specimens an induction furnace, also known as fast thermal treatment unit (FTTU), was used. The FTTU unit which consist of a quenching unit can create a complex heat treatment profile with good accuracy of parameters such as heating rate, temperature, holding time, and cooling rate. One or more N-type thermocouples can be inserted into the specimen to collect the temperature data of the specimens from reheating to the deformation and through cooling with different rates (forced air, water, or mix of both). The specifications of the IMPPETUS TMC machine are shown in Table 3.2.

**Table 3-2** Specifications of the IMPPETUS TMC machine[274].

	Machine characteristics
Actuators	servo-hydraulic
Max strain	$\approx 2$
Max strain rate	$150 - 200 \text{ s}^{-1}$
Max temperature	1200 °C
Max load	500 kN
Quench	either air/water cooled/quenched
Controllable variables	load, displacement
Atmosphere control	none (air)
Temperature measurement	up to 3 thermocouples in specimen

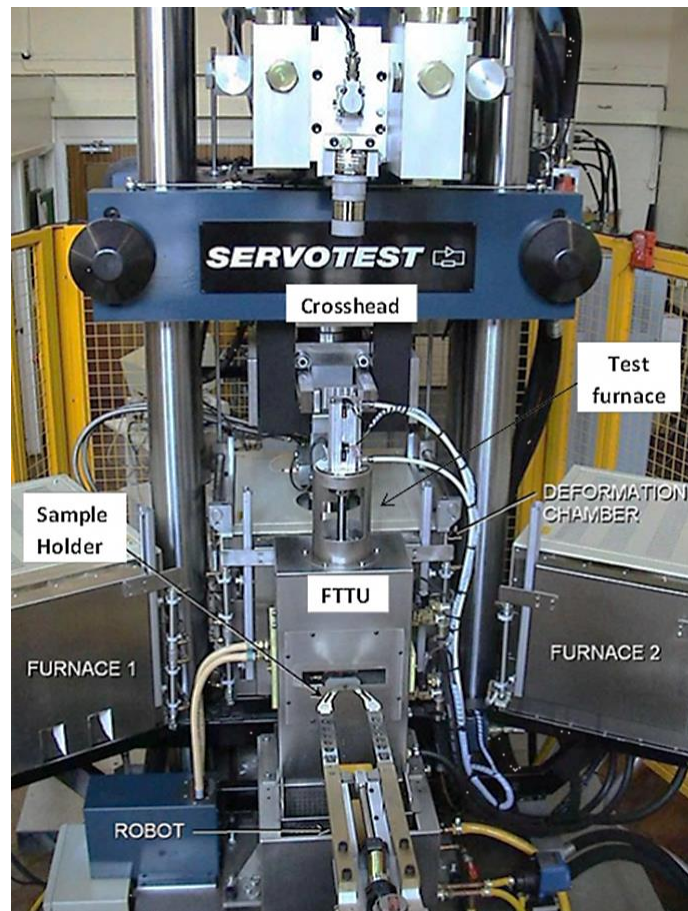


**Figure 3-10** servo-hydraulic test machine[275].

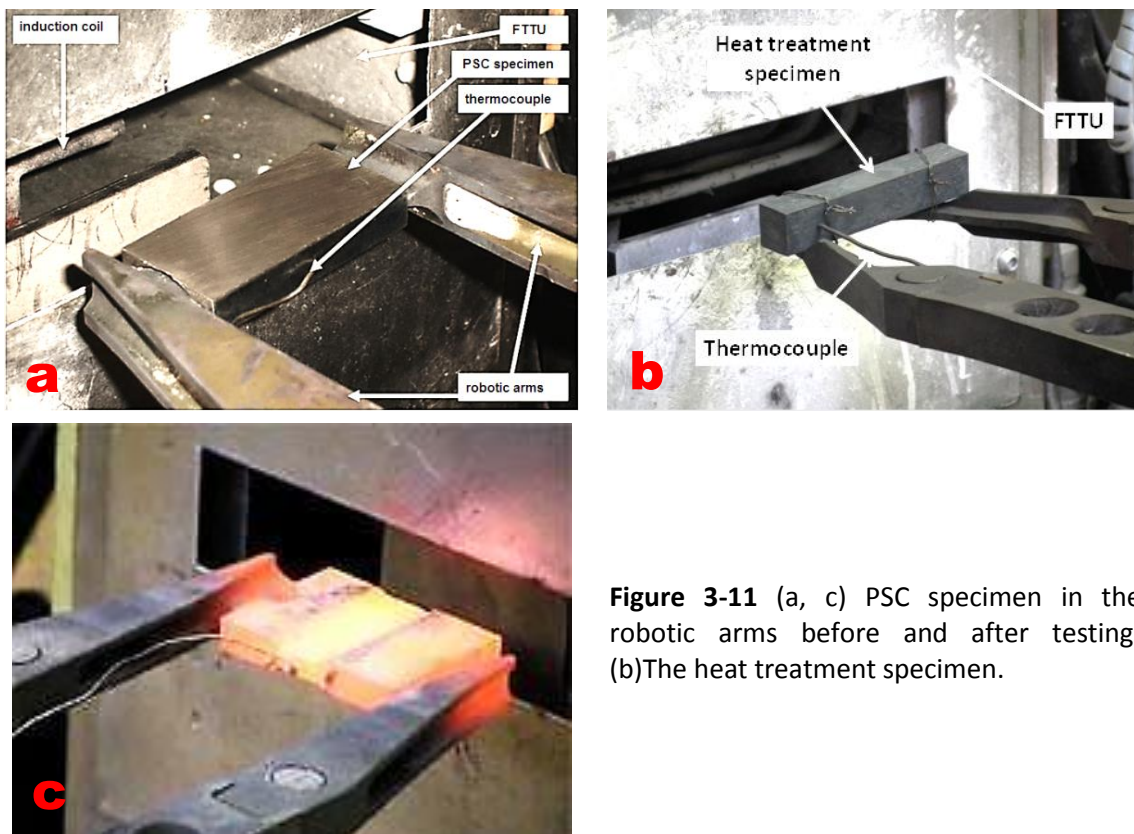


**Figure 3-11** (a, c) PSC specimen in the robotic arms before and after testing. (b)The heat treatment specimen.

### 3.5 Deformation Process

Hot deformation processes such as forging are usually useful for improving the engineering properties of many steel products because they assist in the refinement of austenite grains and produce a fine-grained equiaxed microstructure, thus helping to increase the strength, ductility, and toughness of the material. Austenite grain diameter plays a significant role in determining the subsequent phase transformation (section 2.8.3); therefore, it is necessary to have a good understanding of it during a hot forging. Furthermore, impurities such as inclusions that are formed during casting, which are usually randomly oriented and act as a source of cracks, can be reoriented and made small and spherical by using hot deformation, which leads to a decrease in their danger. Accordingly, the first issue to address during the forging processes is the relationship between the variables that play a role during hot deformation and control the evolution of the microstructure: temperature, strain, strain rate and cooling rate.

### 3.5.1 Isothermal Deformation Process (single hit)

The main purpose of the isothermal deformation processes was to quantify the prior austenite grain size of the 34CrNiMo6 low alloy steel under different deformation conditions. The extent and stability of the austenite phase is affected by chemical composition, the deformation temperature, the holding time before that temperature, strain and strain rate. The process began by heating the specimens to a temperature of either 1100 °C or 1260 °C which represent austenitising temperatures by using the TMC machine. According to the holding time estimation, one hour was the period of holding time for both reheating temperatures (see section 8.1.1).

After soaking at austenitising temperature, the specimen was cooled down to a required deformation temperature. After that deformation took place by using a strain of 0.8 with different strain rates of 0.1, 0.5 and 1 s<sup>-1</sup> at each deformation temperature of 900 °C, 1000 °C, 1100 °C and 1200 °C after the austenitising temperature of 1260 °C, and 900 °C, 950 °C, 1000 °C, and 1100 °C after the austenitising temperature of 1100 °C. Finally, the specimen was water quenched to room temperature directly after deformation, as shown in Figure 3.12.

Moreover, more experiments of isothermal deformation were performed to study the effect of changing the strain on the austenite grain size. The same steps as previously were repeated with an austenitising temperature of 1260 °C, deformation temperature of 1000 °C and strains of 0.4 and 0.6 with strain rates of 0.1, 0.5 and 1 s<sup>-1</sup> at each strain.

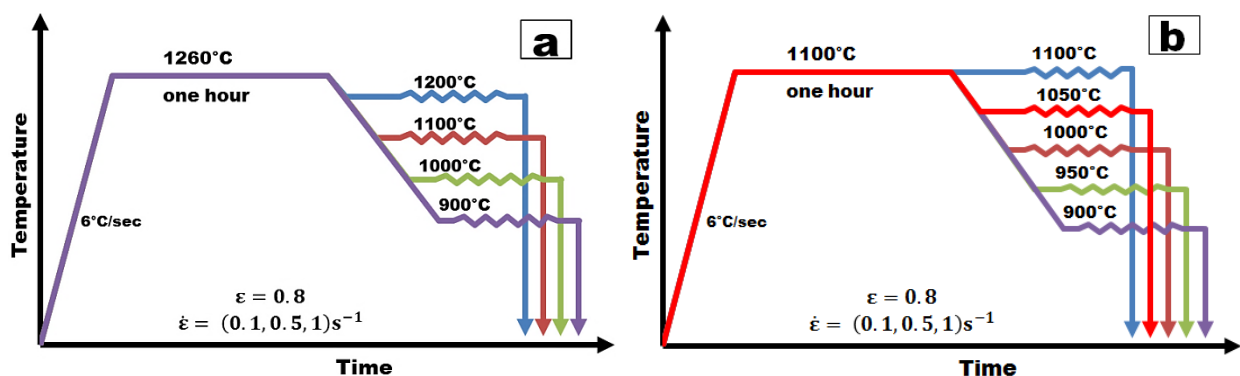


**Figure 3-12** Schematic diagram of the isothermal thermo-mechanical processes, using a strain of 0.8 with different strain rates (0.1, 0.5 and 1 s<sup>-1</sup>) at austenitising temperatures of (A) 1260 °C, at each deformation temperature (900 °C, 1000 °C, 1100 °C and 1200 °C), (B) 1100 °C, at each deformation temperature (900 °C, 950 °C, 1000 °C, 1050 °C and 1100 °C).

### 3.5.2 Non-isothermal Deformation Process (Multi hit)

The real forging process is a non-isothermal deformation process because it is performed at a different range of deformation temperatures. Therefore, to make the experiments more realistic three and four hits of non-isothermal processes were also done in the same range of real deformation temperatures for both austenitising temperatures.

#### 3.5.2.1 Four hits

Deformation in the real forging process begins at a temperature of about 1260 °C and continues until the ingot temperature become close to 900 °C. Therefore, to attempt to simulate this real process as well as to study the influence of changing the deformation start temperature on the final microstructure, two non-isothermal experiments with austenitising temperatures of 1100 °C and 1200 °C were performed. The experiments began by raising the temperature of the specimens to austenitising temperatures of either 1100 °C or 1200 °C with one hour holding time. After that two sets of deformation temperature containing four hits each were applied followed by water quenching to room temperature, as shown in Figure 3.13. The deformation temperature set of 1200 °C, 1100 °C, 1000 °C, and 900 °C was used respectively after austenitising temperature of 1200 °C, while the deformation temperature set of 1100 °C, 1000 °C, 950 °C, and 900 °C was used after the austenitising temperature of 1100 °C. Both 0.5 s<sup>-1</sup> strain rate and the total accumulation strain of 0.8 (0.2 strains at each single deformation hit) were used with each set of deformation temperatures.

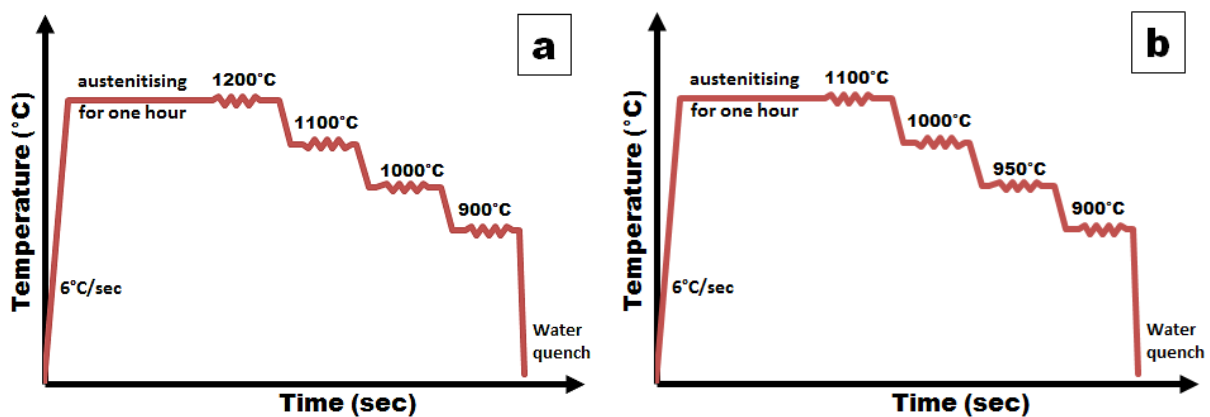


**Figure 3-13** Scheme diagram of four hits of non-isothermal deformation processes at austenitising temperatures of 1200 °C and 1100 °C, using a total strain of 0.8 at each set of deformation temperatures (a) 1200 °C, 1100 °C, 1000 °C, and 900 °C, (b) 1100 °C, 1000 °C, 950 °C and 900 °C, with 0.5 s<sup>-1</sup> strain rate followed by water quenching immediately after each set.



### 3.5.2.2 Three hits

According to results that were obtained from the isothermal deformation process at a temperature of 900 °C, the four hits of the non-isothermal deformation processes were repeated after excluding the deformation at temperature 900 °C. Therefore, the three hits deformation processes at the same austenitising temperatures, strain and strain rates were performed to try to establish the difference in grain size in comparison with the grains obtained from the four hits deformation process. After the cancellation of deformation at a temperature of 900 °C, the same two previous sets of deformation temperatures were used followed by water quenching to room temperature, as shown in Figure 3.14 (A). Furthermore with the three hits experiments, two other different situations were investigated. First, after the three hits the specimens were held for 60 sec and then quenched in water, as shown in Figure 3.14 (B), and in the second case, after the three hits the specimens were cooled to 900 °C in 60 sec then immediately quenched in water, as shown in Figure 3.14 (C). These two different situations were done at austenitising temperature of both 1100 °C and 1200 °C.

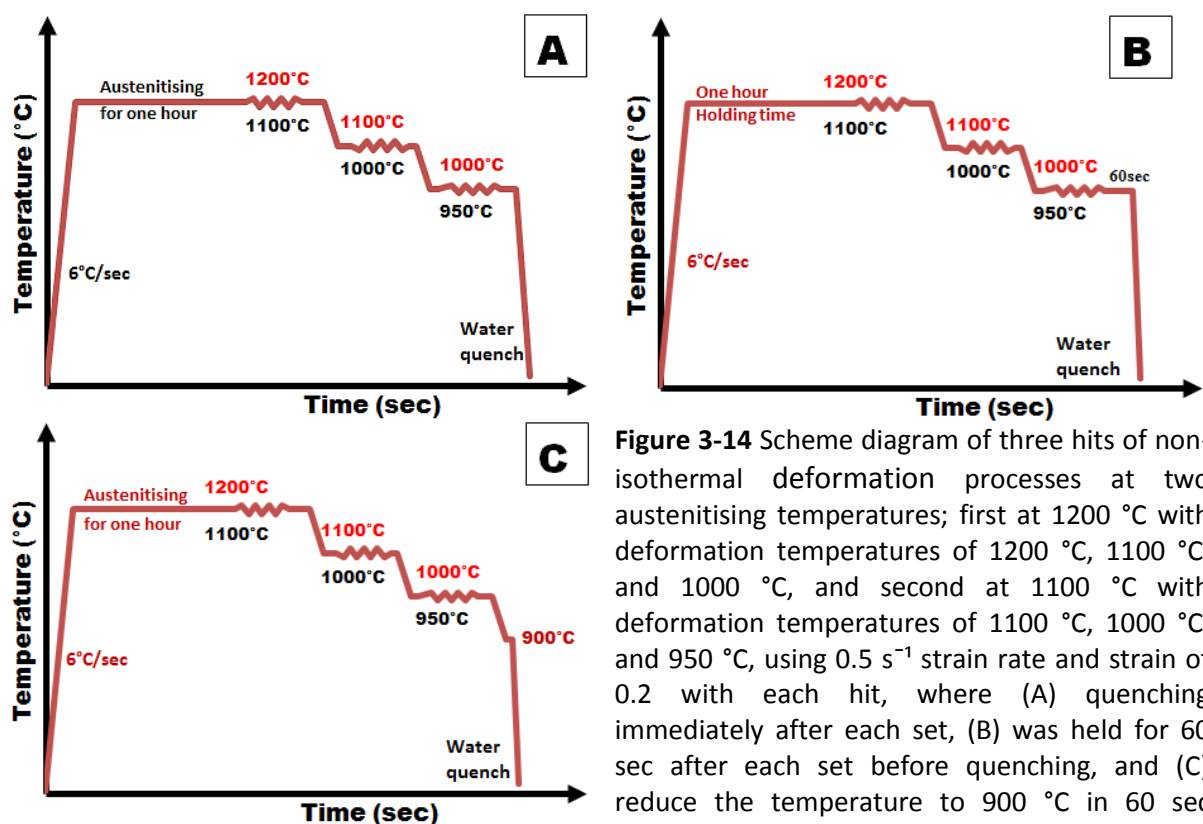


**Figure 3-14** Scheme diagram of three hits of non-isothermal deformation processes at two austenitising temperatures; first at 1200 °C with deformation temperatures of 1200 °C, 1100 °C, and 1000 °C, and second at 1100 °C with deformation temperatures of 1100 °C, 1000 °C, and 950 °C, using 0.5 s<sup>-1</sup> strain rate and strain of 0.2 with each hit, where (A) quenching immediately after each set, (B) was held for 60 sec after each set before quenching, and (C) reduce the temperature to 900 °C in 60 sec before quenching.

### **3.6 Heat Treatment**

In this part of the chapter the normalizing, hardening, and the tempering processes will be described to attempt to investigate the effect of the heat treatment parameters on the grain size and transformation behaviour of austenite. Heat treatment started with a normalizing process; in this step we investigated the effect of austenitising temperature on the normalizing process and compared the austenite grain size after deformation with that produced after a normalizing process at a temperature of 860 °C. Moreover, the effect of increasing the normalizing holding time on the variation in grain size and uniformity of the microstructure, thus the final mechanical properties, was investigated.

The second stage of the heat treatment is the quenching process. The greatest benefit of this process is to obtain martensite through the cross section of the billet. In this step we studied the effect of different cooling rates on the formation of microstructure. The final stage of heat treatment is the tempering process. This process is usually used to obtain desired mechanical properties in the final product. At this point we tried to investigate the effect of the tempering temperature and different cooling rates on the magnitude of the decrease or increase of toughness and ultimate tensile strength.

#### **3.6.1 Create initial conditions to simulate the real heat treatment process**

The results of an austenite grain size with respect to impact toughness for 16 specimens taken from 16 different billets after being subjected to the forging and heat treatment processes (company database), are shown in Figure 3.15. According to the specification design of the final product the impact toughness energy of the material is equal or greater than 50 J at temperature of -20 °C, and from the linear relationship between toughness and austenite grain size in Figure 3.15, the 47 µm austenite grain size will be used as a worst case scenario to simulate the heat treatment process to achieve these standard specifications. The cross section diameter for the studied billet that has the problem is 480 mm.

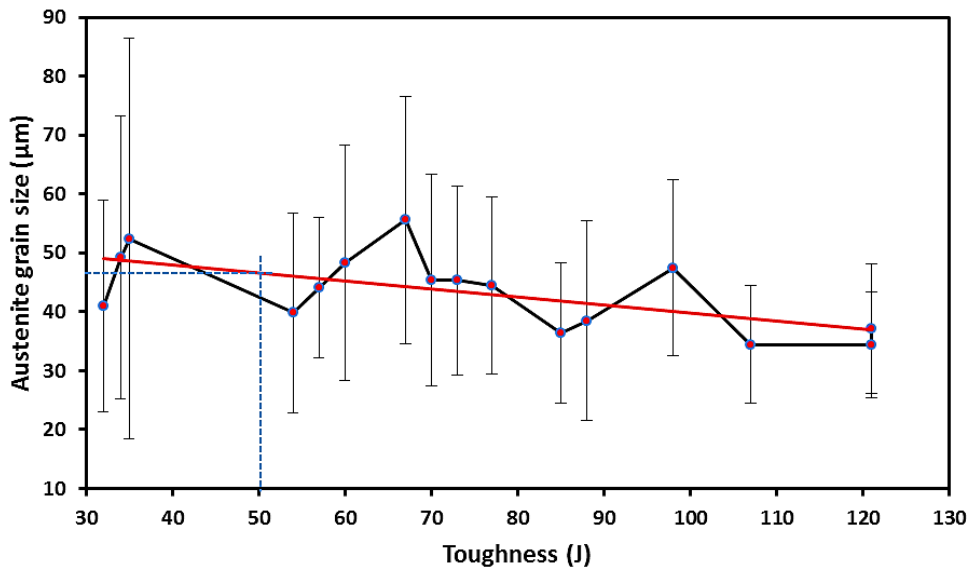


**Figure 3-15** Relationship between toughness and austenite grain size (company data).

According to the company data in Figure 3.16, which shows the cooling rate across the different billet diameter sections, and according to the ABS chain specifications, 0.6 °C/sec was the estimated cooling rate 2/3 from the billet centre for 480 mm diameter. However, for more realistic results this cooling rate (0.6 °C/sec) does not really represent the real cooling rate at 2/3 sampling position for large scale products due to many possible factors such as large variations of austenite grain sizes from the surface to the centre of the billet. Therefore using a cooling rate of 0.3 °C/sec or 0.5 °C/sec, from Figure 3.16, shows a sampling location at 1/3 and even 1/2 radius from the centre is more realistic and gives more reliable results.

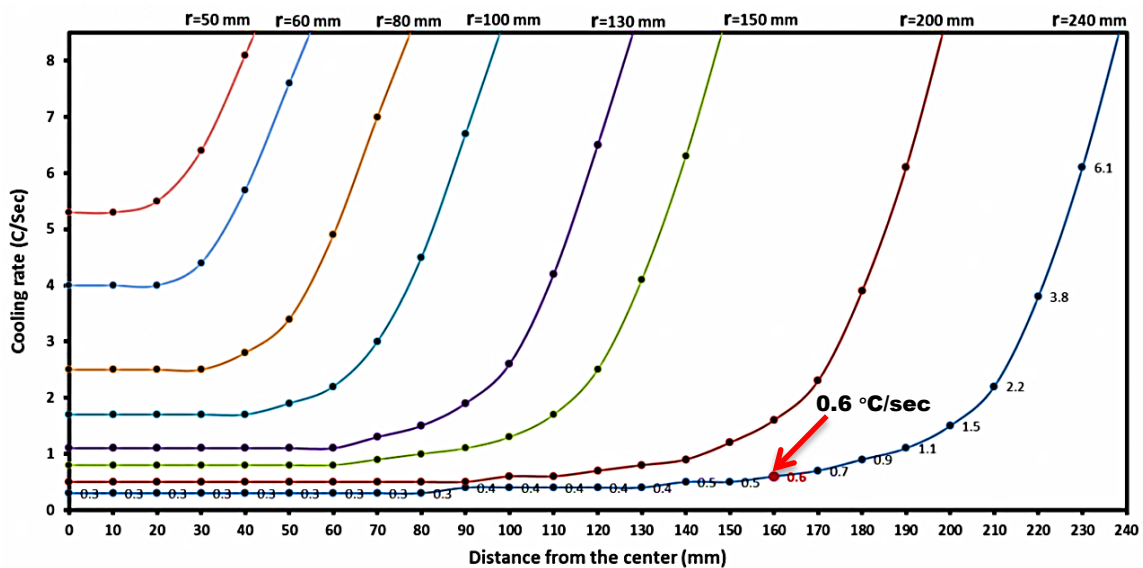


**Figure 3-16** Estimated cooling rate through the cross sections for different billet radiuses (r=radius).

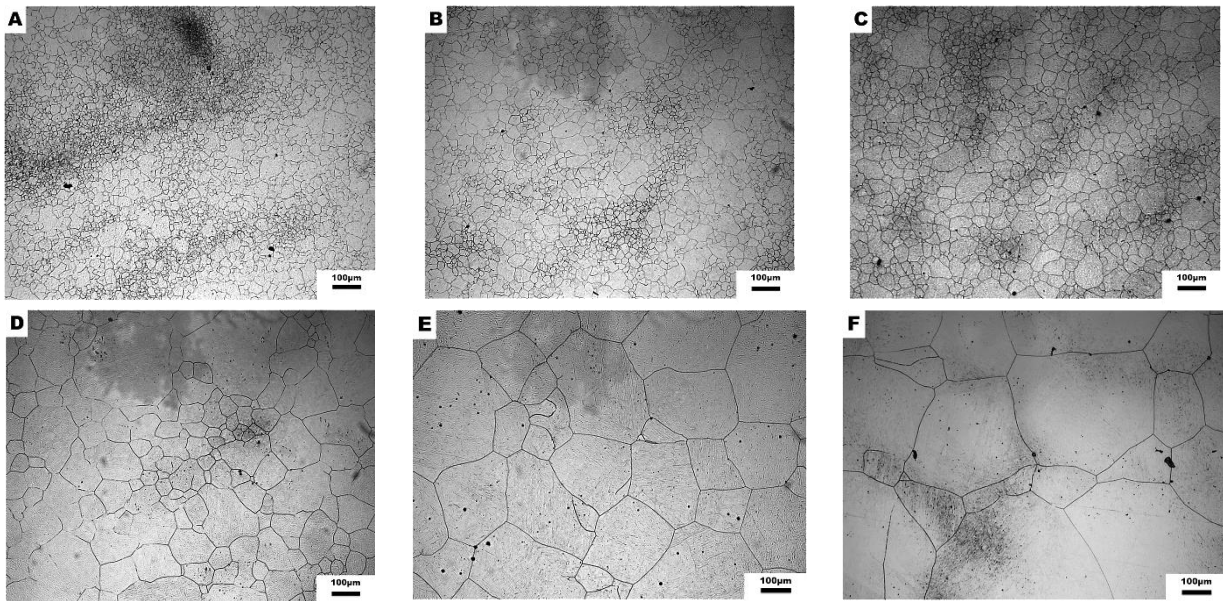


**Figure 3-17** Austenite grain size after holding for one hour at austenitising temperatures of (A)860 °C, (B)900 °C, (C)950 °C, (D)1000 °C, (E)1100 °C, (F)1260 °C (Picric acid) 10X.

According to our previous experimental results, one hour was chosen as an austenitising temperature holding time, which gave the biggest austenite grain size we could achieve in small samples. Optical micrographs for the prior austenite grains after holding for one hour at different temperatures in the range between 860 °C to 1260 °C are shown in Figure 3.17. These microstructures were used to build a diagram as shown in Figure 3.18. Through using this diagram an austenite grain size of 47 µm at one hour holding time can be obtained at a temperature of 960 °C. Therefore, this temperature was used for all experiments to simulate approximately real conditions in the thermo-mechanical process.

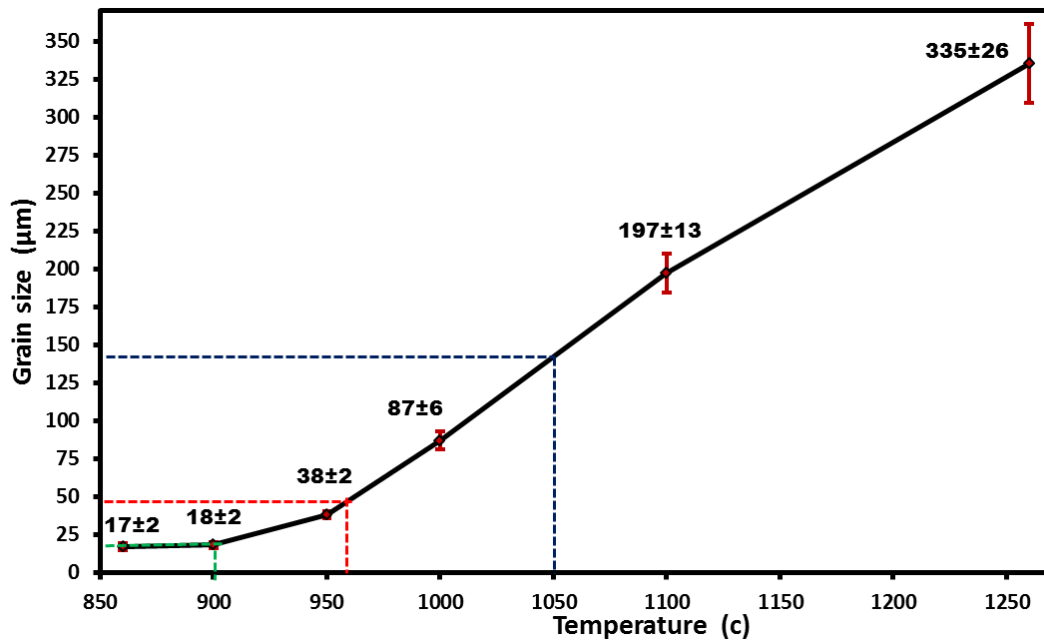


**Figure 3-18** Mean austenite grain size at one hour holding time at different austenitising temperatures.

### 3.6.2 Thermocouple position

The induction furnace in the TMC machine was used to control the rate of heating, holding and cooling temperatures for heat treatment processes. The temperatures were controlled by using an N-type thermocouple attached to the specimens a near-net shape to the Charpy test specimens. These heat treatment samples were to be used later to do a Charpy test, so the thermocouples used to control the temperature were placed in one of the two sides, not in the middle. Therefore, the temperatures between the centre and the sides had to be calibrated to know if there was any difference. Two thermocouples were used as shown in Figure 3.19; one in the middle and the other in the side of the sample to calibrate the differences in all temperatures used in heat treatments. After the samples were heated and held to make the temperature stable, there was no significant difference in the temperature readings between the two thermocouples used.



**Figure 3-19** Heat treatment specimen with two thermocouples.

### **3.6.3 The effect of normalizing process on the deformed austenite grain size**

In this step we attempted to simulate the normalizing process and investigate the effect of this process on the deformed austenite grain size. This was done by comparison between the austenite grains formed after deformation and those produced after the normalizing process. Furthermore, the variation in austenite grains before and after the normalizing process when the normalizing holding time was changed was studied. The experiment was divided into two stages. The first started with heating the specimen up to a deformation temperature of either 1100 °C or 1200 °C. Then the specimen was soaked for ten minutes before being deformed using 0.8 strains and with 1 and 0.5 strain rates at temperatures of 1100 °C and 1200 °C, respectively. Finally the specimen was quenched in water, as shown in Figure 3.20 (a).

In the second stage, the same previous austenitising holding time, deformation temperatures, strain and strain rates were used. However, after deformation the specimens were cooled down under A1 to a temperature of 650 °C with cooling rates of 4.5 °C/sec and 5.5 °C/sec from temperatures of 1100 °C and 1200 °C, respectively. Then, the specimens were held for 5 mins at a temperature of 650 °C after both deformation temperatures. In the last step of the process the specimens were heated up again above A1 to a temperature of 860 °C (which is the temperature of the normalization) and the specimen soaked for 6 mins according to the ratio  $1/2 h/25 \text{ mm}$  as in real process, for both deformation

temperatures of 1100 °C and 1200 °C. Finally, as in the first stage, all the specimens were immediately quenched in water, as shown in Figure 3.20 (b).

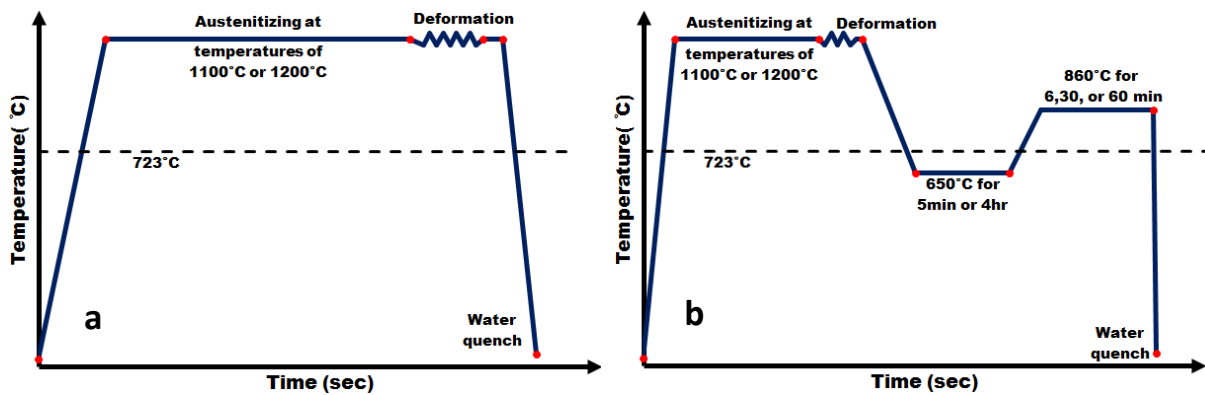


**Figure 3-20** Scheme diagram of isothermal deformation processes, at deformation temperatures of 1200 °C and 1100 °C with different strain rates after being heated for ten minutes, using a strain of 0.8 (a) quenching immediately after deformation (b) Cooled to 650 °C after deformation and then heated to 860 °C before quench.

It is known that the most important benefit of normalizing is refining the austenite grain size. Therefore, in the next step we investigated the effect of increasing the normalizing holding time on austenite grain growth at a temperature of 860 °C. After using the same previous deformation conditions of strain and strain rates with austenitising temperature of 1100 °C and 1200 °C, the specimens were cooled and held for 4 hours at 650 °C to make the whole structure transform to ferrite and pearlite. After that, the specimens were heated to a temperature of 860 °C and held for different times of 6, 30, and 60 mins followed directly by quenching in water, as illustrated in Figure 3.20 (b).

### 3.6.4 Quenching process

After creating initial conditions for the heat treatment process to produce austenite grain sizes similar to those obtained from the real process by using the data in Figures 3.15 and 3.18, specimens for heat treatment and subsequent Charpy impact and hardness testing were prepared. After the normalizing process the next step of heat treatment was quenching, where two austenitising temperatures of 840 °C and 960 °C were used with different cooling rates. The process started with heating the samples up to 960 °C with rate of 4 °C/sec and austenitised for 1 hour to obtain an austenite grain size of approximately 47 µm. Thereafter the temperature was cooled to 860 °C, which represents the austenitization

temperature, and held for 10 mins. Similarly an austenitising temperature of 840 °C with the same heating rate and holding time was used after cooling down to 740 °C and holding for 10 mins for comparison. Both austenitising temperatures were followed with the same different cooling rates down to room temperature, as shown in Figure 3.21.

The TMC machine was used to apply and control the cooling rates of 0.3, 0.6, 0.9, and 1.2 °C/sec. The furnace cooling rate also was used but only for austenitising temperature of 960 °C. To perform the test, two of the chamber furnaces (muffle furnace) with a maximum operating temperature of 1400 °C were used at the same time. The first furnace was heated to a temperature of 960 °C and the sample placed inside when the furnace reached the desired temperature and held for one hour. After that the sample was taken to the second furnace, which had been heated to a temperature of 630 °C, and held for 10 mins. Finally, the chamber furnace was turned off and the sample was left inside to allow cooling to room temperature. A small sample was taken to reveal the microstructure before continuing and subjecting the specimen to a tempering process.

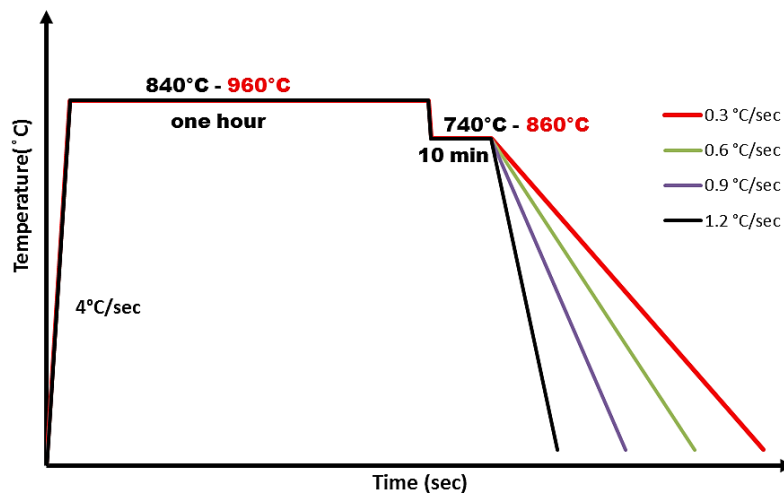


**Figure 3-21** Austenitising temperature and cooling rate profile.

### 3.6.4.1 Quenching process using different austenitising temperatures and cooling rate of 0.6 °C/sec

In the first step of the quenching process an austenitising temperature of 960 °C with cooling rate of 0.6 °C/sec was used, which gives the austenite grain size that represents values comparable to those formed in real product. In addition, to study the effect of changes in the austenitising temperature on the austenite grain size and thus on the final



microstructure that gives desirable mechanical properties, additional austenitising temperatures of 780 °C, 900 °C, 930 °C and 1050 °C were used with the same cooling rate of 0.6 °C/sec, consistent with our previous assumption in the deformation stage when a temperature of 1100 °C was used as an austenitising temperature to try to refine the austenite grain size. Therefore, a small austenite grain size (less than 47 µm) was used to study the effect of grain size refinement on the heat treatment process.

From the curve in Figure 3.18, using temperatures of 780 °C, 840 °C, and 900 °C yields approximate austenite grain size of 19 µm, while using the temperature of 930 °C gives austenite grain size of 30 µm. Furthermore, to study all possible scenarios for influencing austenite grain size in the heat treatment processes, the austenite grain size was increased to more than 45 µm by using an austenitising temperature of 1050 °C. From Figure 3.18, when the temperature rose to 1050 °C we got an austenite grain size of 145 µm. Therefore, as in the previous steps, the heat treatment process shown in Figure 3.21 was repeated with the same conditions after using austenitising temperatures of 780 °C, 840 °C, 900 °C, 930 °C, 960 °C and 1050 °C and a cooling rate of 0.6 °C/sec.

### **3.6.5 Tempering process**

The last stage in the heat treatment process was the tempering process, as seen in Figure 3.5. At this stage two types of experiments were performed. Firstly, the cooling rate for each austenitising temperature was changed, and secondly, the austenitising temperature was changed but the same cooling rate used. After the quenching process the specimens were reheated again to either 520 °C or 630 °C at the rate of 4 °C/sec. Then the samples were held for 40 mins, which represents double the quenching time of the real process, before cooling down at different cooling rates. The tempering temperatures of 520 °C and 630 °C were used with austenitising temperatures of 840 °C and 960 °C respectively, and cooling rates of 0.3 °C/sec, 0.6 °C/sec, 0.9 °C/sec, and 1.2 °C/sec were used with both tempering temperatures, as shown in Figure 3.22.

Since the cooling rate of 0.6 °C/sec was the estimated cooling rate for the sampling position in real product, we used that with austenitising temperatures higher and lower than the previous ones but with the same tempering temperatures of 520 °C and 630 °C.

520 °C was used with austenitising temperatures of 780 °C and 930 °C, whereas 630 °C was used with austenitising temperatures of 900 °C and 1050 °C. The TMC machine was used to perform these tests with all cooling rates.

### 3.6.5.1 The comparison between tempering temperatures of 630 °C and 640 °C

A comparison between tempering temperatures of 630 °C and 640 °C was performed to choose a suitable temperature to improve some mechanical properties, albeit at the expense of other properties, and consequently achieve a good combination of properties. We tried to perform this test on the TMC machine but there was an oscillation of temperature with the heat treatment specimens, because the machine is designed to be more precise with the PSC or axisymmetric specimens. In addition the difference between the two tempering temperatures is not large. Accordingly, the decision was made to be more precise by using a chamber furnace where the temperature can be controlled more easily by using thermocouples.

The three austenitising temperatures of 900 °C, 960 °C and 1050 °C were used with tempering temperatures of 630 °C or 640 °C. The tests were carried out by holding the specimens at temperature of 630 °C or 640 °C for 40 mins then allowing them to cool down to room temperature with a very slow cooling rate inside the furnace. The samples according to the heat treatment conditions of austenitising temperatures, tempering temperatures and different cooling rates are shown in Table 3.3.

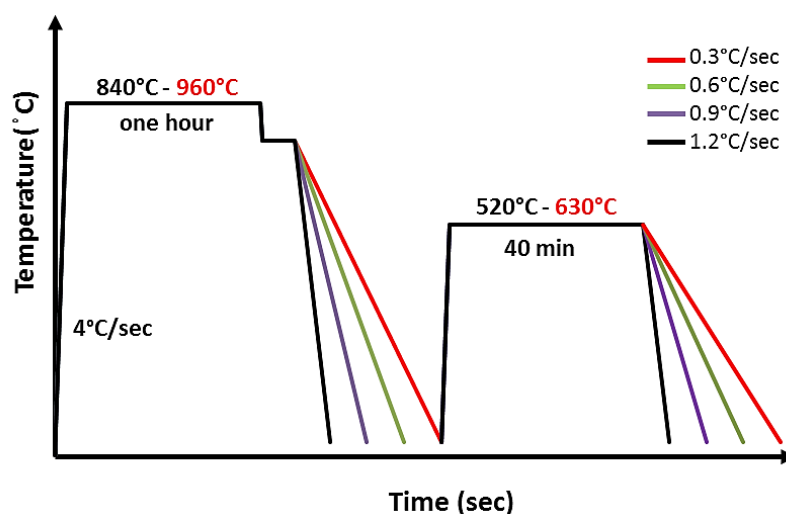


**Figure 3-22** Austenitising temperature followed by tempering temperature profile with using different cooling rates.

**Table 3-3** The samples number according to the heat treatment conditions; austenitising for 1 hr and tempering for 40 mins with different cooling rates. FC (Furnace cooling).

Samples No.	Austenitising temperature (°C)	Tempering Temperature (°C)	Cooling Rate (°C/s)
Sample 1	840	520	0.3
Sample 2			0.6
Sample 3			0.9
Sample 4			1.2
Sample 5	960	630	FC
Sample 6			0.3
Sample 7			0.6
Sample 8			0.9
Sample 9			1.2
Sample 10	780	520	0.6
Sample 11	930		
Sample 12	900	630	
Sample 13	1050		
Sample 14	900	630	FC
Sample 15	1050		
Sample 16	900	640	
Sample 17	960		
Sample 18	1050		

### 3.6.6 Multiple heat treatment processes

In a new step we examined the effect of double heat treatment on the final microstructure to improve the mechanical properties, which are represented primarily in toughness and the UTS. These three processes were doubled and used in different orders to study their influence on grain size refinement.

The double normalizing process is usually used with low alloy steel forged to large dimensions to produce a uniformly fine microstructure to obtain the required properties. Quenching is commonly used to harden steel through producing more martensite within the microstructure. Many studies conducted on some kinds of steel show that when the double

quenching process is used, the prior austenite grain size is refined[276]. The double tempering processes can be useful with some kinds of alloy steels. For instance, it will be of benefit with alloy steels that have a high hardenability and high retained austenite after the first quenching and tempering processes, while tempering will not be needed more than once for steels used to produce large scale products, such as heat treatable alloy steels that form bainite after tempering or that already have a bainitic structure after hardening[277].

Accordingly, a double normalizing, double quenching, and single tempering process was used in this section. In addition, to study all the heat treatment possibilities, the three processes were used in different orders. The TMC machine was used to control the rate of heating, holding and cooling temperatures for heat treatment cycles. These temperatures were controlled using an N-type thermocouple attached to the specimens a near-net shape to the Charpy test specimens. Later we used these specimens to establish the amount of energy that could be absorbed through the Charpy test after each heat treatment process.

#### **3.6.6.1 Cycle 1 (Double normalizing + Quenching + Tempering)**

In the first step of the double heat treatment (cycle 1), as shown in Figure 3.23, we studied the effect of a double normalizing process. This cycle consisted of two normalizing, one quenching, and one tempering process, respectively. The sample was heated to 860 °C which is the normalizing temperature with a rate of 4 °C/sec. Then the sample was held for 20 mins (according to the ratio of 1/2 h/25 mm) before cooling at a very slow rate. 0.6 °C/sec was used to represent the quenching rate as in the sampling position in the real product, whilst furnace cooling was used to represent the air cooling rate. The previous normalizing process was repeated again under the same conditions. The quenching process was started by heating the sample to 860 °C, holding for 20 mins and then cooling to room temperature at a rate of 0.6 °C/sec. The tempering process was the final step in this cycle, where the sample was heated to 640 °C and held for 40 mins (twice the quenching holding time) followed by cooling to room temperature at a rate of 0.6 °C/sec.

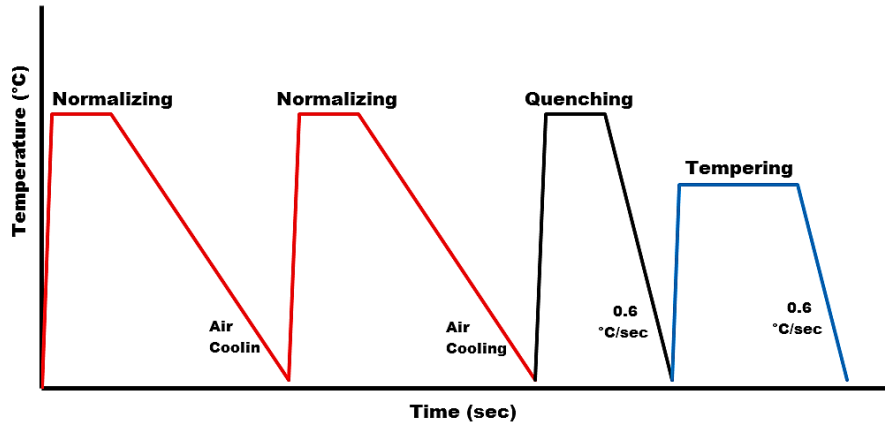


**Figure 3-23** Multiple heat treatment process cycle 1 - double Normalizing followed by Quenching and Tempering process.

### 3.6.6.2 Cycle 2 (Double normalizing + Double quenching + Tempering)

Cycle 2 was the second of the multiple heat treatments, which consisted of double normalizing and double quenching followed by tempering, as shown in Figure 3.24. Both double processes were used in an attempt to produce a more uniformly fine microstructure through double normalizing and also to produce more martensite within the microstructure through double quenching. The normalizing process was performed as earlier, by heating the sample for 20 mins at 860 °C and cooling at the furnace cooling rate. The normalizing process was repeated with the same conditions and then followed by double quenching with a cooling rate of 0.6 °C/sec. As in all cycles, the tempering process was the final step with the sample heated to 640 °C, held for 40 mins and then cooled using the same quenching cooling rate.

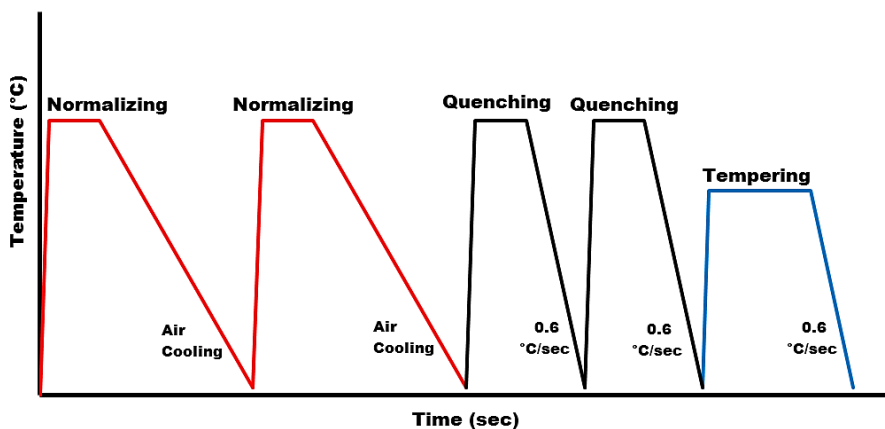


**Figure 3-24** Multiple heat treatment process cycle 2 - double Normalizing followed by double Quenching and one Tempering process.

### 3.6.6.3 Cycle 3 (Normalizing + Quenching + Normalizing + Quenching + Tempering)

In cycle 3 the double normalizing and double quenching processes were used but in a different order. In this step we studied the effect when normalizing and quenching processes were repeated sequentially, as shown in Figure 3.25. The cycle consisted of a normalizing process, where the sample was heated for 20 mins at a temperature of 860 °C and then cooled with a furnace cooling rate tracked by a quenching process with the same normalizing holding time and temperature but with a cooling rate of 0.6 °C/sec. These two processes were repeated and then followed as in previous cycles by a tempering process for 40 mins at a temperature of 640 °C using a cooling rate of 0.6 °C/sec.

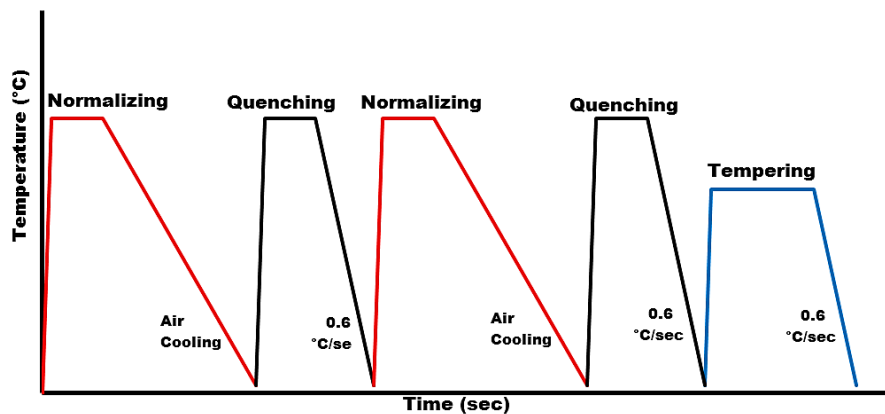


**Figure 3-25** Multiple heat treatment process cycle 3 - double (Normalizing + Quenching) followed by tempering process.

### 3.6.6.4 Cycle 4 (Normalizing + Double quenching + Tempering)

The main purpose of cycle 4 was to study the effect of the double quenching process on the final microstructure in an attempt to improve toughness by increasing the amount of martensite. The cycle, as shown in Figure 3.26, consists of one normalizing, two quenching, and one tempering process, respectively. The normalizing process as previously was started by heating the sample to 860 °C at a rate of 4 °C/sec, held for 20 mins, and tracked by cooling slowly in a furnace. After that two quenching processes were performed sequentially with the same conditions of heating, holding for 20 mins, and cooling to room temperature with a cooling rate of 0.6 °C/sec. Finally, as usual the tempering process was the last step in the heat treatment process, where the sample was heated to 640 °C, held for 40 mins and cooled using the same quenching and cooling rate.

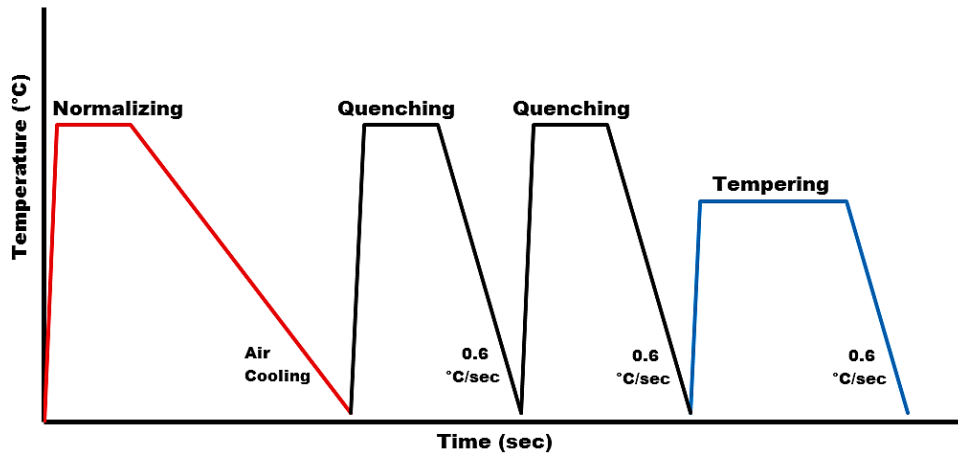


**Figure 3-26** Multiple heat treatment process cycle 4 - Normalizing process followed by double Quenching and one Tempering process.

### 3.7 Metallographic specimen preparation

In this research two types of specimen were used cut from as received material and machined to the appropriate dimensions to investigate two different processes. The standard PSC specimens were used to simulate the forging process and specimens with dimensions of approximately 14 x 14 x 70 mm (subsequently used for a Charpy impact test) were used to simulate the heat treatment process. The same techniques were used with both types of specimen for microstructural investigation and examination using optical or scan electron microscopy.

#### 3.7.1 Sectioning

The two sections that were created to investigate the microstructure are demonstrated in Figure 3.27. The PSC specimens were sectioned parallel to the forging (deformation) direction to expose a surface required for examination, as illustrated in Figure 3.27 (a). That was done when two side shoulders were removed using the Abrasimet cut machine, and the resulting middle deformed section was then cut using an Accutom machine. For the heat treatment specimens approximately 14 x 14 x 2 mm thickness samples were cut from one of the two sides for examination, as illustrated in Figure 3.27 (b).

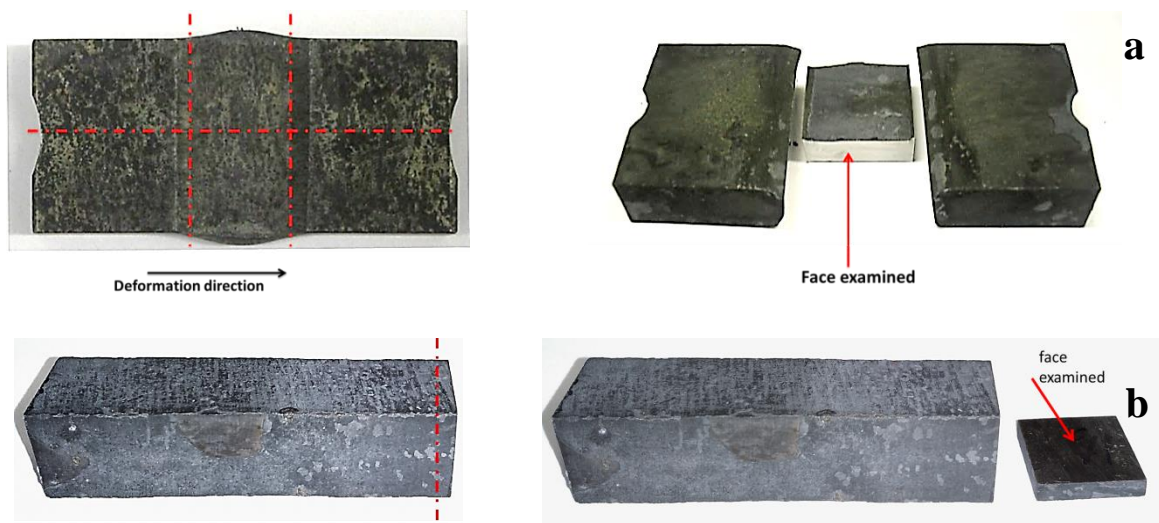


**Figure 3-27** Specimen sectioning (a) PSC specimen. (b) Heat treatment specimen.

### 3.7.2 Grinding, polishing and etching

To prepare the samples that were cut for microstructure analysis, they were first mounted in small discs of bakelite to enable easy handling. The examined surface was subject to a different sequence of operations including grinding, polishing and etching to reveal the microstructure. Finer silicon carbide papers numbered successively from 120 (coarser paper) to 1200 (finer paper) were used to grind the samples. In the last step, to produce a smooth surface, the samples were polished using a cloth covered rotating wheel with a series of 6  $\mu\text{m}$ , 3  $\mu\text{m}$  and 1  $\mu\text{m}$  diamond paste and water based lubricant.

Once the surface of the specimen was ready, etching was used to reveal the microstructure and make the grain boundaries of the metal visible by using an appropriate chemical attack (etchant). In this work two types of etchant were used. The samples that were used for heat treatment with low cooling rates which form martensite-bainite microstructure were etched by immersing the polished surface in Nital 5 % at room temperature several times until the right time was determined, which was 20 to 30 sec. The samples with prior austenite microstructure were etched with picric acid solution after adding two drops of hydrochloric acid and heated to between 75~80  $^{\circ}\text{C}$  to reveal the austenite grain boundaries.



The sample was immersed in the etchant solution for a period of 30 sec to 60 sec. The picric acid solution was swabbed from the surface by rubbing with a piece of cotton wet with soapy water for about 10 sec, washed with water and dried then immediately after covered with alcohol. This process was repeated several times until the grain boundaries were clearly visible. An optical microscope was used to observe the grain boundaries' visibility.

### **3.7.3 Optical microscope**

As soon as the etching was done the samples were ready to investigate the qualitative and quantitative changes that happened in the microstructure after hot deformation or after the heat treatment processes. An optical microscope or light microscope (Polyvar) was used to grab the images and study the surface topography of the specimens. These microscopes uses light and a number of lenses to magnify the images of the samples and show the results directly on a computer screen through coupled software. Digital micrographs received from a microscope camera were used to measure average values of the prior austenite grain size, volume fractions of martensite, analysis and characterization of the impact toughness fracture.

### **3.8 Grain Size Measurement**

The distribution of a variable is a description of the relative numbers of times each possible result will occur in a number of trials. There are several ways of data distribution; the histogram is one of the most common ways. Where the data is usually grouped into bins (intervals) of appropriate size, and plotted as the frequency of each group against the group number. Moreover, the mean grain diameters in all microstructures were measured by using the manual technique of the linear intercept method[278]. Several lines were drawn (on the deformation direction) on the printed image and the lengths and intersections with grain boundaries were noted. These lines were sufficiently spaced so that two adjacent lines did not cross the same grain. After that the real length of the lines was measured by using the scale bar, and then for each line this real length was divided by the number of grain boundaries to get the linear intercept length.

To find mean linear intercept length (a value that tells us the position of the peak, defining the location of the distribution), the linear intercept lengths are summed, and divided by the total number of lines. Finally the collected data are then used to calculate the standard deviation (a value that tells us how broad the peak is; the distribution of the data), which is the most important measure of dispersion. From the standard deviation, the standard error of the mean can be calculated.

Furthermore, the parameter that defines the broadness of the sample means distribution is called the standard error of the sample mean, where there is a link between the standard deviation of the data and the standard error of the sample mean:

$$S(\bar{x}) = \frac{\sigma}{\sqrt{n}} \quad 3-1$$

Higginson and Sellars have shown that the relative standard errors (S) of the mean linear intercept grain size ( $\bar{L}$ ) as well as the number of grains per unit length ( $\bar{N}_L$ ) were

$$\frac{S(\bar{L})}{\bar{L}} = \frac{S(\bar{N}_L)}{\bar{N}_L} \approx \frac{0.65}{\sqrt{n}} \quad 3-2$$

Where n is the number of grains counted. The equations that were used to calculate the grain size diameter and an example for calculation of grain size using the linear intercept method are shown in appendix B.

### 3.9 Scanning electron microscope (SEM)

The microstructures from the as received material and from samples used for Charpy impact tests were imaged by using a JEOL-JSM-6400 scanning electron microscope (SEM) after preparation to observe the areas of interest. An SEM with an operating voltage of 20 kV, spot size of 9, and a working distance of 15 mm was used to provide a high resolution surface imaging for the microstructural investigations. A digital camera was used to record a secondary electron image micrograph. I-Scan associated software, which is capable of acquiring and digitizing images after capture, was used. The high magnification images were stored in an appropriate format.

### **3.10 Energy dispersive X-ray spectroscopy (EDX)**

Energy dispersive X-ray (EDX) microanalysis was used in this study to identify the oxide scales on the surface of specimen cross section. EDX is usually used to obtain the quantitative and qualitative determinations of the elements present in the small selected sample area. After the sample was prepared as for SEM, the JEOL 6400 electron microscope was used for EDX spectroscopy. An X-ray is produced when the sample surface is bombarded with electron beams inside the SEM chamber. The electrons are ejected from the atoms comprising the sample surface where they are received by the X-ray detector to identify and quantify the elemental composition[279]. INCA associated software was used as a microanalysis system.

### **3.11 Mechanical testing**

#### **3.11.1 Hardness test**

Before hardness tests were performed all the specimen surfaces were ground and polished. After that these samples were placed one after another in the hardness testing machine, which consists of a square based pyramidal-shaped indenter made from diamond. Then, after focusing on the surface to make it clear, a 0.3 kg load was applied gently and held in contact for 15 sec. Finally after the load was removed, pyramid diagonals were measured and the Vickers hardness (HV) was calculated. A total of 12 indents were taken from each specimen to obtain statistically meaningful results.

The used hardness testing machine works on Vickers hardness (HV), therefore for comparison with specifications design the results were converted from (HV) to Brinell hardness (HB). Hardness measurements were performed on all specimens for comparison between mechanical properties and microstructure evolution. According to First Subsea specifications design of the manufacturing company, the maximum surface hardness for the material must be greater or equal to 302 HB.

### 3.11.2 Ultimate tensile strength (UTS) calculation:

Several references have shown that the correlation between ultimate tensile strength (UTS) and hardness is represented by the following equation[280, 281]:

$$\text{UTS (MPa)} = k \cdot \text{HB} \quad 3-3$$

Where k is the coefficient and its value ranges between 3.38 and 3.55 for steel[282]. HB is the Hardness and was measured according to Brinnell with a standard indenter and a 3000 kgf load.

### 3.11.3 Charpy impact test

The main purpose of using an impact test is to give an indication of the amount of energy absorbed by the material at fracture[239]. The Charpy impact tests were carried out at a low temperature of -20 °C according to the toughness requirement of the specifications design (DNV and ABS), as shown in Tables 1.1 and 1.2, to investigate the influence of microstructure on low temperature fracture toughness. The requirement of this test is to meet the minimum average required for hardness of 50 J and a minimum single value of 38 J at -20 °C. According to ASTM E32 the standard dimensions for the Charpy impact test are 10x10x55 mm, as seen in Figure 3.28. All tests were carried out in EXOVA TEESSIDE LAB at temperature of -20 °C (see appendix C).

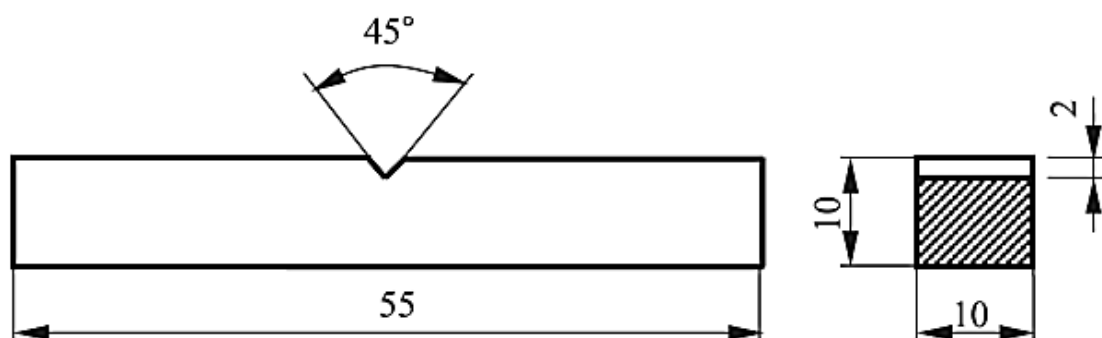


**Figure 3-28** Charpy impact test specimen dimensions.

## Chapter 4 Results of isothermal deformation processes (single hit) in terms of flow behaviour and modelling

Stress-strain curves are a very important graphic for metals, and by using these curves many predictions can be made about the behaviour of a large range of metals under different loading and deformation conditions based on the results obtained from just a small sample. In this chapter the experimental results of isothermal deformation processes (single-hit) in terms of flow behaviour of the 34CrNiMo6 steel obtained from a plane compression testing simulator machine are presented. Furthermore, the flow stress constitutive equations of the work hardening dynamical recovery (DRV) curves and dynamical recrystallisation (DRX) curves were established for 34CrNiMo6 steel and the power law, exponential as well as hyperbolic sine law types of Zener–Hollomon equations were used to determine the hot deformation activation energy ( $Q_{def}$ ). In addition, the constitutive equations were used for modelling and generalising the dynamic recovery (DRV) and dynamic recrystallisation (DRX) of these flow curves.

### 4.1 The austenite grain sizes at different holding times

During hot-working the austenite grain size before deformation is affected by the austenitising temperature and the holding time at that temperature. The curves that represent the relationship between the austenite grain sizes and the different holding times for both austenitising temperatures of 1260 °C and 1100 °C are shown in Figure 4.1. These curves were used to determine the appropriate holding time for both austenitising temperatures. As shown from the Figure, there is a difference between the kinetic relationships of the curves when the same holding times are used.

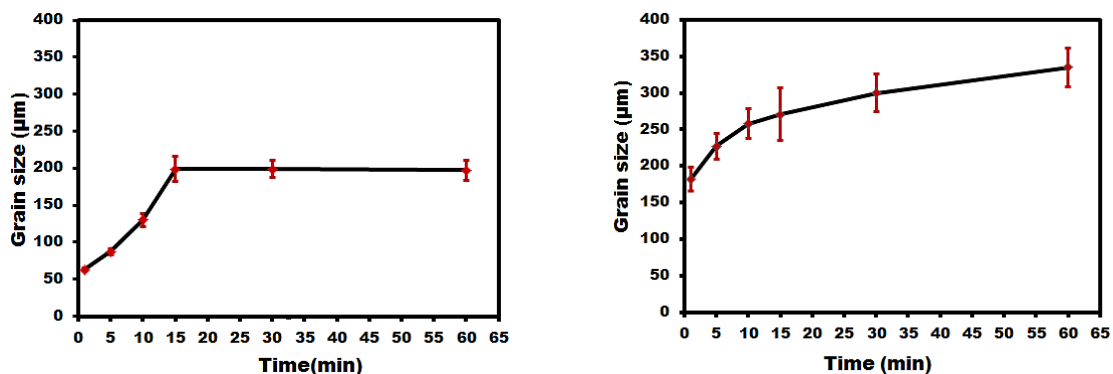


**Figure 4-1** Austenite grain sizes at different holding times for austenitising temperatures of (a) 1100 °C, (b) 1260 °C.

## 4.2 Flow curves at austenitising temperatures of 1100 °C and 1260 °C

Two austenitising and different deformation temperatures were used to investigate the effects of those temperatures on the austenite grain diameter. The microstructure produced by austenitisation and deformation temperatures can influence flow behaviour during subsequent deformation and heat treatment. Typical single hit flow curves for 34CrNiMo6 specimens austenitising at temperatures of both 1260 °C and 1100 °C, maintained at these temperatures for one hour before deformation at different temperatures and strain rates, are shown in Figure 4.2.

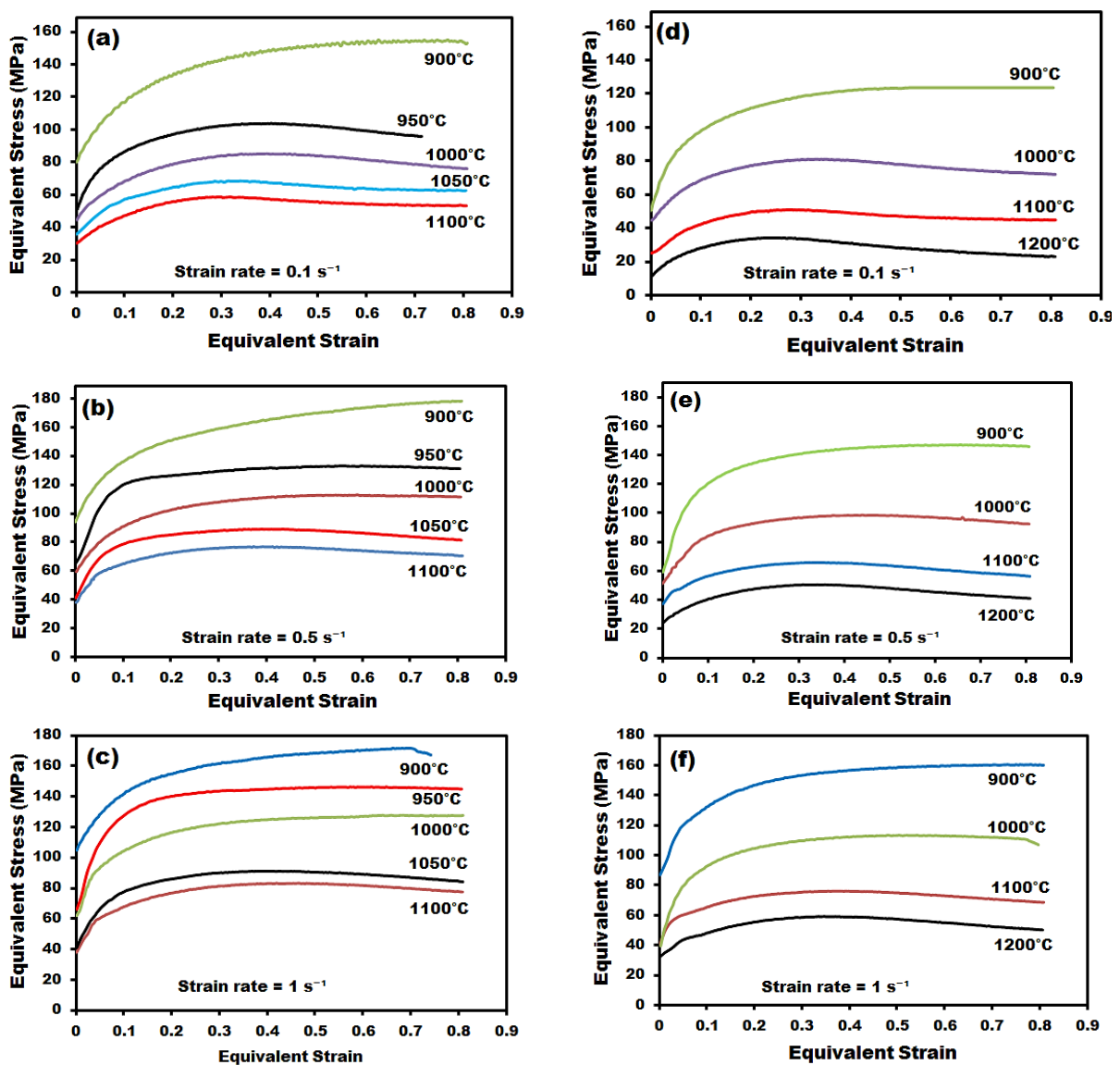


**Figure 4-2** The true stress-true strain curves, after austenitising for one hour [(a, b, c) at temperature of 1100 °C, and (d, e, f) at temperature of 1260 °C] followed by deformation at various temperatures, 0.8 strain and Strain rates of (a, d)  $0.1 \text{ s}^{-1}$ , (b, e)  $0.5 \text{ s}^{-1}$ , and (c, f)  $1 \text{ s}^{-1}$ .

The summary of the peak stress and peak strain with different deformation temperatures and strain rates for austenitising temperatures of both 1100 °C and 1260 °C for all the isothermal deformation testes (single hit) are shown in Table 4.1.

**Table 4-1** Peak stress, and peak strain with different deformation temperatures and strain rates for austenitising temperatures of both 1100 °C and 1260 °C.

Austenitising temperature (C°)	$\dot{\epsilon}$ (s <sup>-1</sup> )	Deformation temperature (C°)	$\epsilon_p$	$\sigma_p$ (MPa)
1260	1	1200	0.34	64
		1100	0.39	76
		1000	0.80	113
		900	0.80	161
	0.5	1200	0.31	56
		1100	0.34	66
		1000	0.44	99
		900	0.80	147
	0.1	1200	0.26	44
		1100	0.28	51
		1000	0.34	81
		900	0.80	124
1100	1	1100	0.42	84
		1050	0.37	91
		1000	0.80	124
		950	0.80	147
		900	0.80	167
1100	0.5	1100	0.37	77
		1050	0.39	90
		1000	0.80	110
		950	0.80	133
		900	0.80	170
	0.1	1100	0.32	57
		1050	0.34	68
		1000	0.44	88
		950	0.40	104
		900	0.80	145

### 4.3 Flow curves at different strains

Strain is one of the other parameters that affects steel microstructure. The true stress–strain curves of the isothermal deformation processes (single hit) austenitised for one hour at temperature of 1260 °C and then cooled to deform at temperature of 1000 °C with strains of 0.4, 0.6, and 0.8 and strain rates of 0.1, 0.5, and 1 s<sup>-1</sup> with each strain, are shown in Figures 4.3. As we can see, some of the flow stress curves have dynamic recrystallisation character with a single peak, where the flow stress increased to a peak and then slightly decreased to a steady state, The others have a recovery recrystallisation character where the flow stress increased to a peak and then increased continuously to reach a steady state in the end.

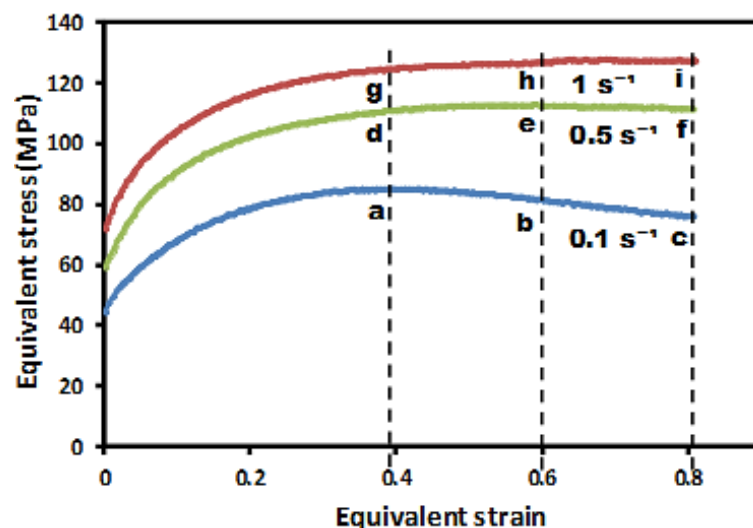


**Figure 4-3** True stress – true strain curves with one hour reheating temperature at 1260 °C and deformed temperature of 1000 °C and strains of 0.4, 0.6, 0.8 with each strain rates of 0.1, 0.5 and 1 s<sup>-1</sup>.

### 4.4 Activation energy and flow stress constitutive equations

Activation energy of deformation ( $Q_{def}$ ) at austenitising temperatures of 1100 °C and 1260 °C was calculated with strain of 0.8, strain rates of 0.1, 0.5, 1 s<sup>-1</sup> and different deformation temperatures. The Arrhenius[72] Eq. 4.1 is widely used to correlate between the flow stress, strain rate and deformation temperature, especially at high deformation temperature [64].

$$\dot{\epsilon} = A f(\sigma) \exp\left(-\frac{Q}{RT}\right) \quad 4-1$$

Also, the influences of strain rate as well as temperature on deformation could be expressed through Zener–Hollomon parameter ( $Z$ ) [283] as shown in Eq. 4.2.



$$Z = \dot{\epsilon} \exp\left(\frac{Q}{RT}\right) \quad 4-2$$

Where  $\dot{\epsilon}$  is strain rate ( $s^{-1}$ ),  $T$  is deformation temperature (K), and  $R$  is the universal gas constant ( $R = 8.314 \text{ J} \cdot (\text{mol} \cdot \text{K})^{-1}$ ).

#### 4.4.1 Flow stress constitutive equations

The Zener–Hollomon Parameter ( $Z$ ) may be regarded as a function of stress, so can be represented mathematically in three types of exponential equation as shown below. The power law description of stress Eq. 4.3 is preferred at lower stress, and the exponential law Eq. 4.4 which is fit when used with high strain rate and low temperature. However, the hyperbolic sine law Eq. 4.5 across the wide range of temperatures and strain rates can be used [284, 285].

$$Z = \dot{\epsilon} \exp\left(\frac{Q}{RT}\right) = f(\sigma) = A' \sigma^n \quad 4-3$$

$$Z = \dot{\epsilon} \exp\left(\frac{Q}{RT}\right) = f(\sigma) = A'' \exp(\beta \sigma) \quad 4-4$$

$$Z = \dot{\epsilon} \exp\left(\frac{Q}{RT}\right) = f(\sigma) = A[\sinh(\alpha\sigma)]^{n'} \quad 4-5$$

Where  $A$ ,  $A'$ ,  $A''$ ,  $n$ ,  $n'$ ,  $\beta$  and  $\alpha$  ( $\alpha \approx \beta/n$ ) are material constants. In many studies, a good approximation between Zener–Hollomon parameter ( $Z$ ) and stress can be obtained from hyperbolic sine law equation, perhaps because it is suitable for a wide range of temperatures and strain rates.

To determine the previous material constants according to the method used in the reference [286], by substitution of  $f(\sigma)$  in the equations 4.3 to 4.5 and taking the logarithm for both sides, the following equations can be derived:

$$\ln \dot{\epsilon} + \frac{Q}{RT} = \ln A' + n \ln \sigma_p \quad 4-6$$

$$\ln \dot{\epsilon} + \frac{Q}{RT} = \ln A'' + \beta \sigma_p \quad 4-7$$

$$\ln \dot{\epsilon} + \frac{Q}{RT} = \ln A + n' \ln[\sinh(\alpha \sigma_p)] \quad 4-8$$

Where  $n$ ,  $\beta$  and  $n'$  are the hot deformation constants. To determine these constants, partial differentiation of Equations 4.6 to 4.8 under the condition of constant temperature were used, that gives the following equations, respectively:

$$n = [\partial \ln \dot{\epsilon} / \partial \ln \sigma_p]_T \quad 4-9$$

$$\beta = [\partial \ln \dot{\epsilon} / \partial \sigma_p]_T \quad 4-10$$

$$n' = [\partial \ln \dot{\epsilon} / \partial \ln [\sinh(\alpha \sigma_p)]]_T \quad 4-11$$

Based on the previous steps, Equation 4.9 was used to get the values of ( $n$ ) from the average of the slopes of the plot  $\ln(\dot{\epsilon})$  against  $\ln(\sigma_p)$ , where the average of the linear regression of these data was 7.1 and 7.8 for austenitising temperatures of 1100 °C and 1260 °C respectively, as shown in Figure 4.4. According to Equation 4.10, the value of ( $\beta$ ) can be obtained from the average of the slopes of the plot  $\ln(\dot{\epsilon})$  against  $(\sigma_p)$ , and the results of average values of linear regression was 0.074 and 0.086 for austenitising temperatures of 1100 °C and 1260 °C, respectively, as shown in Figure 4.5. The value of ( $\alpha$ ) is given from relation of  $\alpha = \beta/n$ , where it was 0.011 for both austenitising temperatures. Equation 4.11 was used to obtain the value of ( $n'$ ) from the average values of the slopes of the plot  $\ln(\dot{\epsilon})$  against  $\ln[\sinh(\alpha \sigma_p)]$ , and the results of the average values were 5.06 and 5.51 for austenitising temperatures of 1100 °C and 1260 °C, respectively, as shown in Figure 4.6.

As shown in the Figures 4.4, 4.5 and 4.6 there are different levels of scattering in data at both austenitising temperatures of 1100 °C and 1260 °C. In all these figures only three data points were used to represent the linear relationships. Where according to the distribution of the data points and since the slope of the lines is the required result from these curves, the relationship should expect to be a linear with high correlation coefficient. In accordance with that, the required data points will be less than those required if the relationship is expected to be non-linear. From the figures at an austenitising temperature of 1100 °C with all the deformation temperatures, and an austenitising temperature of 1260 °C with deformation temperatures of 1200, 1100 and 1000, the scattering in data was too small. whereas at an austenitising temperature of 1260 °C with deformation temperature of 900 °C the scattering in data was a bit bigger in all figures.

Generally, if the number of data points, which used to draw the line of best fit, is small (e.g., three points) random errors should be concerned because it may cause problems during data analysis, thus may leads to a large scatter in the data. In contrast using more data up to six points will allow for the averaging out of these random errors, thus reduce the scattering in data. However, many authors [65, 285, 287, 288] used the three points data to calculate the hot deformation constants that were used in activation energy equations for the different types of steel.

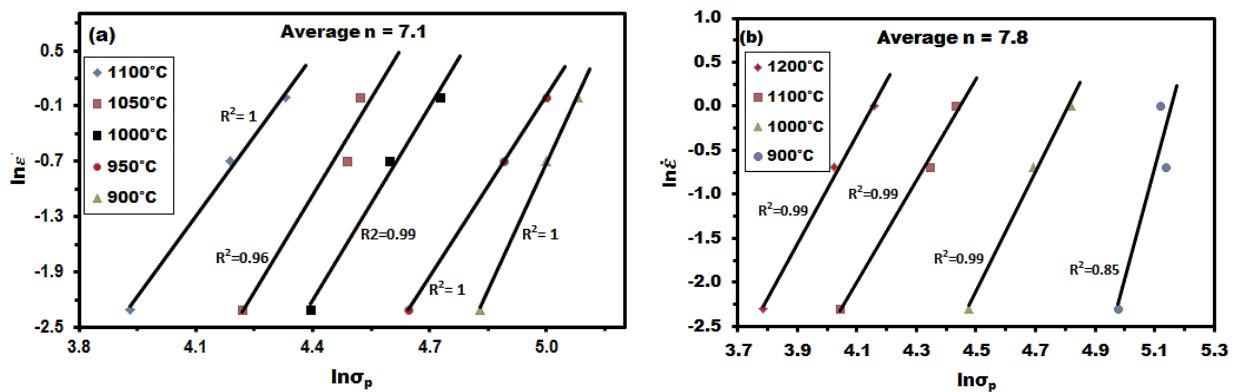


Figure 4-4 Shows plots of  $\ln(\dot{\epsilon})$  versus the  $\ln(\sigma_p)$  that was used for calculation of  $n$  at (a) 1100°C and (b) 1260 °C.

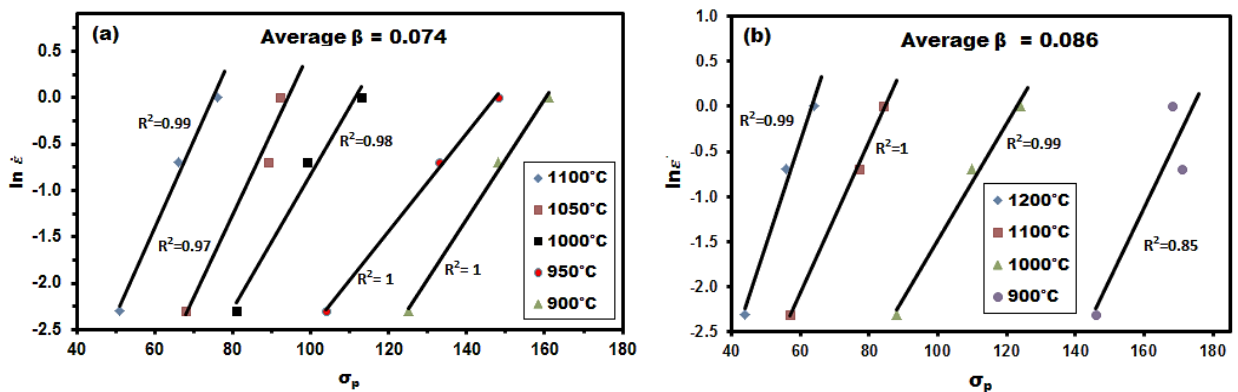


Figure 4-5 Shows plots of  $\ln(\dot{\epsilon})$  versus the  $\sigma_p$  that was used for calculation of  $\beta$  at (a) 1100 °C and (b) 1260 °C.

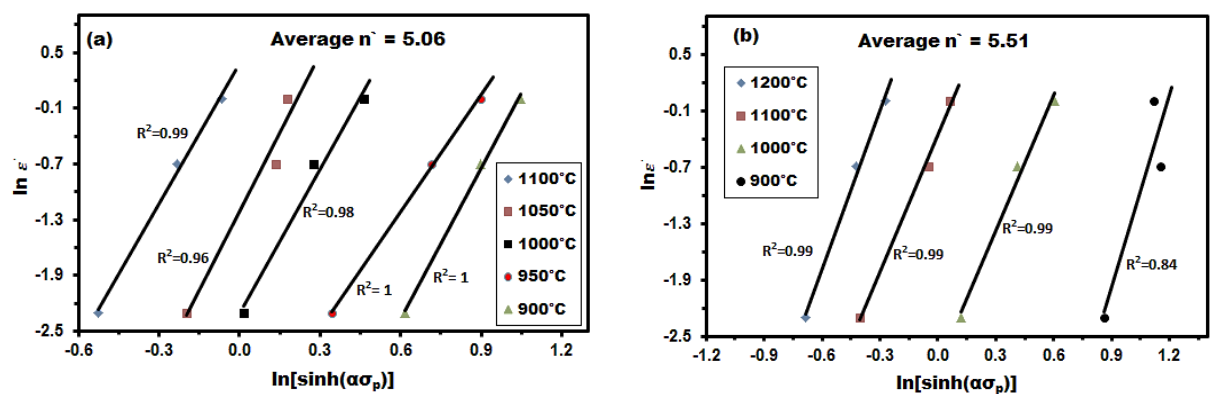


Figure 4-6 Shows plots of  $\ln(\dot{\epsilon})$  versus the  $\ln[\sinh(\alpha\sigma_p)]$  that was used for calculation of  $\hat{n}$  at (a) 1100 °C and (b) 1260 °C.

#### 4.4.2 Calculation of activation energy of deformation

Calculating the correct value of the hot deformation activation energy, according to the same method of references [9, 11] was considered due to the fact that Zener-Hollomon parameter is essentially used in hot working. Partial differentiations of Equations 4.6 to 4.8 under the condition of constant strain rate were used, that give the following equations, respectively:

$$Q = Rn[\partial \ln(\sigma_p) / \partial (1/T)]_{\dot{\epsilon}} \quad 4-12$$

$$Q = R\beta[\partial \sigma_p / \partial (1/T)]_{\dot{\epsilon}} \quad 4-13$$

$$Q = Rn'[\partial \ln[\sinh(\alpha\sigma_p)] / \partial (1/T)]_{\dot{\epsilon}} \quad 4-14$$

Based on these relations, equations 4.12 to 14 were used to obtain the value of (Q) by taking the average of the slopes of the plots of  $\ln(\sigma_p)$ ,  $(\sigma_p)$  or  $\ln[\sinh(\alpha\sigma_p)]$  against  $[1/T(K^{-1})]$  as shown in Figures 4.7 (a-f). A summary of the average values for hot deformation activation energy with three different exponent type equations at two austenitising temperatures are shown below in Table 4.2.

**Table 4-2:** Hot deformation activation energy values

An Exponent Type Equation	Austenitising temperature	
	1100 °C	1260 °C
	Q values (KJ mol <sup>-1</sup> )	
power law	391	411
exponential law	410	446
Hyperbolic sine law	389	400

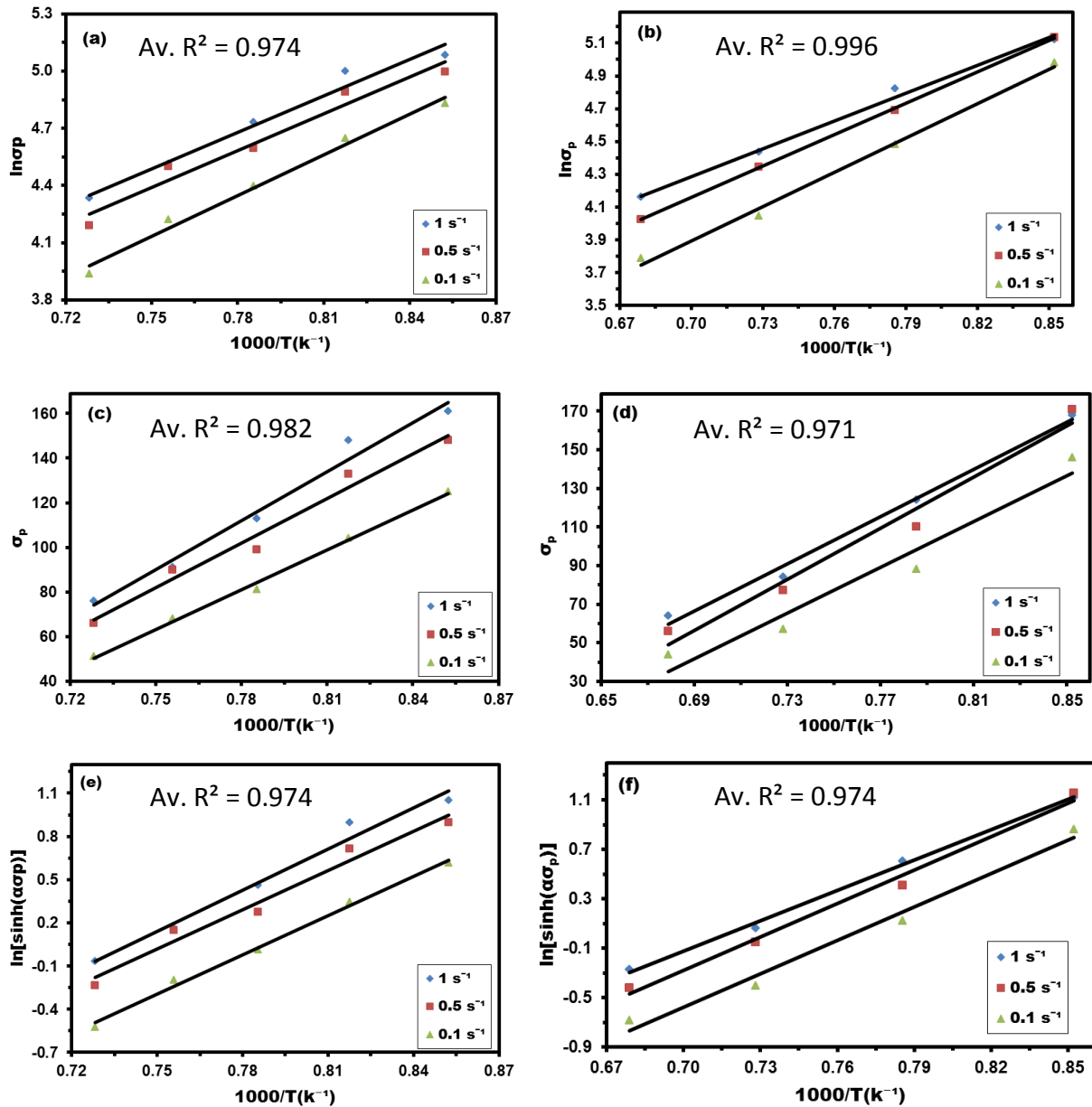


**Figure 4-7** Plots of (a,b)  $\ln \sigma_p$ , (c,d)  $\sigma_p$ , and (e,f)  $\ln[\sinh(\alpha \sigma_p)]$  versus the  $[1/T]$ , where (a, c, and e) are at austenitising temperature of 1100 °C, and (b, d, and f) are at austenitising temperature of 1260 °C.

#### 4.4.3 The Zener–Hollomon Parameter (Z) as a function of stress

The resultant regression equations can be obtained by replacing the values of the material constants and hot deformation activation energy in the previous equations 4.3 to 4.5. The power law, the exponential law, and the hyperbolic sine law resultant regression equations can be seen in Equations 4.15 to 4.17 for austenitising temperatures 1100 °C, and in Equations 4.18 to 4.20 for austenitising temperatures 1260 °C, respectively. According to

that the relationship between (Z) parameter and ( $\sigma_p$ ) may be found, by plotting  $\ln(Z)$  against  $\ln \sigma_p$ ,  $\sigma_p$ , and  $\ln[\sinh(\alpha\sigma_p)]$ , as shown in Figures 4.8 and 4.9.

**Table 4-3:** Material constants and the activation energy for exponential equations at austenitising temperature of 1100 °C

Power law			
A'	n	Q (KJ/mol)	
37.49	7.1	391	
Exponential law			
Ä	β	Q (KJ/mol)	
1.35 x 10 <sup>13</sup>	0.074	410	
Hyperbolic sine law			
A	α	n'	Q (KJ/mol)
1.12 x 10 <sup>15</sup>	0.0105	5.06	389

$$Z = \dot{\epsilon} \exp\left(\frac{391.291}{RT}\right) = A'(\sigma_p)^n = 37.485 (\sigma_p)^{7.086} \quad 4-15$$

$$Z = \dot{\epsilon} \exp\left(\frac{410.212}{RT}\right) = \ddot{A} \exp(\beta \sigma_p) = 1.352 \times 10^{13} \exp(0.074 \sigma_p) \quad 4-16$$

$$Z = \dot{\epsilon} \exp\left(\frac{388.543}{RT}\right) = A[\sinh(\alpha\sigma_p)]^{n'} = 1.123 \times 10^{15} [\sinh(0.0105 \sigma_p)]^{5.062} \quad 4-17$$

**Table 4-4:** Material constants and the activation energy for exponential equations at austenitising temperature of 1260 °C

Power law			
A'	n	Q (KJ/mol)	
4.58	7.82	411	
Exponential law			
Ä	β	Q (KJ/mol)	
4.68 x 10 <sup>13</sup>	0.086	446	
Hyperbolic sine law			
A	α	n'	Q (KJ/mol)
9.93 x 10 <sup>14</sup>	0.011	5.51	400

$$Z = \dot{\epsilon} \exp\left(\frac{411.105}{RT}\right) = A(\sigma_p)^n = 4.58(\sigma_p)^{7.819} \quad 4-18$$

$$Z = \dot{\epsilon} \exp\left(\frac{446.066}{RT}\right) = \tilde{A} \exp(\beta \sigma_p) = 4.68 \times 10^{13} \exp(0.0863 \sigma_p) \quad 4-19$$

$$Z = \dot{\epsilon} \exp\left(\frac{399.910}{RT}\right) = A[\sinh(\alpha \sigma_p)]^n = 9.93 \times 10^{14} [\sinh(0.011 \sigma_p)]^{5.51} \quad 4-20$$

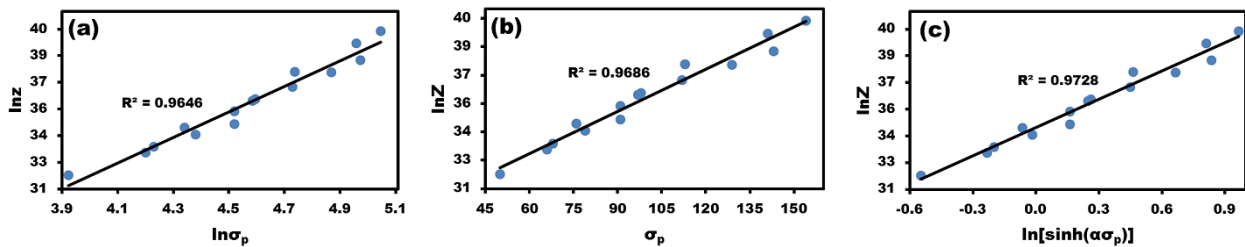


**Figure 4-8** Relations to obtain the resultant regression constant for peak stress ( $\sigma_p$ ) and Z at austenitising temperature of 1100 °C, at (a) Plot of LnZ against  $\text{Ln}\sigma_p$ , (b) Plot of LnZ against  $\sigma_p$  and (c) Plot of LnZ against  $\text{Ln}[\sinh(\alpha\sigma_p)]$ .

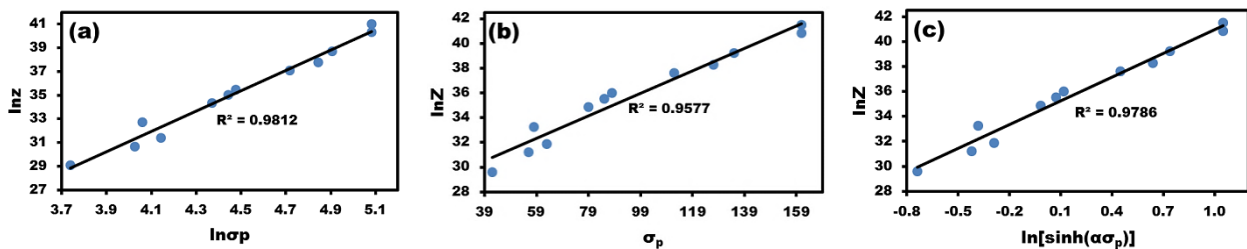


**Figure 4-9** Relations to obtain the resultant regression constant for peak stress ( $\sigma_p$ ) and Z at austenitising temperature of 1260 °C, at (a) Plot of LnZ against  $\text{Ln}\sigma_p$ , (b) Plot of LnZ against  $\sigma_p$  and (c) Plot of LnZ against  $\text{Ln}[\sinh(\alpha\sigma_p)]$ .

#### 4.5 The relation between grain size diameter and the Zener-Hollomon parameter

The main influence factors on the Zener-Hollomon parameter (Z) are the strain rate and deformation temperature, where in the manufacturing process, the equivalent strain rate generally depends on manufacturing equipment. The relationship between the grain size diameter and the natural logarithm of (Z) that results from the isothermal deformation processes (single hit) with one hour holding time at austenitising temperatures of 1100 °C and 1260 °C followed by deformation at different temperatures and different strain rates are shown in Figure 4.10. Strain rates of 0.1, 0.5, and 1 s<sup>-1</sup> were used with all deformation temperatures. Furthermore, as indicated in the Figure 4.10 (b) there was scattering in data at low ln (Z) compared with high ln (Z), and also compared with low ln (Z) at austenitising temperature of 1100 °C.

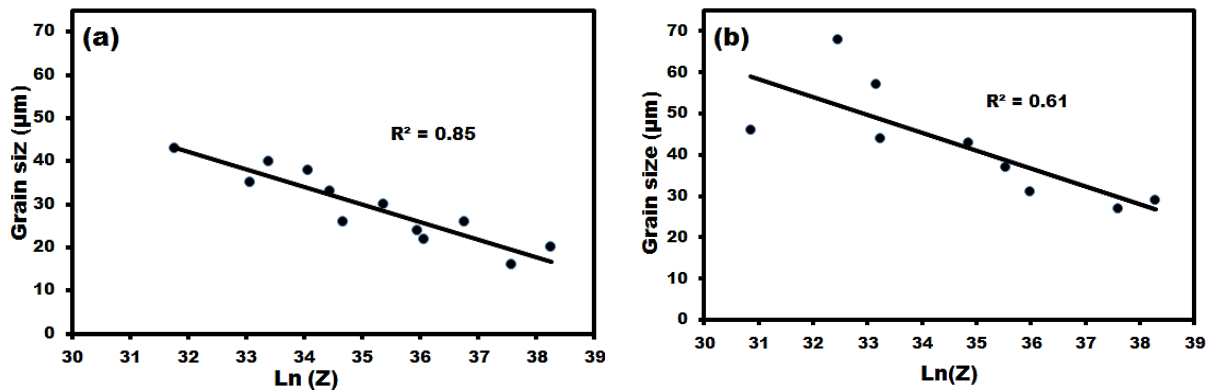


**Figure 4-10** Relationship between grain size diameter and the Ln(Z) in the isothermal processes with one hour austenitising temperature of (a) 1100 °C and (b) 1260 °C, followed by deformation at different temperatures and different strain rates.

#### 4.6 Modelling equations of isothermal stress-strain curves

After the activation energy for hot deformation was calculated, the first stages of constitutive equations were developed into a set of equations that describe continuous curves in terms of engineering variables such as deformation of strain, strain rate and deformation temperature[289]. In addition the constitutive equations were used to model isothermal stress-strain curves of the study steel, using the method proposed by Sellars[72]. As seen in Fig. 4.11, the behaviour of flow curves with deformation at high temperatures can be described by the superposition of two curves. First when just dynamic recovery occurs, the stress–strain curve represents an initial rapid rise in stress as a result of work hardening to a peak stress where then the flow stress curve achieves a steady state value and continues to high strain. This kind of curve can be described by relationship[290, 291].

Stress in the dynamic recovery region( $\varepsilon \leq \varepsilon_c$ ) :

$$\sigma = \sigma_0 + (\sigma_e - \sigma_0)[1 - \exp(-C\varepsilon)]^m \quad 4-21$$

Where  $\sigma_0$  is the maximum stress when  $\varepsilon=0$ ,  $\sigma_e$  is the onset of steady state as illustrated in Fig. 4.11 and C is variable depend on the value of the Zener-Hollomon parameter (Z) were calculated using Eq. (22) as presented by R. LINO [292]. The constant m was measured as 0.5 and is independent of Z[285].

$$C = \frac{1}{\varepsilon_x} \ln \left[ 1 - \left( \frac{\sigma_{\varepsilon_x} - \sigma_0}{\sigma_e - \sigma_0} \right)^{\frac{1}{m}} \right] \quad 4-22$$

$\sigma_{\varepsilon_x}$  is the stress at  $\varepsilon_x$  and  $\varepsilon_x = \varepsilon_p/2$



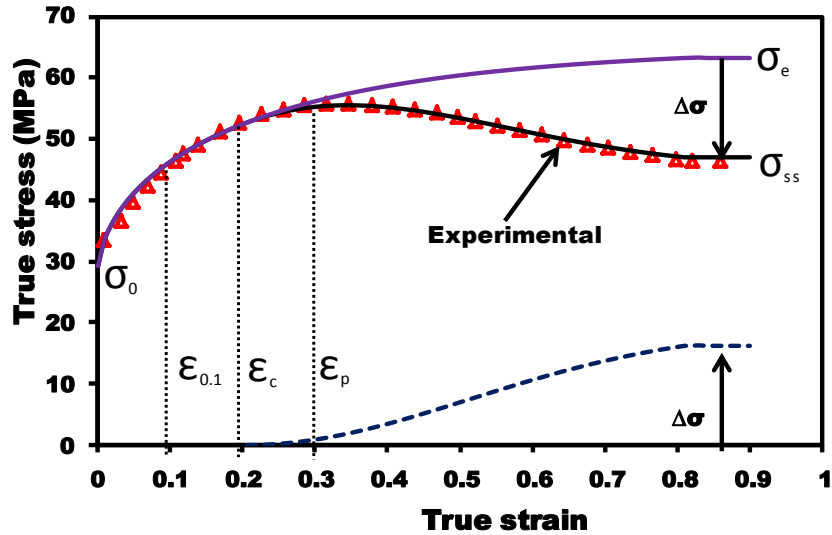


**Figure 4-11** Experimental and calculated stress-strain curves for 34CrNiMo6 steel at deformation temperature of 1200 °C and strain rate of 0.5.

From the stress-strain curves for all samples tested at two austenitising temperatures and different conditions of strain, strain rates and deformation temperatures, just the samples tested at conditions in Table 4.5 indicated the occurrence of DRV. The curves are shown in Figure 4.14.

**Table 4-5** The conditions of samples that indicate the occurrence of DRV.

Austenitising Temperature (°C)	Deformation Temperature (°C)	Strain rate (s <sup>-1</sup> )
1260	1000	1
		0.5
	900	1
		0.5
		0.1
	1100	1000
950		1
		0.5
900		1
		0.5
		0.1

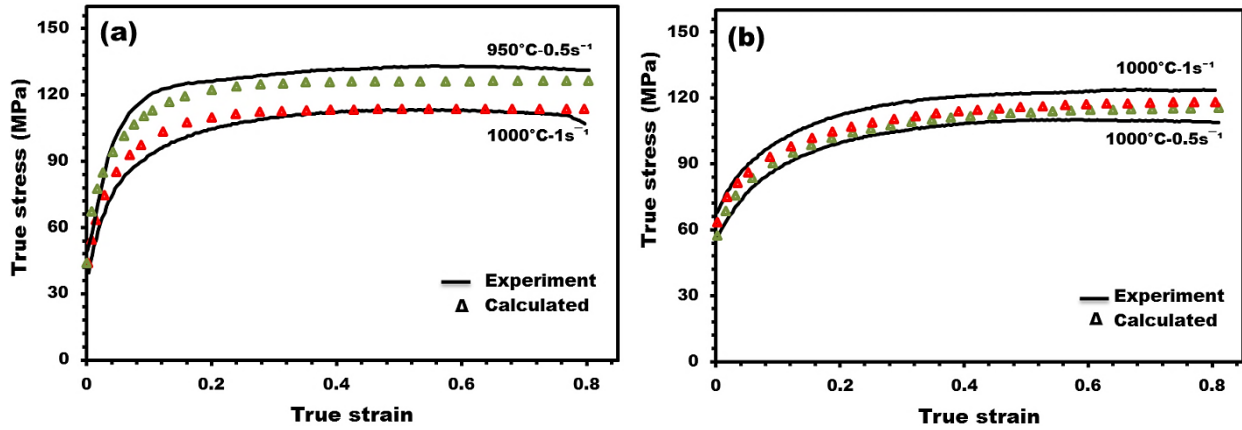


**Figure 4-12** Experimental and calculated stress-strain curves (DRV) at different strain rates, deformation temperature and austenitising temperature of (a) 1100 °C and (b) 1260 °C.

The second case is when the effects of dynamic recrystallisation are combined in the calculations. The flow curve represents two different regions, work hardening to a peak stress followed by decrease in stress when dynamic recovery and dynamic recrystallisation simultaneously occurs which gives an additional softening, and then the curve settles down to a steady state value. The dynamic softening part of the stress-strain curve can be described by using Avrami [290, 292, 293] equation in terms of strain.

Stress in the dynamic recovery and dynamic recrystallisation region ( $\varepsilon \geq \varepsilon_c$ )

$$\Delta\sigma = (\sigma_e - \sigma_{ss}) \left[ 1 - \exp\left(-k \left(\frac{\varepsilon - \varepsilon_c}{\varepsilon_p}\right)^{m'}\right) \right] \quad 4-23$$

As seen in Figure 4.11,  $\sigma_{ss}$  is the onset of steady state conditions,  $\varepsilon_p$  is the peak strain, and  $\varepsilon_c$  is the critical strain[285].  $k$  is a constant and  $m'$  is Avrami coefficient.

$$X = 1 - \exp\left[-k \left(\frac{\varepsilon - \varepsilon_c}{\varepsilon_p}\right)^{m'}\right] \quad 4-24$$

The fraction of dynamic recrystallisation is defined as  $X = \frac{(\sigma_e - \sigma)}{(\sigma_e - \sigma_{ss})}$  and  $\varepsilon_c = 0.6 \varepsilon_p$

From the relationship of  $\ln(\ln(1/(1-X)))$  vs  $\ln((\varepsilon - \varepsilon_c)/\varepsilon_p)$  for each test data the values of  $k$  and  $m'$  can be found.

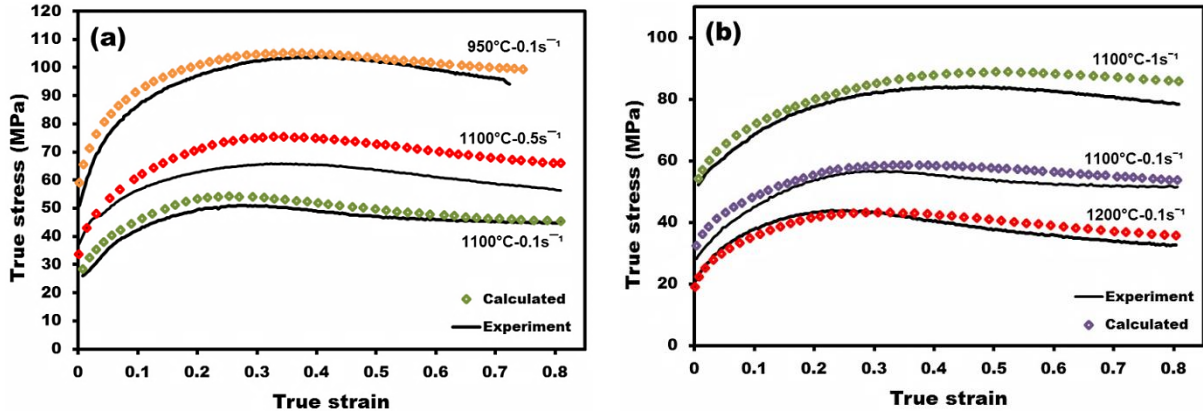


**Figure 4-13** Experimental and calculated stress-strain curves (DRX) at different strain rates, deformation temperature and austenitising temperature of (a) 1100 °C and (b) 1260 °C.

#### 4.6.1 Verification of the constitutive modelling equation:

As can be seen, Fig. 4.13 indicates a good agreement between experimental and predicted flow stresses data for austenitising temperatures of both 1100 °C and 1260 °C. Consequently, to assess and verify the predictability and accuracy of the constitutive equations parameters such as correlation coefficient (R) could be used. R is commonly used as a statistical parameter and provides information about the strength of the linear relationship between experimental and calculated data. However, the higher values of R may not necessarily always indicate better performance of the model, because the tendency of the model could be biased towards higher or lower values[294]. Therefore the average absolute relative error (AARE), which is an unbiased statistical parameter for determining the predictability of the equation, has been found to give a more appropriate assessment as well as comparison of various models[295, 296]. Correlation coefficient (R) and average absolute relative error (AARE) were used and expressed as the following equations:

$$R = \frac{\sum_{i=1}^N (E_i - \bar{E})(P_i - \bar{P})}{\sqrt{\sum_{i=1}^N (E_i - \bar{E})^2 (P_i - \bar{P})^2}} \quad 4-25$$

Average absolute relative error (AARE)

$$AARE (\%) = \frac{1}{N} \sum_{i=1}^N \left| \frac{E_i - P_i}{E_i} \right| \times 100 \quad 4-26$$

Where  $E$  is the experimental data and  $P$  is the predicted value by the constitutive equation.  $\bar{E}$  and  $\bar{P}$  are the mean of  $E$  and  $P$ , respectively.  $N$  is the number of total data used in the study.

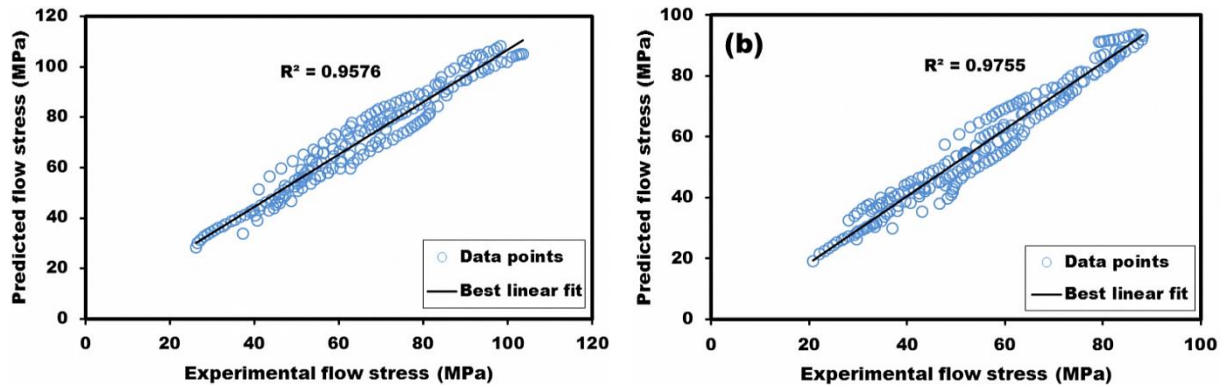


**Figure 4-14** Correlation between experimental and calculated flow stresses data at strain rates of 0.1, 0.5  $1\text{ s}^{-1}$ , different deformation temperature and austenitising temperature of (a) 1100 °C and (b) 1260 °C.

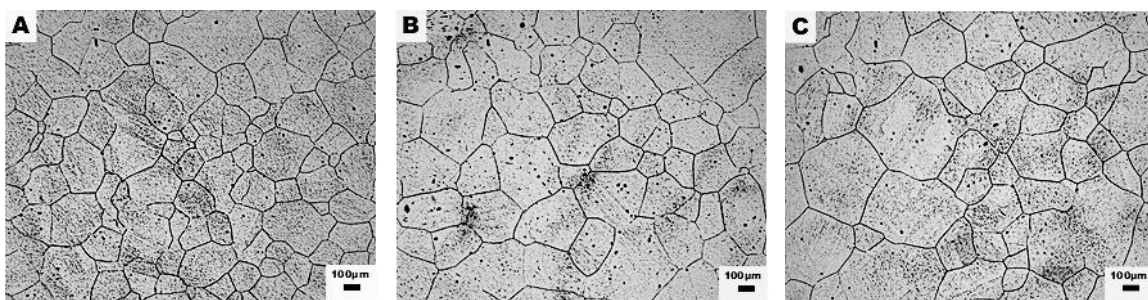
The experimental and calculated flow curves of 34CrNiMo6 steel at strain rates of 0.1, 0.5, and 1  $\text{s}^{-1}$ , different deformation temperature and austenitising temperature of 1100 °C and 1260 °C are shown in Fig. 4.14.

## Chapter 5 Results of isothermal deformation processes (single hit) in terms of microstructures

In this chapter the experimental results of isothermal deformation processes (single-hit) in terms of microstructure obtained from a plane compression testing simulator machine are presented. For examination of the prior austenite microstructure the deformed samples were water quenched after performing the deformations at the specific deformation temperatures as explained before. The reason of this procedure was to quantify and evaluate the prior austenite behaviour in terms of recrystallisation and grain growth under different processing conditions of temperatures, strain and strain rates.

### 5.1 Austenite grain sizes at different holding times

The microstructures of the prior austenite grain size held for times of 1, 5, 10, 15, 30, and 60 mins at austenitising temperatures of both 1260 °C and 1100 °C followed by quenching in water are shown in Figures 5.1 and 5.2, respectively. The linear intercept method was used to measure the prior austenite grain size. The austenite grain size increases as the austenitising temperature and holding time increase. The prior austenite microstructures at austenitising temperatures of 1100 °C have moderately fine and uniform austenite grains, while at austenitising temperatures of 1260 °C the majority of grains are larger with more coarse grains present.



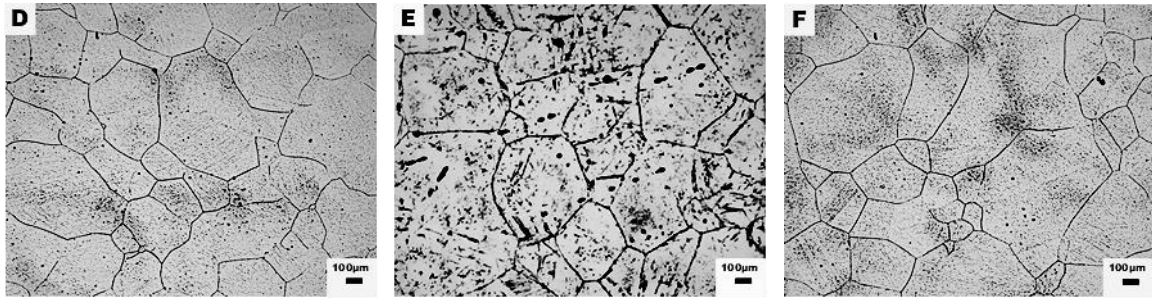


**Figure 5-1** Variation of austenite grain size at austenitising temperature of 1260 °C held for different times: (a) 1 mins, (b) 5 mins, (c) 10 mins, (d) 15 mins, (e) 30 mins, and (f) 60 mins, followed by water quench (5X).

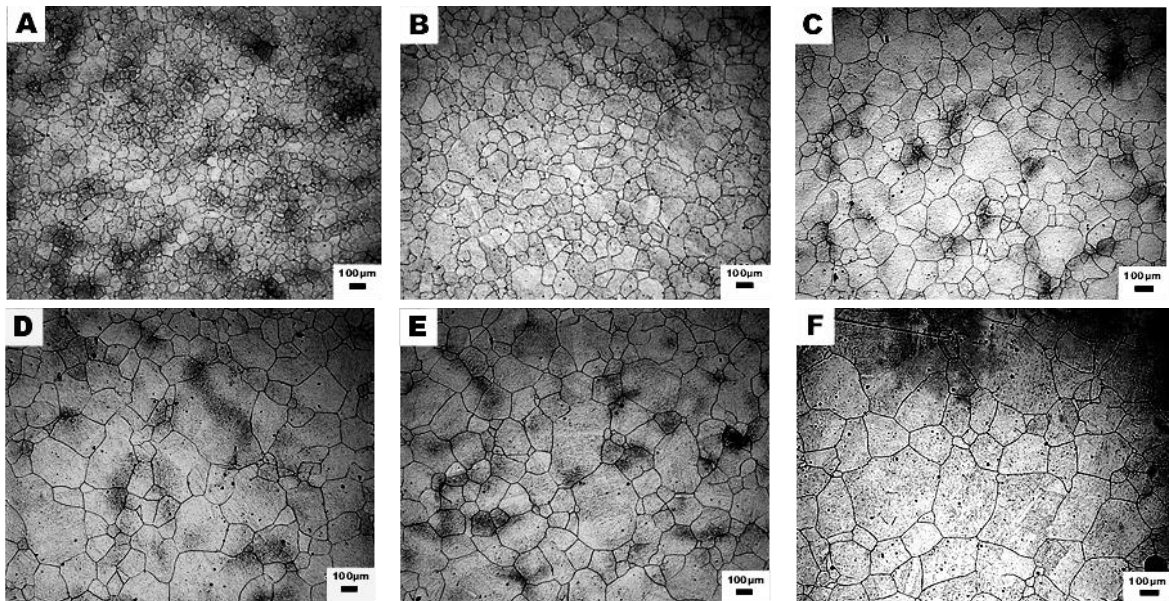


**Figure 5-2** Variation of austenite grain size at austenitising temperature of 1100 °C held for different times: (a) 1 mins, (b) 5 mins, (c) 10 mins, (d) 15 mins, (e) 30 mins, and (f) 60 mins, followed by water quench (5X).

## 5.2 The optical microstructure at austenitising temperatures of 1260 °C and 1100 °C

The prior austenite microstructures following austenitising at temperatures of 1260 °C and 1100 °C for one hour, cooling to the required temperature for deformation, and then water quenching are presented in Figures 5.3 and 5.4. Different deformation temperatures were used and the conditions of 0.8 strains and 1, 0.5, 1 s<sup>-1</sup> were used with each deformation temperature. The microstructure at austenitising temperature of 1260 °C and different deformation conditions was used to simulate the real process and to try to optimize the thermo-mechanical process, whereas the microstructure at austenitising temperature of 1100 °C was to attempt to refine the austenite grain size and to study the effect of changing the austenitising temperature on the resulting microstructure.

Furthermore, as can be seen, the percentage of recrystallisation became smaller as the deformation temperature dropped close to 900 °C especially with an austenitising temperature of 1260 °C. Moreover, the presented images of the microstructures for both austenitising temperatures of 1100 °C and 1260 °C show clear banding in the longitudinal direction, and non-uniform grain size distributions i.e., the grains in the same image have different sizes. These aspects are also important and affect the critical material properties such as strength and toughness and considered not less important than other aspects like grain size refinement.

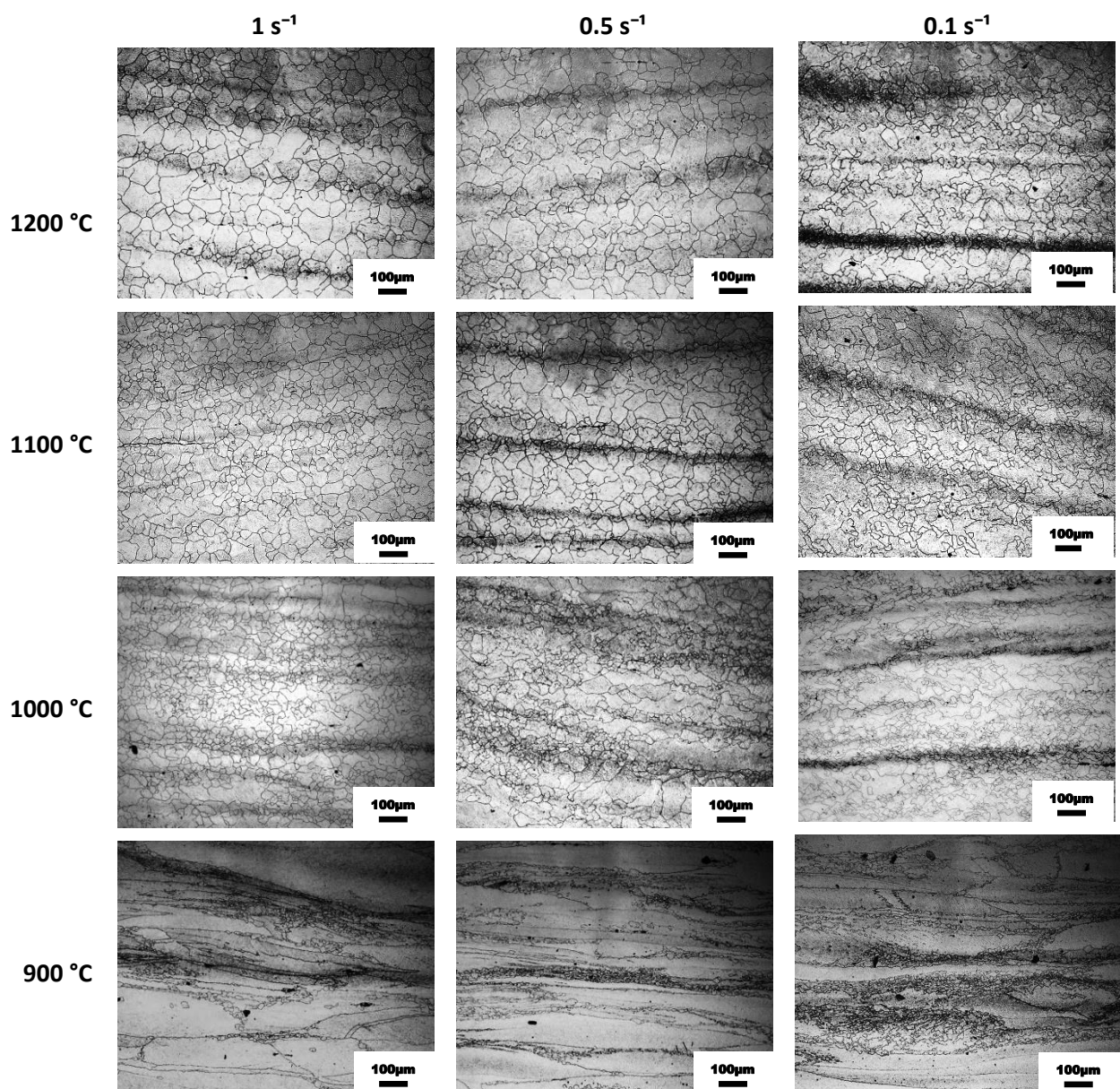


**Figure 5-3** Variation of austenite grain size after austenitising for one hour at temperature of 1260 °C and deformation at different temperatures and different strain rates followed by water quench (10X).

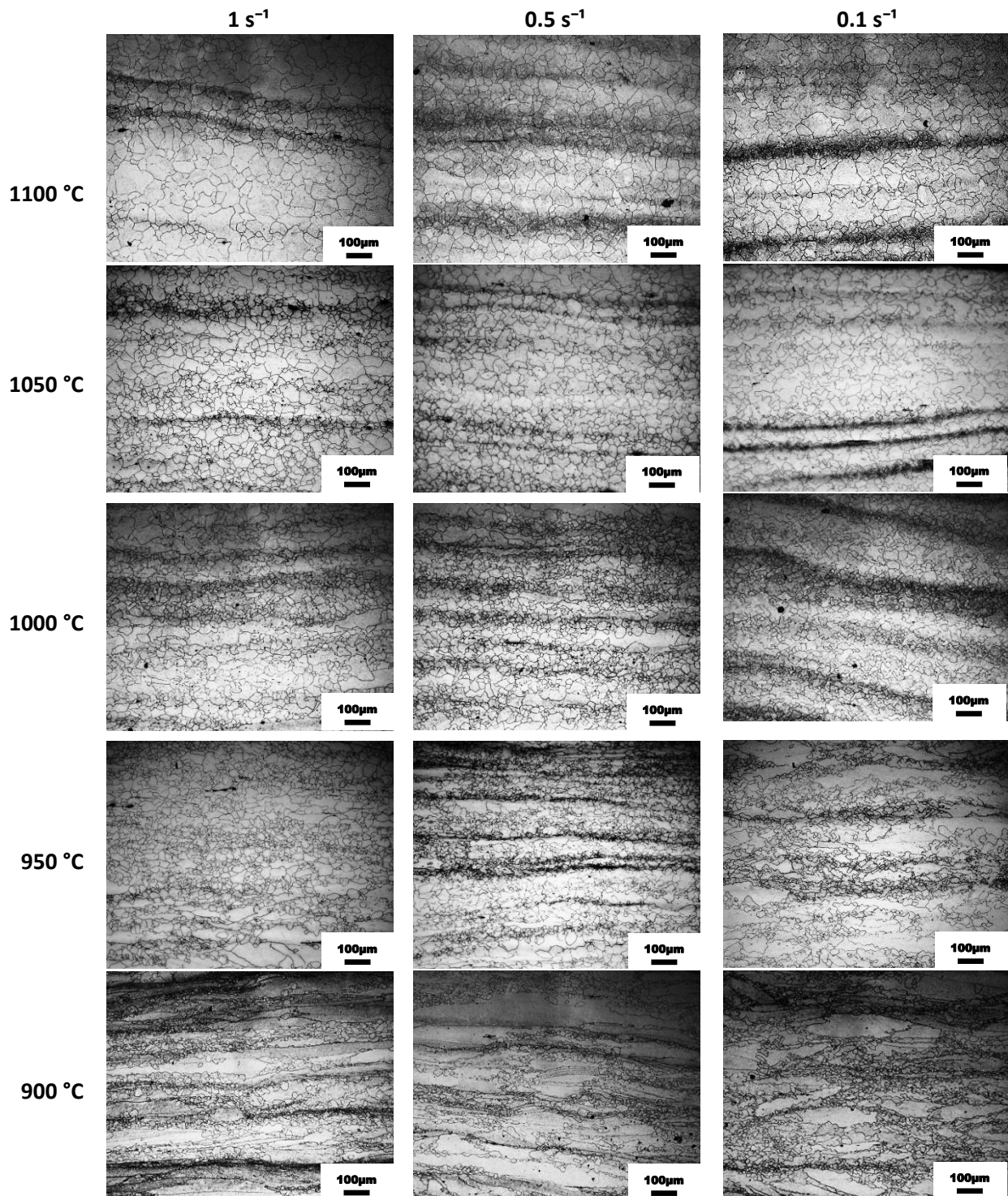


**Figure 5-4** Variation of prior austenite grain size after austenitising for one hour at temperature of 1100 °C and deformation at different temperatures and different strain rates followed by water quench (10X).

The austenite grain size distributions at conditions of austenitising temperatures of 1100 °C with deformation of 1100 °C and austenitising temperature of 1260 °C with deformation temperature of 1200 °C are shown in Figure 5.6. The strain rates of 0.1, 0.5, and 1 s<sup>-1</sup> were used with each deformation temperature.



### 5.3 The relation between grain size diameter and deformation temperatures

The relationship between deformation temperatures and grain size diameters resulting from temperatures with change of strain rate at austenitising temperatures of 1100 °C and 1260 °C are shown in Figure 5.5 (a) and 5.5 (b), respectively. The grain size diameters at the same deformation temperature and different strain rates are almost convergent at all deformation temperatures.

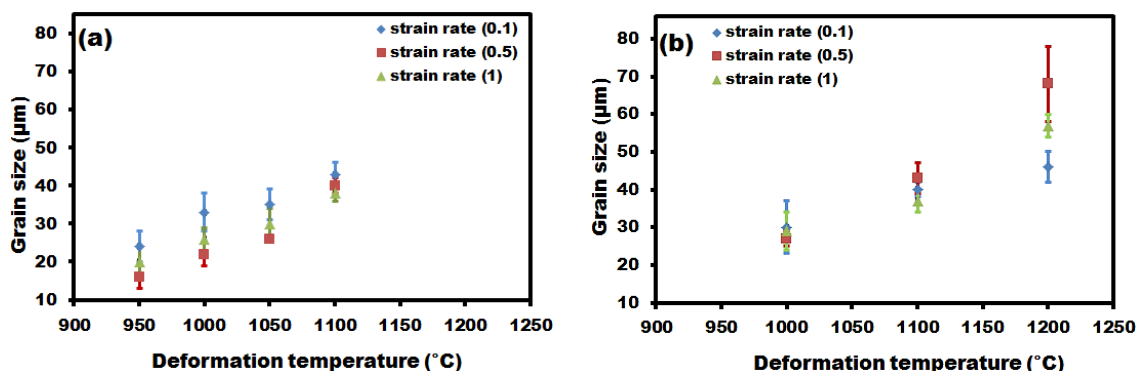
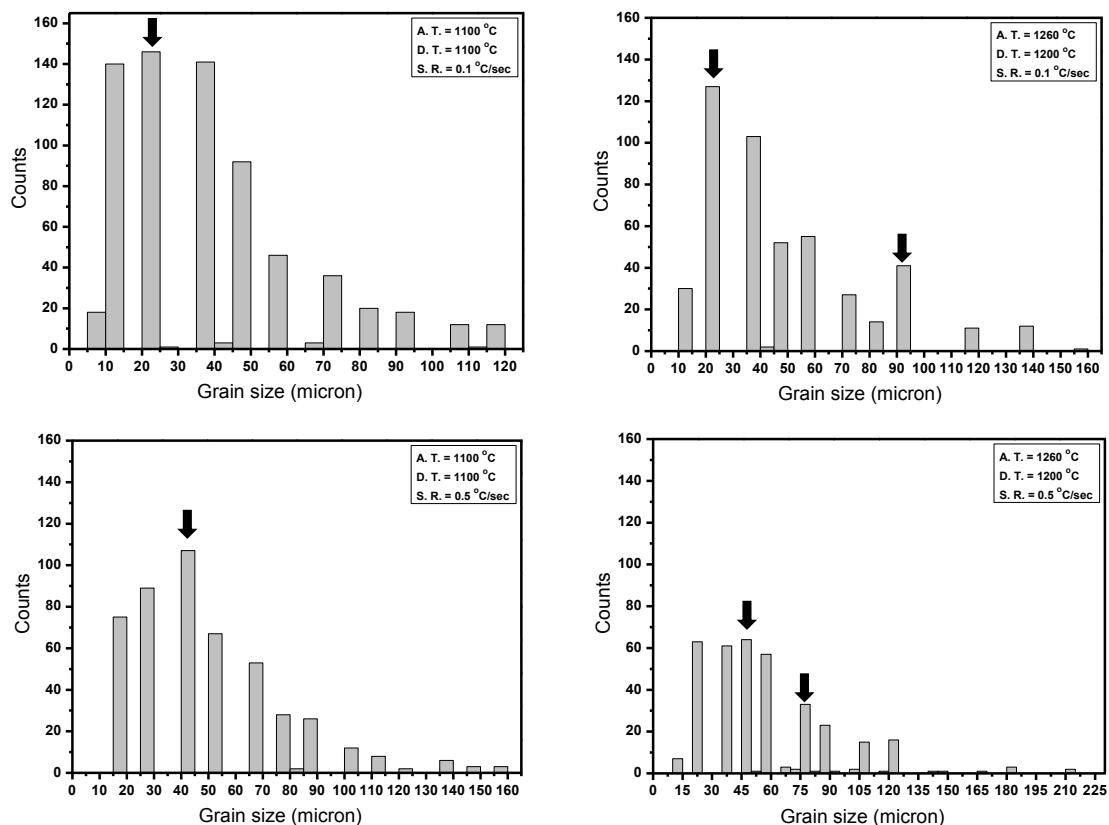
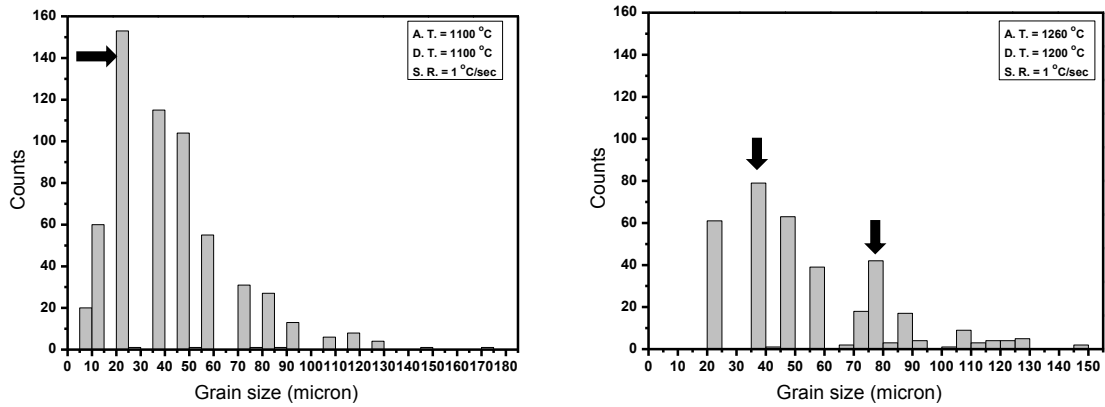


Figure 5-5 The relation between grain size and deformation temperatures at austenitising temperature of (a) 1100 °C, (b) 1260 °C.





**Figure 5-6** The austenite grain size distributions at conditions as shown next to the each graph.  
 A. T. = Austenitising temperature, D.T. = Deformation temperature, S. R. = Strain rate

#### 5.4 The optical microstructure at different strains

The optical micrograph of samples deformed at 1000 °C after soaking for one hour at austenitising temperature of 1260 °C with strains of 0.4, 0.6, 0.8 and strain rates of 1, 0.5, and 0.1 s<sup>-1</sup> with each strain are shown in Figure 5.7. From the resulting microstructure, when different strains were used the highest percentage of recrystallisation was obtained at higher strains with all strain rates.

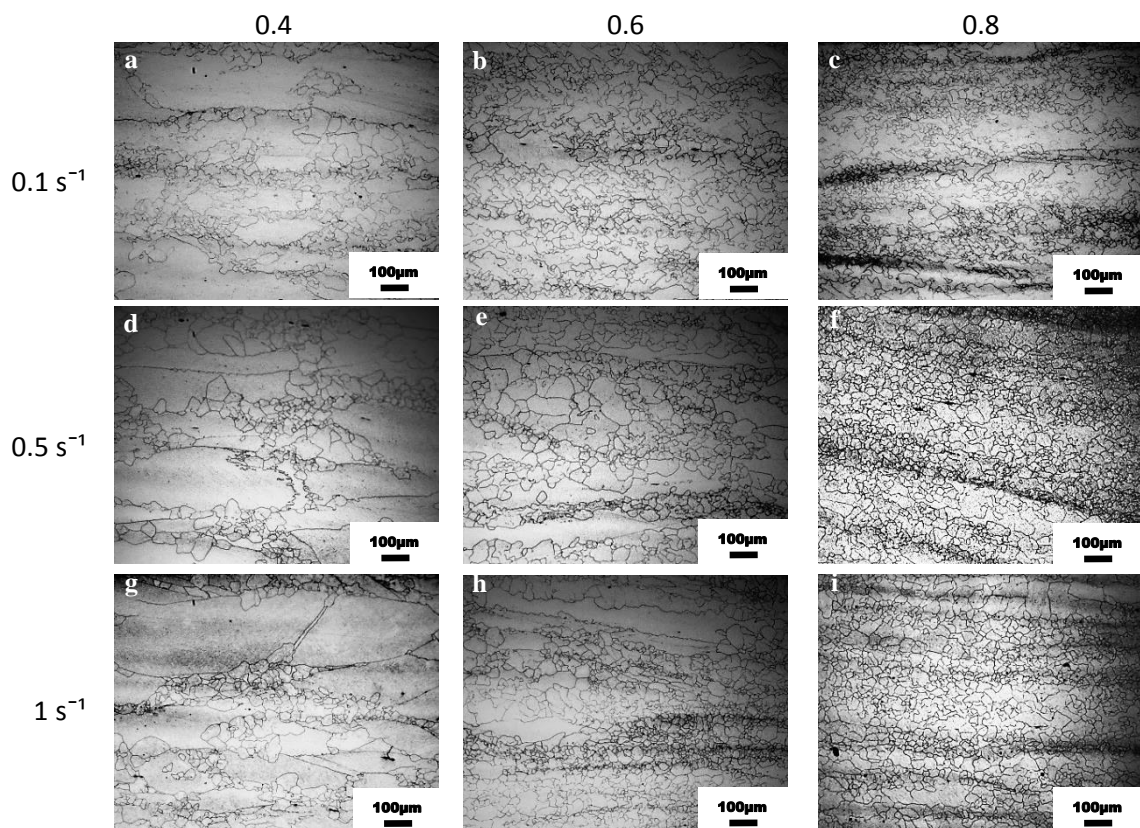


**Figure 5-7** Optical micrograph of samples deformed at 1000 °C after soaking for one hour at 1260 °C, with strain of (a, d, g) 0.4, (b, e, h) 0.6, (c, f, i) 0.8 with strain rates of 1, 0.5, and 0.1 s<sup>-1</sup> (10X).

## Chapter 6 Results of non-isothermal deformation processes (multi hit)

The non-isothermal deformation process was applied to simulate the real forging process through the multi hits deformation at different strain accumulation, strain rate and different deformation temperatures. This process was used to study the prior austenite behaviour and its effect on the evolution of the final transformed microstructure. Furthermore, the multi-hits process was used for comparison with the single-hit deformation process as well as to discover if there are any other factors that can affect the prior austenite grains, such as static and dynamic recrystallisation, when the multi-hits process is applied.

### 6.1 Non-isothermal deformation (Four hits)

This section displays the stress-strain flow curves and the final microstructures that were obtained from typical PSC test samples after being subjected to multi-hits forging under the non-isothermal condition. Typical multi hit flow curves for 34CrNiMo6 steel specimens austenitised at temperatures of 1260 °C and 1100 °C and maintained at these temperatures for one hour prior to deformation at different temperatures are shown in Figure 6.1. The deformation temperature set of 1200 °C, 1100 °C, 1000 °C, and 900 °C was used respectively prior to austenitising for one hour at 1200 °C, and the deformation temperature set of 1100 °C, 1000 °C, 950 °C, and 900 °C also was used respectively after austenitising for the same time at 1100 °C. The deformation conditions of 0.5 s<sup>-1</sup> strain rate and the total strain of 0.8 (0.2 strains at each single deformation hit) were used with each set of deformation temperatures.

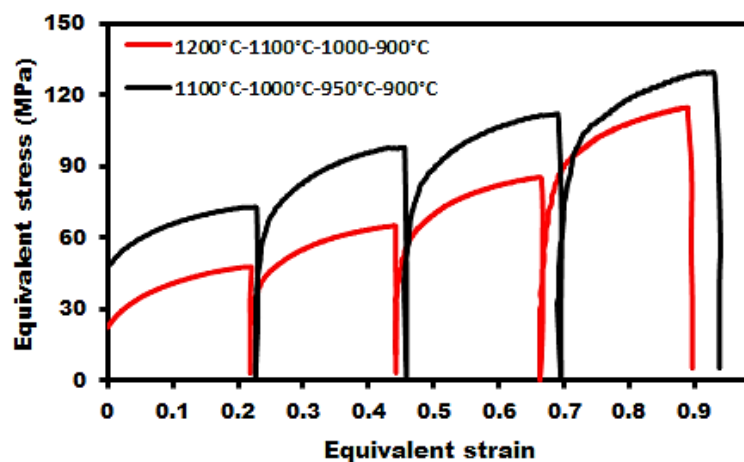


**Figure 6-1** Presents the flow curves for a non-isothermal deformation process using 4 hits at different temperatures after being held for one hour before deformation at temperatures of 1100 °C and 1200 °C, and quenching following the final deformation.

From the flow curves that shown in Figure 6.1, different strains in each step are shown in both curves. As can be seen this difference was small at first hit in both cases and it is increasing as the hits increases, where become bigger in the last hit. Generally, these differences should not be occurred and the equivalent strains should be the same for both non-isothermal tests.

To reveal the prior austenite microstructure throughout the thermo-mechanical processing in these experiments, the deformed specimens were quenched in water directly after the completion of deformation at the specified temperatures. The prior austenite grain diameter was measured by the linear intercept method. As can be seen in Figure 6.2 the microstructure with austenitising temperature of 1100 °C and deformation temperatures of 1100 °C, 1000 °C, 950 °C, and 900 °C has moderately fine and uniform prior austenite grains, in contrast to the structure with austenitising temperature of 1200 °C and deformation temperatures of 1200 °C, 1100 °C, 1000 °C, and 900 °C, where the grains are larger and heterogeneous.

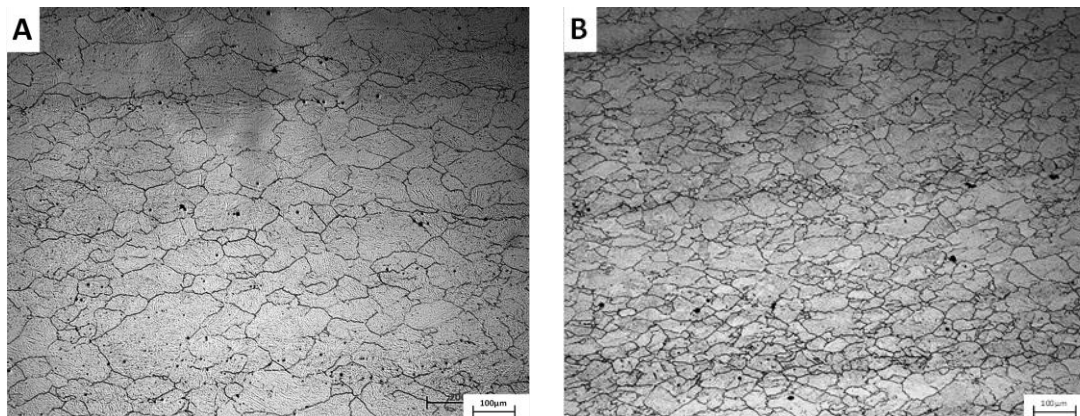


**Figure 6-2** Optical micrograph of four hits of non-isothermal samples. (A) Austenitising for one hour at 1200 °C and deformed at temperatures of 1200 °C, 1100 °C, 1000 °C, and 900 °C, (B) Austenitising for one hour at 1100 °C and deformed at temperatures of 1100 °C, 1000 °C, 950 °C, and 900 °C. (10X Magnification)

## 6.2 Non-isothermal deformation (Three hits)

Based on some of the results that were obtained from the isothermal deformation process at 900 °C, the three-hits of non-isothermal deformation processes were aimed to investigate if 900 °C is the re-crystallisation stop temperature. Accordingly, the four-hit tests were repeated after excluding the deformation at temperature 900 °C to determine the difference in grain size. Figure 6.3 shows the equivalent stress-strain curve for typical three-

hits of deformation tests for the deformation temperature set 1200 °C, 1100 °C and 1000 °C respectively after austenitising for one hour at 1200 °C and deformation temperature set of 1100 °C, 1000 °C and 950 °C respectively after austenitising for the same time at 1100 °C. The 0.5 s<sup>-1</sup> strain rate and the total accumulation strain of 0.6 (0.2 strains at each single deformation hit) were used with each set of deformation temperatures.

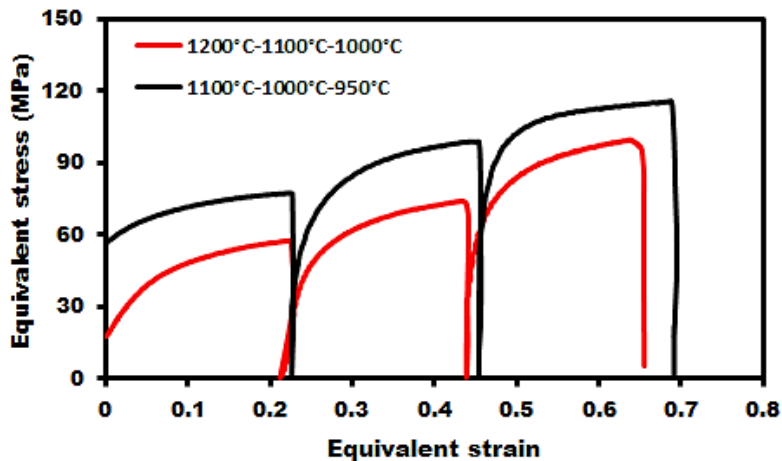


**Figure 6-3** Presents the flow curves for a 3 hits of non-isothermal deformation processes, which was held for one hour before deformation and quenching following the final deformation.

As in the case of four hits, the flow stress curves in Figure 6.3 (three hits) also show different strains in each step. This difference as can be seen from the figure was very small at first hit especially at austenitising temperature of 1200 °C, where it accumulates to become bigger in the last hit in both curves. Furthermore, to study all the possibilities such as static recrystallisation between the deformation temperature of 1000 °C and 900 °C with the austenitising temperature of 1200 °C, and between the deformation temperature 950 °C and 900 °C with the austenitising temperature of 1100 °C, the three-hit deformation processes at the same conditions was repeated with two additional cases. Figure 6.4 shows the optical micrograph for the three-hit deformation tests at three different conditions. Microstructures A and B in this figure represent the three-hit test followed directly by quenching in water, whereas microstructures C and D represent the three-hit followed by holding for 60 sec prior to quenching in water. The microstructures E and F represent the three-hit followed by cooling to 900 °C in 60 sec before quenching in water. The microstructures A, C and E were performed at austenitising temperature 1200 °C, while the microstructures B, D and F were performed at austenitising temperature 1100 °C.

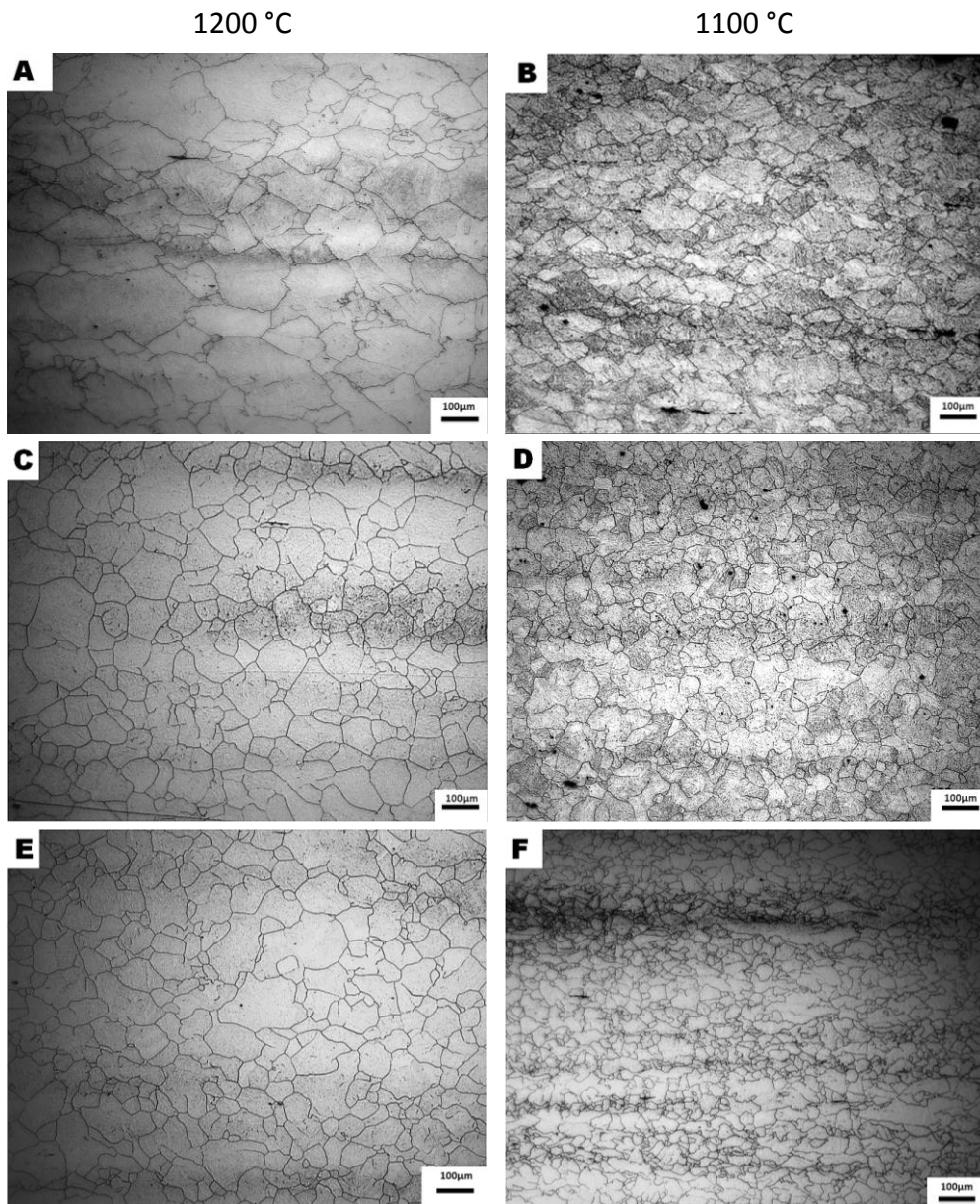


**Figure 6-4** Optical micrograph of non-isothermal deformation processes at two different austenitising temperatures followed by quenching in water after; (A, B) three hits, (C, D) holding for 60 sec after deformation (E,F) cooling to 900 °C in 60 sec after deformation. (10X Magnification)

### 6.3 Summary of grain size results

Tables 6.1 and 6.2 show all the grain size results for the non-isothermal deformation processes of four-hits and three-hits with different situations at austenitising temperatures of 1100 °C and 1200 °C and different deformation conditions, as well as showing the grain size before deformation and after being held for one hour at both austenitising temperatures. The measurements to express the grain size were done by using the manual technique of mean linear intercept.

**Table 6-1** Results of austenite grain size after heating for one hour at temperature of 1200 °C flowed by four hits and three hits with different conditions.

One hour heating at 1200 °C and quench	4 Hits at 1200 °C-1100 °C-1000 °C-900 °C and Quench	3 Hits at 1200 °C-1100 °C-1000 °C		
		Quench	Hold for 60 sec and quench	Cooled to 900 °C in 60 sec and quench
284 ± 20	64 ± 5	88 ± 7	63 ± 3	60 ± 4

**Table 6-2** Results of austenite grain size after heating for one hour at temperature of 1100 °C flowed by four hits and three hits with different conditions.

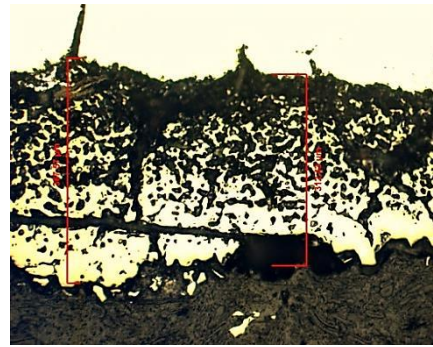
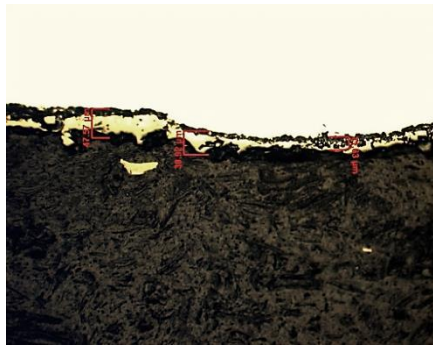
One hour heating at 1100 °C and quench	4 Hits at 1100 °C-1000 °C-950 °C-900 °C and Quench	3 Hits at 1100 °C-1000 °C-950 °C		
		Quench	Hold for 60 sec and quench	Cooled to 900 °C in 60 sec and quench
197 ± 13	37 ± 2	54 ± 9	43 ± 2	42 ± 3

#### 6.4 The oxide scale

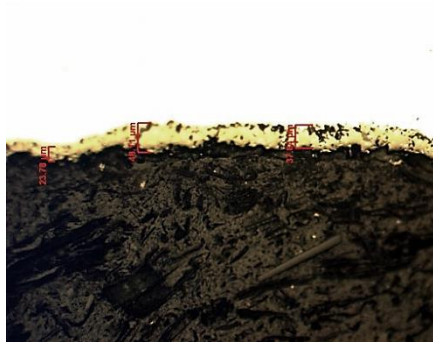
In some metal forming processes such as large scale forging, one of the methods used to enhance cooling rates in the material is producing a near-net shape product to reduce the thickness of the product to the minimum. This means leaving a thin layer to be removed later after finishing from the deformation and heat treatment processes. However, during the tests an oxide scale layer was observed on the surface of the samples when they were heated to an elevated temperature in the presence of air. The behaviour of these oxides on the outer surface of the specimens changed with the austenitising temperature and the holding time at that temperature, as presented in Figure 6.5. These oxide layers became thicker when austenitising temperature increased from 1100 °C to 1200 °C and also when increasing soaking time from 1 hour to 24 hours at these temperatures. A much greater scale layer thickness was observed at temperature 1200 °C than at 1100 °C. Generally these resultant oxide scales are undesirable since they represent the formation of defects such as porosity and cracks within the oxide structure. According to the hardenability problem these oxides can be the cause of many cracks on the outer surface especially if the removed surface layer is thin. Moreover, existence of the oxide scales during hot deformation will affect the friction and heat transfer of the metals during the occurrence of contact between the hot metal and cold die.

Austenitising temperature of 1100 °C

Austenitising temperature of 1200 °C



Soaked for 1 hour (20x)



Soaked for 24 hour (5x)

**Figure 6-5** Oxide scale formed on the outer surface of the specimens at austenitising temperatures of both 1100 °C and 1200 °C.

EDX analysis was used to obtain the qualitative determination of the elements present in the selected sample area. Figure 6.6 shows the SEM images for cross section of the oxide scale layers and the distribution of alloy elements in the selected spectrum, while the EDX point composition analysis results are shown in Table 6.3. From these data, the point analysis results show that Cr, Ni, Mn and O were the highest elements in the oxide layer.

**Table 6-3** SEM EDX composition point analysis (wt %)

Cr	Mn	Fe	Ni	O
2.92	0.52	71.99	1.93	22.65

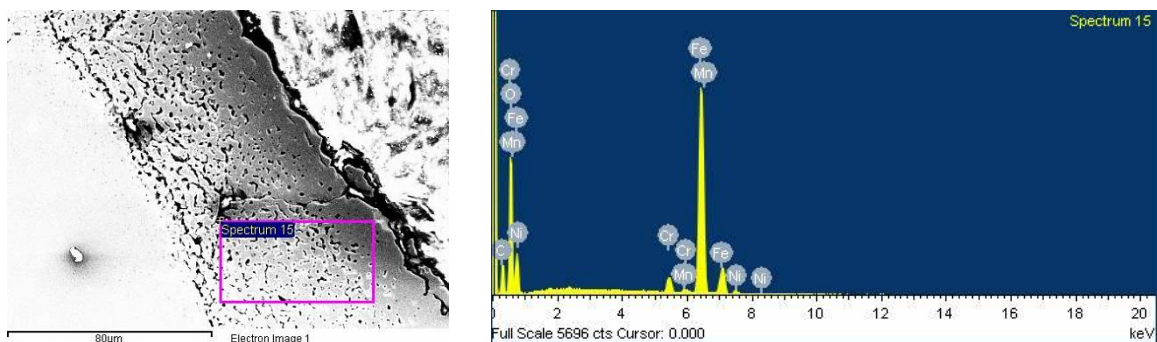


**Figure 6-6** SEM images and EDX of the oxide scale cross section of 34CrNiMo6.



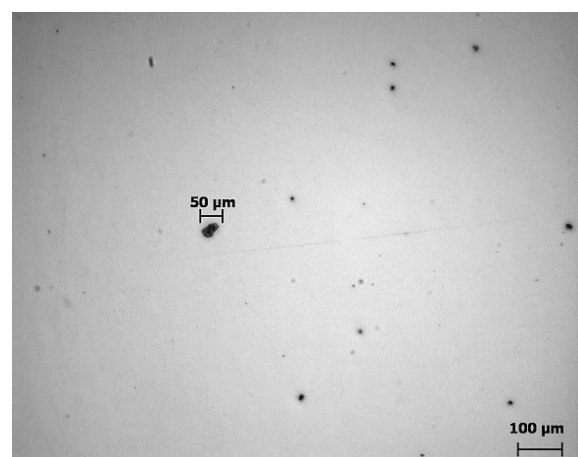
## 6.5 Non-metallic inclusion

The 34CrNiMo6 steel is a medium carbon steel that can be killed really fast during the secondary refining due to the high content of deoxidizer elements such as carbon, manganese, silicon that reacts with oxygen, producing low content of dissolved oxygen in the steel. In addition the alloy elements such as Cr, Mo and V also react with oxygen, thus contributing the reduction of dissolved oxygen in the steel. The process of secondary refinement is performed to refine the steel with a combination of deoxidation, desulphuration and inclusion removal. The 34CrNiMo6 steel in this study has total oxygen and nitrogen content of 35ppm and 80ppm respectively.

Light microscopy usually uses to establish the distributions, shapes, and sizes of inclusions, but it cannot be used to determine the chemistry for these inclusions. Furthermore, inclusions are best observed in as polished surface, but sometimes etching would bring out other features of the microstructures that would make it difficult to view inclusions. Figure 6.7 shows some photographs of the analysed inclusion by using the optical microscope. From the figure can be seen the size, shape and dispersion of non-metallic inclusions in the 34CrNiMo6 steel. Some of inclusions were subjected to energy-dispersive X-ray spectroscopy analysis in the scanning electron microscope to determine the elements present in these inclusions.



Magnification of 20X



Magnification of 10X

**Figure 6-7** Shows the optical images for the size, shape and dispersion of non-metallic in 34CrNiMo6 steel.

Whereas, Figure 6.8 shows the SEM images and EDX analysis for inclusions in the polished cross sections of 34CrNiMo6 steel. As can be seen from the optical micrographs there are

two shapes of inclusions; which are globular or oval and elongated shape inclusions. Randomly one of both shapes was selected to use it for EDX analysis. The EDX spectrum of the upper sample shows sulphur and manganese, while the lower one shows aluminium and manganese and traces of vanadium. From the EDX analysis in Figure 6.8 the steel exhibits both of sulphide inclusions with elongated morphology (green colour) and also globular oxide inclusions.

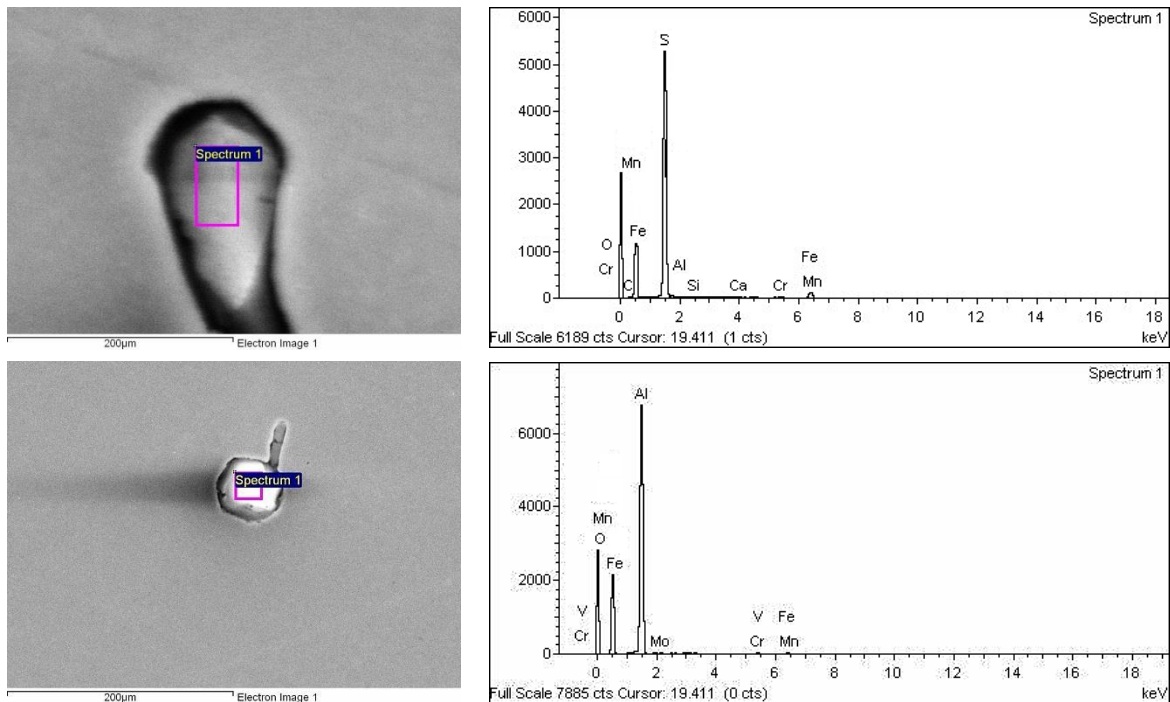


**Figure 6-8** SEM images and EDX for inclusions in the polished cross sections of 34CrNiMo6 steel.

Figure 6.9 shows SEM images of fracture surfaces of Charpy test specimens. The Figure showing some voids and some globular inclusions have formed in these voids.

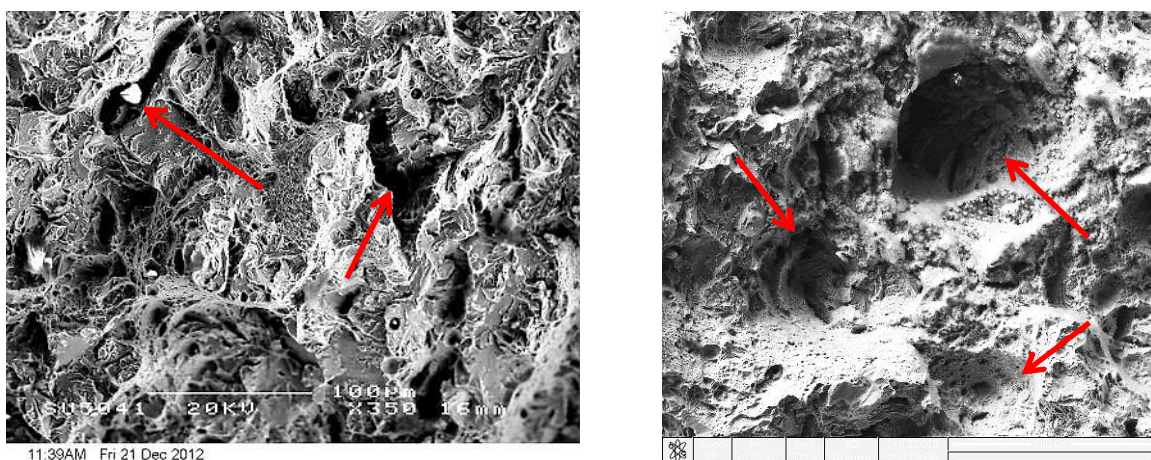


**Figure 6-9** Scanning electron microscope images for the fracture surface specimen. (350X, 302X)

## Chapter 7 Results of heat treatment

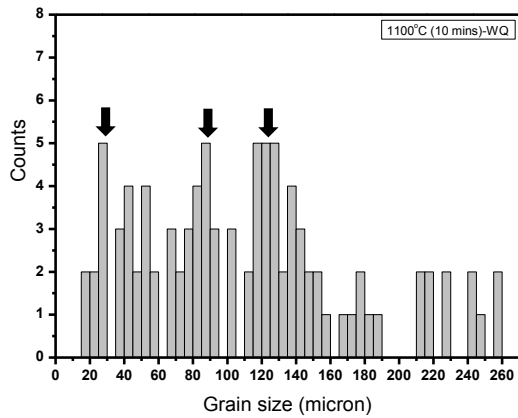
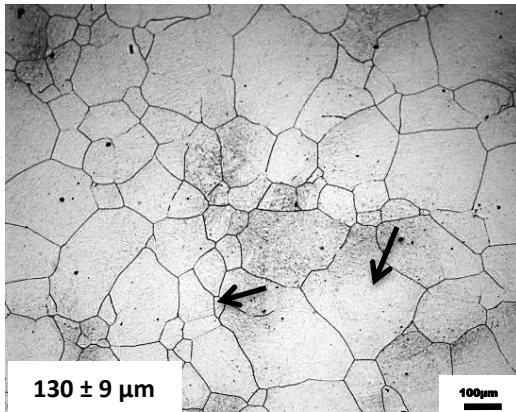
In most types of steel products, especially the larger ones, heat treatment is usually undertaken after the deformation process because the microstructure that is produced after deformation becomes non-uniform and the grains become irregularly shaped and relatively large, which leads to a difference in mechanical properties between the two directions. Therefore the aim of heat treatment is to achieve a required or desired result, such as good toughness or high strength of a material, through controlling the temperatures, soaking times, heating and cooling rates.

### 7.1 The effect of normalising process on the deformed austenite grain size

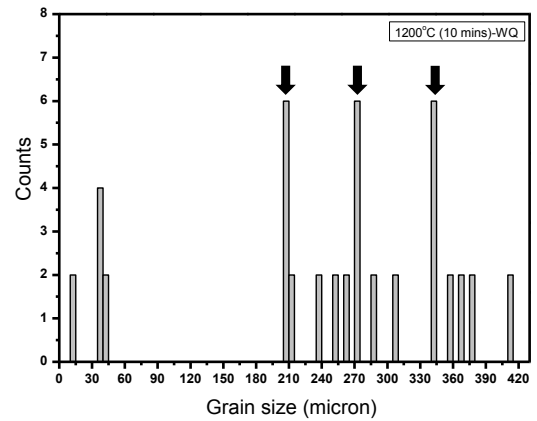
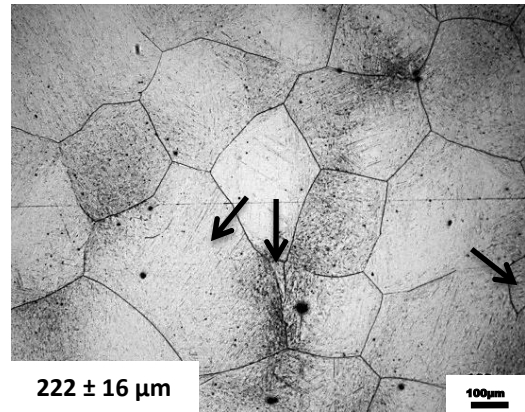
Commonly, a normalizing process is used to remove the internal stresses caused by industrial processes such as forging, refining the grains and providing uniformity in grain size throughout an alloy. Figure 7.1 shows the optical microstructures before and immediately after deformation for the samples that were heated for 10 mins prior to quench. The optical microstructures for the same specimens after being deformed, cooled to a temperature of 650 °C and held for 5 mins before quenching are shown in the same figure. Both the austenitising temperatures of 1100 °C and 1200 °C were used to study the effect on the normalizing process. The optical micrograph of austenite grains after being held for 10 mins at either 1100 °C or 1200 °C, deformed, soaked for 5 mins at 650 °C and normalized at 860 °C for 6 mins before quenching, is also shown.

Moreover, as shown from the microstructure images the grain sizes are non-uniform, and the grains in the same image have different sizes, i.e., there is a great disparity in the grain sizes. The histograms of grain size distributions for these microstructures are shown in figure 7.1. From these curves (Histograms) two types of grain size distribution can be observed; a unimodal, which have one peak, and a bimodal, where the coarse grains present in a matrix of fine grains. Furthermore, as was noted in the case of isothermal deformation microstructures the presented images of the microstructures also show clear banding in the longitudinal direction after deformation process.

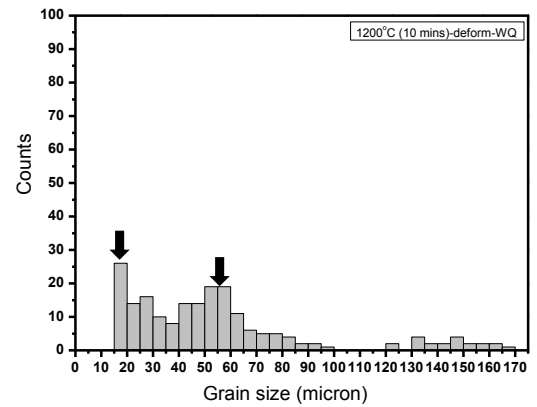
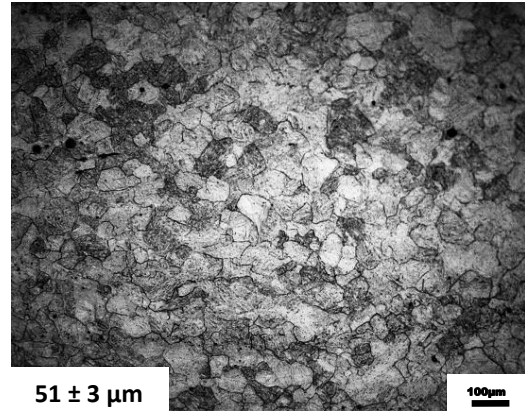
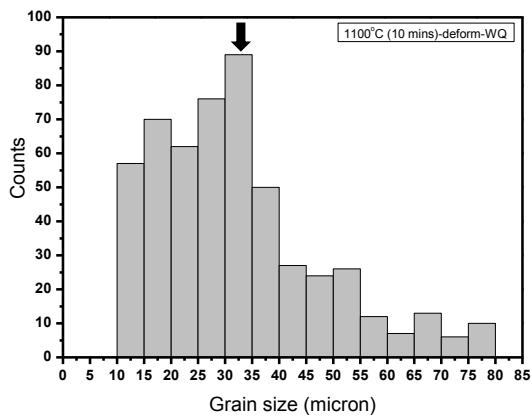
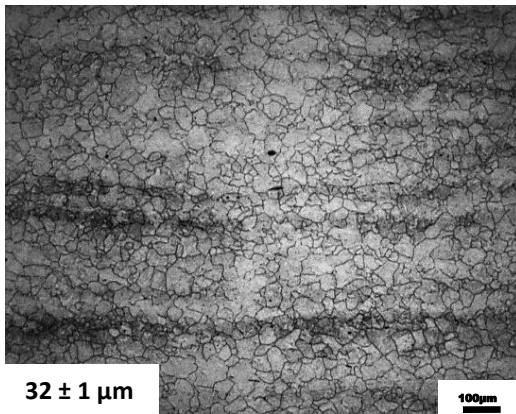
Austenitising temperature of 1100 °C



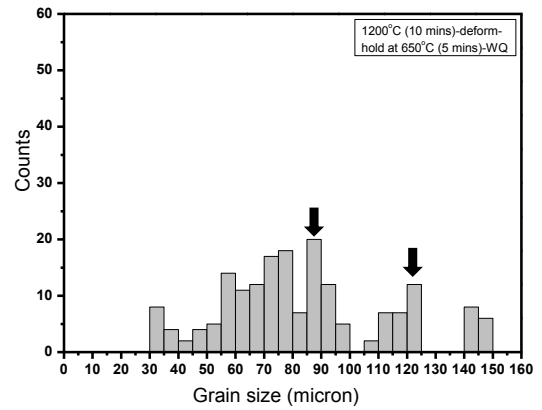
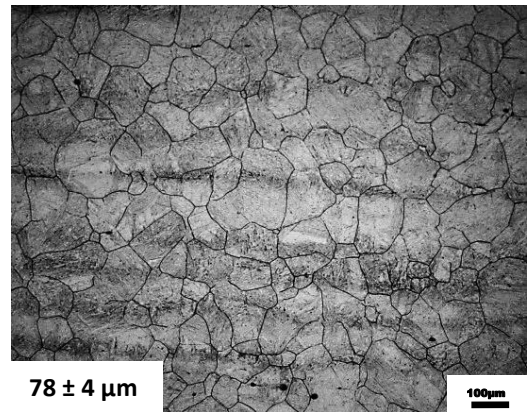
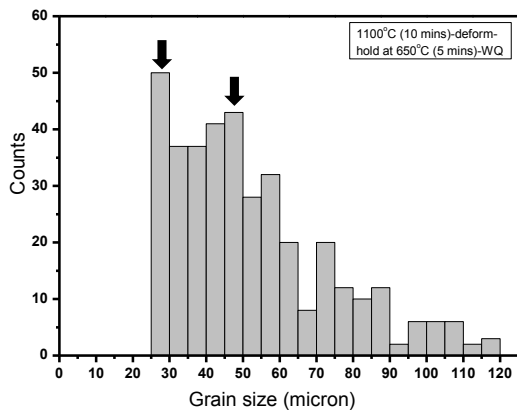
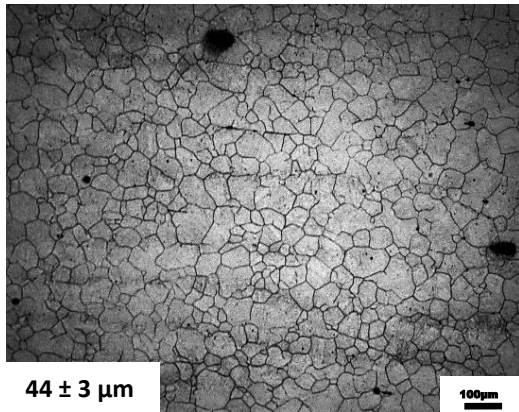
Austenitising temperature of 1200 °C



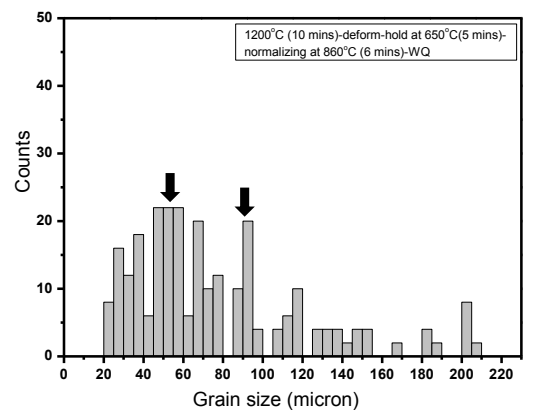
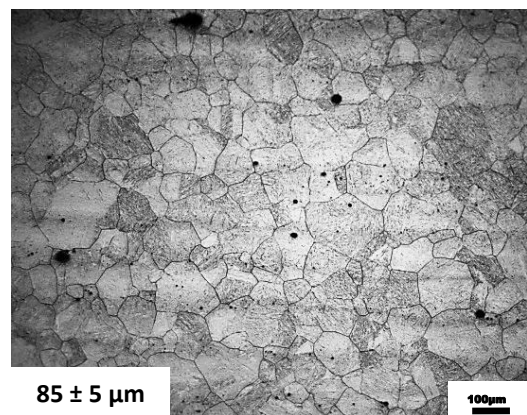
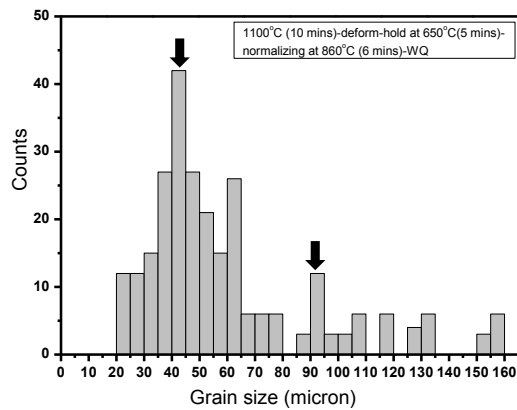
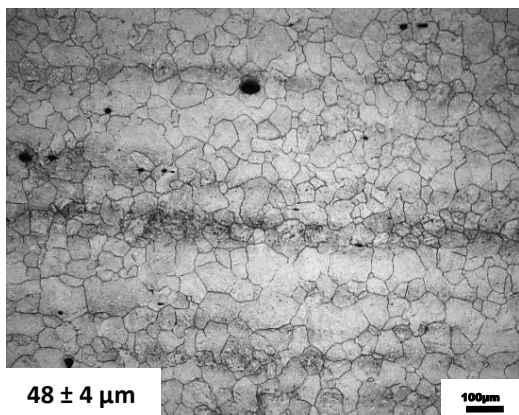
Before deformation



Directly after deformation



Soaked for 5 mins at 650 °C



Soaked for 6 mins at 860 °C

**Figure 7-1** Optical micrograph and size distribution of austenite grains which normalizing at 860 °C for 6 mins after deformation at both 1100 °C and 1200 °C and soaking for 5 mins at 650 °C. (10X)

In the real production process, after completion of deformation the forged piece is placed in a degassing furnace at a temperature of 650 °C with a soaking time of about one week in order to keep the hydrogen content at values less than 2 ppm. To simulate the effect of microstructure changes that occur at this temperature on the normalizing process, 4 hours holding time was used. According to the TTT diagram for 4340 (~ 34CrNiMo6) steel, to make almost the whole structure transform into ferrite and pearlite dual-phase, the specimen should be held for 4 hours at a temperature of 650 °C. Figure 7.2 shows the optical micrograph of ferrite and pearlite microstructure which deformed at both austenitising temperatures of 1100 °C and 1200 °C, soaked for 4 hours at 650 °C before quenching.

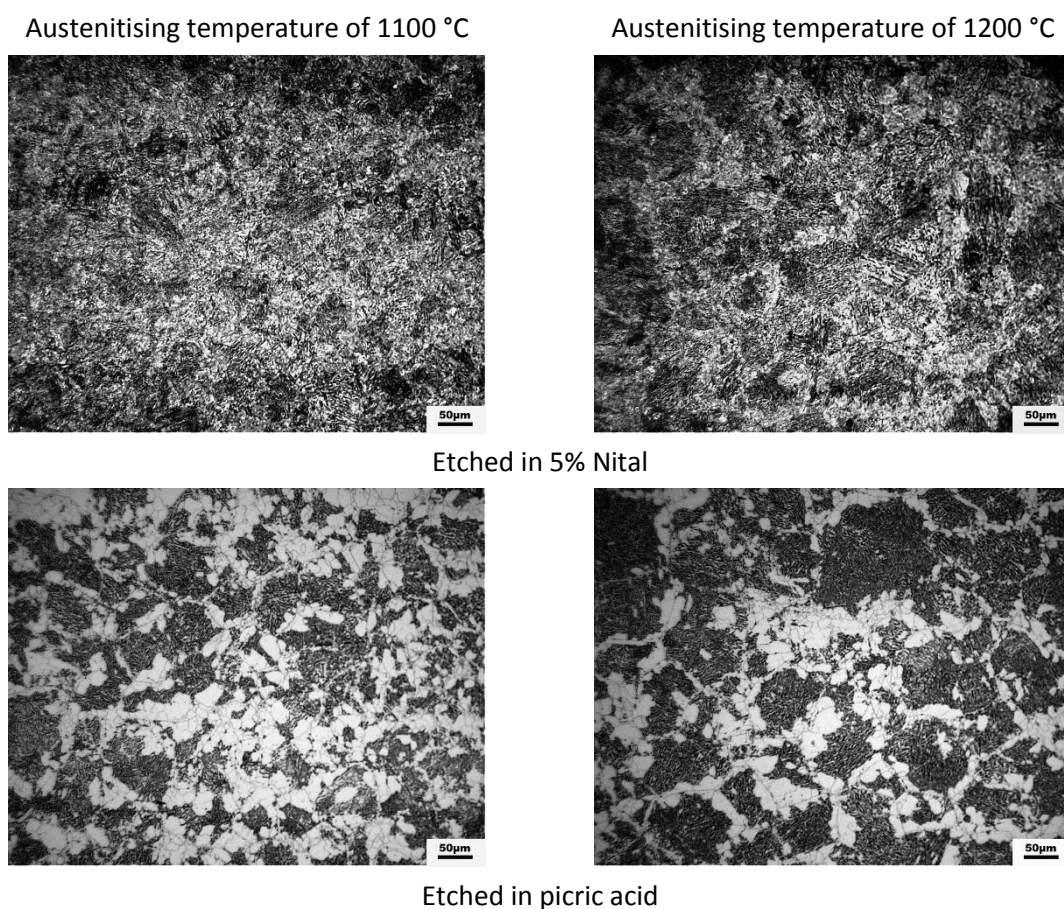


**Figure 7-2** Optical micrograph of the 34CrNiMo6 steel microstructure (ferrite and pearlite) after deforming at both austenitising temperatures and soaking for 4 hours at 650 °C before quenching. (20x)

One of the factors that can affect the variation in austenite grain size after the normalizing process is the holding time. Therefore, the objective of this step was to study the effects of increasing holding time at a normalizing temperature of 860 °C on the refinement and homogenization of microstructure and thus on the mechanical properties. The

microstructures obtained after changing the holding time at normalizing temperature of 860 °C are illustrated in Figure 7.3. Holding times of 6, 30, and 60 mins were used with each austenitising temperature of 1100 °C and 1200 °C after the specimens were deformed and soaked for 4 hours at 650 °C.

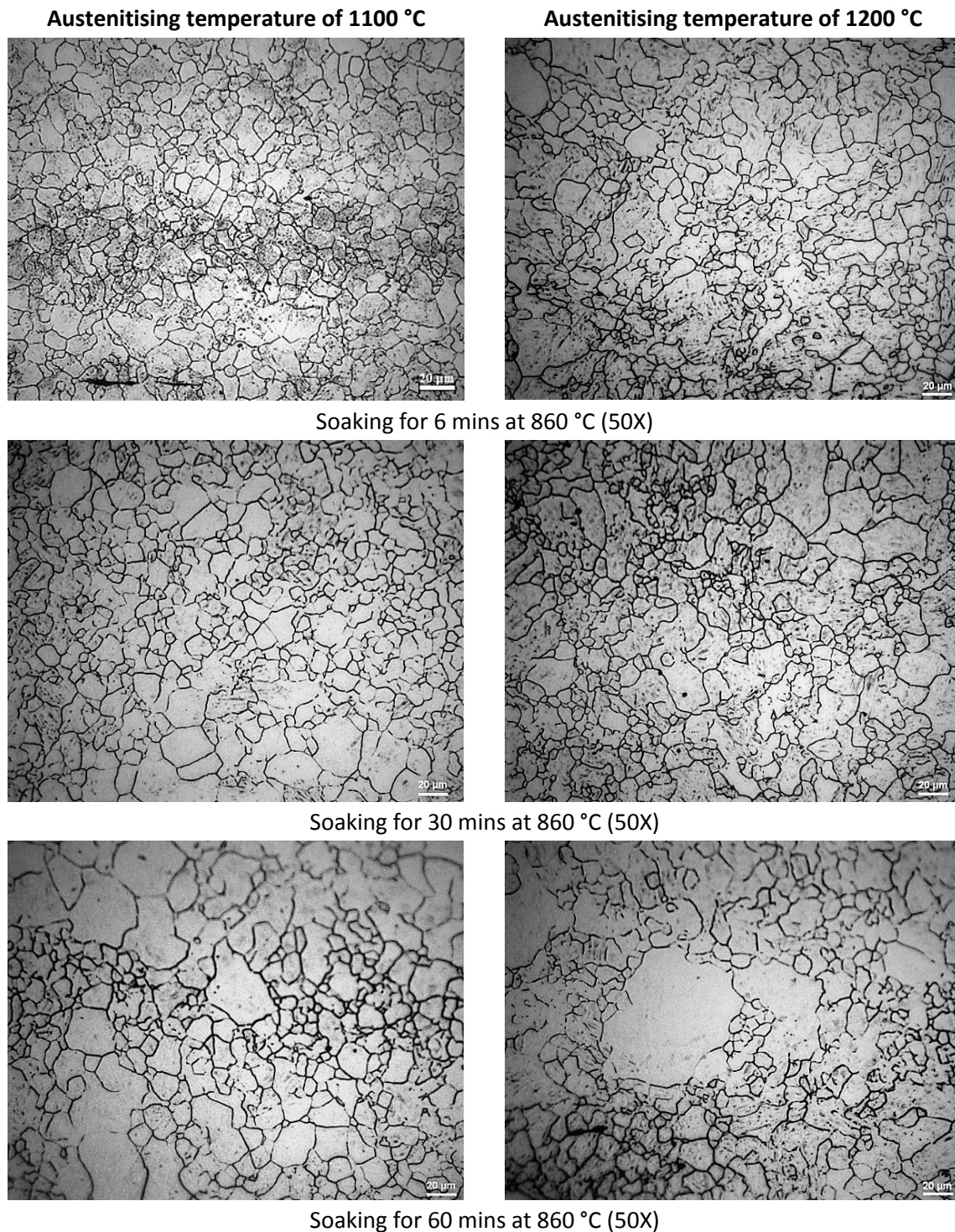


**Figure 7-3** Optical micrograph of the changing of austenite grains with increased of normalizing holding time at 860 °C for 6, 30, and 60 mins after deformation and soaking for 4 hours at 650 °C for both austenitising temperatures.

## **7.2 Quenching and tempering processes**

Different heat treatment processes such as quenching and tempering are applied on the real product made of 34CrNiMo6 alloy steel, in order to achieve required standard specifications. Therefore, a series of heat treatment tests were applied in exactly similar conditions to simulate the real process and to study the microstructural changes and their effects on the final mechanical properties of the studied steel. Moreover, some factors, such as cooling rate, austenitising and tempering temperatures, were modified in order to refine grain size and make it more equiaxed in an attempt to achieve the required combination of high strength and good impact toughness.

### **7.2.1 Using different cooling rates**

The effects of cooling rates on the resulting microstructure and thus on the final mechanical properties of the studied steel were also investigated. For this, austenitising temperatures of 840 °C and 960 °C followed by tempering temperatures of 520 °C and 630 °C respectively were used. Different cooling rates in a range between slow cooling (furnace cooling) and a cooling rate of 1.2 °C/sec were used with each heat treatment cycle (Fig. 3.22) in an attempt to determine the cooling rate necessary to obtain a higher percentage of martensite within the microstructure after the quenching process, which also leads to the required properties being reached after the tempering process.

#### **7.2.1.1 With austenitising temperature of 840 °C and tempering temperature of 520 °C**

In the first step the samples austenitised at 840 °C for 1 hr, normalized at 740 °C for 10 mins, and tempered at 520 °C for 40 mins were subsequently cooled to room temperature at different rates. Figure 7.4 shows the microstructures of samples etched using 5 % Nital and picric acid after using cooling rates of 0.3, 0.6, 0.9, and 1.2 °C/sec. As can be seen from the microstructures, the percentage of austenite phase increases and the grain size decreases with increasing the cooling rate. In addition, the presence of abnormal growth in some of austenite grains, which results in a heterogeneous microstructure from large and small grains within the microstructure, can be seen.



Austenitising temperature of 840 °C

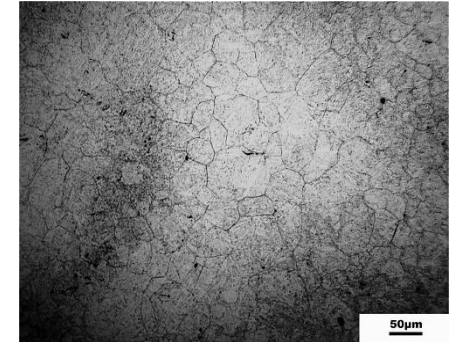
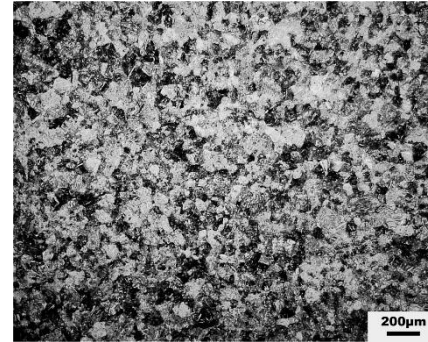
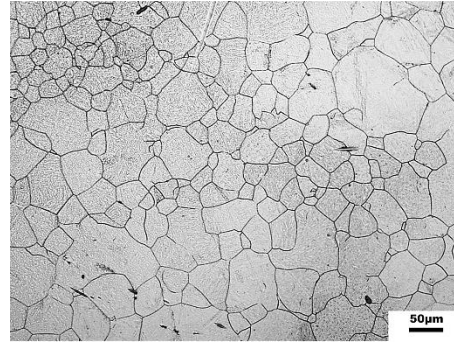
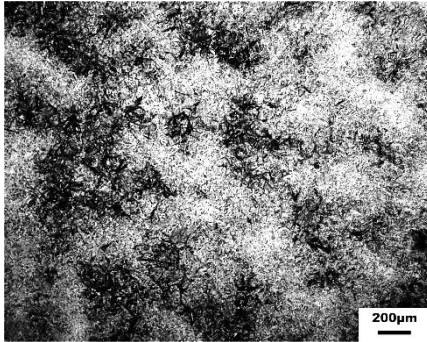
Tempering temperature of 520 °C

Nital 5 % - 5X

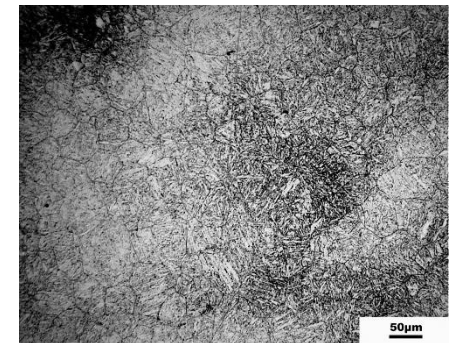
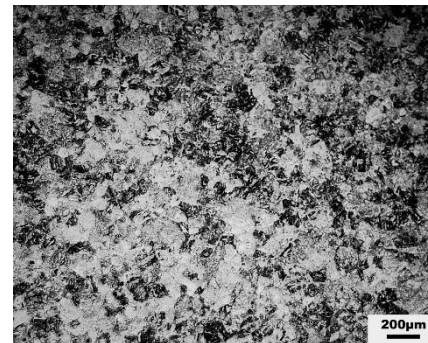
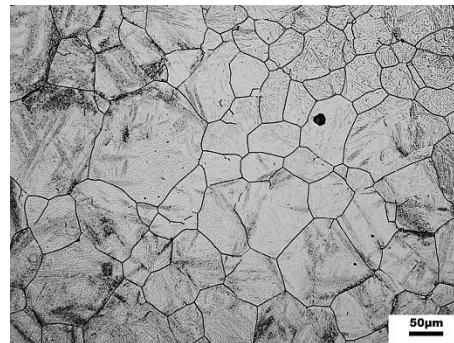
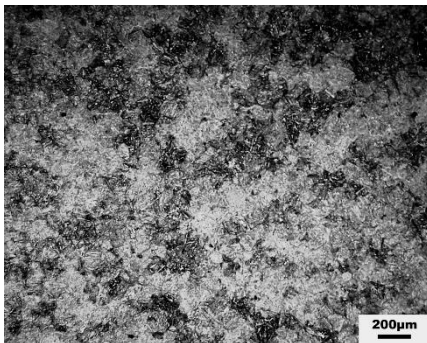
Picric Acid – 20X

Nital 5 % - 5X

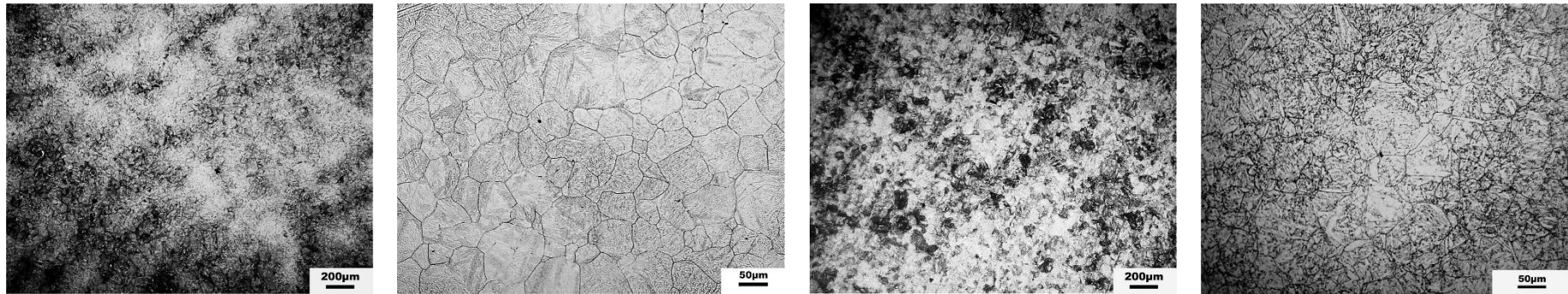
Picric Acid – 20X



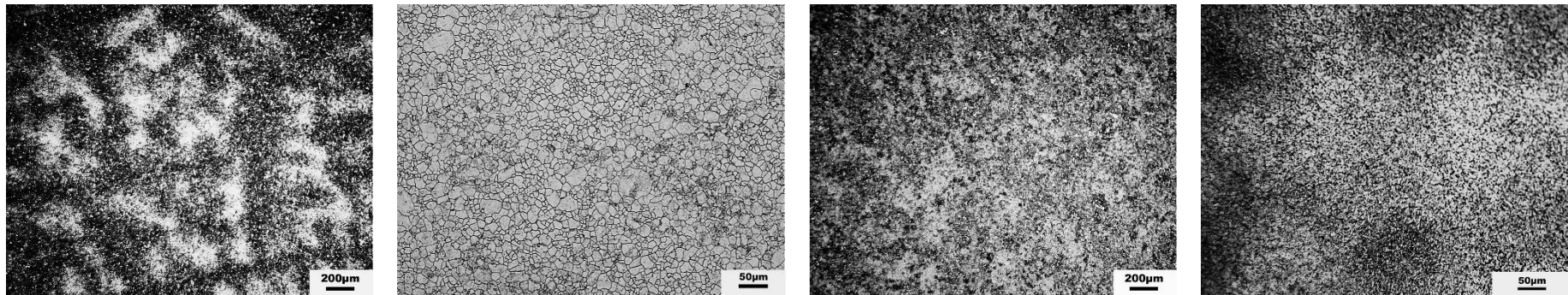
With cooling Rate of 0.3 °C/sec



With cooling Rate of 0.6 °C/sec



With cooling Rate of 0.9 °C/sec



With cooling Rate of 1.2 °C/sec

**Figure 7-4** Microstructure of etched samples austenitised at 840 °C for 1 hr, normalized at 740 °C for 10 mins, tempered at 520 °C for 40 mins then followed by cooling at different rates.

After the heat treatment was accomplished for all samples in this step, V-notch Charpy impact tests were performed on these samples to find out the toughness results. The tests were performed at -20 °C, the temperature required for the standard specifications. Macrographs of the fracture surfaces of tested specimens after austenitising at 840 °C and tempering at 520 °C with different cooling of (a) 0.3 °C/sec, (b) 0.6 °C/sec, (c) 0.9 °C/sec, (d) 1.2 °C/sec are shown in Figure 7.5. The profiles of the propagated cracks at the perpendicular side on the impact v-notch surface are also shown. The samples were numbered according to the heat treatment conditions as shown in Table 3.3.

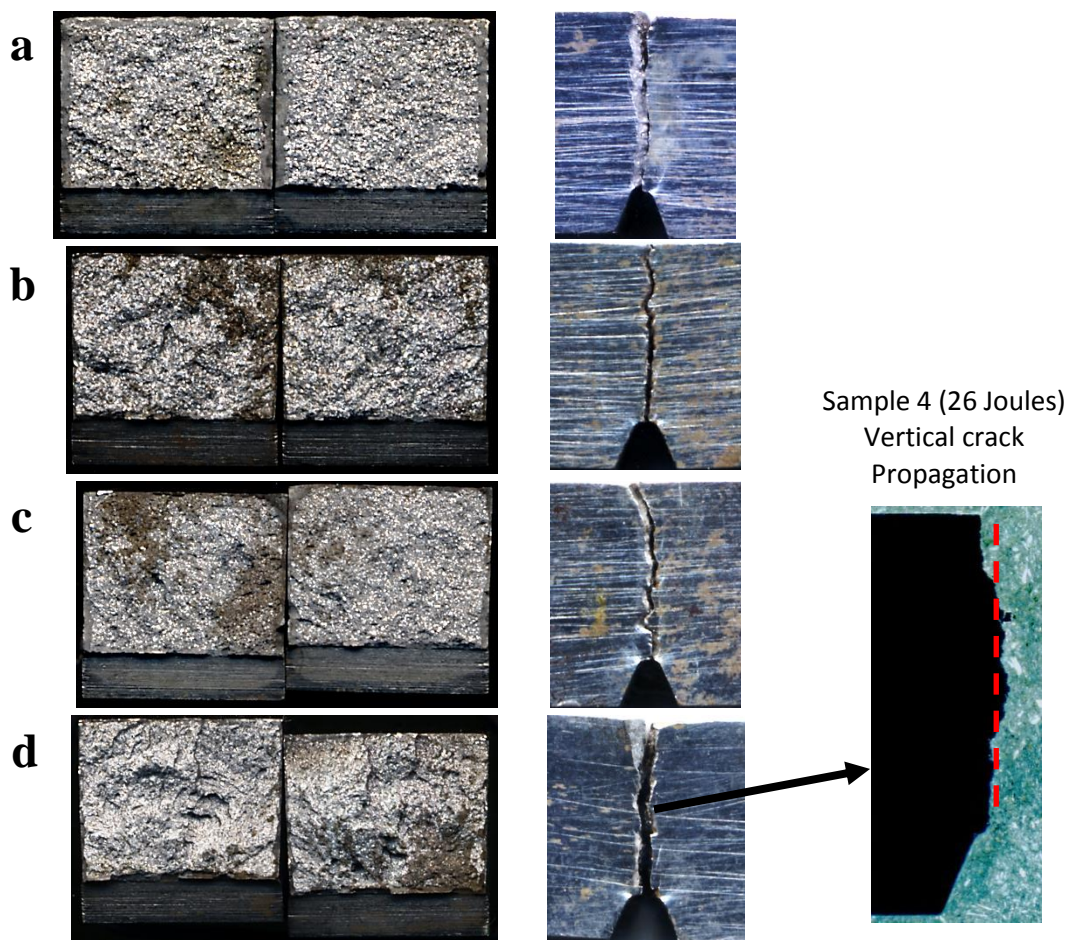


**Figure 7-5** Fracture surfaces of Charpy impact tests after austenitising at 840 °C and tempering at 520 °C followed by cooling (a) 0.3 °C/sec, (b) 0.6 °C/sec, (c) 0.9 °C/sec, (d) 1.2 °C/sec.

### 7.2.1.2 With austenitising temperature of 960 °C and tempering temperature of 630 °C

The previous heat treatment process was repeated after changing the austenitising and tempering temperatures. The same cooling rates as previously were used with the addition of a very slow cooling rate achieved by cooling in a furnace. As formerly, the samples were austenitised at 960 °C for 1 hr, normalized at 860 °C for 10 mins, and tempered at 630 °C for 40 mins then subsequently cooled to room temperature at different rates. Figure 7.6 shows the microstructures of samples etched using 5 % Nital and picric acid after using rates of furnace cooling, 0.3, 0.6, 0.9, and 1.2 °C/sec. Similarly, V-notch Charpy impact tests were carried out at the same temperature (-20 °C) for the samples to find out the toughness results.

A macrograph of the fracture surfaces of tested specimens with variation in toughness after austenitising at 960 °C and tempering at 630 °C with different cooling of (a) furnace cooling (b) 0.3 °C/sec, (c) 0.6 °C/sec, (d) 0.9 °C/sec, (e) 1.2 °C/sec are shown in Figure 7.7. The profiles of the propagated cracks at the perpendicular side on the impact v-notch surface are also shown in the Figure. In comparison with the previous heat treatment process, the austenite grain size was bigger and the hardness values were less, while the toughness values were higher just at higher cooling rates. Moreover, abnormal grain growth was greater than previously, which resulted in a more heterogeneous microstructure.

Austenitising temperature of 960 °C

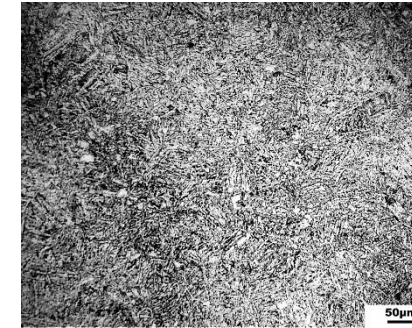
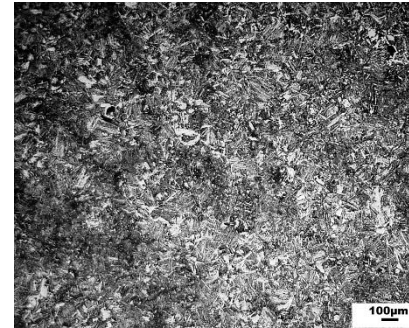
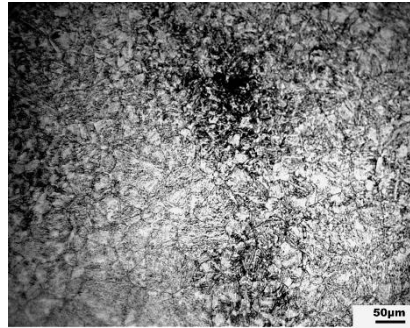
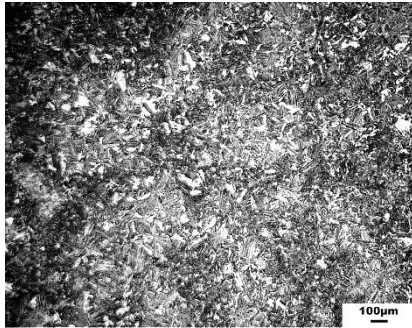
Tempering temperature of 630 °C

Nital 5 % - 5X

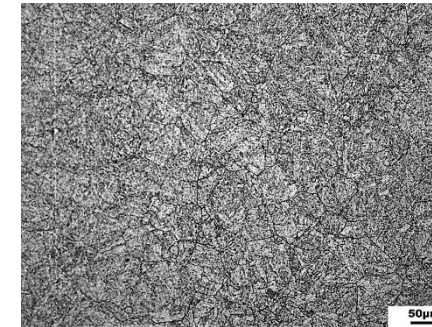
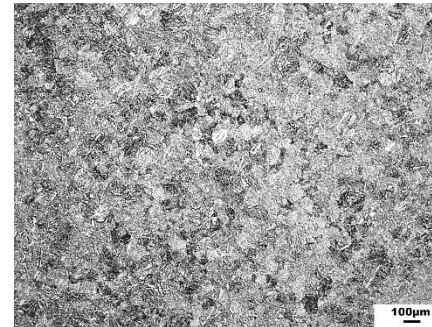
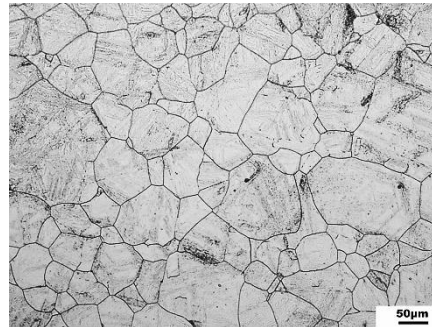
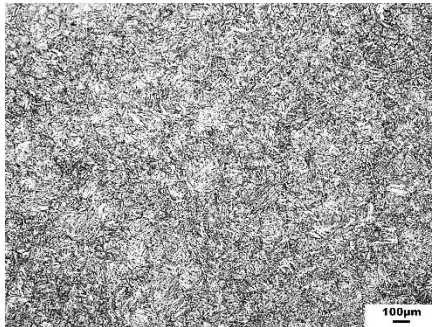
Picric Acid – 20X

Nital 5 % - 5X

Picric Acid – 20X



With furnace cooling Rate



With cooling Rate of 0.3 °C/sec

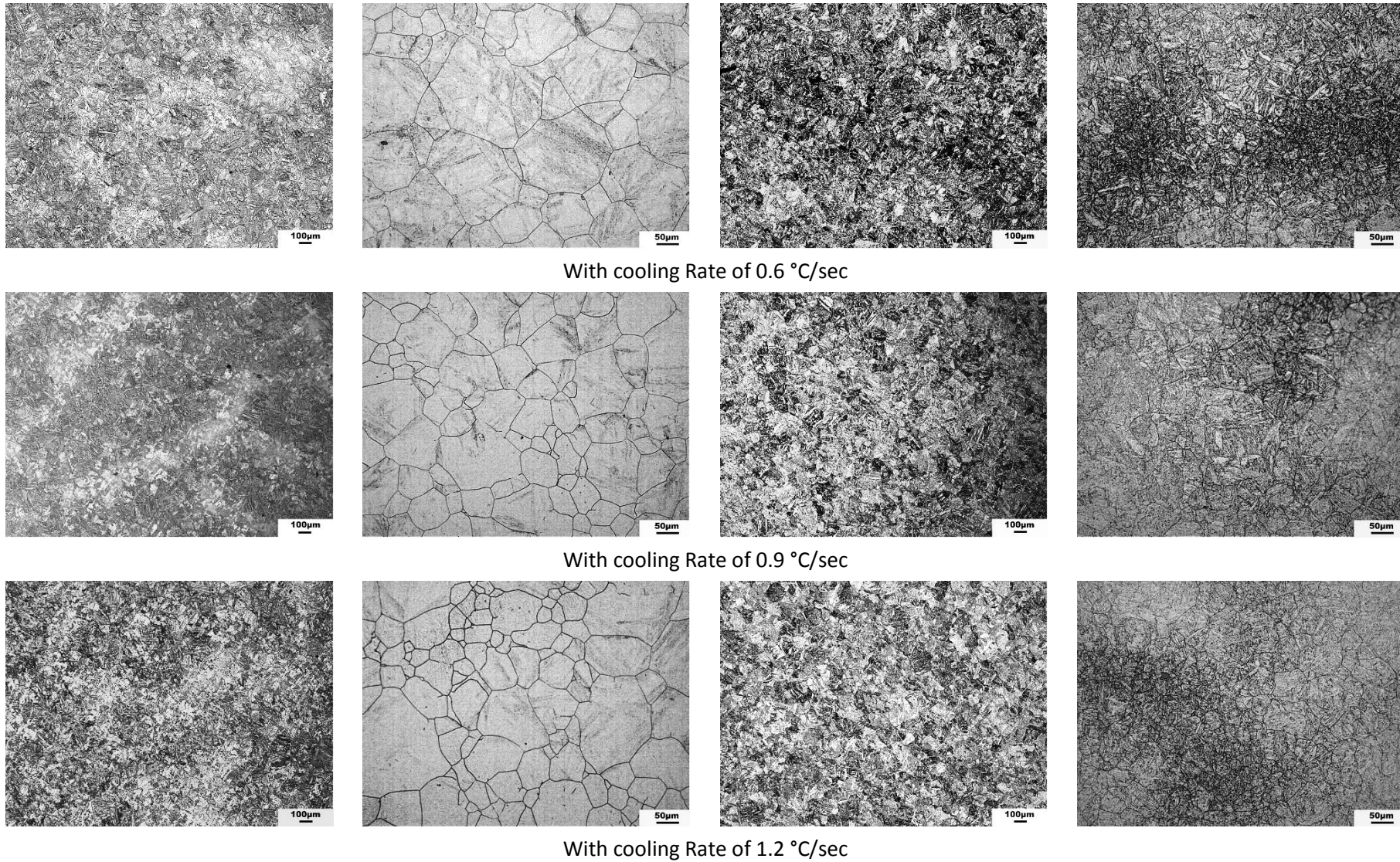


**Figure 7-6** Microstructure of etched samples austenitised at 960 °C for 1 hr, normalized at 860 °C for 10 mins, tempered at 630 °C for 40 mins followed by cooling at different rates.

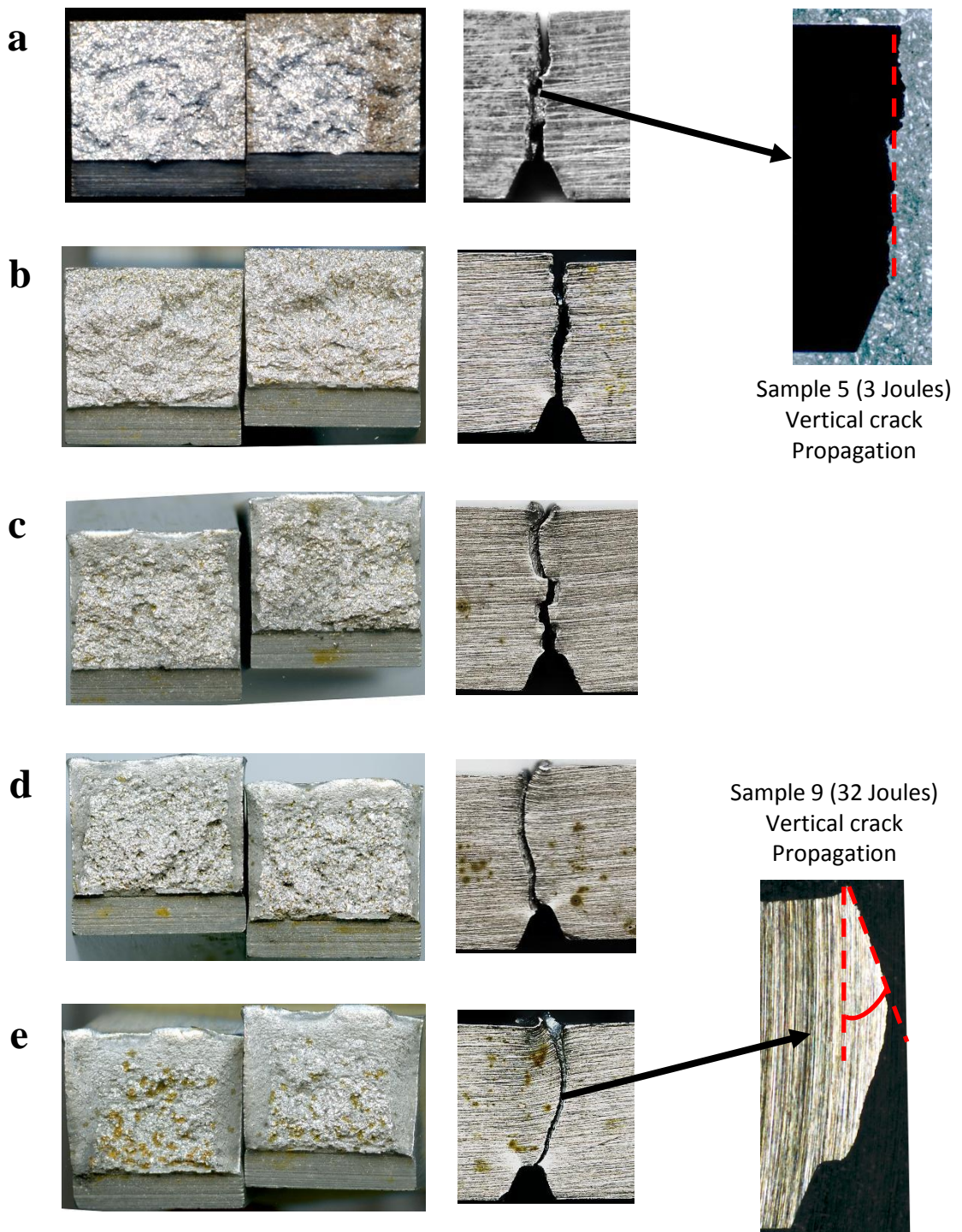


**Figure 7-7** Fracture surfaces of Charpy impact samples with variation in toughness after austenitising at 960 °C and tempering at 630 °C followed by cooling (a) furnace cooling, (b) 0.3 °C/sec, (c) 0.6 °C/sec, (d) 0.9 °C/sec, (e) 1.2 °C/sec.

### 7.2.1.3 Grain size and mechanical properties results

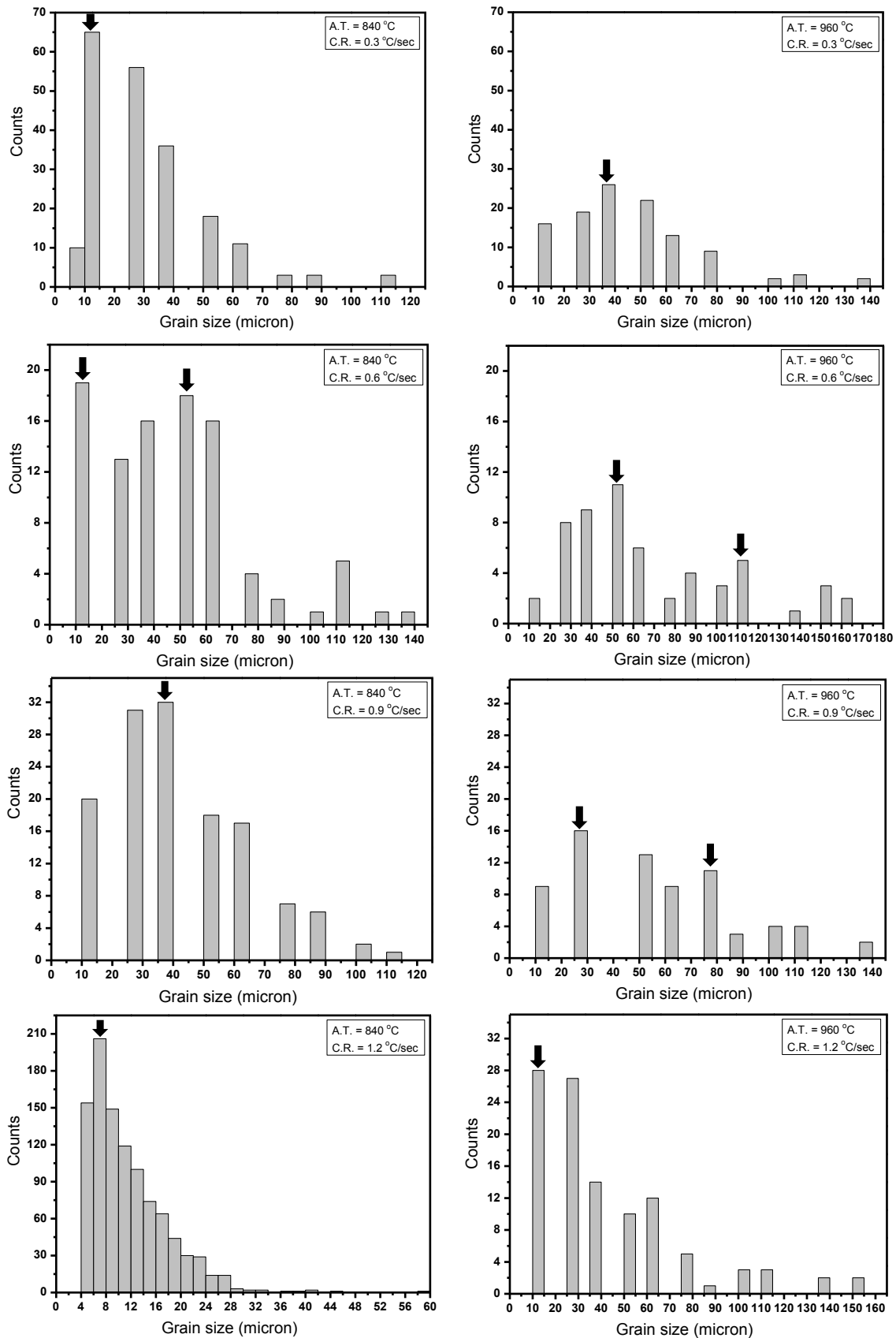
Table 7.1 shows all the Charpy absorbed energy (J), ultimate tensile strength (MPa), and hardness (HB) results of austenitising at both 840 °C and 960 °C followed by tempering temperatures of 520 °C and 630 °C respectively using different cooling rates. From the obtained results it can be seen that toughness and hardness increase with increasing the cooling rate. The relationship between the cooling rate and the grain size is not compatible, as it increases sometimes and decreases at others with an increased cooling rate. Figure 7.9 shows the relationship between different cooling rates and Charpy absorbed energy of the heat treated samples.

**Table 7-1** Charpy absorbed energy (J), ultimate tensile strength (MPa), and hardness (HB) at tempering temperatures of 520 °C and 630 °C followed by different cooling rates after austenitising at temperatures of 840 °C and 960 °C, respectively.

Samples No.	Cooling Rate (°C/s)	Grain size (µm)	Charpy absorbed energy (Joules)	Hardness (HB)	Calculated UTS (MPa)= 3.38HB
Sample 1	0.3	35 ± 5	9	342 ± 6	1157
Sample 2	0.6	47 ± 6	16	366 ± 8	1236
Sample 3	0.9	44 ± 4	17	398 ± 5	1346
Sample 4	1.2	8 ± 1	26	391 ± 4	1323
Sample 5	FC	32 ± 6	3	290 ± 4	980
Sample 6	0.3	48 ± 3	9	304 ± 2	1026
Sample 7	0.6	60 ± 3	17	329 ± 2	1112
Sample 8	0.9	48 ± 2	24	332 ± 4	1123
Sample 9	1.2	43 ± 2	32	341 ± 3	1153

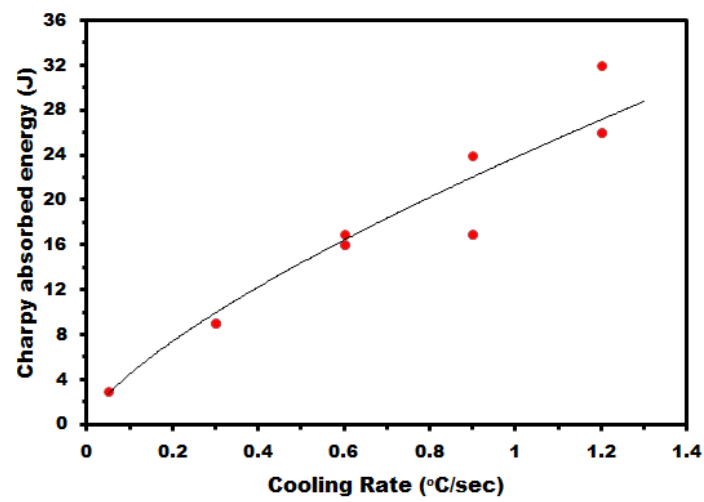
In addition the histograms of grain size distribution for the microstructures at austenitising temperatures of 840 °C and 960 °C and cooling rates of 0.3, 0.6, 0.9 and 1.2 °C/sec with each austenitizing temperature are shown in Figure 7.8. From the figure can be noted that as the cooling rate increase nearly the microstructure become more uniform and the grain size distribution changed from unimodal to bimodal.



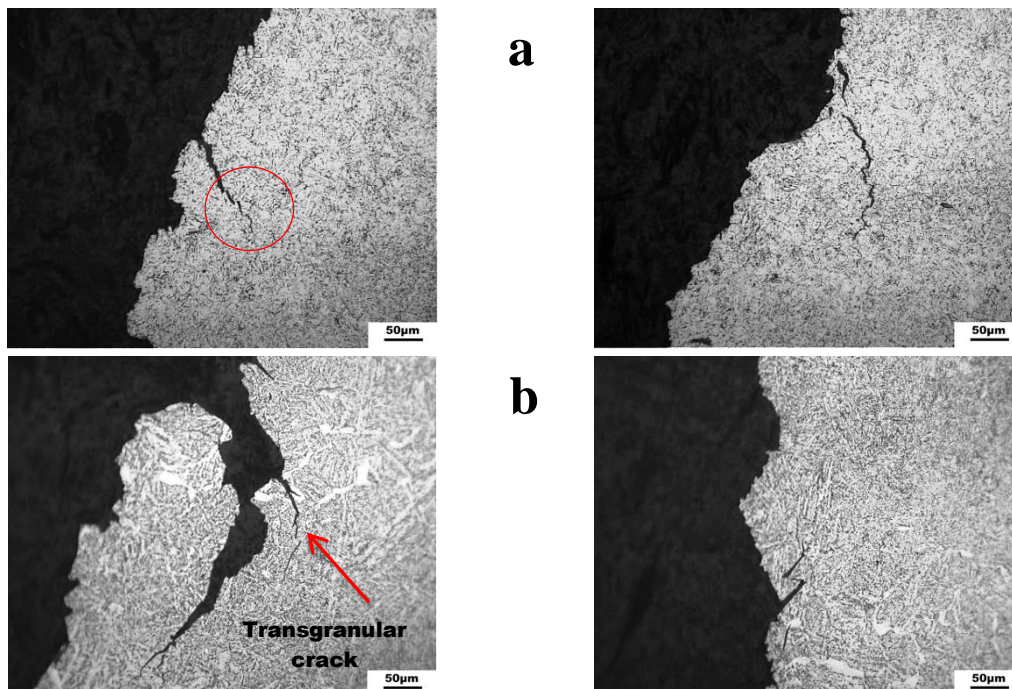


**Figure 7-8** Shows the austenite grain size distributions for the microstructures at austenitising temperatures (A.T.) of 840 °C and 960 °C and cooling rates (C.R.) of 0.3, 0.6, 0.9 and 1.2 °C/sec with each austenitising temperature.

During Charpy tests, when cracks initiate and begin to propagate at the microstructural level they usually follow two main types of paths; intergranular and transgranular. These paths sometimes can be found together in the same microstructure. The crack type (brittle or ductile) can be determined through the crack path and thus the cracks configuration. Figure 7.10 shows the vertical crack propagation of the samples with toughness of (a) sample 4 (26 J), (b) sample 5 (3 J), (c) sample 9 (32 J). All samples were etched with picric acid to reveal the microstructures.



**Figure 7-9** Relationship between Charpy absorbed energy and different cooling rates for quenched and tempered 34CrNiMo6 steel samples.



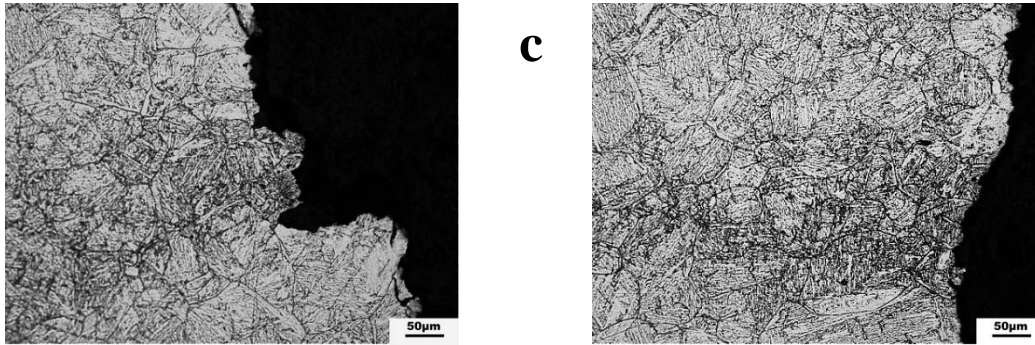


**Figure 7-10** Austenite grains along the vertical crack propagation of (a) sample 4, (b) sample 5, (c) sample 9. Etched with picric acid (20x)

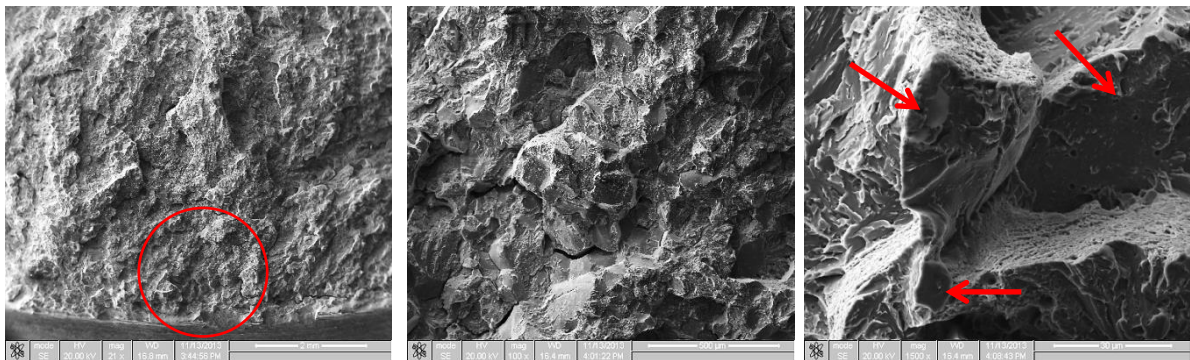


**Figure 7-11** Scanning electron microscope images for the Charpy fracture specimen sample 2. (Austenitised at 840 °C and tempered at 520 °C with cooling rate of 0.6 °C/sec) .(100X, 1500X)

To keep consistency in the results for the hardness values, several measurements were taken in the centre of and around the deformation zone for each sample. The scanning electron microscope (SEM) images of the Charpy fracture surfaces of sample 2 are shown in Figure 7.11. Whereas, Figures 7.12 and 7.13 show the relationship between grain diameter and both hardness (HB) and Charpy absorbed energy (J) with austenitising temperatures of 840 °C and 960 °C followed by tempering temperatures of 520 °C and 630 °C respectively, used with different cooling rates. From the figures it is clear that the relationship between both hardness and toughness with grain diameter is not compatible. This could be attributed to the method of determination of average grain diameter with the presence of abnormal growth of some grains in the microstructure.

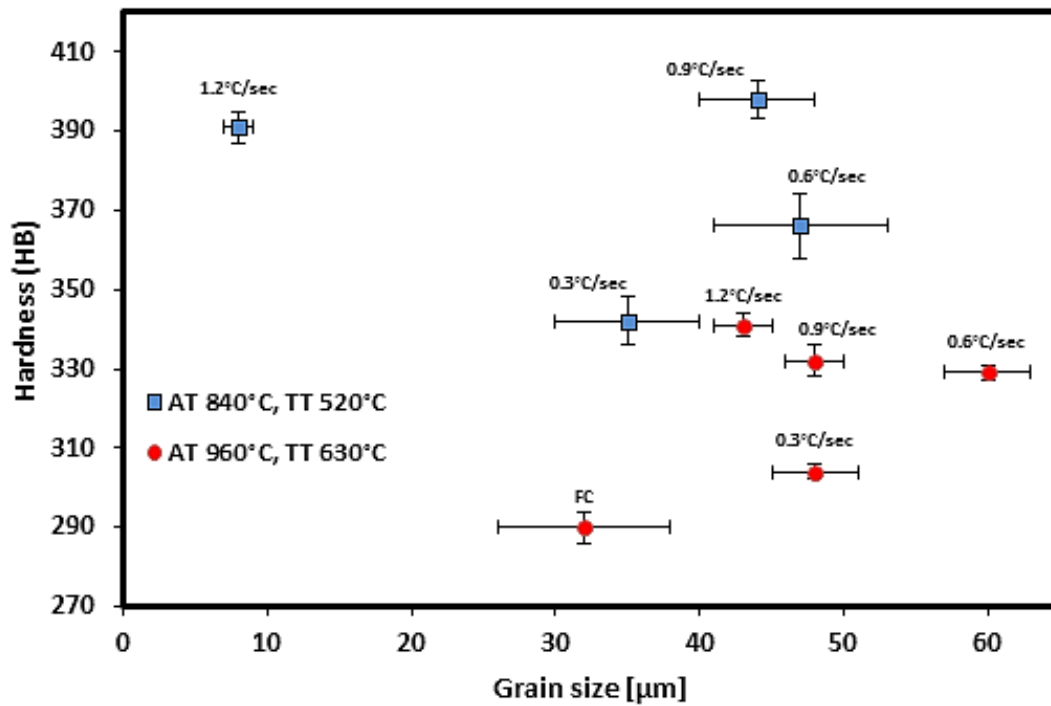


**Figure 7-12** Relationship between grain diameter and hardness (HB)  
(AT = Austenitising temperature, TT = Tempering temperature, FC = Furnace cooling)

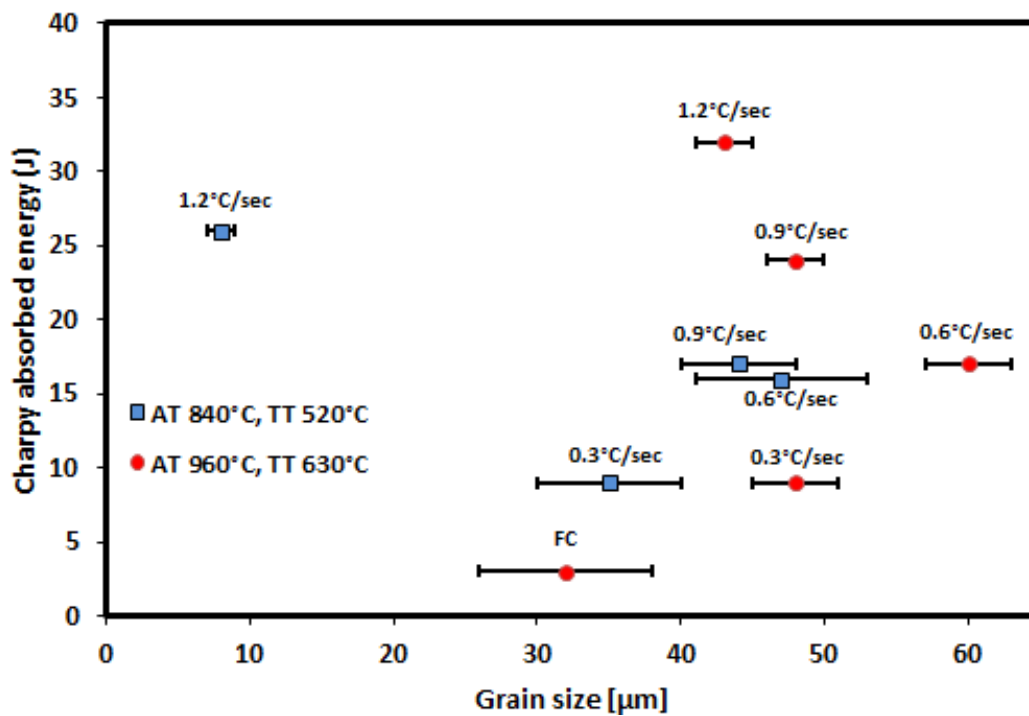


**Figure 7-13** Relationship between grain diameter and Charpy absorbed energy (J)  
(AT = Austenitising temperature, TT = Tempering temperature, FC = Furnace cooling)

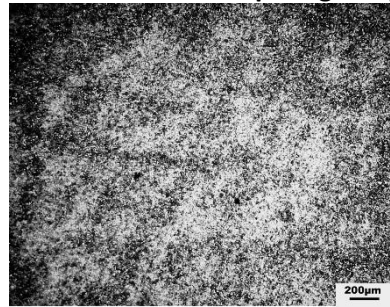
## **7.2.2 Using different austenitising temperatures**

Many studies have been completed about the importance of the effect of austenitising temperatures on mechanical properties, especially fracture toughness. Accordingly at this step the effect of different austenitising temperatures on grain size refinement and homogenization of the microstructure was investigated. The cooling rate of 0.6 °C/sec was used in this step with all austenitising temperatures because it is the estimated cooling rate for the sampling position in real product.

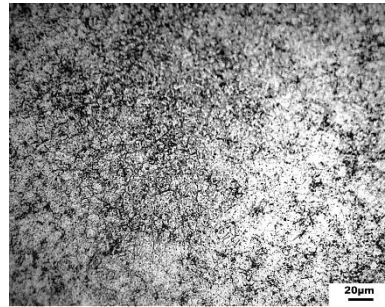
### **7.2.2.1 With tempering temperatures of 520 °C and 630 °C and cooling rate of 0.6 °C/sec**

Two different heat treatment cycles with different austenitising temperatures and two tempering temperatures with cooling rate of 0.6 °C/sec were used. Austenitising temperatures of 780 °C, 840 °C and 930 °C were used with tempering temperature 520 °C, while the austenitising temperatures of 900 °C, 960 °C and 1050 °C were used with tempering temperature 630 °C. The final microstructures of the heat treated samples according to the previous conditions of austenitising temperatures, tempering temperatures, and cooling rates of 0.6 °C/sec, are shown in Figure 7.14. 5 % Nital and Picric acid were used to etch the samples to reveal the microstructures. According to the microstructure, small grains and a high percentage of tempered martensite were obtained at lower austenitising temperatures.

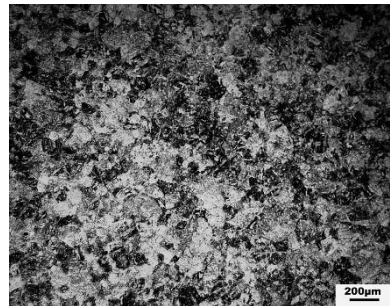
Tempering temperature of 520 °C



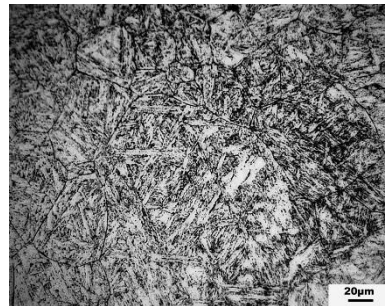
780 °C – 5 % Nital-5x



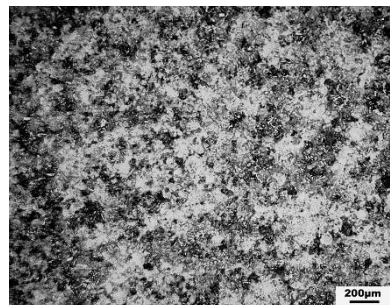
780 °C – Picric acid-50x



840 °C – 5 % Nital-5x



840 °C – Picric acid-50x

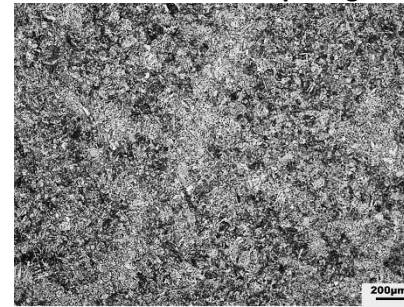


930 °C – 5 % Nital-5x

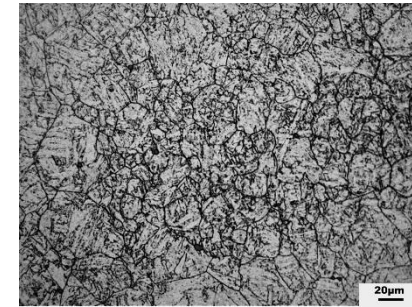


930 °C – Picric acid-50x

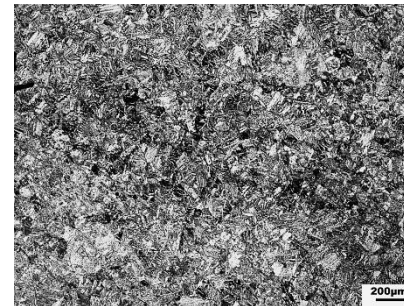
Tempering temperature of 630 °C



900 °C – 5 % Nital-5x



900 °C – Picric acid-50x



960 °C – 5 % Nital-5x



960 °C – Picric acid-50x



1050 °C – 5 % Nital-5x



1050 °C – Picric acid-50x

**Figure 7-14** Microstructures of tempered samples at temperatures of 520 °C and 630 °C with cooling rate of 0.6 °C/sec, and different austenitising temperatures.

### 7.2.2.2 Grain size and mechanical properties results

The results of all the Charpy absorbed energy (J), ultimate tensile strength (MPa), and hardness (HB) tests are shown in Table 7.2. The best results for toughness were obtained at the lowest austenitising temperatures, but it was higher at tempering temperature of 630 °C than tempering temperature of 520 °C. Generally the grain size at the austenitising temperatures of 900 °C, 960 °C and 1050 °C and tempering temperature 630 °C is more compatible than the grain size at the austenitising temperatures of 780 °C, 840 °C and 930 °C and tempering temperature 520 °C.

**Table 7-2** Toughness (J), ultimate tensile strength (MPa), and hardness (HB) at tempering temperatures of 520 °C and 630 °C, cooling rate of 0.6 °C/sec, and different austenitising temperatures.

Samples No.	Austenitising temperature (°C)	Tempering temperature (°C)	Grain size (µm)	Charpy absorbed energy (Joules)	Hardness (HB)	Calculated UTS (MPa)= 3.38HB
Sample 10	780	520	5 ± 1	29	337 ± 4	1138
Sample 2	840		47 ± 6	16	366 ± 8	1236
Sample 11	930		31 ± 4	19	370 ± 5	1251
Sample 12	900	630	25 ± 1	47	313 ± 2	1058
Sample 7	960		60 ± 3	17	329 ± 2	1112
Sample 13	1050		164 ± 31	7	314 ± 2	1062

Figures 7.15 and 7.16 show the fracture surfaces of the Charpy impact specimens with variations in toughness after heat treatment under the conditions described in Table 7.2. The vertical cracks propagation of sample 12 (47 J), sample 2 (16 J) and sample 10 (29 J), are also shown in the same previous figures. From the images of the fracture surfaces it can be seen that some of the fracture surfaces are brittle, which often leaves a rough surface such as in sample 13, while other surfaces are mixed between brittle fractures (rough) and ductile fractures (conchoidal), such as in sample 12. Moreover, it can be seen in the figures that the profiles of the vertical cracks propagation also depend on the type of fracture.

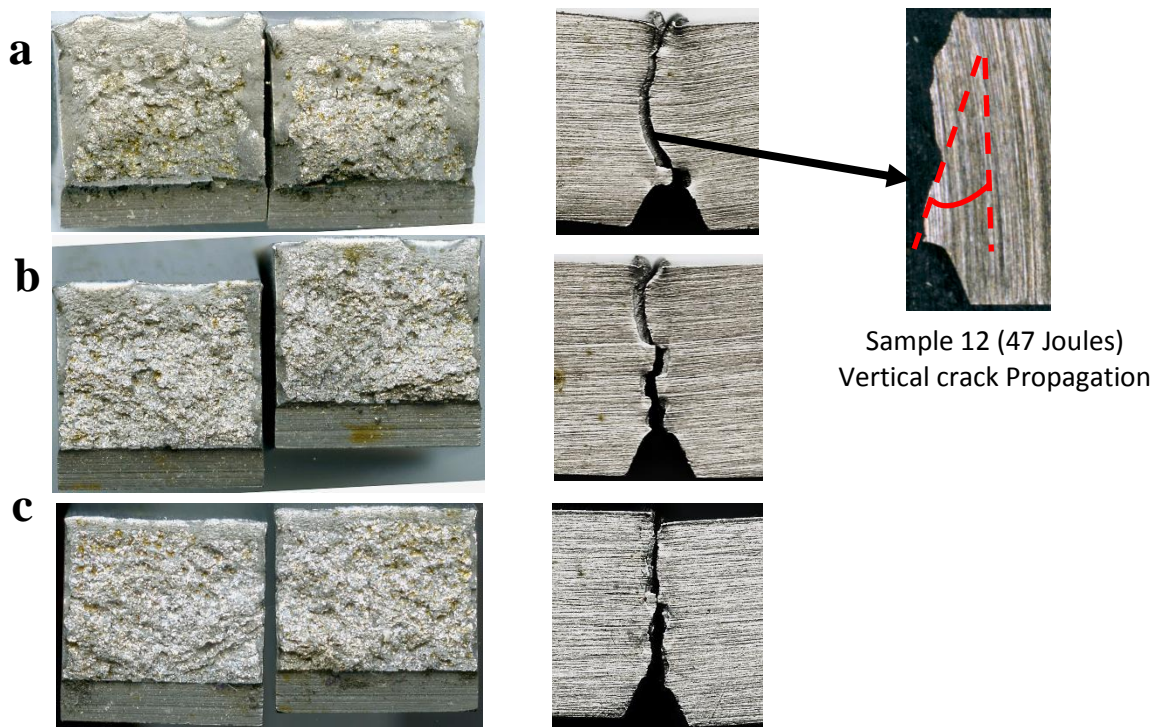
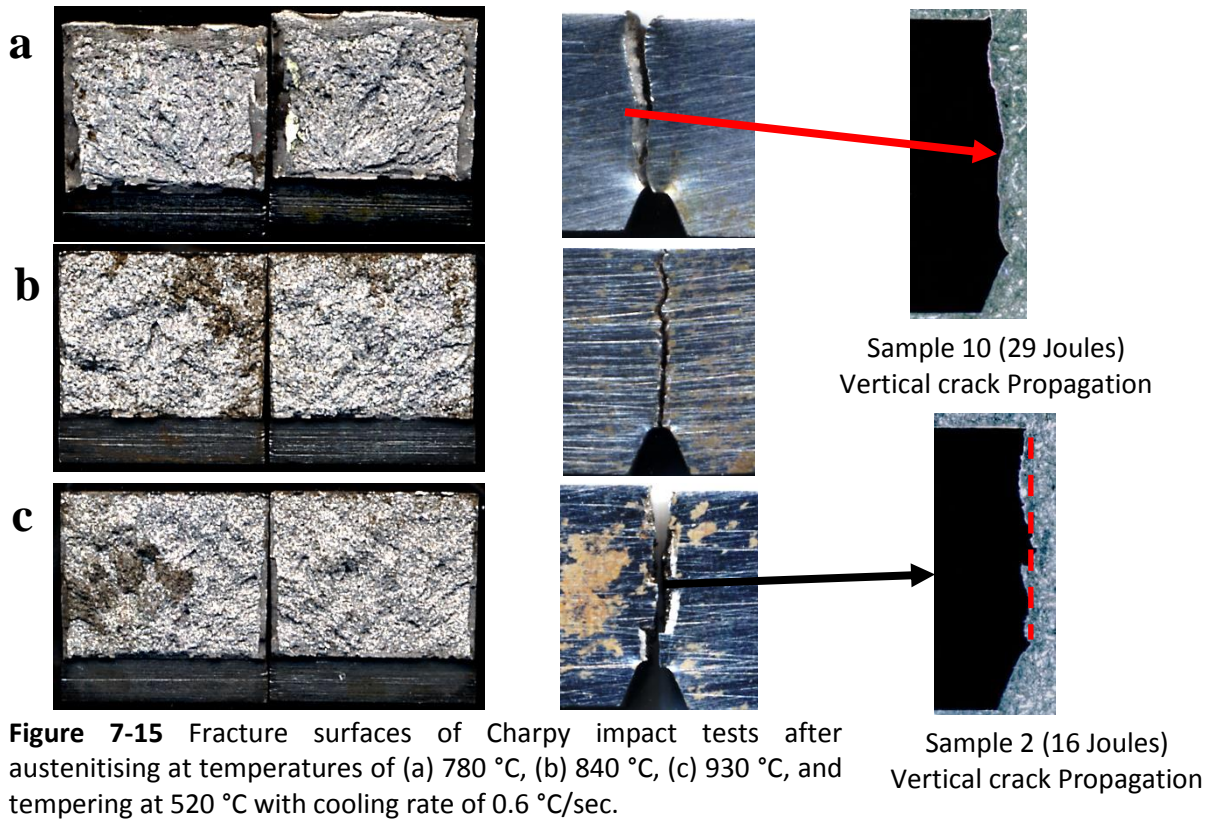
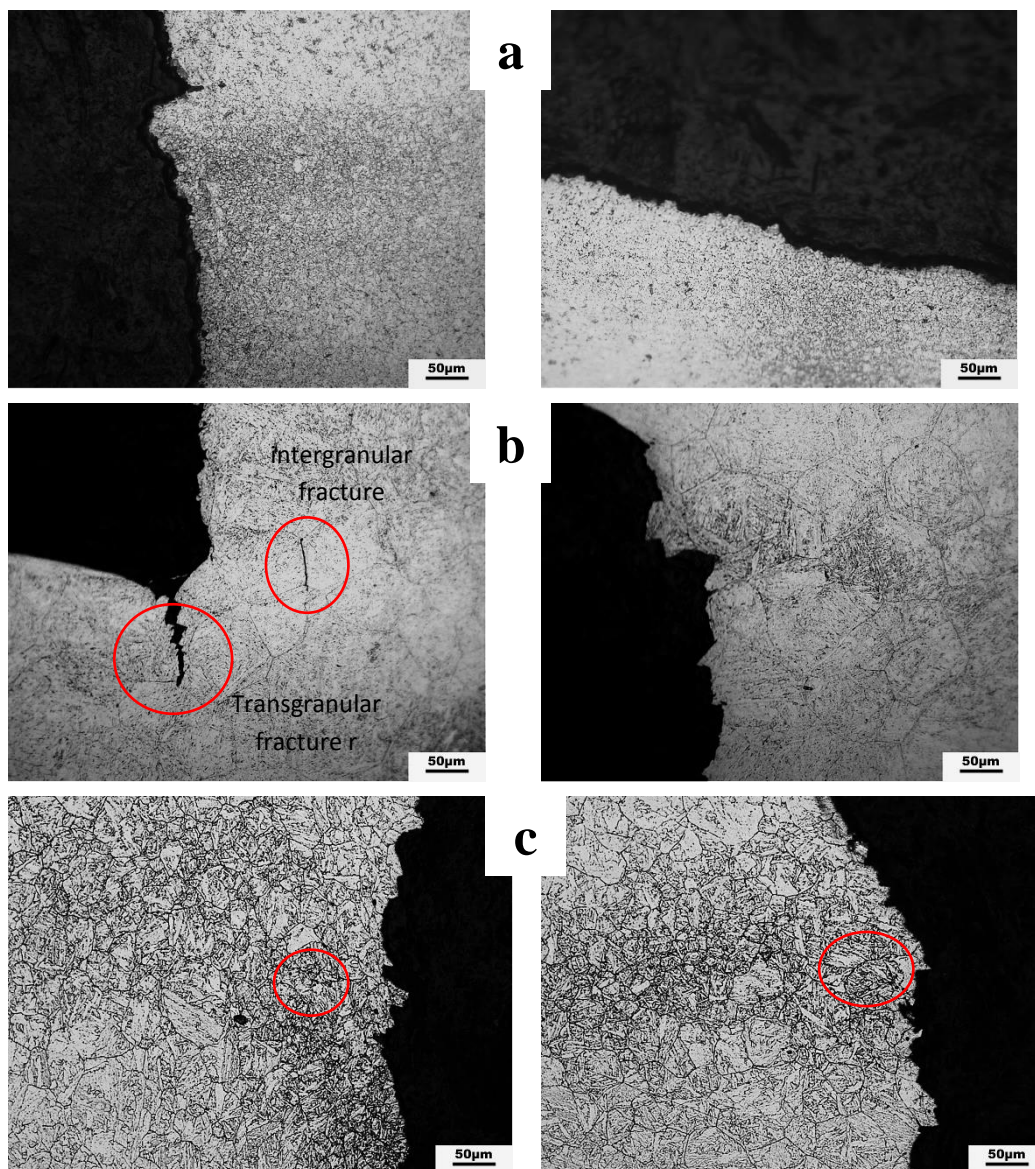


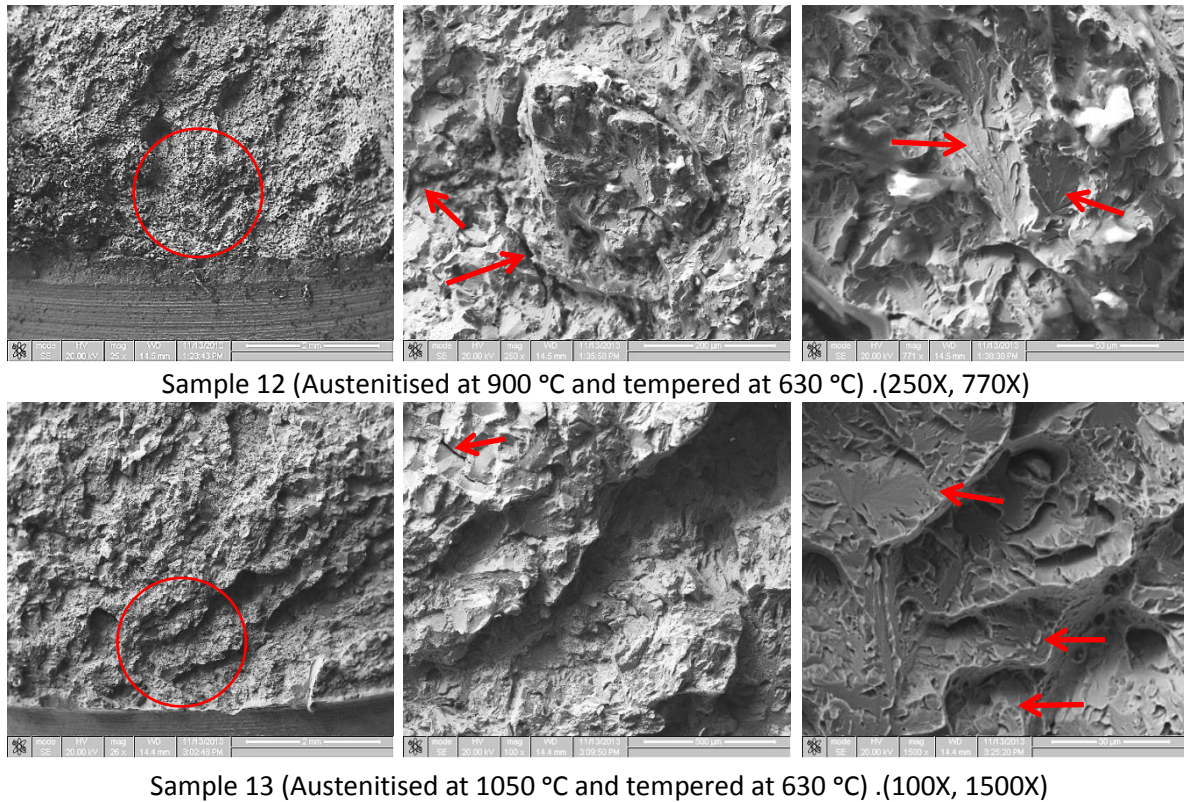


Figure 7.17 shows the fractured grains at the microstructural level for the vertical crack propagation of the specimens with toughness of (a) sample 10 (29 J), (b) sample 2 (16 J), (c) sample 12 (47 J). All samples were etched with picric acid to reveal the microstructures. As can be seen, the microstructure of sample 2 combines two types of crack; intergranular and transgranular. The paths of some of these cracks cross through the grains, while other cracks follow the grain boundaries. Moreover, in sample 12 the cracks are only intergranular and almost all the cracks follow the grain boundaries.



**Figure 7-17** Austenite grains along the vertical crack propagation of (a) sample 10, (b) sample 2, (c) sample 12. Etched with picric acid (20x).

The scanning electron microscope (SEM) images of the Charpy fracture surfaces of samples 12 and 13 are shown in Figure 7.18. Sample 13 revealed a brittle fracture with transgranular cleavage mode at surface, while the sample 12 revealed intergranular fracture mode.



**Figure 7-18** Scanning electron microscope images for the Charpy fracture specimen samples 12 and 13.

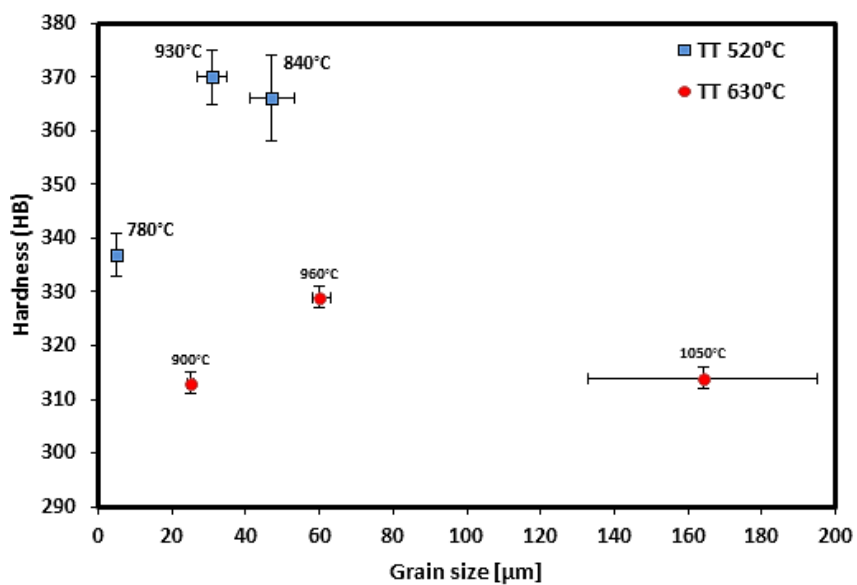


**Figure 7-19** Relationship between grain diameter and hardness (HB) (TT = Tempering temperature)

Figures 7.19 and 7.20 shows the relationship between grain diameter and both hardness (HB) and Charpy absorbed energy (J) with austenitising temperatures of 900 °C, 960 °C and 1050 °C and tempering temperature of 630 °C, and austenitising temperatures of 780 °C, 840 °C and 930 °C and tempering temperature of 520 °C respectively, with different cooling rates. From Figure 7.19 it is clear that the relationship between Charpy absorbed energy and grain diameter is an inverse relationship in which decreasing the grain size increases the toughness.

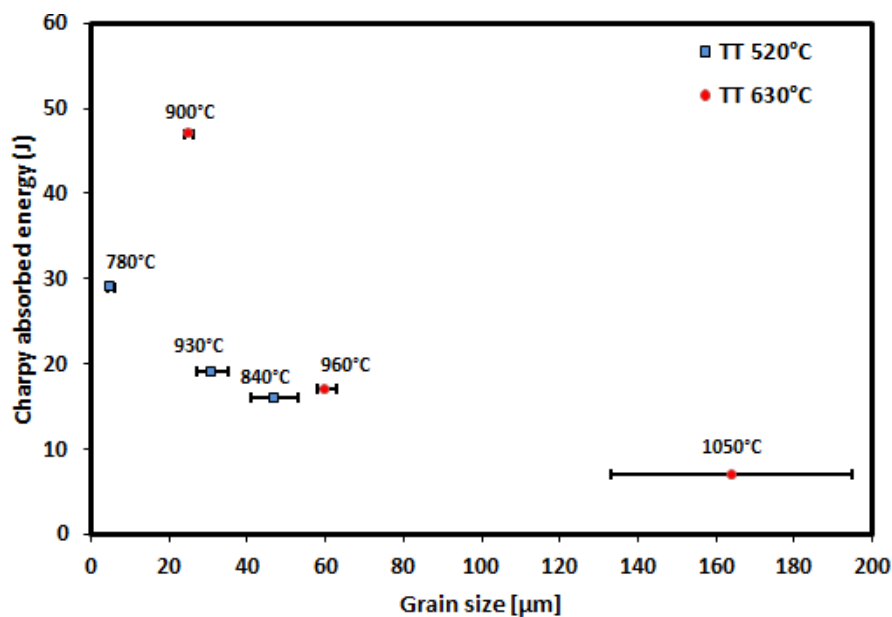


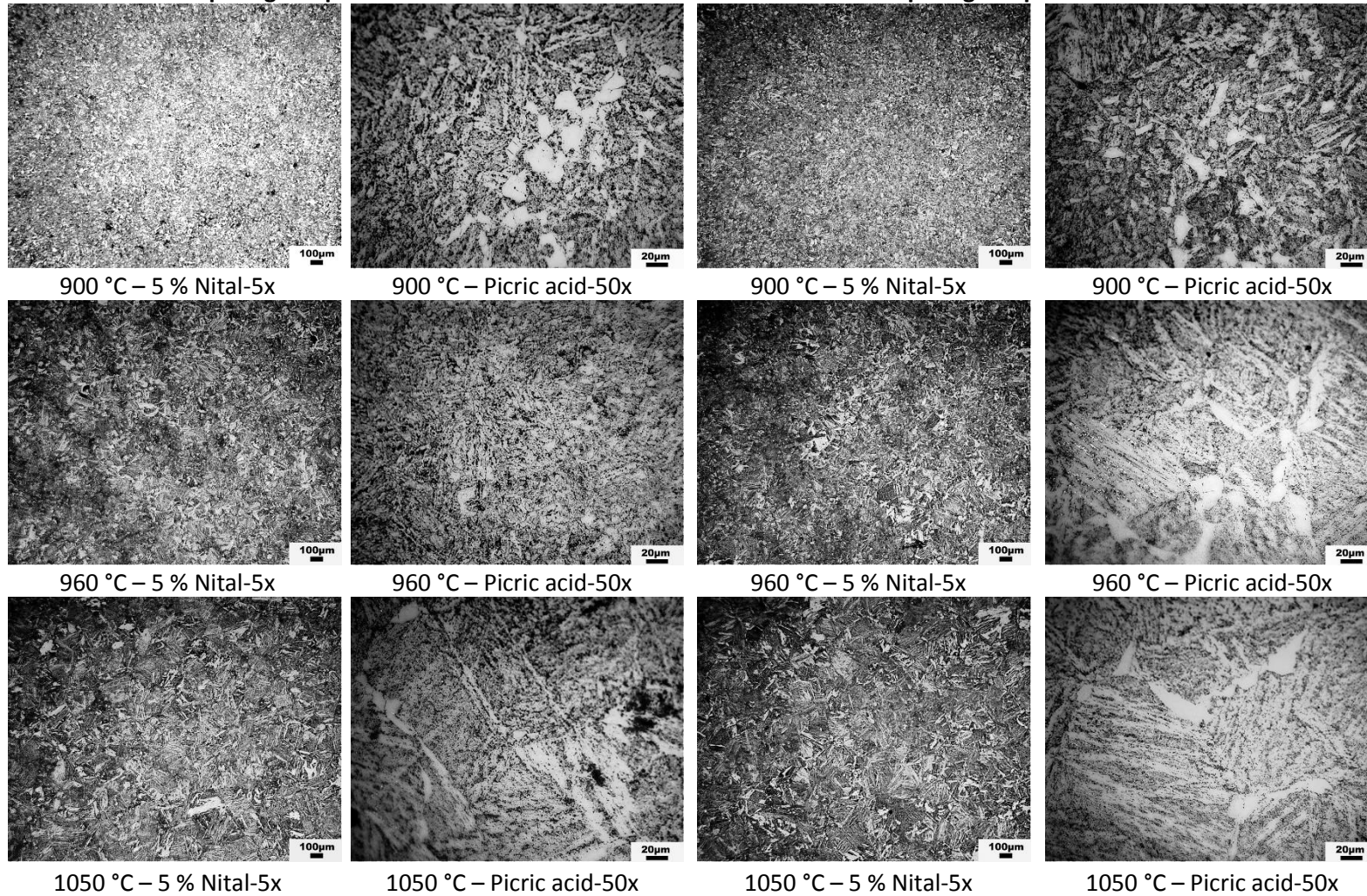
**Figure 7-20** Relationship between grain diameter and Charpy absorbed energy (J). (TT = Tempering temperature)

### 7.2.3 Comparison between tempering temperatures of 630 °C and 640 °C

The tempering temperature is one of the most important variables related to the tempering process that affects microstructure and thus mechanical properties. The real tempering process is carried out at a temperature of 620 °C and, according to the 34CrNiMo6 steel properties, the toughness increases and hardness decreases with increasing tempering temperature (see Fig. 2.45 and Fig. 2.50). Therefore, to increase the toughness without losing too much hardness, the tempering temperature should not be increased to a very high value. Therefore, to attempt to improve some of the mechanical properties and to obtain a good combination of hardness and toughness, tempering temperatures of 630 °C and 640 °C were used.

Tempering temperature of 630 °C

Tempering temperature of 640 °C



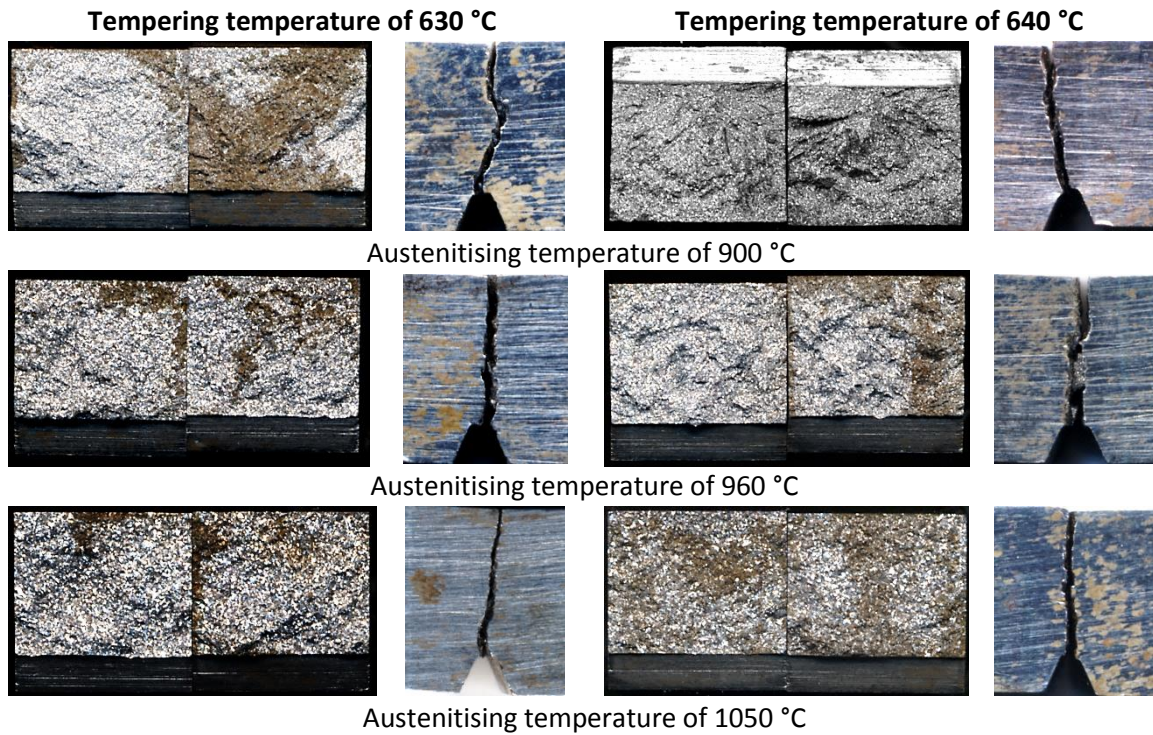
**Figure 7-21** Microstructures of samples tempered at 630 °C and 640 °C followed by furnace cooling after austenitising at different temperatures.

Figure 7.21 shows the microstructures of samples that were austenitised at temperatures of 900 °C, 960 °C and 1050 °C and tempered at tempering temperatures of both 630 °C and 640 °C followed by furnace cooling. 5 % Nital and Picric acid were used to etch the samples to reveal the microstructures. The results of the Charpy absorbed energy (J), ultimate tensile strength (MPa), and hardness (HB) tests at tempering temperatures of 630 °C and 640 °C followed by furnace cooling are shown in Table 7.3. Somewhat higher results for toughness were obtained for the lower austenitising temperatures especially with the tempering temperature of 640 °C. This difference is not too big and it could be considered within the range of experimental error. Otherwise, there were almost no changes in hardness between the tempering temperatures.

**Table 7-3** Toughness (J), ultimate tensile strength (MPa), and hardness (HB) at tempering temperature of 630 °C and 640 °C followed by furnace cooling.

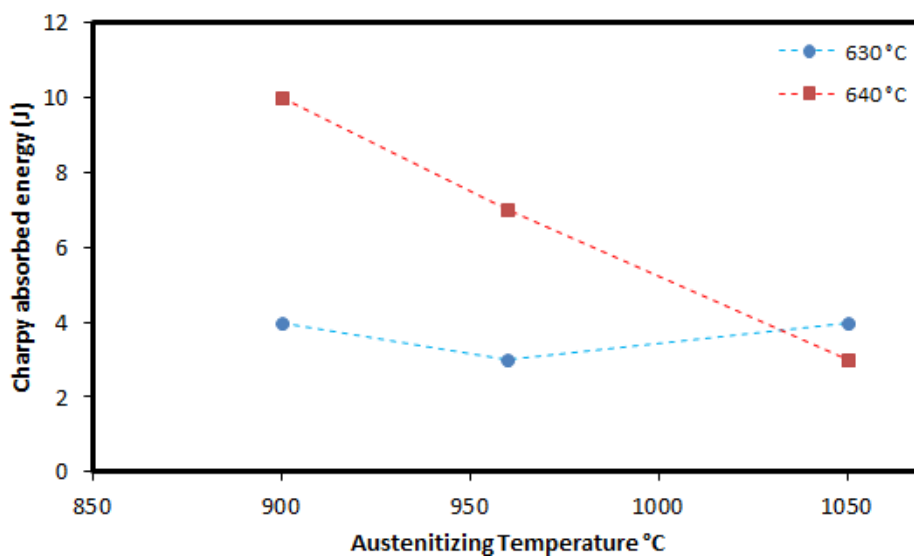
Samples No.	Austenitising temperature (C)	Charpy absorbed energy (Joules)	Hardness (HB)	Calculated UTS (MPa) = 3.38HB
Sample 14	900	4	298 ± 4	1006
Sample 5	960	3	290 ± 4	980
Sample 15	1050	4	312 ± 3	1054
Tempering temperature of 640 °C				
Sample 16	900	10	300 ± 3	1012
Sample 17	960	7	311 ± 4	1051
Sample 18	1050	3	308 ± 5	1041

Figure 7.22 shows the macrograph of the fracture surfaces of Charpy impact specimens that were austenitised at different temperatures prior to tempering at temperatures of both 630 °C and 640 °C and followed by furnace cooling. In addition the profiles of the propagated cracks on the side perpendicular to the V-notch side are also shown in the figure. As can be seen, almost all the fracture surfaces are brittle.



**Figure 7-22** V-notch Charpy impact specimens after the fracture that were tempered at 630 °C and 640 °C followed by furnace cooling after austenitising at different temperatures.

The relation between Charpy absorbed energy (J), austenitising temperature with tempering temperature of both 630 °C and 640 °C using furnace cooling are shown Figure 7.23. The relationship at tempering temperature 640 °C is more compatible than at tempering temperature 630 °C, where the toughness increases with decreased austenitising temperature.



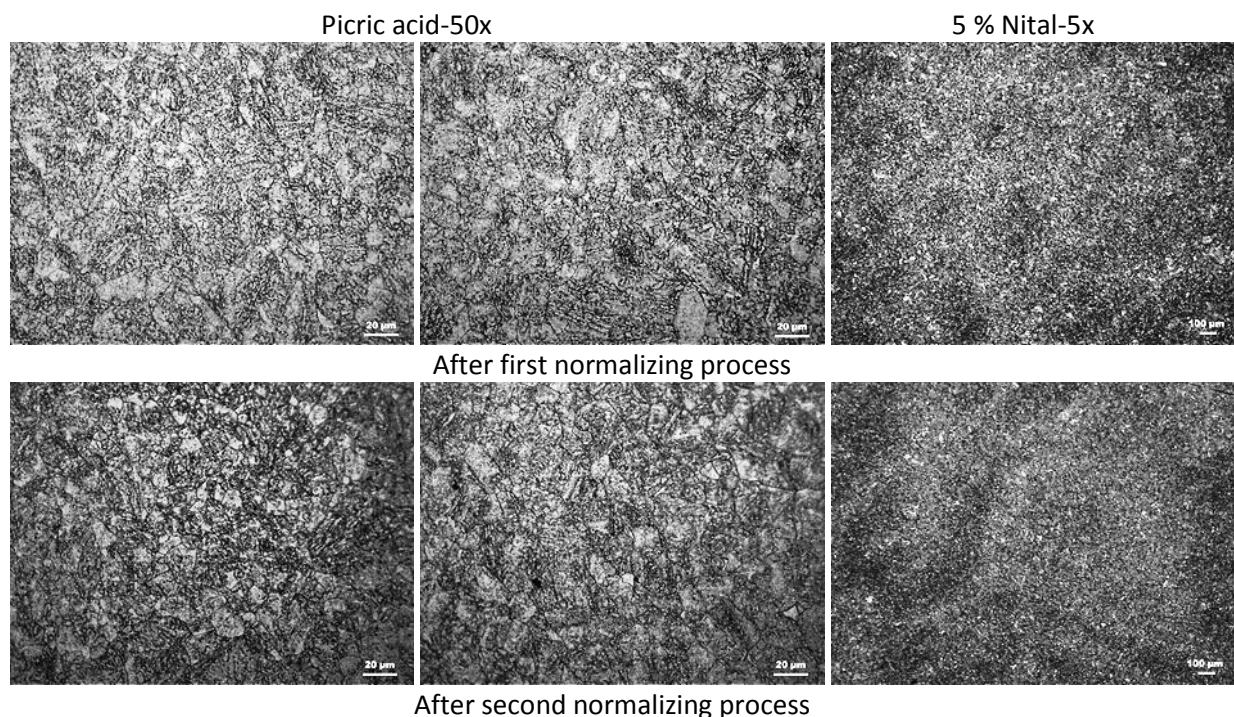
**Figure 7-23** Relation between Charpy absorbed energy (J) and austenitising temperature (°C) at the two tempering temperatures of 630 °C and 640 °C using furnace cooling.

### 7.3 Multiple heat treatment processes

In a new step we tried to refine the grain size and increase the austenite phase percentage within the microstructure using double normalizing, double quenching, and single tempering processes. Furthermore, these processes were used in all possible permutations to investigate their influence on the final microstructure in an attempt to discover the most effective heat treatment cycle and effective sequence for the heat treatment operations.

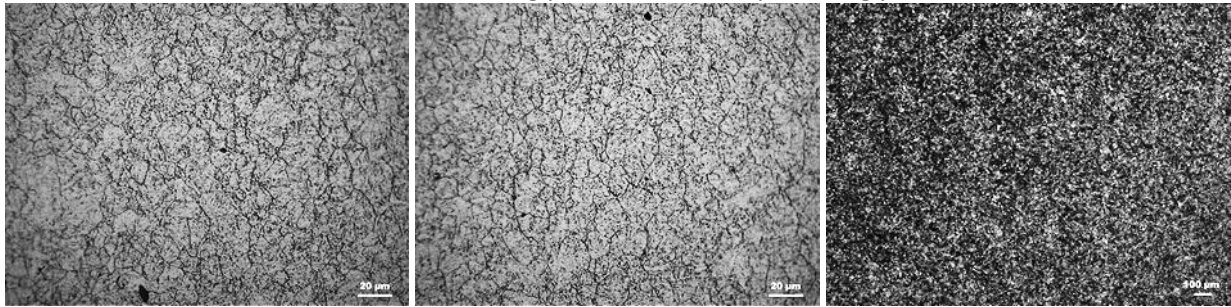
#### 7.3.1 Cycle 1 (Double normalizing + Quenching + Tempering)

The optical micrographs for all the processes that were used in cycle 1 are shown in Figure 7.25. These micrographs were after the first normalizing process, after the second normalizing process, after the double normalizing process followed by a quenching process, and finally after the whole of cycle 1, which consists of double normalizing process, and one quenching process followed by a tempering process. The cooling rate of 0.6 °C/sec was used with the quenching and tempering processes, whilst furnace cooling was used with the normalizing process. 5 % Nital and Picric acid were used to etch the samples to reveal the microstructures. As can be seen from the figure, after quenching the percentage of austenite was significantly increased.





After double normalizing process and one quenching process

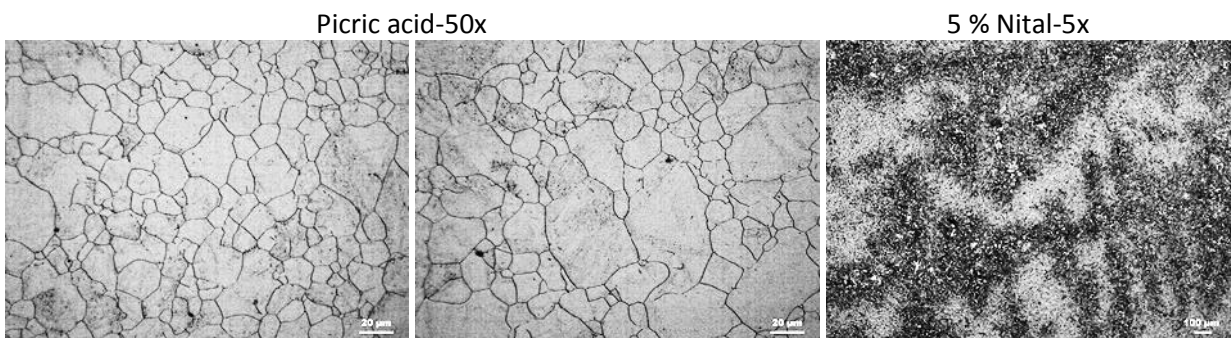


After double normalizing process and one quenching process followed by tempering process

**Figure 7-24** Optical micrographs revealed with both Nital (5x) and Picric acid (50x) for the all steps of cycle 1

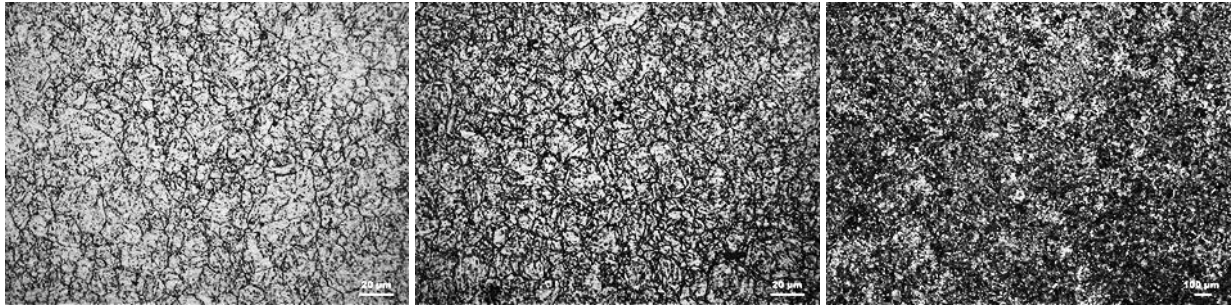
### 7.3.2 Cycle 2 (Double normalizing + Double quenching + Tempering)

The processes of normalizing, quenching and tempering in all cycles were performed under the same conditions of temperature, holding times and cooling rates. Accordingly, some of the optical micrographs are the same as in the other cycles. Figure 7.26 shows the optical micrographs of the heat treated samples for the last two steps of cycle 2. These two steps represent the double normalizing and double quenching processes without and with the tempering process, respectively. In comparison with cycle 1, in cycle 2 the percentage of martensite is less and some grains within the microstructure became more abnormal after the second quenching process. In other words, the second quenching process did not improve the microstructure and therefore did not increase the efficiency of the heat treatment cycle.



After double normalizing and double quenching process



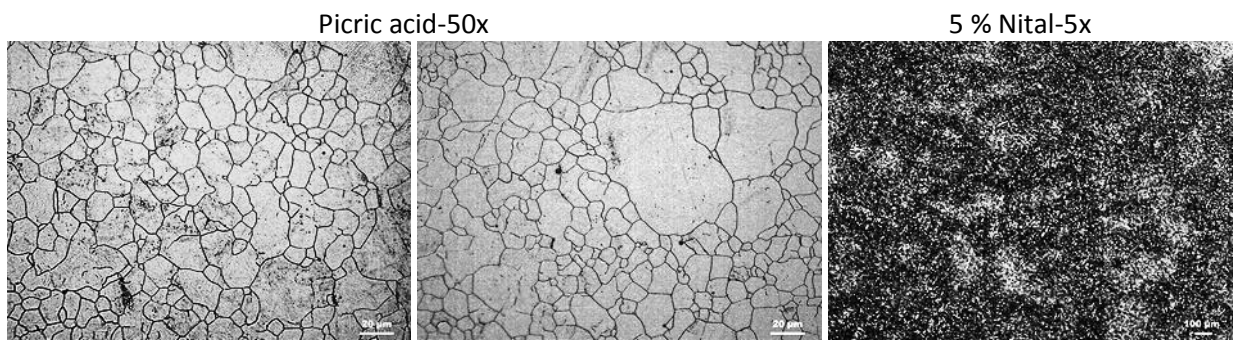


After double normalizing, double quenching and tempering process

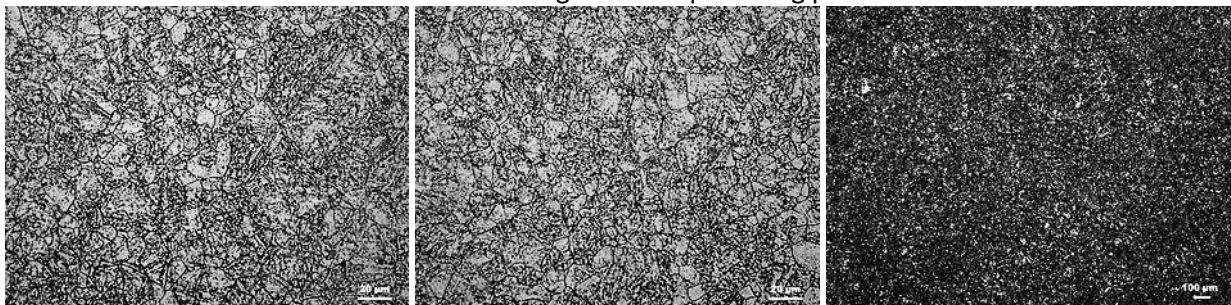
**Figure 7-25** Optical micrographs revealed with both Nital (5x) and picric acid (50x) for the last two steps of cycle 2.

### 7.3.3 Cycle 3 (Normalizing + Quenching + Normalizing + Quenching + Tempering)

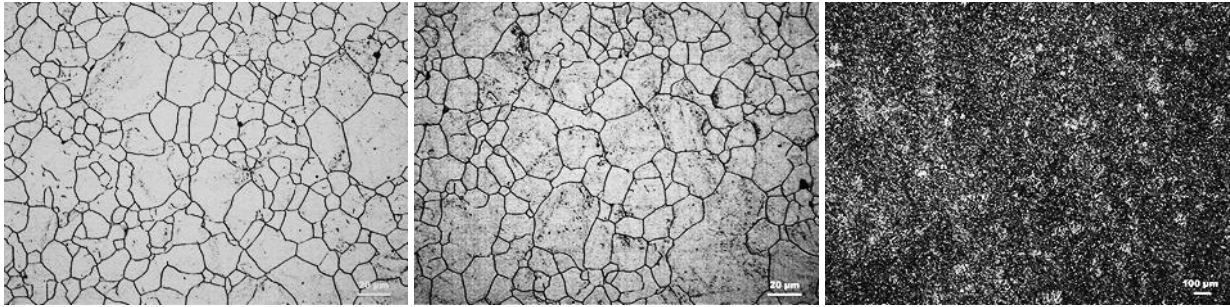
The processes of cycle 3 were the same as in cycle 2 except for the order in which they were carried out. Double normalizing and double quenching processes were used but were repeated sequentially one by one (see Figure 3.25). The optical micrographs for all the processes that were used in this are shown in Figure 7.27. These micrographs were after the first normalizing and quenching processes, after one normalizing, one quenching and the second normalizing process, after repeating the processes of normalizing and quenching twice, and finally after the double (normalizing + quenching) processes followed by the tempering process. As can be seen from the micrographs in Figure 7.27, before tempering, the microstructure becomes more equiaxed but the percentage of martensite is still less than in cycle 1.



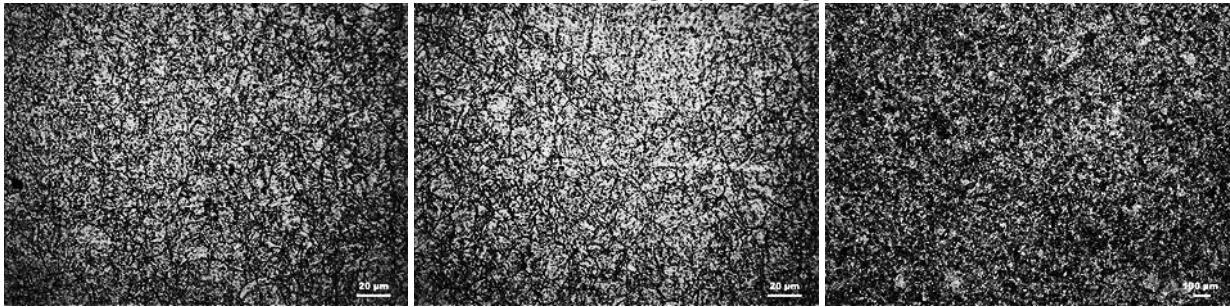
After one normalizing and one quenching process



After one normalizing, one quenching and one normalizing process



Double of (normalizing + quenching)

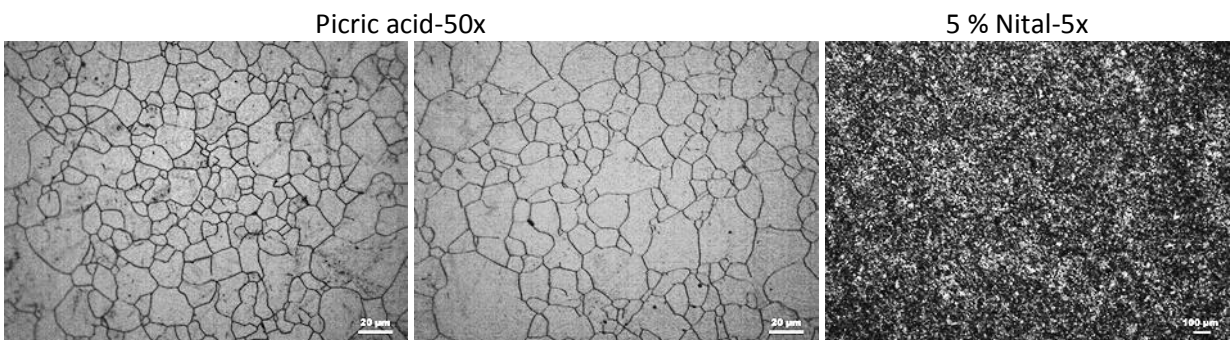


Double of (normalizing + quenching) followed by tempering process

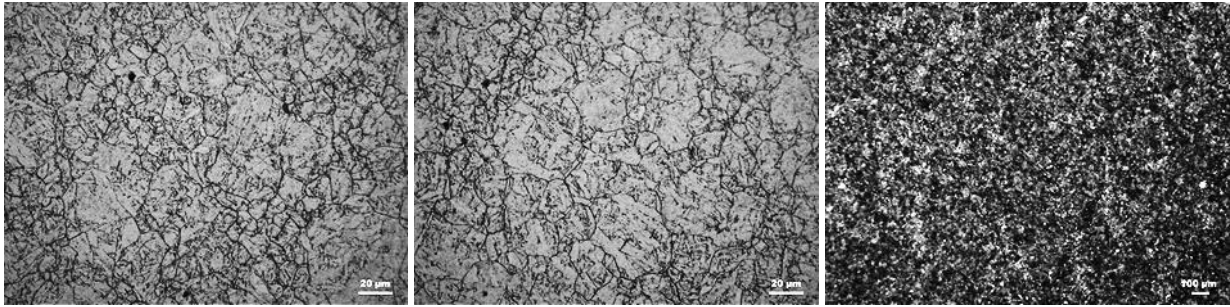
**Figure 7-26** Optical micrographs revealed with both Nital (5x) and picric acid (50x) for all steps of cycle 3 excluding the first normalizing process.

### 7.3.4 Cycle 4 (Normalizing + Double quenching + Tempering)

The optical micrographs of cycle 4, which consisted of one normalizing, two quenching, and one tempering processes respectively, are shown in Figure 7.28. The main purpose of the double quenching process was to increase the amount of martensite within the microstructure. As can be seen from the figure, before tempering the percentage of martensite within the microstructure actually increases compared with the other cycles. However it also seems that after the tempering process the microstructure still contains some bainite or martensite.



After one normalizing and double quenching process



After one normalizing, double quenching and tempering process

**Figure 7-27** Optical micrographs revealed with both Nital (5x) and picric acid (50x) for the last two steps of cycle 4.

After finishing the tempering process in all heat treatment cycles the samples were machined and prepared to perform the hardness and the Charpy impact tests. The results of the Charpy absorbed energy (J), hardness (HB), and ultimate tensile strength (MPa) for all the tests are shown in Table 7.4. Generally, all the results for the toughness and the grain size were closed for all the cycles, where all the tests gave a good toughness and a small grain size. In addition, the best results for toughness were obtained at the smallest grain size in cycle1.

**Table 7-4** Toughness (J), ultimate tensile strength (MPa), and hardness (HB) for different heat treatment cycles with cooling rate of 0.6 °C/sec.

Cycle No.	Grain size (µm)	Charpy absorbed energy (Joules)	Hardness (HB)	Calculated UTS (MPa)= 3.38HB
Cycle 1	13 ± 1	101	295 ± 2	998
Cycle 2	18 ± 2	82	306 ± 2	1036
Cycle 3	14 ± 2	86	304 ± 2	1029
Cycle 4	16 ± 1	80	308 ± 2	1042

The distribution of grain size for the microstructures of cycles 1, 2, 3 and 4 are shown in figure 7.29. As shown from the figure the grain size distributions in all multiple heat treatment cycles were unimodal. This distribution was expected as a result of uniform microstructure and good toughness results.

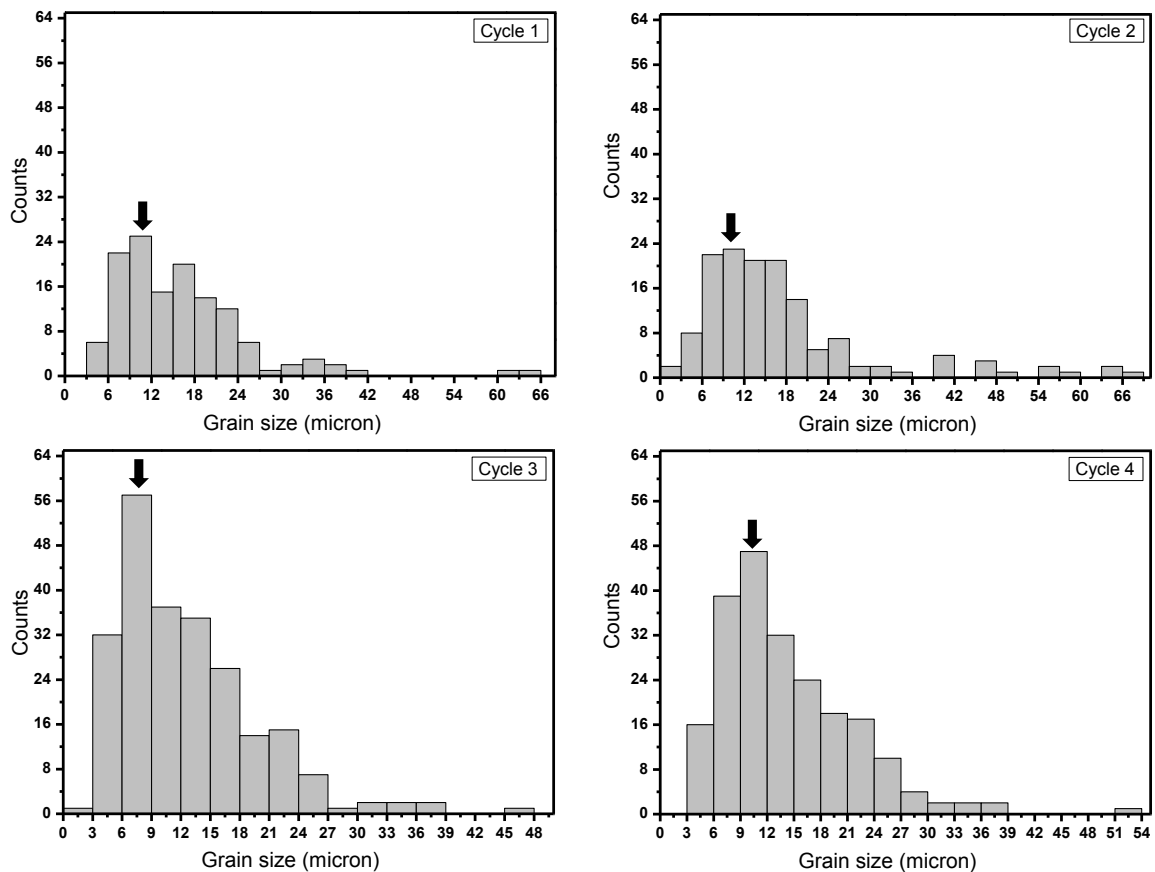


**Figure 7-28** Shows the austenite grain size distributions for the microstructures of cycles 1, 2, 3 and 4.

Macrographs of the fracture surfaces of the Charpy test specimens resulting from the four different heat treatment cycles are shown in Figure 7.30 along with the profiles of the vertical cracks propagation. All the tests were performed at the same temperature as previously,  $-20\text{ }^{\circ}\text{C}$ . From the images it can be seen that all the surface fractures are ductile. Furthermore, the Figure 7.31 show the fractured grains at the microstructural level for the vertical crack propagation of the specimens that were heat treated using cycles 1, 2, 3 and 4. From the figure, it seems that all the cracks in the samples are intergranular fracture mode where almost all the cracks follow the grain boundaries. The scanning electron microscope (SEM) images of the Charpy fracture surfaces of cycle 2 are shown in Figure 7.32.

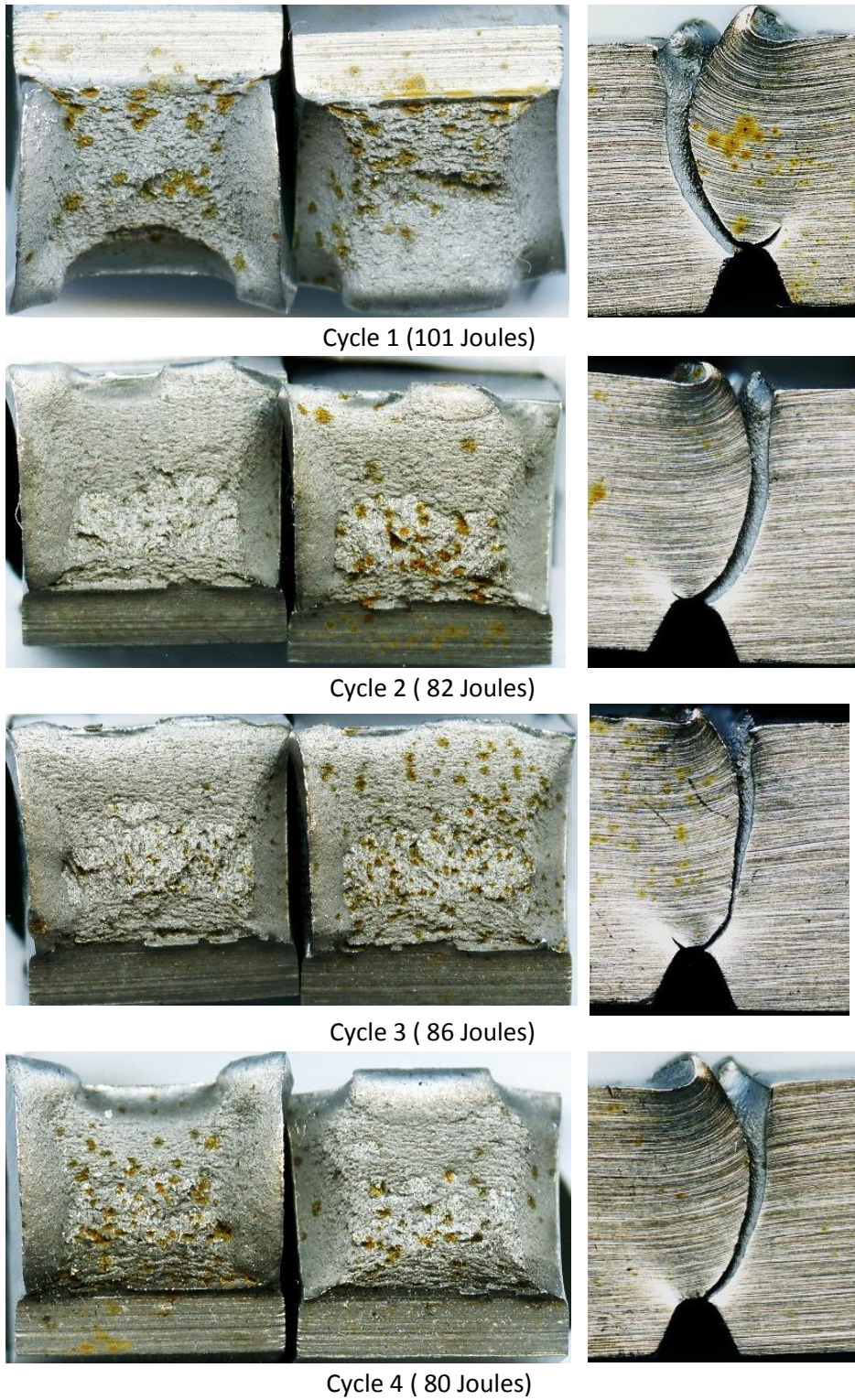


**Figure 7-29** Fracture surfaces of V-notch Charpy impact specimens and the profiles of the vertical cracks propagation that resulted from cycles 1 to 4.

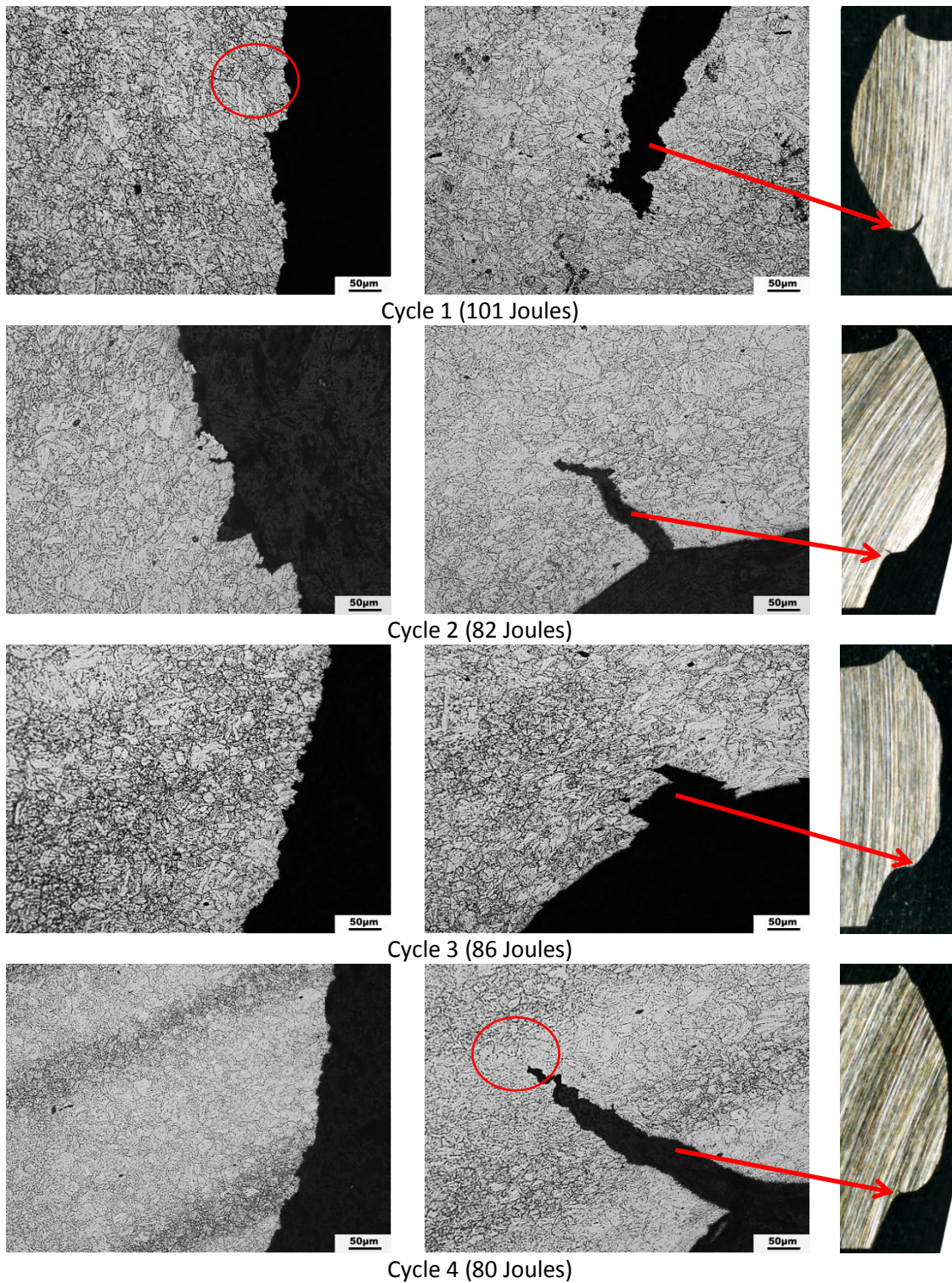


**Figure 7-30** One side fracture of the Charpy specimens and the austenite grains along the vertical crack propagation of cycles 1 to 4 (20x).

Figures 7.33 and 7.34 shows the relationship between grain diameter and both of hardness (HB) and Charpy absorbed energy (J) for all fractured samples. From the Figures it is clear that by increasing the grain diameter the toughness decreases and the hardness increase.

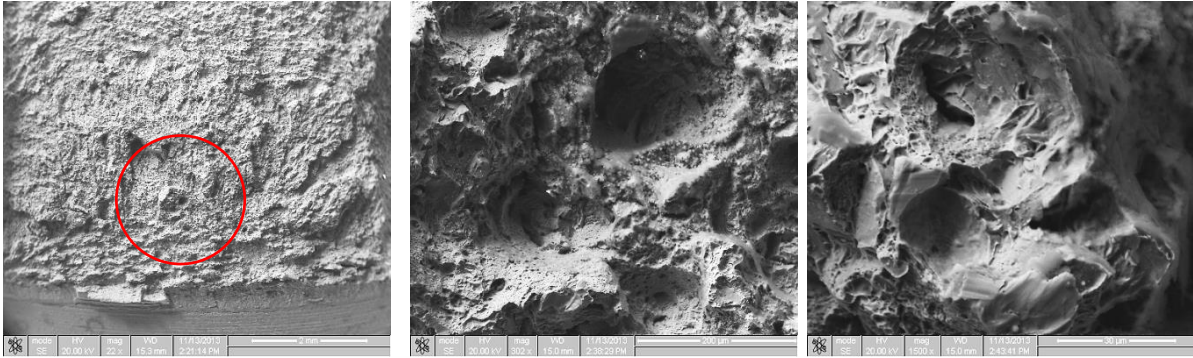


**Figure 7-31** Scanning electron microscope images for the fracture surface of the cycle 2 Charpy specimen. (300X and 1500X)

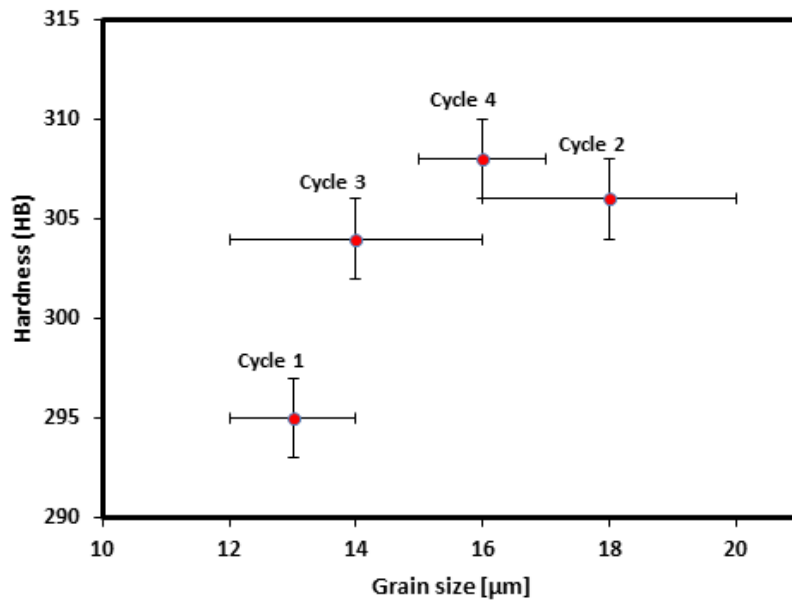


**Figure 7-32** Relationship between grain diameter and hardness (HB) for all cycles.

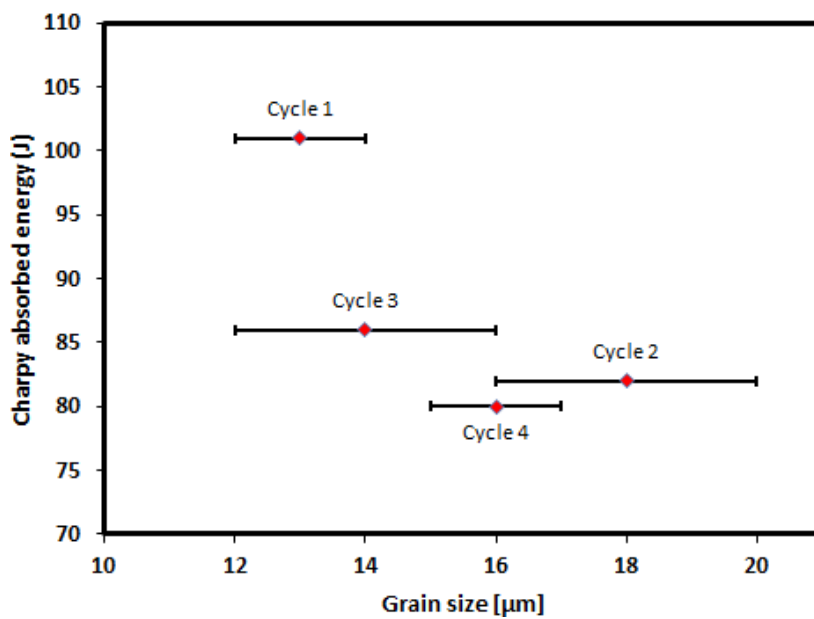


**Figure 7-33** Relationship between grain diameter and Charpy absorbed energy (J) for all cycles.

#### 7.4 Fracture surfaces of the some impact tested (Charpy) samples showing the facet sizes

Fracture surfaces of the impact tested (Charpy) samples with fracture energies 16 J, 47 J, 7 J are shown in Figure 7.24 (a-c), respectively. These Fracture surfaces are showing the different facet sizes (fine and coarse). The sample 2 in Figure 7.24 (a) with grain size of  $47\pm 6\ \mu\text{m}$ , were austenitised at temperature of  $840\ ^\circ\text{C}$  and tempered at temperature of  $520\ ^\circ\text{C}$ . While the samples 12 and 13 in Figure 7.24 (b and c) with grain sizes of  $25\pm 1\ \mu\text{m}$  and  $164\pm 1\ \mu\text{m}$ , were austenitised at temperatures of  $900\ ^\circ\text{C}$  and  $1050\ ^\circ\text{C}$ , respectively, and both tempered at temperature of  $630\ ^\circ\text{C}$ . The cooling rate of  $0.6\ ^\circ\text{C}/\text{sec}$  was used with all three samples. From the figures, the fracture surfaces of samples 2 and 13 have facets of different sizes comparing with sample 12. However, the sample 13, which has the biggest grain size, also has the biggest facet size.

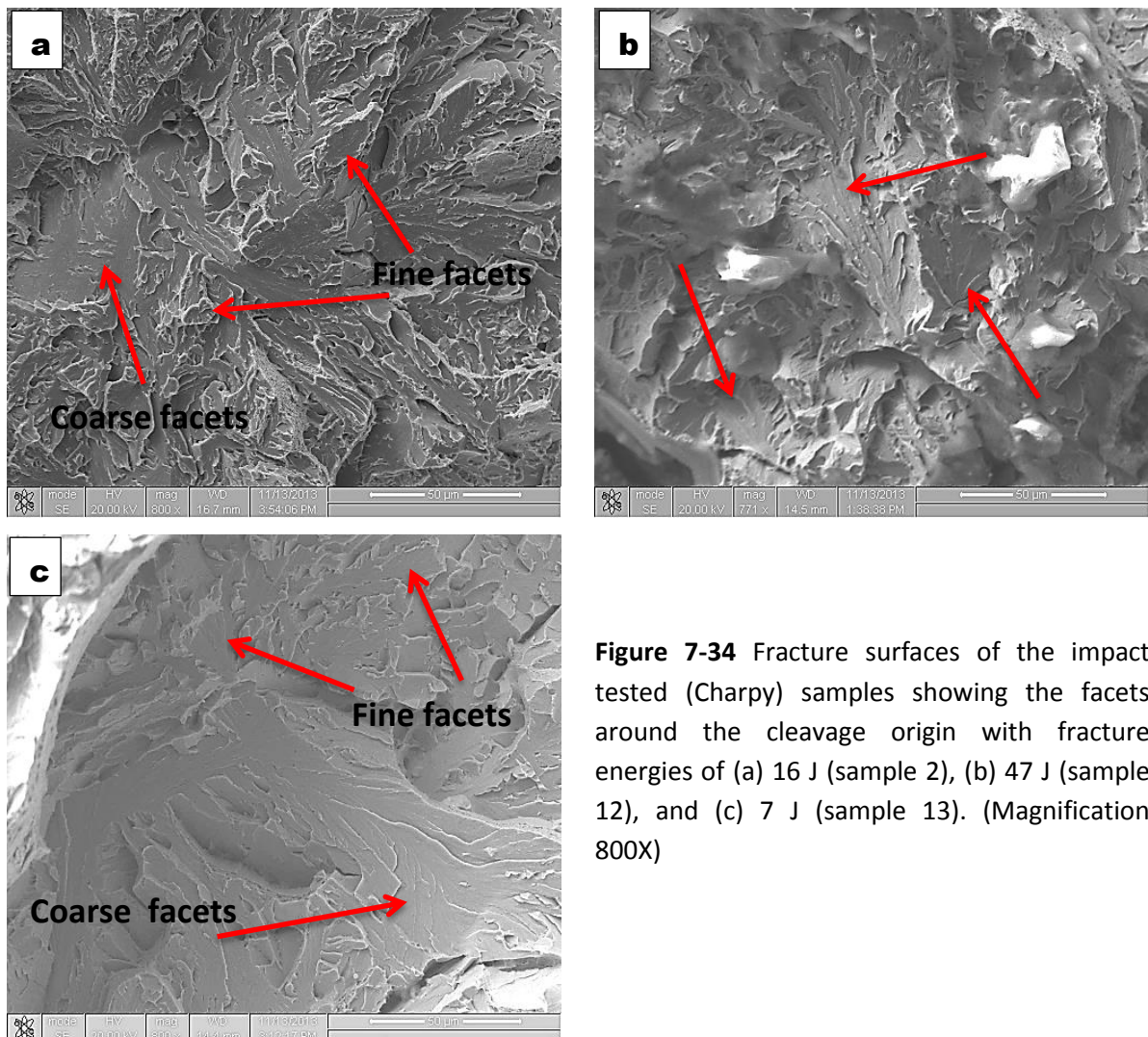
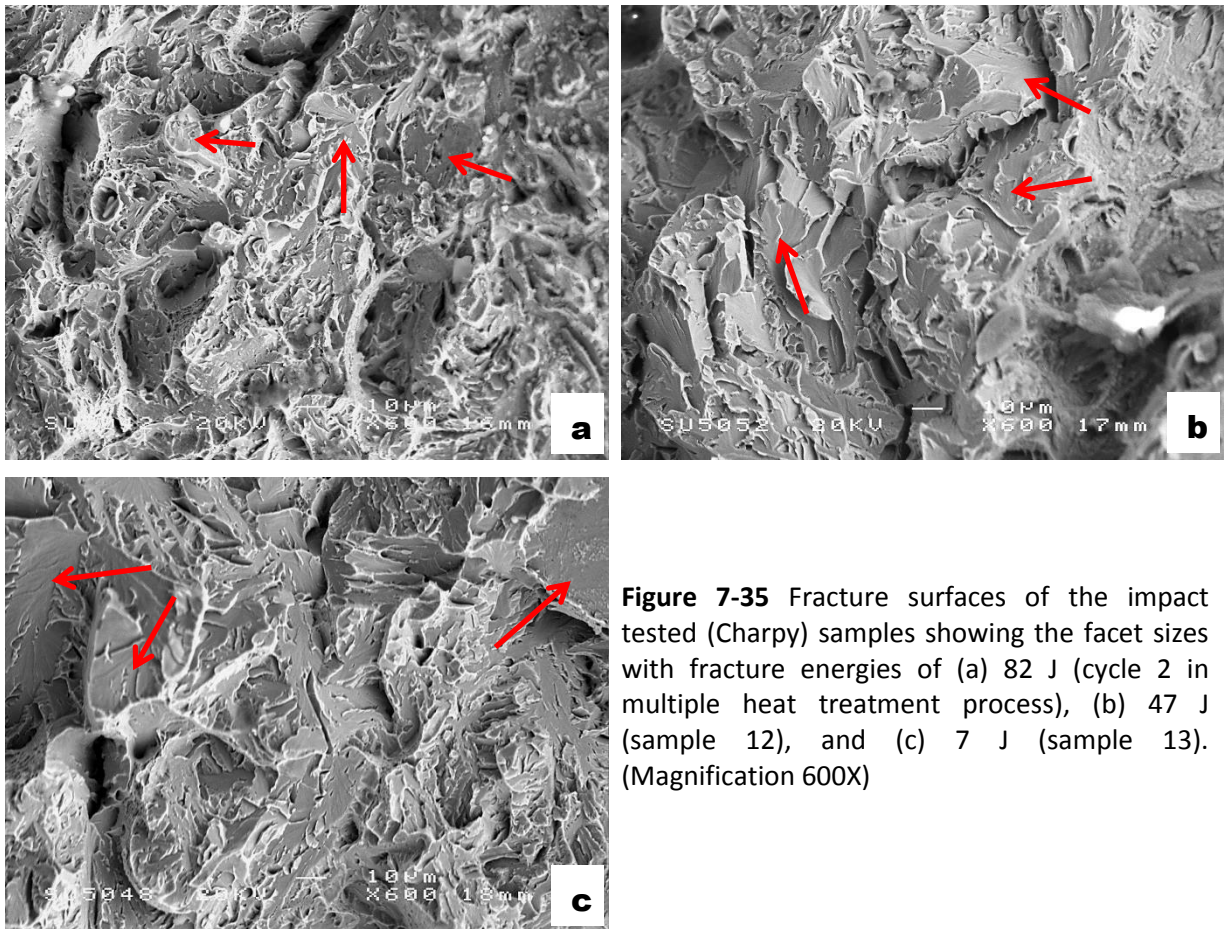


**Figure 7-34** Fracture surfaces of the impact tested (Charpy) samples showing the facets around the cleavage origin with fracture energies of (a) 16 J (sample 2), (b) 47 J (sample 12), and (c) 7 J (sample 13). (Magnification 800X)



Moreover, fracture surfaces of the impact tested (Charpy) for the samples 13 and 14, and cycle 2 in multiple heat treatment process (at lower magnification) are shown in Figure 7.25 (a-c). The cycle 2 in Figure 7.25 (a) with grain size of  $18\pm 2\ \mu\text{m}$  and fracture energy of 82 J, was subjected to the double normalizing and double quenching processes before tempering process, respectively.



## Chapter 8 Discussion

In this chapter, the results that have been presented in Chapters 4, 5, 6 and 7 will be discussed. The discussion follows the same order as the chapters; the isothermal deformation processes (single hit) in terms of flow behaviour and modelling, and in terms of microstructures; the non-isothermal deformation processes (multi hit); and finally the heat treatment processes.

### 8.1 Isothermal deformation processes (single hit)

#### 8.1.1 Austenitising temperatures and holding time

Austenite grain growth is affected by both the austenitising temperature and the holding time, but the effect of the austenitising temperature is stronger than that of the holding time[297]. An austenitising temperature of 1260 °C was used to simulate the real process and to try to optimize the thermo-mechanical process when some deformation parameters are changed. Furthermore, to attempt to refine the austenite grain size and to study the effect of changing the austenitising temperature on the resulting microstructure, an austenitising temperature of 1100 °C was also used. The relation between austenite grain sizes and different holding times for both austenitising temperatures of 1260 °C and 1100 °C, shown in Figure 4.1, was used to determine the appropriate holding time for both austenitising temperatures.

The microstructures of austenite grain size at austenitising temperature of 1260 °C and 1100 °C held for different times are shown in Figures 5.1 and 5.2. The biggest austenite grain size, obtained at austenitising temperature of 1260 °C, was  $335\pm 26$   $\mu\text{m}$  at one hour holding time; after this time the increase in grain size will be slightly less compared to the bigger increase in holding time. The biggest austenite grain size obtained at an austenitising temperature of 1100 °C was  $199\pm 17$   $\mu\text{m}$  at 15 mins holding time, where the grain size remained the same even when heated for one hour. For comparison, the holding time used must be the same for both austenitising temperatures. Therefore one hour austenitising holding time for both austenitising temperatures was chosen to be used for all experimental tests so as to start with the biggest austenite grain size, which represents the worst case scenario before the deformation process.

Furthermore, as shown in Figure 4.1, there is a difference between the kinetic relationships of the curves. This figure shows that the austenite grain size at temperature 1260 °C increases gradually with time from the beginning to the end. The austenite grain growth was significant during the first 30 minutes, but in the latter 30 minutes growth was relatively slower, whereas at a temperature of 1100 °C, the austenite grain size increases rapidly until 15 minutes is reached and then becomes nearly constant. However, as shown from the normal trend of the curves, in the first 15 minutes the increment in austenite grain size was bigger at 1100 °C than at 1260 °C. This difference in kinetics may be related to the presence of alloying elements such as vanadium in the chemical composition, which at 1100 °C precipitate at grain boundaries with increased time, causing grain growth inhibition. Moreover, vanadium nitride particles have a low solubility compared with vanadium carbide and vanadium carbo-nitride particles, so it is the most likely to cause grain growth inhibition at this temperature. The undissolved nitride particles disperse and prevent the growth of grains by pinning the austenite grain boundaries. In contrast, at a temperature of 1200 °C all the vanadium dissolves and the precipitated particles are ineffective in inhibiting austenite grain growth.

In addition, other elements usually present in small amounts in steels and that may remain during steelmaking, such as aluminium (e.g., 0.004 Al% in 34CrNiMo6 steel), are used for grain size refinement. If aluminium is present with nitrogen, aluminium nitride particles will be formed, which may also inhibit austenite grain growth at 1100 °C. For example, Militzer et al. [298] studied the austenite grain growth kinetics in two commercial plain carbon steels, A36 and DQSK. The study showed that, with the existence of aluminium nitride precipitates, there was very little grain growth during isothermal annealing at temperatures below 1100 °C, while fast grain growth took place at 1150 °C. Accordingly, they suggested that the dissolution of aluminium nitride in their steel was complete above the temperature of 1100 °C, thus was responsible for the large grain growth.

### 8.1.2 Flow curves and optical microstructure at both austenitising temperatures of 1260 °C and 1100 °C

Figures 4.2 (a-f) shows the true stress–strain curves at two austenitising temperatures followed by different deformation temperatures, 0.8 strain, and different strain rates. The effects of deformation temperatures and strain rates can be seen in all curves, where at the lower deformation temperature the higher flow stress was obtained; at the same time at the higher strain rate the higher flow stress was achieved. The reason is that high temperatures as well as low strain rates give a longer time for energy accumulation and higher ability to move at grain boundaries for the nucleation and growth of dynamically recrystallised grains and dislocation faded. This is consistent with the fact that flow stress decreases at low strain rates and high temperatures[297]. Furthermore, a single peak was observed in all the flow stress curves.

In the case of austenitising temperature of 1260 °C, as can be seen in Figures 4.2 (d-f), the flow stress increased to a peak and then slightly decreased to a steady state accompanied by dynamic recrystallisation at all deformation temperatures and strain rates. In this case, when the stress reached the peak value, dynamic recrystallisation softening took place and the peak flow stress decreased slowly. After that, hardening and softening balanced and the flow stress curve reached a steady state. Excluded from all that the deformation at temperature of 1000 °C with strain rates of  $1 \text{ s}^{-1}$  and the deformation at temperature of 900 °C with all strain rates, where with these deformation conditions the flow stress increased to a peak and then continued to increase until finally it reached a steady state. The reason for that may be the return to the resulting massive elongated grains with a small percentage of recrystallised grains, especially at a deformation temperature of 900 °C which is approximately the recrystallisation stop temperature. According to the optical micrographs in Figure 5.3, the percentages of recrystallisation at deformation temperature of 900 °C were approximately 11 %, 6 % and 5 % at strain rates of 0.1, 0.5 and  $1 \text{ s}^{-1}$  respectively.

All the results of peak stress and peak strain with all deformation conditions are shown in Table 4.1. As we can see from the table, the peak flow stress increases with increase of deformation strain rate, where for example at the deformation temperature of 1000 °C the peak stress was 81, 99, and 113 MPa when the deformation strain rate was 0.1, 0.5 and  $1 \text{ s}^{-1}$ , respectively. Moreover, the peak flow stress increases with decreasing the deformation

temperature, where for instance at the strain rate of  $0.1 \text{ s}^{-1}$  the peak stresses were 44, 51, 81 and 124 MPa with deformation temperatures of 1200, 1100, 1000 and 900 °C, respectively. In addition, increasing strain rate and decreasing deformation temperature will delay the beginning of dynamic recrystallisation. The peak strain value as shown in Table 4.1 ranges from 0.26 to 0.80.

In the situation of austenitising temperature of 1100 °C, as can be seen in Figure 4.2 (a-c), the stress-strain curves have approximately the same characteristics as the flow stress curves at austenitising temperatures of 1260 °C. Where at strain rate of  $0.1 \text{ s}^{-1}$  almost all the flow stress curves are dynamically recrystallised with a single peak apart from that the flow stress curve at deformation temperatures of 900 °C, likewise at strain rates of 0.5 and  $1 \text{ s}^{-1}$  apart from that the flow stress curves at deformation temperatures of 900 °C, 950 °C and 1000 °C. At the rest of flow stress curves dynamic recovery occurred, where the work hardening dominant at the beginning of deformation increases the flow stress. Then hardening and softening achieved balance when deformation reached a certain degree, flow stress curve reached steady state. Due to the presence of some alloying elements such as Cr in the chemical composition of the studied steel, dynamic recrystallisation is retarded, which leads to an increase in the temperature of crystallization. According to the optical micrographs in Figures 5.4, at deformation temperature of 900 °C there was a partial recrystallisation where just some nuclei germinated dynamically on the original grain boundaries of deformed grains. The percentages of recrystallisation were approximately 24 %, 15 % and 23 % at strain rates of 0.1, 0.5 and  $1 \text{ s}^{-1}$ , respectively. These percentages are higher compared with those at the same deformation temperature with austenitising temperature of 1260 °C.

Furthermore, from the optical micrographs in Figures 5.3 and 5.4 two other important aspects can be observed. First, the images presented in these figures show the presence of clear banding. These regions, which are manifested by presence bands of quite different microstructures, generally exist in closely spaced pairs of lines parallel to the deformation direction. Generally, these bandings usually result in interdendritic variations in chemistry, producing alternating areas of high and low concentration of different solute elements such as Cr, Mn, and P that are elongated during deformation. In almost all images presented in Figures 5.3 and 5.4 at austenitising temperatures of both 1260 °C and 1100 °C respectively,

these bandings were noted as regions of small equiaxed austenite grains compared with the surrounding grains, which are bigger and have different sizes. Excluding from that the deformation at temperature of 900 °C in both figures, where the banded regions, which are fine recrystallized grains, surround the large non-recrystallized elongation grains. Some authors mention that band morphology, which is represented in thickness, geometry, continuity, etc., depends on the type of deformation[299] and heat treatment[300] employed. Moreover, MAJKA et al. mention that microstructural banding is severely influenced by austenite grain size, austenitising temperature, and cooling rate[301].

Several investigations were carried out about the effect of this banding on mechanical properties. In these studies, a consensus was reached on the detrimental effects of banding on some of these properties e.g., fracture toughness, while there were contradictory results about other properties such as ductility which varied from no effect, to a little effect, to a significant effect [302-304]. In many cases, an aligned banded microstructure produced during deformation is difficult to separate from the effect of aligned inclusion particles, which may make it difficult to determine the effect of banding on mechanical properties[305].

A study by A. Bor[306]of the effect of pearlite banding on the mechanical properties of hot rolled steel plates concluded that the banding exerts no significant effect on strength properties, thus yield strength and tensile strength in the material are little affected. However, it has a significant effect on impact toughness properties and the evolution of banded structures becomes worse with the presence of a level of anisotropy in the material. Furthermore, a study by Grange[303] investigated tensile and notch impact properties in wrought steel containing 0.25%C and 1.5%Mn, with and without elongated inclusions. The specimens were divided into severely banded or nearly free of microstructural banding for comparison. The study results show that both banding and elongated inclusions cause anisotropy in tensile ductility and impact energy. In contrast, by eliminating banding the ductile fracture and anisotropy were significantly improved in clean steel, but in steel with high elongated inclusion the results showed only modest improvement. Accordingly, it can be summarized from these two studies that banded occurrence of the microstructure has an impact mainly on the ductility and the impact energy of the steel, while other mechanical properties are not significantly changed.

The second important aspect that can be observed in Figures 5.3 and 5.4 is the grain size distribution. The prior austenite grain sizes in most of these microstructure images are not uniform, and coarse grains and very fine grains (especially in the banding area) are clearly present. Moreover, Figure 5.6 shows the austenite grain size distributions for the microstructures at conditions of austenitising temperatures of 110°C with deformation temperature of 1100°C and austenitising temperature of 1260°C with deformation temperature of 1200°C. Strain rates of 0.1, 0.5, and 1 s<sup>-1</sup> were used with each deformation temperature. From the figure, two austenite grain size distributions are shown; a unimodal, which has one peak, and a bimodal, where the coarse grains present in a matrix of fine grains. At the austenitising temperature of 1100°C, deformation of 1100°C, and all strain rates, unimodal grain size distributions with a positive skew were obtained. The peaks for these distributions are shown with an arrow in Figure 5.6.

However, at austenitising temperature 1260°C, deformation 1200°C, and the same previous strain rates, bimodal grain size distributions were obtained. The coarse and fine grain regions in these bimodal grain size distributions are also shown with an arrow. The bimodal grain size distribution at the strain rate of 0.5 s<sup>-1</sup> is wider than the distribution at strain rates of 0.1 and 1 s<sup>-1</sup>, while the difference in grain size between the peaks corresponding to the coarse and fine grain populations is higher at 0.1 s<sup>-1</sup> than for 0.5 and 1 s<sup>-1</sup>. Generally, the bimodal grain size has a significantly larger distribution microstructure than unimodal grain distribution microstructures. According to that the average grain size in unimodal distributions is more convergent than in bimodal distributions. Average grain sizes of 43, 40 and 38 μm were obtained in unimodal distributions, whereas average grain sizes of 46, 68 and 57 were obtained in bimodal distributions, at the strain rates of 0.1, 0.5, and 1 s<sup>-1</sup>, respectively.

As was discussed in section 2.7, bimodal grain size has an effect on mechanical properties, especially toughness. In accordance with some studies, the larger difference between the coarse and fine grain sizes, which is usually due to the wider grain size distribution and the larger separation between the coarse and fine grain regions, is usually responsible for scatter in the measured toughness values. Chakrabarti et al.[151] have reported that the differences in the local notch root microstructure were related to the distance of a coarse

grain sized band from the notch root, where If the notch root is located close to this band, the cleavage fracture stress as well as impact energy is going to be lower, and vice versa.

According to what has been discussed earlier (**section 2.4.2**) the main conditions giving rise to dynamic recrystallisation (DRX) can be summarised as following:

- Effect of solutes, precipitates and deformation bands

The precipitation and segregation that develop during casting have a direct effect on the dynamic recrystallisation. The presence of alloying elements in equilibrium solid solution or in supersaturation and therefore acting as precipitate formers generally changes the shapes of the flow curves.

- Effect of initial grain size

The initial grain size also has a significant effect on the kinetics of dynamic recrystallisation of austenite. The results of some researches indicated that the rate of recrystallization will increase in presence of fine grain structure.

- The microstructure variation

In some cases, such as in large scale products, the initial structure which is represented in grain size inhomogeneity within a whole billet also has influence on dynamic recrystallisation. Where the different grain sizes within the billet recrystallize at various rates, and also the growth rate during recrystallisation is not constant through the microstructure.

- Effect of strain rate and deformation temperature changes

The temperature compensated strain rate ( $Z$ ) value also has some bearing on the dynamic recrystallization, where an increase in  $Z$ , by decreasing deformation temperature and increasing strain rate will delay the beginning of dynamic recrystallisation.

- The influence of chemical content

The outcomes of some researches on the effect of chemical composition on dynamic recrystallisation indicated that the beginning of dynamic recrystallisation is delayed and the rate of recrystallisation decreases due to the presence of some alloying elements such as Cr.



### **8.1.3 The relation between grain size diameter and deformation temperatures**

The relationship between grain size and deformation temperature with changing strain rate at both austenitising temperatures of 1100 °C and 1260 °C is shown in Figures 5.5 (a) and 5.5 (b), respectively. As can be seen from the figure, at austenitising temperature of 1100 °C, there was a difference in grain size accompanied with a change in the strain rate at almost all deformation temperatures. The smallest grain size was obtained with a strain rate of 0.5 s<sup>-1</sup>; otherwise, with austenitising temperature of 1260 °C the difference in grain size was just at deformation temperature of 1200 °C, while at deformation temperatures of 1000 °C and 1100 °C there was no difference and the grain size was nearly the same. In other words the changing of strain rate in range of 0.1 - 1 s<sup>-1</sup> will not have any effect on grain size at low deformation temperatures.

### **8.1.4 Calculation of activation energy of deformation**

The curves that are shown in Figures 4.4, 4.5 and 4.6 are used to determine the hot deformation constants, which later will be used in activation energy equations. By comparing these curves it can be seen that at an austenitising temperature of 1100°C the scattering in the data was too small, and the correlation coefficient in all figures was more than 0.96, while at an austenitising temperature of 1260°C the scattering was very small just at deformation temperatures of 1200°C, 1100°C and 1000°C, and the relations were nearly straight lines with correlation coefficient of 0.99. However, at a deformation temperature of 900°C the scattering in data was a bit bigger in all figures with a correlation coefficient of about 0.85.

Comparing to others, Sajadifar et al.[307] used the three points of data to calculate the activation energy for 4340 steel (~34CrNiMo6), and also there was scattered data at temperature of 900°C. Moreover, from Figure 4.2, at a deformation temperature of 900°C the flow curves dynamically recovered at all strain rates. The reason for that may be returned to the change the dynamic recrystallisation to the work hardening when the deformation temperature decreased to 900°C, where the microstructures presented in Figures 5.3 and 5.4 at the deformation temperature of 900°C, which is approximately the recrystallisation stop temperature, show massive elongated grains with a small percentage

of recrystallised grains. As discussed in section 2.4.2.1 a microalloying element such as vanadium causes the retardation of recrystallization. According to the optical micrographs in Figure 5.3, at austenitising temperature of 1260°C the percentages of recrystallisation at deformation temperature of 900°C were approximately 11%, 6% and 5% at strain rates of 0.1, 0.5 and 1 s<sup>-1</sup> respectively. The scattering in data is obvious at strain rates of 0.5 and 1 s<sup>-1</sup> more than at 0.1 s<sup>-1</sup> which is consistent with the recrystallization percentage, where the percentages of recrystallization are small at these strain rates.

As can be seen in Table 4.2, there is a difference between the values of deformation activation energy ( $Q_{def}$ ) resulting from the three exponential equations used at both austenitising temperatures. Among these exponential equations only one has a suitable value of  $Q_{def}$  for the hot working process. This value will be determined in accordance with the linear regressions of the average results data that were used to calculate the  $Q_{def}$  (Fig. 4.7 a-f) for all the exponential equations at both austenitising temperatures. At austenitising temperature of 1100 °C, as shown in Figure 4.7 (a, c, e), the hyperbolic sine law has the highest value of correlation coefficient ( $R^2$ ). Consequently, the activation energy of hot working condition was considered to be 389 (kJ/mol) and in consequence the equation 4.14 is appropriate relation. This is compatible with the reason for using a wide range of temperatures and strain rates[288]. Moreover, according to Figure 4.7 (b, d, f), at austenitising temperature of 1260 °C the power law has the highest value of ( $R^2$ ). Therefore, the activation energy of hot working condition was considered to be 411 (kJ/mol) and thus the equation 4.12 is the appropriate relation, which usually gives good results with low stresses.

The activation energy of deformation is sensitive to any change in chemical composition. Accordingly, comparing the resulting values to the results of others cannot be convergent, unless the chemical composition is the same. Medina and Hernandez[308] have studied the effect of each of the alloying elements C, Mn, Si, Mo, Ti, V, Nb on the Zener-Hollornon parameter  $Q_{def}$ . They conclude that, except in the case of carbon, which has the opposite effect, increasing any of these elements in the content of the alloy was found to increase the activation energy of deformation ( $Q_{def}$ ). In other words, except carbon, which causes a slight softening, all other investigated elements in solution have a hardening effect on the austenite. Niobium followed by titanium has a greater hardening effect than similar

amounts of the rest of the alloying elements. However, some other authors[71, 309] mention that an increase in the carbon content of austenite gives rise to an increase in the value of  $Q_{def}$ . Furthermore, Hamada et al.[310] investigated the influence of aluminium on hot deformation behaviour of high Mn TWIP steels. They found that adding aluminium to the alloy increases the activation energy. The activation energy value for 25Mn steel was 377 kJ/mol, while it was 397 kJ/mol for the 25Mn3Al steels.

In this thesis we used three types of exponential equation; the power law, the exponential law and hyperbolic sine law. However, most authors used the hyperbolic sine law equation to calculate the activation energy of deformation, because it can be used across a wide range of temperatures and strain rates. Consequently, comparison with other previously published values will be made using the same type of equation (Hyperbolic sine law). Nevertheless, this equation also represents appropriate relations for our results. In our work, by using hyperbolic sine law equation average  $Q_{def}$  values of 400 kJ.mol<sup>-1</sup> and 389 kJ.mol<sup>-1</sup> were obtained at austenitising temperature of 1260 °C and 1100 °C respectively. These values are compared with those of other steels, which are listed in Table 8.1. As can be observed, these values which have been found clearly show that results are dependent on the nature of the metal and sensitive to changes in the chemical composition

As mentioned earlier (section 1.1), according to their composition, AISI 4340 steel is considered one of the 34CrNiMo6 steel grades. Accordingly, in comparison with the activation energy value for 4340 steel, which is 427 kJ.mol<sup>-1</sup>, our results may be considered to be very close, taking into account the slight differences in the percentages of contents of both alloys. Moreover, the presence of a small amount of V (0.07 wt%) in the 34CrNiMo6 steel also will help to make the activation energy a little higher. In addition, the material constants that were used to calculate the  $Q_{def}$  for 4340 steel are also close to our results, as can be seen in figure 8.2. The activation energy value of Mn-Cr steels, which is 379 kJ.mol<sup>-1</sup>, is also considered relatively close to our result, especially that at austenitising temperature of 1260°C. As for the other types of steel, the activation energy of 34CrNiMo6 steel is higher than the activation energy of typical 4140 steels. On the other hand, as compared to the  $Q_{def}$  value of 42CrMo steels and stainless, the 34CrNiMo6 steel has a lower value.

**Table 8-1** Comparison of activation energies of deformation values for various steel alloys, using the hyperbolic sine law equation.

Alloy	Q (KJ*mol <sup>-1</sup> )	Reference
34CrNiMo6 steel (1100 °C)	389	our results
34CrNiMo6 steel (1260 °C)	400	our results
4340 steel	427	[307]
4140 steel	318	[311]
Mn-Cr steel	379	[312]
42CrMo steel	463	[313]
Stainless steel	508	[314]

**Table 8-2** Comparison of material constants values for 4340 steels in table 8.1 with our values.

Alloy steel	n	$\beta$	$\alpha$	n`
34CrNiMo6 steel (1100 °C)	7.1	0.074	0.0105	5.06
34CrNiMo6 steel (1260 °C)	7.82	0.086	0.011	5.01
4340 steel	7.74	0.096	0.012	-

The  $Q_{def}$  in isothermal compression of 300M steel was investigated by Luo et al.[315]. The mechanical properties of 300M steel were modified by adding alloying elements of 1.6% silicon and 0.1% vanadium in 4340 steel. They found that the  $Q_{def}$  of deformation values for this steel was in the range of 332±61 to 397±31 kJ/mol. They mentioned that the reason for variation in the activation energy for deformation with strain is attributed to microstructural evolution of steel. Considering that the 300M steel is close in chemical composition to the 4340 steel, these values of  $Q_{def}$  are also close to our values, especially in the higher range.

### 8.1.5 The Zener–Hollomon Parameter (Z) as a function of stress

The relationship between Zener–Hollomon Parameter (Z) and the peak stress as a function of used exponential equations (The power law, the exponential law, and the hyperbolic sine law) for both austenitising temperatures of 1100 °C and 1260 °C is shown in Figures 4.8 and 4.9, respectively. According to Figure 4.8 (a-c) the hyperbolic sine equation (Eq. (4.17)) has the highest correlation coefficient ( $R^2$ ), which makes the relation 4.14 more appropriate for

analysis, whereas the highest correlation coefficient at austenitising temperature of 1260 °C, as shown in Figure 4.9 (a-c), was obtained with the power law equation (Eq. (4.18)), which usually give good results with low stresses. The hyperbolic sine law also has a good fit at austenitising temperature of 1260 °C. In summary, the peak stress of 34CrNiMo6 low alloy steel under the deformation conditions that were used in this study can be expressed by rearranging Eq. 4.17 with austenitising temperature of 1100 °C, and by rearranging Eq. 4.18 with austenitising temperature of 1260 °C.

### 8.1.6 The relation between grain size diameter and the Zener-Hollomon parameter

As is known, the main influencing factors on the Zener-Hollomon parameter ( $Z$ ) are the strain rate and deformation temperature. In the manufacturing processes, equivalent strain rate usually depends on manufacturing equipment, especially in large scale products. Accordingly, small values of strain rates (0.1, 0.5, 1 s<sup>-1</sup>) were used with all deformation temperatures. Figure 4.10 shows the relationship between the grain size and the natural logarithm of  $Z$  for austenitising temperatures of both 1100 °C and 1260 °C. From the figure it can be seen that small  $Z$  values were obtained with a big grain size, which is associated with a decrease in strain rate and increase of deformation temperature which facilitates recrystallisation. In contrast, big  $Z$  values were obtained with a small grain size, and that usually happens with an increase in strain rate and decrease of deformation temperature, which facilitates dynamic recovery. In addition, from linear regressions of the results in Figure 4.10, a good relation between grain size and the natural logarithm  $Z$  was obtained with austenitising temperature of 1100 °C, which is represented in the following equation [ $d=4.1 \ln(Z) + 173$ ]. The linear regressions of the results at austenitising temperature of 1260 °C were lower because the data were slightly scattered at higher temperature of 1200 °C, which is represented in equation [ $d=-4.2 \ln Z + 187$ ].

However, as illustrated in Figure 4.10 (b) there was scattering in data at low  $\ln(Z)$  compared with high  $\ln(Z)$ , and also compared with low  $\ln(Z)$  in Figure 4.10 (a). The figure shows that the scattering was specifically at austenitising temperature of 1260 °C and deformation temperature of 1200 °C with all strain rates of 0.1, 0.5, and 1 s<sup>-1</sup>. Since the parameters that relate to the natural logarithm of ( $Z$ ) are either constant (e.g.,  $Q$  and  $R$ ) or

have specific values (e.g., strain rate) at all deformation temperatures, the grain size diameter is responsible for this scattering in data. The existence of some alloying elements such as vanadium and aluminium, which precipitate as AlN and VN at austenite grain boundaries with increased time at temperatures below 1100 °C, caused grain growth inhibition through the pinning effect. In contrast, the complete dissolution of these precipitates above the deformation temperature of 1100 °C will cause large grain growth at a deformation temperature of 1200 °C. Accordingly, this will cause a difference between the grain size at deformation temperature of 1200 °C (large grains), and grain size that was formed at deformation temperatures 900°C, 1000 °C and 1100 °C (small grains). The precipitation can be observed from the Figure 4.1, where a difference between the kinetic relationships of the curves can be seen. The precipitation of vanadium nitride particles which have a low solubility compared with vanadium carbide and vanadium carbo-nitride particles is the most likely reason for that. The undissolved nitride particles disperse and prevent the growth of grains by pinning the austenite grain boundaries. In contrast, at a high temperature (1200 °C) all the vanadium dissolves and the precipitated particles are ineffective in inhibiting austenite grain growth, as shown in the same figure.

In addition, the second aspect that may cause the scattering in data is the grain size distribution. According to Figure 5.6, at the austenitising temperature of 1260 °C, deformation temperature of 1200 °C, and all strain rates (i.e., low  $\ln(Z)$ ) bimodal grain size distributions were obtained. Generally, bimodal grain size has a significantly larger distribution microstructure compared to unimodal grain distribution microstructures. The average grain size rapidly increases above deformation temperature of 1100 °C. At a larger deformation temperature, data set of grain sizes has a larger standard deviation to the average size value, and data spread out over a wide range of values. However, at a lower deformation temperature, data set of grain sizes has a smaller standard deviation to the average size value. As deformation temperature decreases, the microstructure becomes more and more uniform. The average grain size decreases with the increase of Zener-Hollomon parameter.

### 8.1.7 Modelling equations of isothermal stress-strain curves

As described in section 4.6, the constitutive equations were used for modelling isothermal stress-strain curves of the studied steel, using the method proposed by Sellars. Moreover, the Avrami equation was used to describe the dynamic softening part of the stress-strain curve. Some researchers when they used these equations said that the value of  $m'$  is constant and equal to about 1.4, but this value does not conform to the results of our experiments. From the relationship of  $\ln(\ln(1/(1-x)))$  vs  $\ln((\epsilon-\epsilon_c)/\epsilon_p)$  for each test data it can be seen that the lines are not parallel with each other, which indicates that the Avrami coefficient  $m'$  is not a constant under different deformation conditions. For the study experiment conditions, the values of  $m'$  ranged from 1.3 to 3.2 with austenitising temperature of 1100 °C, and from 1.4 to 2.3 with austenitising temperature of 1260 °C. Similarly, there was variation in the value of constant  $k$ , where it ranged from 0.5 to 1.3. Accordingly, this means that  $k$  and  $m'$  are not constants and clearly depend on the deformation parameters, which agrees with other authors [293, 316]. In summary, as can be seen in Figures 4.12 and 4.13, the data that have been applied gave reasonable agreement between the predicted data based on the models and the experimental data, especially with the data obtained at austenitising temperature of 1100 °C.

### 8.1.8 Verification of the constitutive modelling equation

The relationship between experimental and calculated flow curves of 34CrNiMo6 steel at strain rates of 0.1, 0.5, and 1 s<sup>-1</sup>, different deformation temperature and austenitising temperatures of 1100 °C and 1260 °C are shown in Fig. 4.14. As can be seen the model has good prediction capabilities of flow stress using the constitutive equations in the range of experimental conditions for both austenitising temperatures. A good correlation has been obtained, which was found to be 0.9576 and 0.9755 for austenitising temperatures of 1100 °C and 1260 °C, respectively. Also the average absolute relative error (AARE) was found to be 8.60 % and 5.96 % for the same austenitising temperatures respectively, which suggests a good predictability of the constitutive equation.

### 8.1.9 Flow curves and optical microstructure at different strains:

The stress–strain curves of isothermal process after austenitising for one hour at temperature of 1260 °C and cooled down to deform at temperature of 1000 °C with strains of 0.4, 0.6, and 0.8 and strain rates of 0.1, 0.5, and 1 s<sup>-1</sup> with each strain are shown in Figure 4.3. The flow stress curve with strain rate of 0.1 s<sup>-1</sup> was dynamically recrystallised with a single peak, where the flow stress increased to the peak and then slightly decreased to a steady state. With strain rates of 0.5 and 1 s<sup>-1</sup> the flow stress curves were dynamically recovered, where the flow stress increased to a peak and then increased continuously to reach a steady state in the end. The percentages of recrystallisation at strain of 0.6 and strain rates of 0.1, 0.5 and 1 s<sup>-1</sup> were approximately 41 %, 38 % and 37 % respectively, as shown in Figure 5.6 (b, e, h), whilst at strain of 0.4, recrystallisation occurred with percentages less than those at strain of 0.6, where the percentages at strain rates of 0.1, 0.5 and 1 s<sup>-1</sup> were approximately 29 %, 26 % and 24 % respectively, as shown in Figure 5.6 (a, d, g). From this it can be concluded that, when strains of 0.4, 0.6 and 0.8 are used, the highest percentage of recrystallisation was obtained at the highest strain of 0.8 with all strain rates at the same deformation conditions.

Furthermore, as in the previous microstructures in this chapter, the optical micrographs in Figure 5.7 also show the presence of clear banding especially at high strain rate of 0.8 with all strain rates of 1, 0.5, and 0.1 s<sup>-1</sup>. Generally, banding has its origins in the casting of steels, where dendritic solidification result in a chemically segregated microstructure. This banding that is a result of the microsegregation of elements such as Cr, Mn and P that are elongated during deformation, where alternating bands of different microstructures, parallel to the forging direction develop in steel products, especially in slow cooled carbon and alloy steels. Moreover, the austenitising temperature, austenite grain size, and cooling rate the most factors that influence the severity of microstructural banding[301].

Thompson and Howell[317] investigated banding in 0.15 %C, 1.40 %Mn steel and concluded that increasing the cooling rate from the austenitic condition reduces the intensity of banding because it reduces the Ar<sub>3</sub> temperature differences of the segregated bands. Caballero and his partners[318] in the study of the microstructural evolution during the whole manufacturing process of a dual phase steel has showed that banding eliminated



by fast cooling during hot rolling will appear after intercritical annealing at 800 °C. In that case, the degree of banding will increase as the transformation proceeds resembling the original chemical segregation. Furthermore, some authors mention that band morphology, which is represented in thickness, geometry, continuity, etc., depends on the type of deformation[299]. Other researchers mentioned that the tendency for deformation banding in f.c.c. crystals depends on the applied strain, the amount of constraint, the crystal orientation and stacking fault energy for the material subjected to deformations[319, 320].

From the figure 5.7 it can be observed that the banding regions increase or widespread with increased strain. The deformation bands that appearing as groups of approximately parallel lines occupying all or part of a grain, but not crossing grain boundaries. They are visible in some grains from very early in the deformation, but become more intense and widespread as strain increases. Some grains contain more than one family of bands, often aligned at different angles and occasionally intersecting. The occurrence of intersecting bands increases at higher strains. Additionally, some researchers such as Van Houtte et al. [321] and Duggan et al.[322] assume some degree of co-ordination between the deformation bands to retain compatibility with the macroscopic strain.

The images also shown austenite grain size distributions (see section 2.7), where at strain of 0.4 the microstructures consists of fine recrystallized grains, surrounded by large non-recrystallized elongation grains. The grain distributions become less as the strain increases from 0.4 to 0.6 to 0.8, respectively and the grains become smaller and more equiaxed. Nonetheless, the microstructure at a high strain of 0.8 still shows a variation in grain size distributions at all strain rates. Regarding the effect of used strain rates on grain size distribution, the variation in distributions at strain rates of 0.5 and 1 s<sup>-1</sup> are less than at the strain rate of 0.1 s<sup>-1</sup>, although the average grain sizes at strain rate of 0.8 and strain rates of 0.1, 0.5 and 1 s<sup>-1</sup> were convergent, with values of 30±7, 27±2, and 29±5 μm, respectively.

## **8.2 Non-isothermal deformation processes (multi hit)**

The main purpose of non-isothermal deformation process is to attempt to simulate the real forging process. This can be done through making the deformation experiment more realistic by performing it at different deformation temperatures. In addition deformation

temperatures of both 1100 °C and 1200 °C were used to compare the influence of change of austenitising temperature on the microstructure. Therefore, tests of four and three hits at different temperatures were performed with the two above-mentioned austenitising temperatures, as shown in Figures 3.13 and 3.14, respectively. All these experiments were performed at conditions of one hour of holding time for each austenitising temperature, strain rate of  $0.5 \text{ s}^{-1}$  and strain of 0.2 at each deformation step.

By analysing the stress-strain curves that are shown in Figure 6.1 and 6.3 for three and four hits it can be observed that at both austenitising temperatures the flow stress increases with a decrease in deformation temperature. Additionally, in the four hits flow curve with austenitising temperature of 1100 °C, there were gaps between the 2nd and 3rd hits and also between the 3rd and 4rd hits, in comparison with the flow curve at austenitising temperature of 1200 °C. These gaps occurred according to a little softening that took place between the deformation temperatures. This is assumed to be due to differences in deformation temperature between these hits, where it was 50 °C less than four hits at austenitising temperature of 1200 °C. Furthermore, from Figures 6.1 and 6.3, for four and three hits respectively, the flow stress curves show different strains in each step. As can be seen from the figures, this difference was small at the first hit in both cases and increases as the hits increase, becoming bigger in the last hit. Under perfect test conditions these differences should not occur and the equivalent strains should be the same for both non-isothermal tests. Because all the hits are performed at the same strain, strain rates and holding time between the different hits, these differences are usually a slight machine effect, not a material effect. Sometimes when a TMC machine (Section 3.4.1) is used for long periods without maintenance its efficiency drops e.g., in the oil pressure pump, therefore the input data is slightly adjusted by increasing or decreasing in an attempt to get the exact results required. Unfortunately sometimes this causes a very slight difference, such as that in the first hit in Figures 6.1 and 6.3.

In isothermal tests this difference has almost no effect, but in non-isothermal tests when multiple hits are used this difference accumulates in each hit, as seen after the last hit in both figures. For instance, if a strain of 0.8 is needed, from the user's experience the strain is increased a little to 0.85 to get the required value, but sometimes the machine gives the exact strain, i.e. 0.85. In that case the difference in strain is probably a control issue, i.e.

each deformation set is not as it is designed to be, especially since most of our tests were carried out at different intervals of time. However, most tests are imperfect and so there are always differences. For example, in Figures 6.1 (four hits) the strain was about 0.22 after the first hit, and increased until it reached about 0.9 after the fourth hit, instead of 0.8 (the required strain at austenitising temperatures of 1200 °C), while the strain was about 0.23 after the first hit, and increased until it reached about 0.92 after the fourth hit at austenitising temperatures of 1100 °C.

Furthermore, the slight accumulative difference in strain may also occur during analysis and correction of data that were collected from the testing machine. The raw data that can be collected from the TMC machine during tests, including load, displacement, velocity of the ram and temperature, will correct for the effects of machine compliance, deviation from the plane strain conditions and for the effects of friction between the specimen and the tools[323] (See Appendix A). These data are used later for analysis and to draw the stress-strain curves. For example the difference maybe occurred during the origin correction, where the raw displacement data are corrected for possible errors in the zero position, as shown in Appendix Figure (A-1). In addition, as known the calculation of the equivalent strain depends on the initial and the final dimensions of the tested specimen. The presence of oxide scales, which were observed on the final deformed surfaces of the tested samples (section 6.4), may also affect the equivalent strain. Accordingly, the accumulation of these scales may cause an increase in the final deformed surface dimensions, thus making a small difference in the strain calculation.

The optical micrograph for these three and four hits at both deformation temperatures of 1100 °C and 1200 °C are shown in Figures 6.2 (A-B) and 6.4 (A-B). From the figures, the grain size at an austenitising temperature of 1200 °C appears bigger and the microstructure was non-uniform compared with the austenitising temperature of 1100 °C. In addition, there was a significant difference in average grain size between four and three hits. Moreover, according to the results obtained from the isothermal deformation process at deformation temperature of 900 °C, which seems to be the approximate recrystallisation stop temperature. The recrystallization stop temperature is the temperature where no recrystallization occurs for a given hold time. The microstructure form above this temperature and below non-recrystallization temperature is usually results in a mixture

including some recrystallized grains and some deformed grains. Some researchers such as Cuddy[324] mentioned that this critical temperature increased by increasing the initial solute level (e.g. V and Nb). The triple hits tests were repeated with some modifications, as shown in figures 3.14 (b) and 3.14 (c). In this step we tried to determine the difference in grain size when the deformation process is stopped before a temperature of 900 °C. In both cases, when the specimen was held for 60 sec after the three hits and prior quenching, or was cooled down to a temperature of 900 °C then quenched, the grain size was almost same.

On the other hand, by comparison with the two processes of four hits with and without formation at a temperature of 900 °C, the results were convergent for both austenitising temperatures. Thus, at four hits the average austenite grain sizes were  $64\pm 5\ \mu\text{m}$  and  $37\pm 2\ \mu\text{m}$  at austenitising temperatures of 1200 °C and 1100 °C respectively, as shown in Figures 6.2 (A) and 6.2 (B), whereas the grain size at the four hits without deformation at temperature of 900 °C were  $60\pm 4\ \mu\text{m}$  and  $42\pm 3\ \mu\text{m}$  at the same austenitising temperatures respectively, as shown in Figures 6.4 (E) and 6.4 (F). This means that the change in austenite grain size between these two processes was not due to an increase in strain at the fourth hit causing dynamic recrystallisation but because of static recrystallisation.

### **8.3 The oxide scale**

During the performance of different tests, the presence of oxide scales was observed on the specimens' surfaces after deformation, and also sometimes on the surface of the deformation tool. These oxides formed very small layers in some cases, but at other times were significantly present. All the tests were performed in the presence of air to simulate large scale forging during the real deformation process. According to our investigations, the thickness of these oxides on the outer surface of the specimens changed with changing the austenitising temperature and the holding time at that temperature, as presented in Figure 6.5. According to experiments, these oxide layers become thicker when austenitising temperature increased from 1100 °C to 1200 °C and also when the soaking time increased from 1 hour to 24 hours at these temperatures. Consequently, the thickest oxide scale layers were obtained at austenitising temperature of 1200 °C after a holding time of 24 hours.

Generally, the scale type should not change between these temperatures, thus more experiments should be performed to investigate the reasons for these results. However, the presence of these oxide scales is undesirable since they may cause defects such as cracks within the metal surface, and also may influence tool wear, and thus the surface finishing of the final product, during deformation. Furthermore, several authors mention that the friction and heat transfer characteristics of metals change dramatically in the presence of oxide scale during hot deformation, when contact occurs between the hot metal (e.g., billet) and cold deformation tool (e.g., die).

Li and Sellars[325] conducted a study about interfacial heat transfer behaviour during hot forging and rolling of steel with oxide scale formation. They concluded that in both forging and rolling processes, the different heat transfer rates at the interface are basically because of the differences in deformation behaviour of oxide scales. However, the effective interfacial heat transfer coefficients in hot rolling of steel with oxide formation are higher than those in hot forging of steel under nearly the same conditions. Moreover, Matsumoto, et al.[326] recently worked on a study about reduction in friction of steel covered with oxide scales in hot forging. They concluded that during the hot forging process the presence of oxide scales led to maintaining a high temperature in the steel workpiece because of low thermal conductivity of the oxide scales. In the same study these oxide scales exhibited low friction characteristics during hot forging. The oxide scales under specific forging conditions during the hot forging process may possibly act as a lubricant.

#### **8.4 Non-metallic inclusions**

Non-metallic inclusions, as discussed in section 2.6, have an effect on some properties of steel such as strength, machinability and toughness. The influence of these inclusions on the properties of steel depends very much on their composition, shape, size, and distribution, in addition to the stress system imposed during deformation. During the preparation of samples for optical micrographs, especially during the polishing process, it was considered difficult to maintain the inclusions on the surface of the samples. Subsequently, a small number of inclusions will be available for the energy dispersive X-ray spectroscopy (EDX) analysis. Furthermore, inclusions usually are easy to observe in a well-prepared surface, but sometimes the preparation process brings out other features of the microstructure that

make it difficult to see the inclusions. As can be seen in Figure 6.7 there are two shapes of non-metallic inclusions; the elongated morphology in the direction of deformation, which from the polished surfaces are small in quantity, about 30  $\mu\text{m}$  length. The other is spherical or oval shaped inclusions, which are greater in quantity with different diameters, but some of these particles are very small, and we cannot be sure these are inclusions for the reasons aforementioned. Furthermore, the scanning electron microscope (SEM) images and EDX for some polished cross-section samples are shown in Figure 6.8. The EDX spectrum of the upper sample shows sulphur and manganese, while the lower one shows aluminium, manganese, oxygen and vanadium. Accordingly, from the EDX analysis, these inclusions were identified as manganese sulphide (MnS) and aluminium oxide ( $\text{Al}_2\text{O}_3$ ). The  $\text{Al}_2\text{O}_3$ , considered as a hard non-metallic inclusion, has greatest influence on fatigue strength, whereas the MnS, which makes more deformable inclusions, has less effect. Moreover, the SEM images for the fracture surfaces of Charpy impact test specimens are shown in Figure 6.9. The figure shows some voids, especially in the right-hand side of the image, where the voids are very clear. These voids probably were places for inclusions compatible with the fact that globular inclusions served as hard particles for void initiation. However, even though these voids were near the fracture initiation area, there is no certain evidence to prove that these voids were caused by inclusions.

## **8.5 Heat treatment**

### **8.5.1 The effect of normalizing process on the deformed austenite grain size**

During study of the normalization process the grain sizes before deformation, after deformation, and before and after normalizing were calculated, as shown in Figures 7.1, 7.2 and 7.3. As with all previous experiments, austenitising temperatures of 1100 °C and 1200 °C were used. Before deformation and with the same holding time, a higher austenitising temperature gives a bigger grain size. The percentage of the difference in austenite grain size before and after deformation was approximately the same for both austenitising temperatures used. As shown in Figure 7.1, the grain size prior to deformation was 130  $\mu\text{m}$  and 220  $\mu\text{m}$ , while after the process of deformation it was 32  $\mu\text{m}$  and 51  $\mu\text{m}$ , so that the percentages of grain size reduction were about 25 % and 23 % at austenitising temperatures of 1100 °C and 1200 °C, respectively.

In addition, the histograms of the grain size distribution for the microstructures are also shown in Figure 7.1. At both austenitising temperatures of 1100 °C and 1200 °C, the microstructures showed a big variation in grain size distributions after holding for 10 mins, and the distributions were heavily bimodal. The grain size distribution range at the austenitising temperature of 1100 °C (15 to 260 µm) was much higher than the distribution range at the austenitising temperature of 1200 °C. In addition, at the austenitising temperature of 1200 °C there was no distribution for the grains in the range of (45 to 200) µm. However, after the isothermal deformation, the grain size distribution showed less variation. The microstructure at the austenitising temperature of 1100 °C becomes more uniform with unimodal distribution than at the austenitising temperature of 1200 °C with bimodal distribution. Furthermore, as was noted in the case of the isothermal deformation microstructures the presented images of the deformed microstructures also show clear banding in the longitudinal direction after deformation process.

At the first stage, directly after deformation the temperature of the sample was cooled to 650 °C, held for 5 mins, then heated up to 860 °C and held for 6 mins before quenching in water. In this step there was no change in microstructure after 5 mins soaking at 650 °C for both austenitising temperatures, where the structure was still almost all austenite because the time was not long enough to change the structure to ferrite or pearlite. Also, because the temperature was low, the average austenite grain size remained the same before and after the hold period of 5 mins. As shown in figure 7.1, the grain size was  $44\pm 3$  µm and  $78\pm 4$  µm at austenitising temperatures of 1100 °C and 1200 °C, respectively. After the temperature rose to 860 °C and was held for 6 mins, a slight increase occurred in the austenite grain size to  $48\pm 4$  µm and  $85\pm 5$  µm at austenitising temperatures of 1100 °C and 1200 °C respectively, as also shown in Figure 7.1.

Moreover, from the grain size distribution histograms that shown in Figure 7.1, the microstructures exhibited a variation in grain size distributions (bimodal type) at both austenitising temperatures of 1100 °C and 1200 °C after holding at temperature of 650 °C for 5 mins. However, the grain size distribution at the austenitising temperature of 1100 °C was around the grain size average (i.e., the big grain size counts were around the average) than at the austenitising temperature of 1200 °C, where the big counts were higher than the average size. When the temperature rose to the 860 °C and held for 6 mins, the distribution

of the grain size stayed the same with bimodal distribution type, but the distribution range become wider especially at austenitising temperatures of 1200 °C (20 to 210 µm).

From the TTT diagram for 34CrNiMo6 steel, the structure almost entirely transformed to ferrite and pearlite after being held for 4 hours at a temperature of 650 °C. The specimens etched with 5 % Nital and also with picric acid are shown in Figure 7.2. As can be seen from the figure, the volume fraction of ferrite to pearlite was almost convergent at an austenitising temperature of 1100 °C, while at an austenitising temperature of 1200 °C the volume fraction of pearlite was higher compared to the ferrite. After the samples were held for 4 hours at 650 °C the temperature was raised to 860 °C and held for 6 mins, resulting in a nucleation of new grains and thus the microstructure transformed again to austenite. The austenite grain size was refined and the obtained results were small grains, on average  $9\pm 1$  µm and  $10\pm 2$  µm at austenitising temperatures of 1100 °C and 1200 °C respectively.

As can be seen in Figure 7.3, after 6 mins the grain size on average was approximately the same for both austenitising temperatures. However, it was equiaxed with more uniform structure at austenitising temperature of 1100 °C than at 1200 °C, which gives more desirable mechanical properties. When the normalizing holding time was increased from 6 mins to 30 mins (equivalent to five times longer), the average austenite grain size remained almost the same as at 6 mins, nearly  $10\pm 1$  µm and  $11\pm 1$  µm at the same austenitising temperatures respectively. However, at the level of the microstructure a little change occurred where a small growth happened to some of the grains; thus the microstructure became less uniform especially at an austenitising temperature of 1200 °C.

Likewise increasing the holding time to 60 mins (ten times longer) did not produce any significant changes to the average austenite grain size. As shown in Figure 7.3, the average grain size increased by a very small amount ( $12\pm 2$  µm) and was equal for both austenitising temperatures. However, substantial changes occurred to the grains at an individual level. Two different sizes of grain appeared which made the microstructure become heterogeneous. Where some grains were refined at the same time abnormal growth occurred for other grains. The presence of abnormal austenite grains can be observed more clearly at an austenitising temperature of 1200 °C, which may contribute to reduce the toughness of the material.



In summary, using different austenitising temperatures of 1100 °C and 1200 °C with normalizing process gave nearly the same average austenite grain size. Moreover, at both austenitising temperatures increasing the normalizing time did not influence the increase of average austenite grain size, where the size of the grains remaining approximately the same despite a significant increase in time. The reason for that may be due to the normalizing temperature, which was low and therefore insufficient for austenite grain growth even with a longer holding time. On the other hand, the optical microstructures of the normalizing grains showed a difference in terms of the shape and distribution of grains although the average grain size was the same, which will cause the scattering of data, thus affect the material properties.

## **8.6 Quenching and tempering processes**

### **8.6.1 Using different cooling rates**

Generally, decreasing the austenitising temperature from 960 °C to 840 °C and tempering temperature from 630 °C to 520 °C did not give good results, with the hardness increasing and the toughness decreasing, especially with high cooling rates. As shown in Figure 3.22, different cooling rates in a range between slow cooling rate (furnace cooling) and a cooling rate of 1.2 °C/sec were used with two heat treatment cycles. The microstructures for these heat treatment cycles after being etched by using 5 % Nital and picric acid are shown in Figures 7.4 and 7.6. As shown in these figures the final microstructure consists of two different carbon region concentrations. The first, which is dark with high carbon concentration and the second, is light in colour with low carbon concentration. It is clear from the microstructures that there was a variation in percentages of these regions between samples, where this percentage varies with used cooling rates. Furthermore, from these optical images the main phases are not clear, and it may become clearer with using of SEM images. However, according to CCT diagrams were constructed for 34CrNiMo6 steel using JMatPro software database shown in Figures 3.2 and 3.3, and also according to the CCT diagrams shown in Figures 2.29 and 2.31 (section 2.5.2), it can be concluded that the final microstructure consists of tempered bainite and tempered martensite microstructures in the range of used cooling rates (0.3 to 1.2 °C/sec).

Moreover, from the figures, a variation in bainite / martensite volume fraction and colony size also can be seen. Approximate percentages of bainite / martensite volume fraction were determined for the final microstructure in both figures 7.4 and 7.6 at the used cooling rates. At tempering temperature of 520 °C the percentages of martensite in the microstructures were 35%, 40%, 25% and 60% at cooling rates of 0.3, 0.6, 0.9 and 1.2, respectively. whereas, at tempering temperature of 630 °C in figure 7.6, the percentages of martensite were 21%, 34%, 38%, 47% and 57% at cooling rates of furnace, 0.3, 0.6, 0.9 and 1.2, respectively. It is clearly to see the variation of percentages of martensite between samples with high and low toughness values, where samples with High toughness values exhibits high percentage of martensite. Contrary, the microstructural analysis of the samples show that samples with low toughness exhibits high percentages of bainite. Presumably, this bainite structure is upper bainite that is typical of medium carbon steel such as 4340 at low cooling rate. According to experimental cooling rate and also from previous theoretical review, microstructure constituted with high percentage of martensite will give better toughness response.

Furthermore, from the literature, this variation would be expected to cause scattering in some the mechanical properties. The toughness, strength and ductile-brittle transition temperature (DBTT) are the most properties that expected to scatter. In quenching and tempering high strength steel, the formation of martensite is desirable because tempered martensite structure has higher toughness than that of the upper bainite that forms during continuous cooling transformation.

Yoshiyuki Tomita[327] made a research by investigating the effect of the cooling transformation product on the mechanical properties in medium carbon steel 4340. In this study, structures of tempered martensite with different percentage of Upper Bainite (25%, 50% and 75%) were studied. The mechanical properties for these different structures show markedly increment of DBTT and also reduction of strength with the presence of more upper bainite. Toshio Okuno[125] also made a study on the effect of microstructure on the toughness of three quenching and tempering hot work tool steels. These three steel also exhibited the same microstructural effect on toughness by the formation of upper bainite, where with increase in volume fraction of upper bainite, results in deterioration of the toughness. They reasoned that, the increment in the size and fraction of upper bainite, its

change in morphology, precipitation and agglomeration of carbide particles along the prior austenite grain and bainite grain boundary and also fine dispersion of carbides in matrix produced during tempering promote the deterioration of the steel toughness.

In addition, from the figures it can be seen that the presence of abnormal growth in some of the austenite grains resulted in heterogeneity of grain size within the microstructure. To improve the toughness of the material, it is necessary not just to get a small austenite grain size, but also a large difference between grain sizes within the microstructure must be avoided (see section 2.8.3). The Figure 7.8 shows the austenite grain size distribution histograms for the microstructures at austenitising temperatures of 840 °C and 960 °C, with the cooling rates of 0.3, 0.6, 0.9 and 1.2 °C/sec at each austenitising temperature. As shown from the figure, at austenitising temperatures of 840 °C the distributions of the grain size were unimodal with all strain rates except at a strain rate of 0.6 °C/sec where it was heavily bimodal distribution type.

In addition, as the cooling rate increased the highest frequency value of grain size become close to the average grain size and the distribution range become narrow. For instance, at cooling rate of 0.3 °C/sec the highest frequency value of grain size was between (10 to 15)  $\mu\text{m}$  and the average value of grain size was  $35\pm 5$   $\mu\text{m}$  and the distribution range was between (5 to 115)  $\mu\text{m}$ , while at cooling rate of 1.2 °C/sec the highest frequency value of grain size was between (6 to 8)  $\mu\text{m}$  and the average value of grain size was  $8\pm 1$   $\mu\text{m}$  and the distribution range was between (5 to 60)  $\mu\text{m}$  with positively skew. Generally, at austenitising temperatures of 960 °C the behaviour of the distributions were the same, excluded from that a strain rate of 0.9 °C/sec where the distribution was also bimodal type. Furthermore, the highest frequency value of grain size at cooling rate of 1.2 °C/sec is not close to the average grain size. A macrograph of the fracture surfaces and the profiles of the propagated cracks at the perpendicular side on the impact surface are shown in Figures 7.5 and 7.7. As can be seen from these figures, the fracture surfaces varied from brittle to a mixture between brittle and ductile. From the obtained results in Table 7.1, the toughness and the hardness increased with increasing the cooling rate.

The tempered bainite structure is soft compared to tempered martensite structure which usually reflects low hardness. However, a low hardness value does not mean a tough

material unless it is certain that the material has a homogeneous microstructure across the section. The relationship between the cooling rate and the grain size is not compatible, where it increases sometimes and decreases in other times with increasing cooling rate. The crack propagation response in the samples with low toughness values was vertical, which seems to indicate the presence of transgranular fracture.

The scanning electron microscope (SEM) images of the impact (Charpy V-notch) fracture surface of sample 2 with fracture energy of 16 J are shown in Figure 7.11. The sample 2 was austenitised at 840 °C and tempered at 520 °C with cooling rate of 0.6 °C/sec. The figure shows the fracture initiation site of the sample 2. As can be seen the fracture is showing intergranular fracture surface. At higher magnification the images showing intergranular fracture surface, where the crack occurs along the grain boundaries. Moreover, the fracture shows different faceted sizes appeared with different cleavage steps. From Figures 7.12 and 7.13 it is clear that the relationship between both the hardness and toughness with the grain diameter is not compatible. This could be attributed to the method of determination of average grain diameter with the presence of abnormal grain growth within the microstructure.

In summary, the results of this step did not meet the required toughness specifications in the place of tested samples shown in Table 1.1. By using the tests conditions mentioned in Table 3.3 for samples numbered 1 to 9, the toughness requirements will not be achieved. This may sometimes attributed to non-uniformity microstructure because of the variation in grain size distributions, which usually causes scattering in the measured data (e.g., toughness) especially when one test sample is used. Moreover, it may attribute to the lower hardenability in the 34CrNiMo6 steel where we could not get a high percentage of martensite within the microstructure of the tested samples. Therefore to achieve 100 % martensite in the sampling position with previous test conditions, the cooling rate should be more than 1.2 °C/s for the big section billet with diameter of 480 mm.

### **8.6.2 Using different austenitising temperatures**

Two different heat treatment cycles consisting of two different sets of austenitising temperatures, two tempering temperatures and using cooling rate of 0.6 °C/sec were used.

Tests conditions for these cycles are mentioned in Table 3.3 for samples numbered 2, 7 and from 10 to 13. As in the previous step, the best results were obtained with the heat treatment cycle with tempering temperature of 630 °C than the heat treatment cycle with tempering temperature of 520 °C. The grain size at the austenitising temperatures of 900 °C, 960 °C and 1050 °C and tempering temperature 630 °C is more compatible than the grain size at the austenitising temperatures of 780 °C, 840 °C and 930 °C and tempering temperature 520 °C. According to the microstructures, small grains and a high percentage of martensite were obtained at lower austenitising temperatures as shown in Figure 7.14.

From the macrograph of the fracture surfaces as shown in Figures 7.15 and 7.16 it can be seen that some of the fracture surfaces are brittle, often leaving a rough surface such as in sample number 13, while the other surfaces were mixed between brittle fracture (rough) and ductile fracture (conchoidal), such as in sample number 12. Moreover, it can be seen in the figures that the profiles of the vertical cracks propagation also depend on the type of fracture. Figure 7.17 shows the fractured grains at the microstructural level for the vertical crack propagation of some selected specimens. As can be seen from the figure, the microstructure of sample 2, which is brittle fracture with low toughness, seems to be a mixture of intergranular and transgranular fracture, where some of these cracks make their paths cross through the grains, while other cracks follow the grain boundaries. The cracks in sample number 12, which is ductile with high toughness, were not vertical and exhibited high plastic flow zone through the fracture, as shown in Figure 7.16.

The mode of failure at any given strain rate and temperature depends on the value of the yield or flow stress relative to the brittle or fracture stress. Moreover, toughness depends on microstructure, austenite grain size, impurities, carbide particles, temperature and also inclusions. The variation in the austenite grain size and the uniformity of microstructure will effect on the type of fracture thus on the toughness. Some research has been done for high strength steel with a bainite and martensite structure at which the prior austenite grain size, martensite and bainite colony size within the austenite grain has effect on the toughness of the material. D. Lonsdale[328] made a study of the effect of prior austenite grain size, bainite colony size and individual lath size on toughness for F22 (2.25%Cr, 1%Mo steel). The microstructure is constituted of upper bainite with no evidence of retain austenite.

- The colony size varies linearly with the prior austenite grain size.
- The effective grain size is the upper bainite packet size where the higher numbers of the quasi-cleavage surface at which the fracture takes place corresponds to the bainite colony size in comparison with the austenite grain size, this analysis was made for prior austenite grain size of 80um ( unembrittled steel, charpy test at -196C ). However the percentage of intergranular fracture increases when the austenite grain size is greater than 80 um producing cracks predominantly along the prior austenite grain boundary.

Furthermore, the variation of  $K_{ic}$  is explained by Robert O. Ritchie[329, 330] with a term called characteristic distance. Characteristic distance is referred to the distance between second phase particles that produces microvoids and can be altered with the size of the austenite grain size that also modified the martensite pocket and finally the increment of the particles spacing. For This reason, there are certain inconsistency between impact V-notch toughness and plain fracture toughness ( $K_{ic}$ ) where large austenite grain size produces low toughness value but highest  $K_{ic}$  value. Obviously this analysis is only deal with ductile fracture because when the material exhibits temper embrittlement due to segregation of residual elements in the austenite grain size, large austenite grain size can causes low values of both  $K_{ic}$  and Toughness.

The scanning electron microscope (SEM) images of fracture surfaces of samples 12 and 13 with fracture energies of 47 J and 7 J respectively are shown in Figure 7.18. The figure shows the fracture initiation sites of both samples. As can be seen, the surfaces are showing presence of some cracks in both samples. At higher magnification the images of sample 12 showing fracture surface,with different facet sizes; small and long ones. Moreover, the fracture surface of the sample 13 shows different faceted sizes with different cleavage steps as a result of the brittle fracture surface. From Figures 7.19 and 7.20 that show the relationship between grain diameter and both hardness (HB) and toughness (J), it is clear that the relationship between grain diameter and toughness is an inverse relationship while it is a direct relationship with the hardness, where the toughness decreases and the hardness increases with increasing the grain size.

In summary, changing austenitising temperatures has an effect on mechanical properties, especially fracture toughness. According to Figure 3.18, reducing the austenitising

temperature to 900 °C gave an austenite grain size of nearly 19 µm, resulting in a good agreement with the required toughness specification. Moreover a good percentage of martensite was achieved within the microstructure. From this austenitising temperature a 47 J value of toughness has been obtained that meets the toughness requirement (ABS specification Table 1.1) of minimum single value of 38 J at -20 °C.

Also, a hardness value of 313±2 HB was obtained that is considered close to the required hardness of the studied material (302 BHN) according to the producing company's specification. Accordingly, starting with a small austenite grain size before the heat treatment process will help to obtain the required mechanical properties. however, because of the variation in grain size distributions in most of microstructures, which usually cause scattering in data, and also because of using one test sample, this result cannot be reliable unless more specimens are tested.

### **8.6.3 Comparison between tempering temperatures of 630 °C and 640 °C**

Changing the tempering temperature is a very important factor for the balance between toughness and hardness. Toughness increases and hardness decreases with increasing tempering temperature (see Fig. 2.45 and Fig. 2.50). Consequently, we tried to increase the tempering temperature from 630 °C to 640 °C to increase the toughness without losing too much hardness. Figure 7.21 shows the microstructures of samples that were austenitising at different temperatures and tempered at tempering temperature of both 630 °C and 640 °C. Generally, from the figure it can be observed that there is no significant difference in microstructures at both tempering temperatures. The results of the toughness and hardness at tempering temperature of 630 °C and 640 °C are shown in the Table 7.3.

A slightly higher result for toughness was obtained at tempering temperature of 640 °C compared with that at tempering temperature of 630 °C; this obtained result is not too big and the differences are still considered to be within the experiment's error range. Furthermore, from the relation between toughness and austenitising temperature at the two tempering temperatures as shown in Figure 7.23, the results of toughness at a temperature of 640 °C were more consistent than those at a temperature of 630 °C, where the toughness decreases with increasing the grain size. Also at the level of hardness no

significant change occurred. Figure 7.22 shows the macrographs of the resulting fracture surfaces of Charpy impact specimens. From the figure almost all the fracture surfaces are brittle.

In summary, using a tempering temperature of 640 °C did not improve the toughness and hardness results at high austenitising temperatures, but there was a slight improvement at low temperatures.

## 8.7 Multiple heat treatment processes

The cycles of multiple heat treatments that were used in this study are shown in Figures 3.23 to 3.26. Accordingly, the optical micrographs of these cycles, which consist of two normalizing, two quenching and one tempering process in different orders, are shown in Figures 7.24 to 7.27. As can be seen from these figures, in cycle 1 after a double normalizing process and one quenching process the percentage of austenite phase was increased significantly compared with the previous results. Moreover, the grain size of the final microstructure appears small and the variation of grain size distribution is somehow less, which made the microstructure more homogeneous. In cycle 2 (double normalizing, double quenching and one tempering) the results also were good, but the percentage of martensite was less than with cycle 1. Furthermore, the microstructure became more heterogeneous, where some of the grains grew more abnormally after the second quenching process.

In the case of cycle 3, where the normalizing and quenching processes were used twice and sequentially one by one, as can be seen in the micrographs in Figure 7.26, the microstructure became more equiaxed but the percentage of martensite was still less than in cycle 1. Finally, in cycle 4, as can be seen from Figure 7.27, after the double quenching process the percentage of martensite became more within the microstructure compared with the other cycles. However, the microstructure was still not homogeneous and there is some variation in grain size distribution. The distribution of grain size for the microstructures of cycles 1, 2, 3 and 4 are shown in figure 7.28. As shown in the figure, the grain size distributions in all multiple heat treatment cycles were unimodal and positively skewed. This distribution was expected as a result of fine average grain size, more uniform microstructure (i.e., better than the single heat treatment) and good toughness results.



However, although the final average grain sizes were small in all cycles, there was abnormal growth for some grains in the microstructures with very small frequencies. For instance, in cycle 1 the main grain size distribution was in the range of (3 to 42)  $\mu\text{m}$ , but there were some abnormal grain sizes with very little frequencies in the distribution range of (60 to 66)  $\mu\text{m}$ . Generally, the average grain sizes of the final microstructures for all cycles are also considered relatively close to the highest grain size counts.

However, the average grain sizes of the final microstructure of cycle 1 with fracture energies of 101 J, which is  $13\pm 1$   $\mu\text{m}$  is considered the closest to the highest grain size count, which is about 11  $\mu\text{m}$ . In cycle 2 with fracture energies of 82 J the grain size distribution in a range of (6 to 18)  $\mu\text{m}$  nearly has the same high frequencies.

The results of toughness, hardness and grain size for all cycles are shown in Table 7.4. Overall, the hardness and grain size values for all the cycles were closed and, in accordance with the required standard specification, good hardness values and a small grain sizes were obtained for all the cycles. Compared to all heat treatment cycles, a good hardness value of  $295\pm 2$  HB and a small grain size of  $13\pm 1$   $\mu\text{m}$  were best results obtained with cycle 1, while the highest hardness value of  $308\pm 2$  HB was obtained with cycle 4 and the highest grain size of  $18\pm 2$   $\mu\text{m}$  obtained with cycle 2. As for toughness, the values obtained from heat treatment cycles 2, 3 and 4 were convergent, while the highest value of 101 J was obtained with cycle 1. This may be attributed to the double quenching process that leads to an increase in the amount of martensite within the microstructures and consequently an increase the percentage of the retained austenite. This retained austenite later will be transformed to bainite and martensite depending on tempering temperature and holding time which causes a reduction in the toughness. A macrograph of the fracture surfaces and the vertical cracks propagation for all the multiple heat treatment specimens is shown in Figure 7.30. From the images it can be seen that all the surface fractures are a mixture of brittle with shiny grey colour surrounded by ductile with dull grey colour, but the surface area of the ductile was bigger than the brittle.

Scanning electron microscope (SEM) fractography obtained from the fracture surface of the Charpy impact test specimen (cycle 2), are shown in Figure 7.31. The figure shows the original initiation site of the fracture; some voids also exist in this site. These voids may

serve as inclusion nucleation sites compatible with the fact that the globular inclusions served as hard particles for voids initiation. Although these voids existed in the fracture initiation area, there is no certain evidence proving that these voids were caused by inclusions. As was discussed in section 2.6.1, coalescence of these voids leads to crack propagation and may cause a ductile fracture.

Furthermore, Figure 7.30 shows vertical crack propagation at the microstructural level for all the specimens. From this microstructural level, it seems to be that the cracks in the samples are intergranular fracture mode where the cracks follow the grain boundaries. Figures 7.32 and 7.33 show the relationship between grain diameter and both hardness and toughness, where it is clear that by increasing the grain diameter the toughness decreases and the hardness increases.

In summary, by using a multiple heat treatment process consisting of double normalizing, double quenching and single tempering in different orders, values of high toughness and good hardness within the required specifications can be obtained. Moreover, the obtained microstructures were more uniform and less variation in grain size distributions comparing to the single heat treatment, which usually helps to reduce the scattering in data. By comparison of all heat treatment cycles, a good hardness value of  $295\pm 2$  HB and a high toughness value of 101 J were the best results, obtained using cycle 1.

## **8.8 Fracture Surface Facets**

Grain size influences the type of fracture, as the existence of coarse grains may enhance brittle fracture while fine grains can resist fracture initiation and also help to delay crack propagation, resulting in higher fracture energy. From the results it can be observed that fracture energies significantly correlated with average grain size, with fracture energy decreasing with increased average grain size. For instance, a fracture energy of 16 J was obtained in sample 2 with an average grain size of  $47\pm 6$   $\mu\text{m}$ , while sample 13 with grain size of  $164\pm 1$   $\mu\text{m}$  gave a fracture energy of 7 J. Generally, the three samples shown in Figure 7.24 (a – c) relatively have different facet sizes. However, the fracture surfaces of samples 2 and 13 have more variation in facet sizes compared with sample 12.

From the SEM images in Figure 7.25 (a – c), it can be observed that the average facet size, which represents the biggest fraction of the area in the fracture surface, increases with decrease of fracture energy. For example the facet size in the fracture surface of sample 13 with fracture energy of 7 J is bigger than the facet size in the fracture surface of cycle 2 with fracture energy of 82 J. In other words, the samples that have a bigger grain size also have a bigger facet size. Moreover, by increasing the percentage of large facet sizes in the fracture surface, variation in facet size also increases, which in turn increases the scatter in data.

According to these SEM images the effect of grain size bands near the notch-root on the fracture energy is not completely clear because most of the microstructures have a mix of fine and coarse grain structure (bimodal distribution). Accordingly, more experiments should be undertaken to study this issue and make it clearer. More SEM images with different magnifications should be taken around the crack initiation area and the facet sizes should be measured to compare with the average grain size.

## Chapter 9 Conclusions

The aim of this investigation was to study the influence of hot deformation and heat treatment processes on the evolution of microstructure refinement and the final mechanical properties of 34CrNiMo6 steel. Therefore, a study was undertaken on the austenite microstructure with particular emphasis on the grain refinement and the effect on it of thermo-mechanical variables. The following conclusions can be drawn from Chapters 4, 5, 6, 7 and 8 presented in this study:

### - Isothermal deformation processes (single hit)

- Consistent with the fact that fine and equiaxed grains of material lead to improvement in toughness as well as strength, investigation results of all isothermal deformation tests with both austenitising temperatures showed that using an austenitising temperature of 1100 °C gives better equiaxed grains and higher recrystallisation percentages than using an austenitising temperature of 1200 °C.
- Unimodal grain size distributions with a positive skew were obtained at the austenitising temperatures of 1100 °C, deformation temperature of 1100 °C, and strain rates of 0.1, 0.5 and 1 s<sup>-1</sup>, while at the austenitising temperatures of 1260 °C and deformation of 1200 °C, the bimodal grain size distributions were obtained at the same strain rates.
- Almost all the optical microstructures at both austenitising temperatures of 1100 °C and 1260 °C shown presence of clear banding, which represented by dark lines parallel to the direction of deformation.
- When the samples were tested under the selected isothermal deformation conditions of austenitising and deformation temperatures, strain and strain rate, the smallest grain sizes were obtained at an austenitising temperature of 1100 °C and strain rate of 0.5 s<sup>-1</sup> with all tested deformation temperatures.
- The 34CrNiMo6 steel has a high recrystallisation temperature, and 900 °C is approximately the recrystallisation stop temperature at which some nuclei germinated dynamically on the original grain boundaries of deformed grains (See Figures 5.3 and 5.4). Accordingly, in order

to refine grain size thermo-mechanical processing must be performed above this temperature.

- Using deformation temperature of 900 °C with an austenitising temperature of 1100 °C, the percentages of recrystallisation were approximately 24 %, 15 % and 23 % at strain rates of 0.1, 0.5 and 1 s<sup>-1</sup> respectively. These percentages were higher when compared with an austenitising temperature of 1260 °C, which reduced them to approximately 11 %, 6 % and 5 % at the same strain rates respectively.
- The average value of  $n$  and  $n'$  for the 34CrNiMo6 low alloy steel at austenitising temperature of 1100 °C and in the deformation temperature range of 900 °C-1100 °C and strain rate of 0.1, 0.5, 1 s<sup>-1</sup> is 7.1 and 5.06, respectively, whereas at austenitising temperature of 1260 °C, and same strain rate in the deformation temperature range of 900 °C - 1200 °C it is 7.8 and 5.51, respectively.
- Some researchers have mentioned that the value of activation energy of deformation ( $Q_{def}$ ) is a function of the chemical composition of the steel and usually changes with the alloy content[331]. However, consistent with the results of our experiments it also seems to be affected by the austenitising temperature. At an austenitising temperature of 1100 °C the values of  $Q_{def}$  were 391, 389 and 410 (KJ mol<sup>-1</sup>) depending on an exponent type equation, while with austenitising temperature of 1260 °C the values were higher and equal to 400, 411 and 446 (KJ mol<sup>-1</sup>).
- The calculation of the activation energy for hot working of 34CrNiMo6 steel showed that at austenitising temperature of 1100 °C the hyperbolic sine law was found to be the appropriate relation, which resulted in a value of 389 (kJ/mol), while at austenitising temperature of 1260 °C, the power law was found to be the appropriate relation, which resulted in the value of 411 (kJ/mol).
- Peak stress of 34CrNiMo6 steel at both austenitising temperatures of 1100 °C with deformation temperature range of 900 °C - 1100 °C, and 1260 °C with deformation temperature range of 900 °C - 1200 °C under the same deformation conditions of 0.8 strains and strain rates of 0.1, 0.5, and 1 s<sup>-1</sup> can be expressed by the following Equations respectively after rearranged:

$$\dot{\epsilon} \exp\left(\frac{389}{RT}\right) = A[\sinh(\alpha\sigma_p)]^{n'} = 1.123 \times 10^{15} [\sinh(0.0105 \sigma_p)]^{5.062}$$

$$\dot{\epsilon} \exp\left(\frac{411}{RT}\right) = A'(\sigma_p)^n = 4.58(\sigma_p)^{7.819}$$

- The constitutive equations that have been used to model the hot isothermal deformation behaviour of 34CrNiMo6 steel and the data that have been applied gave reasonable agreement between the model curves and the experimental data obtained. Both flow stress models for dynamic recovery and dynamic recrystallisation gave good agreement between the predicted and the experimental data especially with that obtained at austenitising temperature of 1100 °C (See Figures 4.12 and 4.13).
- The model has good prediction capabilities of flow stress using the constitutive equations, where it gave a good accuracy in the range of experimental conditions of deformation temperature, strain and strain rate. The average absolute relative error (AARE) was found to be 8.60 % and 5.96 %, while the correlation coefficient (R) was found to be 0.9576 and 0.9755 for austenitising temperatures of 1100 °C and 1260 °C, respectively (See Figure 4.14).
- When the strains of 0.4, 0.6 and 0.8 were used with the same deformation conditions, the highest percentage of recrystallisation was obtained with the highest strain (0.8) at all strain rates (See Figure 5.7).

#### - **Non-isothermal deformation processes (multi hit)**

- In the case of using non-isothermal deformation tests (four hits) the austenitising temperature of 1100 °C gave smaller grain size than austenitising temperature of 1200 °C. The obtained grain size with austenitising at 1100 °C was approximately 37±2 µm, while it was approximately 64±5 µm with austenitising at 1200 °C.
- By comparing austenite grain size after the non-isothermal deformation tests (multi-hit) with and without deformation at temperature of 900 °C, the results were convergent for both austenitising temperatures. Change in the austenite grain size, which occurred between the third and fourth hits, can be explained because of the static recrystallisation and not because of increasing strain in the fourth hit.

- During the tests oxide scale layers were observed on the surface of the samples and increasing the austenitising temperature and time would increase the thickness of the layers. These oxides are undesirable because they lead to the formation of defects such as porosity and cracks within the surface structure, especially when the outer surface layers, which should be removed after the thermo-mechanical process, is thin. For instance, when producing a near-net shape product as in the case of large-scale forgings for trying to increase the material hardenability. Moreover, presence of the oxide scales through the deformation would affect the friction and heat transfer of the metals during the contact between the hot metal and cold die.
- According to the optical images, two kinds of non-metallic inclusions were recognised in the studied steel; sulphide inclusions with elongated morphology (green colour) and globular oxide inclusions. From the EDX analysis, these inclusions were identified as Manganese Sulphide (MnS) and Aluminium Oxide (Al<sub>2</sub>O<sub>3</sub>).

#### - Heat treatment

- By using the normalization process the prior austenite grain sizes were refined for both austenitising temperatures. The grains were refined from 32 µm to 10 µm and from 51 µm to 12 µm when austenitising temperatures of 1100 °C and 1200 °C were used, respectively. This result is good and consistent with the fact that the strength and impact toughness can be improved by refinement of the prior austenite size.
- The kinetics of grain growth are higher at an elevated temperature than at a faster cooling rate, so using a temperature of 1100 °C as the deformation temperature can help to obtain a smaller grain size than 1200 °C when the same cooling rate is used.
- From the TTT diagram for 34CrNiMo6 steel, the structure almost entirely transformed to ferrite and pearlite after being held for 4 hours at temperature of 650 °C.
- Using austenitising temperatures of 1100 °C and 1200 °C with the normalizing process gave almost the same austenite grain size. However, at 1100 °C the grains were equiaxed with more uniform structure than at 1200 °C, which helps to improve desired mechanical properties. Furthermore, it was clear from the normalized microstructure the volume

fraction of ferrite to pearlite was almost convergent at an austenitising temperature of 1100 °C, while at 1200 °C the volume fraction of pearlite was higher than the ferrite.

- Increasing the normalizing holding time did not influence the average austenite grain size, as the grain size remained approximately the same despite a significant increase in normalizing holding time to ten times the previous, but increasing to this time resulted in an abnormal growth of austenite grains, particularly at an austenitising temperature of 1200 °C, which may lead to reduced toughness. This abnormal grain growth may be due to the lack of enough elements such as Al in the steel composition to avoid grain coarsening.
- Decreasing the austenitising temperature from 960 °C to 840 °C and tempering temperature from 630 °C to 520 °C did not help to achieve good results, as the hardness increased and toughness decreased, especially with high cooling rates.
- Microstructural analysis of the samples showed that specimens with low toughness exhibited high percentages of acicular ferrite (bainite). Most probably this acicular ferrite structure is typical of medium carbon steel such as 34CrNiMo6 at low cooling rate (See sections 2.2 and 2.11). Moreover, the presence of abnormal grain sizes is also an important factor that contributed to the low toughness of the material.
- At very low cooling rates the toughness requirements will not be achieved. This may be attributed to the lower hardenability in the 34CrNiMo6 steel, where we cannot get a high percentage of martensite within the microstructure of the tested samples. Therefore to achieve 100 % martensite in the sampling position, the cooling rate should be more than 1.2 °C/s for a big section billet with diameter of 480 mm.
- Samples with low toughness have a brittle fracture (rough) where clear evidence of the transgranular fracture is produced by the presence of bainite, but there is also a possibility of a intergranular fracture due to the presence of abnormal growth of austenite grain size found in some tested samples ( See Figures 7.10 and 7.17 ).
- Results for samples that were tested with different cooling rates showed that the toughness increased with increasing hardness (see Table 7.1). This result means that a soft material that can be characterized by low hardness does not always exhibit good toughness. However, for samples that were tested with 0.6 °C/sec and different austenitising



temperatures, the results of the toughness was oscillatory, sometimes increasing and at other times decreasing with increased hardness (see Table 7.2). Consequently hardness cannot be a good factor to determine whether the material has good toughness or not.

- Experiments performed on the samples made of 34CrNiMo6 steel showed that when different cooling rates of 0.3, 0.6, 0.9, and 1.2 °C/sec with austenitising temperatures of 840 °C and 960 °C and tempering temperatures of 520 °C and 630 °C were used respectively, the toughness and hardness increased with increasing the cooling rate (See Table 7.1). These results support the idea of having 100 % martensite for a good toughness response (See Fig. 7.9). However, a low hardness value does not mean a tough material unless the material has a homogeneous microstructure and exhibits good hardenability across the section.
- Changing the austenitising temperature by reducing it to 900 °C, which according to Fig. 3.18 gave an austenite grain size of nearly 19 µm, has an effect on the mechanical properties especially fracture toughness. Accordingly, starting with a small austenite grain size before the heat treatment process will help to obtain the required mechanical properties.
- Toughness value of 47 J and a hardness value of 313±2 HB were obtained when the austenitising temperature was reduced to 900 °C, which is considered a good result according to required specifications.
- Using a tempering temperature of 640 °C instead of 630 °C did not improve the results of toughness and hardness at high austenitising temperatures, but there was a slight improvement at low temperatures (See Figure 7.22).

#### - **Multiple heat treatment processes**

- Using a multiple heat treatment process consisting of double normalizing, double quenching and single tempering in different orders gave values of high toughness and good hardness within the required specifications. However, using the multiple heat treatment will increase production costs due to repeating the processes many times. Furthermore, there would be a delay in release of the product as a result of the length of heat treatment processes.

- The microstructure which has a 100 % martensite has the highest hardness value in comparison with a mixture microstructure of martensite and bainite (See Figures 7.6 and 7.22).
- The resulting microstructures were more uniform and less variation in grain size distributions comparing to the single heat treatment, which usually helps to reduce the scattering in data
- The grain size distributions in all multiple heat treatment cycles were unimodal with positively skewed
- The best results of a good hardness value of  $295\pm 2$  HB and a high toughness value of 101 J were achieved by using heat treatment cycle 1.

## **Chapter 10 Suggestion for the future**

In this chapter some solutions will be proposed for future work, based on the outcomes that have been achieved from the thesis. After what had been done to improve the factors affecting the thermo-mechanical process and from the discussion of results the main problem was how to achieve 100 % martensite in the sampling position for the big section of billet (485 mm diameter) after being quenched in water. This makes the hardenability the main problem, which should be improved to overcome the problem. In that respect suggestions to try to solve this problem have been divided into two main sections.

### **10.1 Study the possibility of increasing the cooling rate**

#### **10.1.1 Use near net-shape forging**

As the billet diameter increases the toughness will become poor in the direction of the centre especially if the steel has a hardenability problem. Therefore, increasing the cooling rate to achieve 100 % martensite in the sampling position is one of the aspects to be taken into consideration when the mechanical properties of the big section of billet (485 mm diameter) are required to be improved. One of the suggestions is producing a near-net shape product before the heat treatment process to try to increase the steel hardenability. This step is an attempt to make the cross section of the billet as small as possible where just a thin layer should be left for a final finishing.

#### **10.1.2 Study the performance improvement of Somers Forge quenching tank**

The other suggestion is to try to improve the performance of the quenching tank as much as possible to increase the hardenability. Sometimes improvement of the water tanks that are used for the quenching process is reflected in an improvement of the convective heat transfer coefficient which consequently leads to enhanced hardenability. For example, using high volume pumps to circulate the water inside the tank can help to achieve good quench tank agitation. At other times the quenching tank should be completely redesigned in order to get a consistent flow rate along the length and around the cross section of the billet.

## 10.2 Modifying the chemical composition of the 34CrNiMo6 alloy steel

The other important aspect that can be modified or changed to improve the hardenability is the chemical composition. As mentioned in Section 9.2, there are several types of elements that can be used to increase the hardenability. Elements such as Mn and Ni are used to increase the hardenability of steel (Figure 10.1), but the balance between added elements and the cost of the steel should be taken in consideration because the addition of some elements in large quantities increases the cost. Moreover, Vanadium is one of the most important elements that contribute to increase the hardenability in the chemical composition of 34CrNiMo6 steel. It must be taken into account that the right conditions for heat treatment are the only way to achieve a good efficiency in hardenability with Vanadium. Some alloying elements which should be in solid solution can reduce the rate of austenite decomposition either by retarding the growth rate, such as Chrome and Molybdenum, or by retarding the nucleation rate of ferrite-pearlite or bainite, such as Vanadium, Nickel and Manganese.

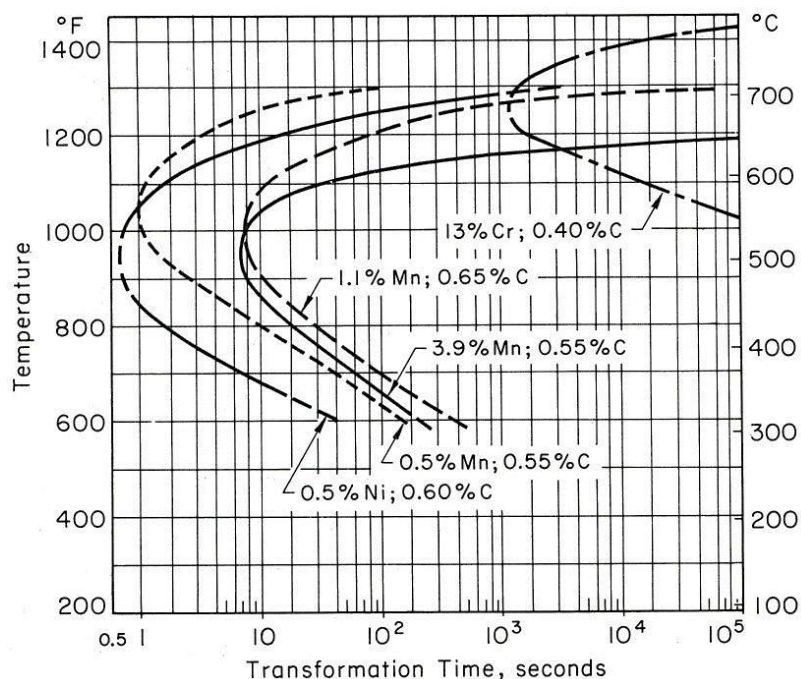


**Figure 10-1** Comparative time intervals for 50 % isothermal transformation in steels containing different amounts of alloying elements, Nickel, Manganese and chromium[332].

### **10.2.1 The addition of niobium (Nb) instead of vanadium (V) in the chemical composition of 34CrNiMo6 steel**

The effect of using niobium instead of vanadium in the composition of 34CrNiMo6 steel may lead to an improvement in some of the required properties. As was discussed in section 2.11.3.2, niobium is an important component of some high strength alloy steels; it is a very strong carbo-nitride former which inhibits grain growth of both austenite and ferrite. Moreover, niobium is used to improve strength and ductility within a structure. Niobium is mainly used for grain refinement purposes and also precipitation strengthening. Generally elements such as Mn, Ni, Nb, C are used to help to increase hardenability. Furthermore, if niobium is used in combination with Mn, the Nb solubility in austenite will increase, which in turn further lowers the austenite transformation temperature and also limits the premature precipitation of Nb in austenite[333].

### **10.3 Bimodal grain size distribution and its effect on scatter in toughness results**

The presence of bimodal (mixed coarse and fine) grain size distribution in some resultant microstructures must be taken into consideration, especially when unsatisfactory results are obtained despite the fact that the average grain size of the microstructure is small. This bimodal distribution, as discussed earlier, adversely affects the mechanical properties by causing scatter in cleavage fracture values. Accordingly, the effect of this distribution on scatter in toughness results should be studied. Moreover, the link between grain size distribution in forging and the microalloy precipitate type, size, and distribution as a consequence of as-cast inhomogeneous microalloying precipitate distributions should also be studied.

### **10.4 The effect of microstructural banding on mechanical properties and fracture behaviour**

As observed, most of the microstructures after deformation showed banding, which may affect some mechanical properties. Thus the effect of this banding and its influence on impact fracture properties behaviour should be investigated. Furthermore, the effect of heat treatment processes, especially normalizing, as a tool to reduce or remove the banded condition should also be studied. This could be done by replacing the martensite that

concentrated in bands with randomly dispersed small volumes of martensite in the steel microstructure, which may improve some subsequent mechanical properties.

### **10.5 The effect of non-metallic inclusions on fracture toughness properties**

As was discussed in section 2.6, non-metallic inclusions have an effect on some properties of steel such as strength, machinability and toughness. The shape, critical size and distribution of non-metallic inclusions inside a steel ingot are the important parameters that influence these mechanical properties. According to the optical images that were shown in section 6.1, two kinds of non-metallic inclusions were recognised in the 34CrNiMo6 steel; sulphide inclusions with elongated morphology (e.g. MnS) and also some globular oxide inclusions (e.g.  $Al_2O_3$ ). These inclusions usually have an important role in the fracture process, where they or their traces (e.g. voids) often show at the centre of the fracture surfaces of tested specimens. Consequently, more research is needed into the effect of inclusions on the impact fracture toughness of 34CrNiMo6 steel.

### **10.6 The effect of oxide scales on interfacial heat transfer and friction during hot forging**

Several authors mentioned that the friction and heat transfer characteristics of metals change dramatically in the presence of oxide scale during hot deformation, when contact between the hot metal (e.g. during hot forging) and the cold deformation tool (e.g. die) occurs. Consequently, during the tests we observed that the oxide layers became thicker when the austenitising temperature increased from 1100 °C to 1200 °C and also when increasing soaking time from 1 hour to 24 hours at these temperatures, although the scale type usually should not change between these temperatures. However, the presence of these oxide scales may affect the rate of heat transfer, which is usually used to calculate the heat transfer from equilibrium state to another during cooling. Furthermore, these oxide scales during deformation may also affect the friction between the hot metal and cold die. Accordingly, the effects of these oxide scales on both heat transfer through the metal and friction between the deformed metal and the die halves should be investigated.

## **10.7 Optimization of the austenitising temperature before deformation**

In this study an austenitising temperature of 1260°C, which represented the real deformation temperature, was used to simulate the real process. Furthermore, an austenitising temperature of 1100°C was also used to study the effect of changing the austenitising temperature on the resulting microstructure. The results showed that reducing the austenitising temperature to 1100°C gave moderately fine and more uniform austenite grains and higher recrystallisation percentages than using an austenitising temperature of 1200°C. According to that, further tests should be done using different temperatures to optimize the austenitising temperature before deformation so as to improve the resulting microstructure, and thus subsequent mechanical properties.

## **10.8 Verification of double normalizing and double quenching results in the heat treatment process**

For reasons that we have mentioned earlier we could not use more than one sample for toughness test results. Accordingly, verification of the good results that were obtained from the toughness specimens after using double normalizing, double quenching or both in the heat treatment process are required by using more test samples. Moreover, the main parameters of the second process (normalizing and quenching) such as holding time and temperature could also be tested to optimise results.

# Appendix A: PSC Test Data and calculations

Table A-1 Example of workout sheet for raw, calculated, and corrected PSC stress-strain data

Specimen dimension (mm)

Equivalent Stress (MPa)

Equivalent Strain

Time [s]	Sample Temp. 2. C [Load]	Displacement [mm]	Velocity [mm/s]	Final Load [N]	Total Displacement / Zero offset [mm]	Corrected End Stop	stress-Mpa							f	stress-Mpa	Beta	Corrected Strain		
							σ <sub>1</sub>	σ <sub>2</sub>	σ <sub>3</sub>	σ <sub>4</sub>	σ <sub>5</sub>	σ <sub>6</sub>	σ <sub>7</sub>					σ <sub>8</sub>	σ <sub>9</sub>
3857.4	1189.193188	-0.33986	16.825722	41.844711	-0.33986	0.759	-7.9992456	0.4542506	1.6186	26.4749	0.8292963	5.192574	-0.13999	0.6049124	0.6333378	-1.04984	-0.70223726	0.045	1.30041477
3857.407	1189.672485	-0.33989	16.871036	50.521217	-0.33989	0.504	-7.7449896	-0.1940898	18.361	26.57449	0.83961781	5.125104	-0.13005	0.6191408	0.6191542	-1.04742	-0.69634115	0.045	1.27142232



## A.1 Plane strain compression testing origin correction

The raw displacement data collected from the TMC machine were analysed and corrected on a spread sheet, as shown in Table A-1, and this was performed according to Loveday[334]. The important variables acquired during the deformation simulation were time, specimen temperature, load, and the displacement and velocity of the ram. The raw displacement data were corrected for possible errors in the zero position.

The final deformed specimens were measured as described in section 3.5 for thickness; the measurements were averaged over five readings. In the breadth direction the average was weighted towards the central measurement, with this being counted twice during the calculation. The cold final measurements were then used to calculate the hot final measurements of the specimen.

In order to take into account the changing area between the tool and the specimen an empirical formula was used to define the breadth spread coefficient  $C_b$  from the specimen dimensions before and after deformation test and obtained from Equation A.1.

$$C_b = \frac{(b_f/b_0)-1}{1-(h_f/h_0)^{0.5}} \quad \text{A.1}$$

where  $b_f$  is the average breadth after deformation,  $b_0$  is the average breadth before deformation,  $h_f$  is the average thickness after deformation, and  $h_0$  is the average thickness before deformation, and the instantaneous breadth was obtained from Equation A.2.

$$b = b_0[1 + C_b - C_b(h/h_0)^{0.5}] \quad \text{A.2}$$

The appropriate origin correction was applied to the analysed data in the zero position as shown in Figure (A-1).

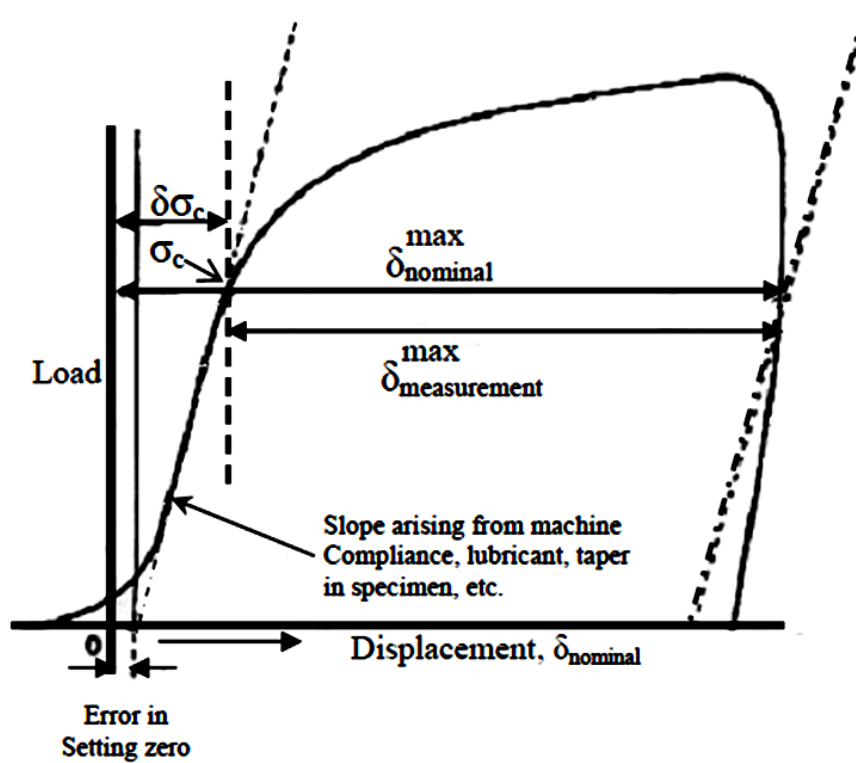


**Figure A-1** Schematic of the load corrected tool displacement curve[334].

In order to determine the flow stress of the tested material, the load exerted by the ram  $L$  was converted to pressure using the instantaneous breadth  $b$  and the platen width  $w$  and calculated using Equation A.3.

$$\bar{p} = \frac{L}{wb} \quad \text{A.3}$$

The friction conditions, sliding, partial sticking or sticking, are determined by the relationship between the values of the position in the tool width  $Z_0$  and platen width  $w$ .

$$Z_0 = \left(\frac{h}{2\mu}\right) \ln\left(\frac{1}{2\mu}\right) \quad \text{A.4}$$

Where  $h$  is the instantaneous thickness and  $\mu$  is the friction coefficient.

If  $2Z_0 > w$ , then sliding friction is occurring.

$$\frac{\bar{p}}{2k} = \frac{1}{bw} \left[ \frac{2h^2}{\mu^2} + \frac{(b-w)h}{\mu} \right] \left[ \exp\left(\frac{\mu w}{h}\right) - 1 \right] - \frac{2h}{\mu b} \quad \text{A.5}$$

If  $w > 2Z_0 > 0$ , then partial sticking is occurring.

$$\frac{\bar{p}}{2k} = \frac{1}{\mu w} \left( \frac{1}{2\mu} - 1 \right) + \frac{(w/2) - z_0}{\mu w} + \frac{[(w/2) - z_0]^2}{hw} + \frac{1}{\mu b} \left( \frac{2z_0^2}{w} - z_0 - \frac{2hz_0}{\mu w} + \frac{h}{2\mu} - h + \frac{h^2}{w\mu^2} - \frac{2h^2}{\mu w} \right) + \frac{1}{hb} \left( z_0^2 - \frac{4z_0^3}{3w} - \frac{w^2}{12} \right) \quad \text{A.6}$$

If  $0 > 2Z_0$ , then sticking is occurred

$$\frac{\bar{p}}{2k} = 1 + \frac{w}{4h} - \frac{w^2}{12hb} \quad \text{A.7}$$

Also during deformation tests especially at multiple hits, the heating which occurs on the first deformation can raise the temperature for the second deformation, particularly when the second hit is at a low temperature and with short inter-pass times. Therefore, the stress strain data are corrected for the effects of temperature rise during the deformation using the equation below.

$$\sigma_{iso} = \sigma + \frac{Q}{\beta R} \left( \frac{1}{T_{iso}} - \frac{1}{T_{inst}} \right) \quad \text{A.8}$$

Where  $\sigma_{iso}$  isothermal stress, Q is Activation energy of deformation, R is the Universal gas constant ( $8.314 \text{ J K}^{-1} \text{ mol}^{-1}$ ),  $T_{iso}$  the desired isothermal temperature,  $\beta$  is the material strength constant and  $T_{inst}$  the instantaneous temperature recorded using a thermocouple. The corrections were applied to the obtained test data by using an Excel spreadsheet as shown in Table A-1.

## Appendix B: Grain size measurement: Linear intercept method

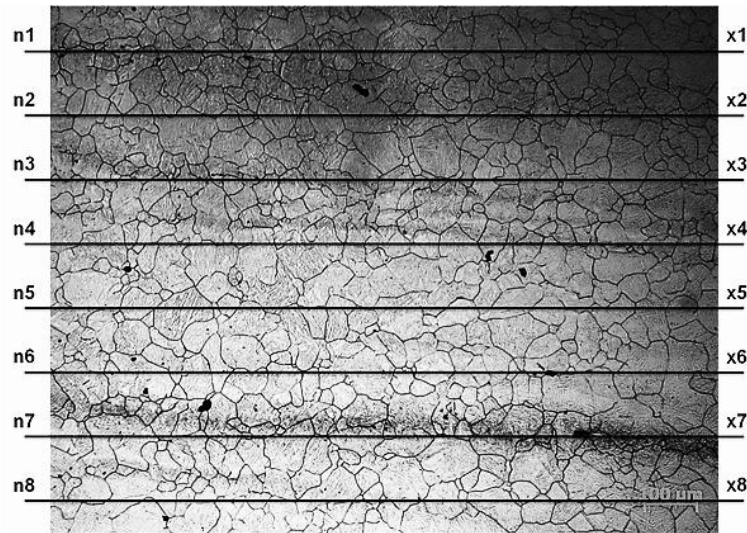


**Figure B-1** The linear intercept method for grain size determination.

First the real length of the lines was measured by using the scale bar, and then for each line this real length was divided by the number of grain boundaries to get the linear intercept length.

$$L_i = \frac{\text{real length}}{x_i} \quad \text{B. 1}$$

To find mean linear intercept length, the linear intercept lengths ( $L_i$ ) are summed, and divided by the total number of lines ( $n$ ).

$$\bar{L} = \frac{\sum L_i}{n} \quad \text{B. 2}$$

The data collected are then used to calculate the standard deviation as follows:

$$S^2 = \frac{(L_i - \bar{L})^2}{(n - 1)} \quad \text{B. 3}$$

$$\text{(Standard Deviation) } S = \sqrt{\frac{(L_i - \bar{L})^2}{(n - 1)}} \quad \text{B. 4}$$

From the standard deviation, the standard error of the mean can be calculated as follows:

$$S(\bar{L}) = \frac{S}{\sqrt{n}} \quad \text{B. 5}$$

From the standard error of the mean, the 95% confidence limit can be calculated using the relevant **t** value (taken from the statistics Table) as follows:

Confidence Interval (95% confidence level) =  $\bar{L} \pm (t_{95n-1}) * S(\bar{L})$

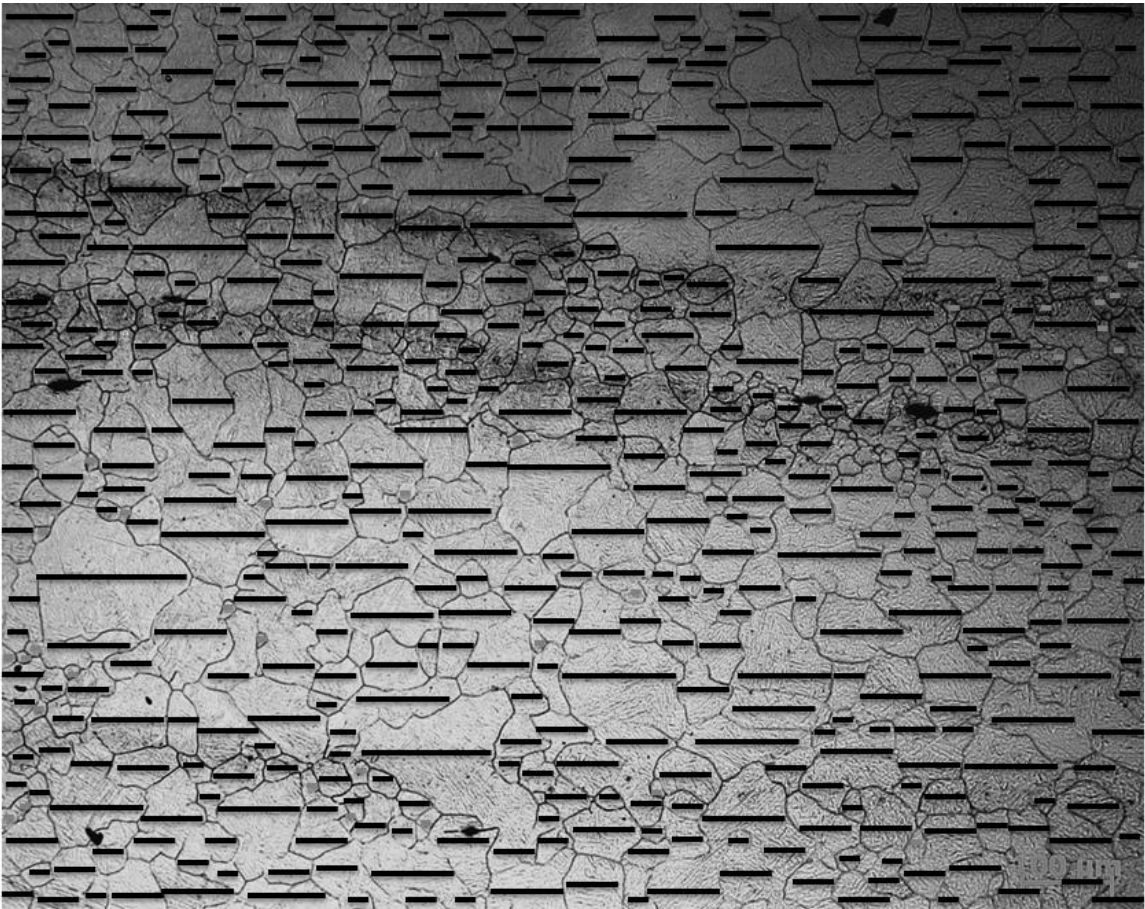
B.6

**Table B-1** The calculation of grain size using the linear intercept method

$n_i$	$x_i$	$L_i (\mu\text{m})$	$(L_i - \bar{L})^2$
1	20	50.0	38.1
2	26	38.5	28.7
3	25	40.0	14.6
4	21	47.6	14.4
5	25	40.0	14.6
6	25	40.0	14.6
7	26	38.5	28.8
8	19	52.6	77.5
		$\Sigma L_i = 347.2$	$s^2 = \frac{\Sigma(L_i - \bar{L})^2}{n-1} = 33$
		$\bar{L} = \Sigma L_i / n = 43.4 \mu\text{m}$	$s = 5.75$

**- Grain size distribution example:**

An example for a manual method that was used to determination the grain size distribution.



## Appendix C: Charpy specimens results sheets

Exova (UK) Ltd  
Holwick Road  
Riverside Park  
Middlesbrough  
United Kingdom  
TS2 1QS

T: 01642 250336  
F: 01642 250337  
E: Teesside@Exova.com  
W: www.exova.com



### Test Certificate

EXOVA - TEESSIDE LAB  
HOLWICK ROAD  
RIVERSIDE PARK  
MIDDLESBROUGH  
TS2 1QS

REF No  
Page  
Ord No  
Date Tested  
Date Reported

T 204117 : Issue 1  
1 of 1  
PRO FORMA  
07/08/12  
16/08/12

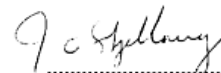
Attn: NASAR ALI

Item - 12 X CHARPY IMPACTS - TEST ONLY  
NI-HARD MATERIAL?

Specification - Client Requirement

Charpy Test - ASTM E23 : 2007A							
	Position	Dimensions [mm]	Denomination	Test Temp [°C]	Energy Absorbed [Joules]	Average [Joules]	Comments
001:Pre-machined Sample	0	10x10x2V	N/A	-20.0	17	17	Nil
002:Pre-machined Sample	1	10x10x2V	N/A	-20.0	10	10	Nil
003:Pre-machined Sample	2	10x10x2V	N/A	-20.0	3	3	Nil
004:Pre-machined Sample	3	10x10x2V	N/A	-20.0	9	9	Nil
005:Pre-machined Sample	4	10x10x2V	N/A	-20.0	4	4	Nil
006:Pre-machined Sample	5	10x10x2V	N/A	-20.0	3	3	Nil
007:Pre-machined Sample	6	10x10x2V	N/A	-20.0	16	16	Nil
008:Pre-machined Sample	7	10x10x2V	N/A	-20.0	4	4	Nil
009:Pre-machined Sample	8	10x10x2V	N/A	-20.0	7	7	Nil
010:Pre-machined Sample	10	10x10x2V	N/A	-20.0	26	26	Nil
011:Pre-machined Sample	11	10x10x2V	N/A	-20.0	19	19	Nil
012:Pre-machined Sample	12	10x10x2V	N/A	-20.0	29	29	Nil

Tested by EXOVA TEESSIDE

  
.....  
Jon Skjelhaug  
Production Engineer  
For and on authority of  
Exova (UK) Ltd

This document may not be reproduced other than in full, except with the prior written approval of the issuing laboratory.  
These results pertain only to the item(s) tested as sampled by the client unless otherwise indicated.



Exova (UK) Ltd  
 Holwick Road  
 Riverside Park  
 Middlesbrough  
 United Kingdom  
 TS2 1QS

T: 01642 250336  
 F: 01642 250337  
 E: Teesside@Exova.com  
 W: www.exova.com



## Test Certificate

UNIVERSITY OF SHEFFIELD  
 DEPARTMENT OF MATERIALS  
 SCIENCE AND ENGINEERING  
 SHEFFIELD  
 S1 3JD

REF No T 205713 : Issue 1  
 Page 1 of 1  
 Ord No N/A  
 Date Tested 24/10/12  
 Date Reported 24/10/12

Attn: NASAR ALI

Item - 10 OFF CVN SAMPLES FOR TEST ONLY


Specification - Client Requirement

Charpy Test - Client Requirement							
	Position	Dimensions [mm]	Denomination	Test Temp [°C]	Energy Absorbed [Joules]	Average [Joules]	Comments
001:Pre-machined Sample	SAMPLE 0	10x10x2V	N/A	-20.0	9	9	N11
002:Pre-machined Sample	SAMPLE 1	10x10x2V	N/A	-20.0	40	40	N11
003:Pre-machined Sample	SAMPLE 2	10x10x2V	N/A	-20.0	47	47	N11
004:Pre-machined Sample	SAMPLE 3	10x10x2V	N/A	-20.0	17	17	N11
005:Pre-machined Sample	SAMPLE 4	10x10x2V	N/A	-20.0	32	32	N11
006:Pre-machined Sample	SAMPLE 5	10x10x2V	N/A	-20.0	24	24	N11
007:Pre-machined Sample	SAMPLE 6	10x10x2V	N/A	-20.0	80	80	N11
008:Pre-machined Sample	SAMPLE 7	10x10x2V	N/A	-20.0	82	82	N11
009:Pre-machined Sample	SAMPLE 8	10x10x2V	N/A	-20.0	86	86	N11
010:Pre-machined Sample	SAMPLE 11	10x10x2V	N/A	-20.0	101	101	N11

### Certificate Comments

----- End of Text -----

Tested by EXOVA TEESSIDE

  
 .....  
 Liam Overend  
 Metallurgist  
 For and on authority of  
 Exova (UK) Ltd

This document may not be reproduced other than in full, except with the prior written approval of the issuing laboratory. These results pertain only to the item(s) tested as sampled by the client unless otherwise indicated.

The contents of this report are governed by the terms and conditions outlined.  
 Registered Office: Exova (UK) Ltd, Lochend Industrial Estate, Newbridge, Midlothian, EH28 8PL, United Kingdom, Reg No. SC 70429



Exova (UK) Ltd  
Holwick Road  
Riverside Park  
Middlesbrough  
United Kingdom  
TS2 1QS

T: 01642 250336  
F: 01642 250337  
E: Teesside@Exova.com  
W: www.exova.com



## Test Certificate

UNIVERSITY OF SHEFFIELD  
DEPARTMENT OF MATERIALS  
SCIENCE AND ENGINEERING  
SHEFFIELD  
S1 3JD

REF No  
Page  
Ord No  
Date Tested  
Date Reported

T 206688 : Issue 1  
1 of 1  
NARAR A ALI  
12/12/12  
12/12/12

Attn: NASAR A ALI

Item - TWO PRE-MACHINED CHARPY SAMPLES  
REF: 1-1 + 2-2

Specification - Client Requirement

Charpy Test - ASTM E23 : 2007A							
	Position	Dimensions [mm]	Denomination	Test Temp [°C]	Energy Absorbed [Joules]	Average [Joules]	Comments
001:Pre-machined Sample	SAMPLE 1-1	10x10x2V	N/A	-20.0	7	7	Nil
002:Pre-machined Sample	SAMPLE 2-2	10x10x2V	N/A	-20.0	91	91	Nil

### Certificate Comments

----- End of Text -----

Tested by EXOVA TEESSIDE

.....  
Liam Overend  
Metallurgist  
For and on authority of  
Exova (UK) Ltd

This document may not be reproduced other than in full, except with the prior written approval of the issuing laboratory.  
These results pertain only to the item(s) tested as sampled by the client unless otherwise indicated.





Appendix D - 1: Certificate of conformity for chemical composition of 34CrNiMo6 steel

Steel SEM

Sheffield Forgemasters Steel Ltd  
 PO Box 288 Brightside Lane  
 Sheffield S9 2RW  
 t: 0114 244 9071  
 f: 0114 251 9035

Certificate of Conformity

Works Order No.						Specification										
8014870                      8889						34 Cr.Ni.Mo 6 Electrically Melted Vacuum Degassed Steel										
Customer & Customer Order Reference																
Somers Forge                      30.05659																
Cast No.	C	Si	Mn	P	S	Cr	Mo	Ni	V	Al	Cu	Sn			H	
75500	.33	.22	.51	.009	.010	1.52	.23	1.86	.07	.003	.13	.010			1.6 ppm	
Ingot Type                      42 x 92																
No. Off                                      5																
Identities                                      A-AB, B-BC, C																
Delivery Condition                      As Cast																
Additional Data																

SOMERS VERIFIED COPY  
 SIGNED *A Sh*  
 TITLE: QUALITY MANAGER  
 DATE 05/06/2008

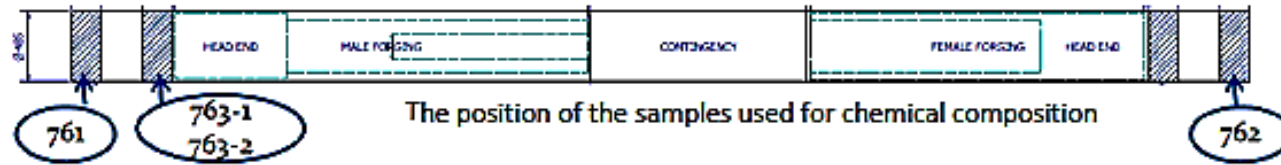
*S. Hunt*  
 10/3/07

Certified that, unless otherwise stated above, the whole of the above mentioned parts have been manufactured, tested and inspected in accordance with the terms of the contract/order applicable thereto and conforms fully to the standard/specification quoted. The quality systems adopted in respect of these supplies have accented with the conditions of our BS EN ISO 9001 registration FM 12816. Certified in accordance with BS EN 10204 3.1.2.

Signed: *JMC*                                      Date: *9.7.07*  
 For and on behalf of Sheffield Forgemasters Steel Limited

Witness / Review  
 Signed: *[Signature]*  
 Date: *06/06/2008*

D - 2: The chemical composition and toughness from 4 positions along the length of the billet



The chemical composition of samples from different position along the length of the billet

ID	Toughness (Joules)	Chemical Analysis %									ppm		
		C	Si	Mn	P	S	Cr	Mo	Ni	Cu	N	H	O
761	77	0.33	0.24	0.48	0.008	0.006	1.5	0.22	1.63	0.12	80	2	40
763-1	54	0.34	0.25	0.49	0.007	0.005	1.5	0.22	1.68	0.12			
763-2	121	0.34	0.26	0.46	0.006	0.006	1.5	0.22	1.68	0.12			
762	57	0.34	0.24	0.48	0.01	0.006	1.5	0.22	1.63	0.12	80	2	30
Max		0.34	0.26	0.49	0.01	0.006	1.5	0.22	1.68	0.12	80	2	40
Min		0.33	0.24	0.46	0.006	0.005	1.5	0.22	1.63	0.12	80	2	30
Average		0.34	0.25	0.48	0.008	0.006	1.5	0.22	1.65	0.12	80	2	35

## Appendix E: Examples of equivalent grades of 34CrNiMo6 steel

1-

Equivalent grades of grade 34CrNiMo6 (1.6582)											
Warning! Only for reference											
USA	Germany	Japan	France	England	Italy	China	Sweden	Poland	Czechia	Russia	Inter
-	DIN, WNr	JIS	AFNOR	BS	UNI	GB	SS	PN	CSN	GOST	ISO
4340	34CrNiMo6 GS- 34CrNiMo6V	SNM447	35NCD6	817M40	35CrNiMo6 35NiCrMo6KB	34CrNi3Mo 34CrNiMo ZG34CrNiMo	2541	34HNM	16342 16343 16444	36KH2N2MFA 38KH2N2MA 40KH2N2MA	36CrNiMo6

Equivalent grades of grade 34CrNiMo6 (1.6582)[335]

2-

**OYAL METAL ÇELİK**  
SAN. VE TİC. LTD. ŞTİ

Güvenebileceğiniz İsim



The name you can trust



English

Ana Sayfa	Üretim Programı	Çelikler Hakkında	İletişim	Hakkımızda	Dökümanlar	Haberler
-----------	-----------------	-------------------	----------	------------	------------	----------

Alt Başlıklar	VCNMO150																		
Soğuk İş Takım Çelikleri	<p style="text-align: center;"><b>Identification</b></p> <table border="1"> <thead> <tr> <th colspan="6">Designation by Standards</th> </tr> <tr> <th>Brand Name</th> <th>Ravne No.</th> <th>Mat. No.</th> <th>DIN</th> <th>EN</th> <th>AISI</th> </tr> </thead> <tbody> <tr> <td>VCNMO150</td> <td>748</td> <td>1.6582</td> <td>34CrNiMo6</td> <td>34CrNiMo6</td> <td>4337/4340</td> </tr> </tbody> </table>	Designation by Standards						Brand Name	Ravne No.	Mat. No.	DIN	EN	AISI	VCNMO150	748	1.6582	34CrNiMo6	34CrNiMo6	4337/4340
Designation by Standards																			
Brand Name		Ravne No.	Mat. No.	DIN	EN	AISI													
VCNMO150		748	1.6582	34CrNiMo6	34CrNiMo6	4337/4340													
Sıcak İş Takım Çelikleri																			
Düşük Alaşımli Takım Çelikleri																			
Yüksek Hız Takım Çelikleri																			
Özel Çelikler																			
Alaşımlı Çelikler																			

Designation by standards[119]

3-

Metal Ravne Steel Selector													
<p>Alphabetical Steel Index Keyword Search Cold Work Tool Steel Hot Work Tool Steels Low Alloyed Tool Steels High Speed Steels Special Steels Alloyed Cast Steels</p>	<p>Steel VCNMO150 (Mat.No. 1.6582, DIN 34CrNiMo6, AISI 4337/4340)</p> <p>Designation by Standards</p> <table border="1"> <thead> <tr> <th>Brand Name</th> <th>Ravne No.</th> <th>Mat. No.</th> <th>DIN</th> <th>EN</th> <th>AISI</th> </tr> </thead> <tbody> <tr> <td>VCNMO150</td> <td>748</td> <td>1.6582</td> <td>34CrNiMo6</td> <td>34CrNiMo6</td> <td>4337/4340</td> </tr> </tbody> </table>	Brand Name	Ravne No.	Mat. No.	DIN	EN	AISI	VCNMO150	748	1.6582	34CrNiMo6	34CrNiMo6	4337/4340
Brand Name	Ravne No.	Mat. No.	DIN	EN	AISI								
VCNMO150	748	1.6582	34CrNiMo6	34CrNiMo6	4337/4340								

Designation by standards[336]

## References

- [1] <http://en.wikipedia.org/wiki/Forging#History>.
- [2] "Standard of steel SR EN 10083-1:1995."
- [3] W. C. Leslie, "The physical metallurgy of steels," ed Auckland ; London: McGraw-Hill, 1983, 1982, pp. 142-144.
- [4] G. Krauss, "Steels: Processing, Structure, And Performance," ed: ASM International, 2005, p. 126.
- [5] G. Krauss, "Steels: Processing, Structure, And Performance," ed: ASM International, 2005, p. 125.
- [6] E. B. Damm and M. Merwin, "Austenite formation and decomposition," ed Warrendale, Pa.: TMS, 2003, pp. 196-197.
- [7] K.-E. Thelning, "Steel and its heat treatment," 2nd ed London ; Boston: Butterworths, 1984, p. 4.
- [8] F. G. C. Carlos Capdevila, "The Role of Inclusions and Austenite Grain Size on Intragranular Nucleation of Ferrite in Medium Carbon Microalloyed Steels," *Materials Transactions*, vol. Vol.45. NO.8, pp. 2678-2685, 2004.
- [9] H. K. D. H. Bhadeshia and R. W. K. Honeycombe, "Steels : microstructure and properties," 3rd ed. ed Amsterdam ; London: Butterworth-Heinemann, 2006, pp. 42-44.
- [10] F. C. C. Capdevila, "Modelling of Kinetics of Isothermal Allotriomorphic and Idiomorphic Ferrite Formation in Medium Carbon Vanadium–Titanium Microalloyed Steel," *ISIJ International*, vol. Vol. 41, pp. 1083–1092, 2001.
- [11] S. M. K. Yamamoto, T. Haze, R. Chijiwa and H. Mimura., *Symposium On Residual and Unspecified Elements in Steel*, ASTM, Philadelphia, (1989), 266.
- [12] H. I. Aaronson, "Symposium on the Mechanical Properties of Phase Transformations in Metals," *Institute of Materials*, London 1995.
- [13] [http://en.wikipedia.org/wiki/Acicular\\_ferrite](http://en.wikipedia.org/wiki/Acicular_ferrite).
- [14] H. K. D. H. Bhadeshia, *Interpretation of the microstructure of steels*, 2005.
- [15] H. K. D. H. Bhadeshia, "Bainite in steels : transformations, microstructure and properties," 2nd ed London: IOM Communications, 2001, p. 262.
- [16] H. K. D. H. Bhadeshia and R. W. K. Honeycombe, "Steels : microstructure and properties," 3rd ed. ed Amsterdam ; London: Butterworth-Heinemann, 2006, p. 44.
- [17] H.-W. Yen, P.-Y. Chen, C.-Y. Huang, and J.-R. Yang, "Interphase precipitation of nanometer-sized carbides in a titanium–molybdenum-bearing low-carbon steel," *Acta Materialia*, vol. 59, pp. 6264-6274, 2011.
- [18] W. D. Callister, Jr. / Rethwisch, David G., "Materials science and engineering: an introduction," 8th ed: John Wiley & Sons, 2009, pp. 360-361.
- [19] H. K. D. H. Bhadeshia, "Bainite in steels : transformations, microstructure and properties," 2nd ed. ed London: IOM Communications, 2001, p. 189.
- [20] S. J. M. a. R. F. Hehemann, "Institute of Metals Division - The Structure of Bainite in Hypoeutectoid Steels," *Trans. Met. Soc. , AIME* 221 (1961) 179–185.
- [21] H. K. D. H. Bhadeshia, "Bainite in steels : transformations, microstructure and properties," 2nd ed. ed London: IOM Communications, 2001, p. 129.
- [22] H. K. D. H. Bhadeshia and R. W. K. Honeycombe, "Steels : microstructure and properties," 3rd ed. ed Amsterdam ; London: Butterworth-Heinemann, 2006, p. 129.
- [23] H. K. D. H. Bhadeshia and J. W. Christian, "Bainite in steels," *Metallurgical Transactions A*, vol. 21, pp. 767-797, 1990.
- [24] F. B. Pickering, *Transformation and hardenability in steels* Ann Arbor: Climax Molybdenum, Ann Arbor USA, (1967) 109-132.

- [25] M. Takahashi and H. K. D. H. Bhadeshia, "Model for transition from upper to lower bainite," *Materials Science and Technology*, vol. 6, pp. 592-603, 1990.
- [26] G. E. Totten, "Steel Heat Treatment Metallurgy and Technologies," in *Steel Heat Treatment Handbook*, Second Edition ed, 2006, p. 101.
- [27] H. K. D. H. Bhadeshia, "Bainite in steels : transformations, microstructure and properties," 2nd ed. ed London: IOM Communications, 2001, p. 65.
- [28] A. G. Guy, "Reconstructive and displacive phase transformations," *Metallurgical Transactions*, vol. 3, pp. 2535-2536, 1972/09/01 1972.
- [29] C. H. Gur, "Handbook of thermal process modeling of steels," ed Boca Raton, Fla.: CRC ; London : Taylor & Francis., 2009, p. 359.
- [30] G. E. Totten, "Steel Heat Treatment Metallurgy and Technologies," in *Steel Heat Treatment Handbook*, Second Edition ed, 2006, p. 134.
- [31] "<http://www.keytometals.com/page.aspx?ID=CheckArticle&site=KTS&NM=144.>"
- [32] H. K. D. H. Bhadeshia, "Bainite in steels : transformations, microstructure and properties," 2nd ed. ed London: IOM Communications, 2001, pp. 73-74.
- [33] G. Krauss, "Steels: Processing, Structure, And Performance," ed: ASM International, 2005, p. 90.
- [34] G. Krauss, "Steels: Processing, Structure, And Performance," ed: ASM International, 2005, p. 91.
- [35] J. D. Verhoeven, "Steel metallurgy for the non-metallurgist," ed Materials Park, Ohio: ASM International, 2007, p. 38.
- [36] H. K. D. H. Bhadeshia, "Bainite in steels : transformations, microstructure and properties," 2nd ed. ed London: IOM Communications, 2001, pp. 66-68.
- [37] N. F. K. a. J. S. Bowles, *J. Aust. Inst. Metals*, vol. 5, 1960.
- [38] H. K. D. H. Bhadeshia and R. W. K. Honeycombe, "Steels : microstructure and properties," 3rd ed. ed Amsterdam ; London: Butterworth-Heinemann, 2006, p. 133.
- [39] H. K. D. H. Bhadeshia, "Bainite in steels : transformations, microstructure and properties," 2nd ed. ed London: IOM Communications, 2001, pp. 189-190.
- [40] N. Kennon, "Schematic transformation diagrams for steel," *Metallurgical Transactions A*, vol. 9, pp. 57-66, 1978/01/01 1978.
- [41] G. Krauss, "Steels: Processing, Structure, And Performance," ed: ASM International, 2005, p. 55.
- [42] H. K. D. H. Bhadeshia and R. W. K. Honeycombe, "Steels : microstructure and properties," 3rd ed. ed Amsterdam ; London: Butterworth-Heinemann, 2006, p. 95.
- [43] D. A. Porter, K. E. Easterling, and M. Y. Sherif, "Phase transformations in metals and alloys," 3rd ed. / David A. Porter, Kenneth E. Easterling, and Mohamed Y. Sherif. ed Boca Raton, Fla. ; London: CRC, 2009, pp. 367-370.
- [44] G. Krauss, "Steels: Processing, Structure, And Performance," ed: ASM International, 2005, pp. 60-63.
- [45] G. Krauss, "Steels : heat treatment and processing principles," ed Materials Park, Ohio: ASM International, 1990, pp. 52-54.
- [46] W. D. Callister, Jr. / Rethwisch, David G., "Materials science and engineering: an introduction," 8th ed: John Wiley & Sons, 2009, pp. 363-364.
- [47] G. Krauss, "Steels : heat treatment and processing principles," ed Materials Park, Ohio: ASM International, 1990, pp. 47-50.
- [48] G. Krauss, "Steels : heat treatment and processing principles," ed Materials Park, Ohio: ASM International, 1990, p. 49.
- [49] G. E. Totten, "Steel Heat Treatment Metallurgy and Technologies," in *Steel Heat Treatment Handbook*, Second Edition ed, 2006, pp. 133-134.

- [50] G. Krauss, "Steels: Processing, Structure, And Performance," ed: ASM International, 2005, pp. 71-82.
- [51] G. Krauss, "Steels: Processing, Structure, And Performance," ed: ASM International, 2005, p. 72.
- [52] G. Krauss, "Steels: Processing, Structure, And Performance," ed: ASM International, 2005, p. 79.
- [53] H. K. D. H. Bhadeshia and R. W. K. Honeycombe, "Steels : microstructure and properties," 3rd ed. ed Amsterdam ; London: Butterworth-Heinemann, 2006, pp. 116-117.
- [54] J. D. Verhoeven, "Steel metallurgy for the non-metallurgist," ed Materials Park, Ohio: ASM International, 2007, p. 31.
- [55] J. D. Verhoeven, "Steel metallurgy for the non-metallurgist," ed Materials Park, Ohio: ASM International, 2007, p. 112.
- [56] H.-S. Yang and H. K. D. H. Bhadeshia, "Austenite grain size and the martensite-start temperature," *Scripta Materialia*, vol. 60, pp. 493-495, 2009.
- [57] K.-E. Thelning, "Steel and its heat treatment," 2nd ed London ; Boston: Butterworths, 1984, pp. 301-302.
- [58] J. J. Jonas, C. M. Sellars, and W. J. M. Tegart, "Strength and structure under hot-working conditions," *Materials Reviews*, vol. 14, pp. 1-24, 1969.
- [59] W. D. Callister, Jr. / Rethwisch, David G., "Materials science and engineering: an introduction," 8th ed: John Wiley & Sons, 2009, p. 417.
- [60] [http://en.wikipedia.org/wiki/Hot\\_working](http://en.wikipedia.org/wiki/Hot_working).
- [61] G. E. Dieter and D. Bacon, "Mechanical metallurgy," SI metric ed. ed: McGraw-Hill, 1988, pp. 72-75.
- [62] J. J. Jonas, C. M. Sellars, and W. J. M. Tegart, "Strength and structure under hot-working conditions," *Metallurgical Reviews*, vol. 14, pp. 1-24, 1969.
- [63] M. J. Luton and C. M. Sellars, "Dynamic recrystallization in nickel and nickel-iron alloys during high temperature deformation," *Acta Metallurgica*, vol. 17, pp. 1033-1043, 1969.
- [64] H. Yang, Z.-h. Li, and Z.-l. Zhang, "Investigation on Zener-Hollomon parameter in the warm-hot deformation behavior of 20CrMnTi," *Journal of Zhejiang University - Science A*, vol. 7, pp. 1453-1460, 2006.
- [65] M. Meysami and S. A. A. Mousavi, "Study on the behavior of medium carbon vanadium microalloyed steel by hot compression test," *Materials Science and Engineering: A*, vol. 528, pp. 3049-3055, 2011.
- [66] H. Mirzadeh, J. M. Cabrera, J. M. Prado, and A. Najafizadeh, "Hot deformation behavior of a medium carbon microalloyed steel," *Materials Science and Engineering: A*, vol. 528, pp. 3876-3882, 2011.
- [67] S. V. Sajadifar, M. Ketabchi, and B. Bemanizadeh, "Dynamic recrystallization behavior and hot deformation characteristics in 4340 steel," *Metallurgist*, vol. 56, pp. 310-320, 2012/07/01 2012.
- [68] R. W. K. Honeycombe, "The plastic deformation of metals," 2nd ed. ed London: Edward Arnold, 1984, pp. 237-238.
- [69] G. E. Dieter and D. Bacon, "Mechanical metallurgy," SI metric ed. ed: McGraw-Hill, 1988, pp. 189-191.
- [70] T. Gladman, "The physical metallurgy of microalloyed steels," ed London: Institute of Materials, 1997, pp. 39-40.
- [71] C. M. a. T. Sellars, W.J. McG, *Mem. Sci. Rev. Met*, vol. 63, pp. 731-746, 1966.
- [72] C. M. Sellars and W. J. McTegart, "On the mechanism of hot deformation," *Acta Metallurgica*, vol. 14, pp. 1136-1138, 1966.

- [73] G. E. Dieter and D. Bacon, "Mechanical metallurgy," SI metric ed. ed: McGraw-Hill, 1988, pp. 203-205.
- [74] B. Verlinden and R. W. Cahn, "Thermo-mechanical processing of metallic materials," ed Amsterdam ; London: Pergamon, 2007, pp. 69-72.
- [75] C. M. Sellars, "Modelling microstructural development during hot rolling," *Materials Science and Technology*, vol. 6, pp. 1072-1081, 1990.
- [76] F. J. Humphreys and M. Hatherly, "Recrystallization and related annealing phenomena," 2nd ed. ed Amsterdam ; London: Elsevier Science Ltd, 2004, p. 428.
- [77] N. Tsuji, Y. Matsubara, and Y. Saito, "Dynamic recrystallization of ferrite in interstitial free steel," *Scripta Materialia*, vol. 37, pp. 477-484, 1997.
- [78] R. Sandström and R. Lagneborg, "A model for hot working occurring by recrystallization," *Acta Metallurgica*, vol. 23, pp. 387-398, 1975.
- [79] F. J. Humphreys and M. Hatherly, "Recrystallization and related annealing phenomena," 2nd ed. ed Amsterdam ; London: Elsevier Science Ltd, 2004, p. 431.
- [80] I. Weiss, T. Sakai, and J. J. Jonas, "Effect of test method on transition from multiple to single peak dynamic recrystallization," *Metal Science*, vol. 18, pp. 77-84, 1984.
- [81] F. J. Humphreys and M. Hatherly, "Recrystallization and related annealing phenomena," 2nd ed. ed Amsterdam ; London: Elsevier Science Ltd, 2004, p. 435.
- [82] C. Maidorn and D. Blind, "Solidification and segregation in heavy forging ingots," *Nuclear engineering and design*, vol. 84, pp. 285-296, 1985.
- [83] P. J. Wray, "The Hot Deformation of Austenite, J.B. Bailance, ed," *TMS-AIME, New York, NY*, pp. 86-112, 1977.
- [84] F. J. Humphreys and M. Hatherly, "Recrystallization and related annealing phenomena," 2nd ed. ed Amsterdam ; London: Elsevier Science Ltd, 2004, p. 248.
- [85] F. J. Humphreys and M. Hatherly, "Recrystallization and related annealing phenomena," 2nd ed. ed Amsterdam ; London: Elsevier Science Ltd, 2004, p. 241.
- [86] F. J. Humphreys and M. Hatherly, "Recrystallization and related annealing phenomena," 2nd ed. ed Amsterdam ; London: Elsevier Science Ltd, 2004, p. 247.
- [87] P. J. Wray, "Effect of composition and initial grain size on the dynamic recrystallization of austenite in plain carbon steels," *Metallurgical Transactions A*, vol. 15, pp. 2009-2019, 1984/11/01 1984.
- [88] F. J. Humphreys and M. Hatherly, "Recrystallization and related annealing phenomena," 2nd ed. ed Amsterdam ; London: Elsevier Science Ltd, 2004, p. 482.
- [89] E. M. Lauridsen, D. J. Jensen, H. F. Poulsen, and U. Lienert, "Kinetics of individual grains during recrystallization," *Scripta Materialia*, vol. 43, pp. 561-566, 2000.
- [90] C. M. Sellars and J. A. Whiteman, "Recrystallization and grain growth in hot rolling," *Metal Science*, vol. 13, pp. 187-194, 1979.
- [91] T. Gladman, "The physical metallurgy of microalloyed steels," ed London: Institute of Materials, 1997, p. 235.
- [92] D. G. J. Sellars C. M., "Hot working and forming processes : proceedings of an International Conference on Hot Working and Forming Processes," London, 1980.
- [93] T. Gladman, "The physical metallurgy of microalloyed steels," ed London: Institute of Materials, 1997, pp. 236-237.
- [94] D. R. Barraclough and C. M. Sellars, "Static recrystallization and restoration after hot deformation of Type 304 stainless steel," *Metal Science*, vol. 13, pp. 257-268, 1979.
- [95] F. J. Humphreys and M. Hatherly, "Recrystallization and related annealing phenomena," 2nd ed. ed Amsterdam ; London: Elsevier Science Ltd, 2004, pp. 227-228.

- [96] F. J. Humphreys and M. Hatherly, "Recrystallization and related annealing phenomena," 2nd ed. ed Amsterdam ; London: Elsevier Science Ltd, 2004, pp. 159-164.
- [97] F. J. Humphreys and M. Hatherly, "Recrystallization and related annealing phenomena," 2nd ed. ed Amsterdam ; London: Elsevier Science Ltd, 2004, pp. 228-229.
- [98] B. Dutta and C. M. Sellars, "Effect of composition and process variables on Nb(C, N) precipitation in niobium microalloyed austenite," *Materials Science and Technology*, vol. 3, pp. 197-206, 1987.
- [99] [http://www.matter.org.uk/steelmatter/metallurgy/7\\_1\\_2.html](http://www.matter.org.uk/steelmatter/metallurgy/7_1_2.html).
- [100] W. D. Callister, Jr. / Rethwisch, David G., "Materials science and engineering: an introduction," 8th ed: John Wiley & Sons, 2009, pp. 356-360.
- [101] [www.msm.cam.ac.uk/phase-trans/2012/Manna/Part2.ppt](http://www.msm.cam.ac.uk/phase-trans/2012/Manna/Part2.ppt).
- [102] M. R. M. a. S. J. Rosenberg, *Trans. ASM*, vol. vol. 46, p. 1225, 1954.
- [103] S. S. T. Maki, and I. Tamura, *Metall. Trans*, vol. vol. 2, p. 2944, 1971.
- [104] G. Krauss, "Principles of heat treatment of steel," ed Metals Park, Ohio: American Society for Metals, 1980, p. 91.
- [105] W. C. Leslie, "The physical metallurgy of steels," ed Auckland ; London, 1982, p. 261.
- [106] W. C. Leslie, "The physical metallurgy of steels," ed Auckland ; London, 1982, p. 259.
- [107] G. F. Vander Voort, "Atlas of time-temperature diagrams for irons and steels," ed Materials Park, Ohio: ASM International, 1991, p. 147.
- [108] G. F. Vander Voort, "Atlas of time-temperature diagrams for irons and steels," ed Materials Park, Ohio: ASM International, 1991, p. 35.
- [109] R. E. R. Hill, "Physical metallurgy principles," 2d ed. ed [S.I.]: Van Nostrand Reinhold, 1972, pp. 701-704.
- [110] D. A. Porter, K. E. Easterling, and M. Y. Sherif, "Phase transformations in metals and alloys," 3rd ed. / David A. Porter, Kenneth E. Easterling, and Mohamed Y. Sherif. ed Boca Raton, Fla. ; London: CRC, 2009, p. 333.
- [111] W. D. Callister, Jr. / Rethwisch, David G., "Materials science and engineering: an introduction," 8th ed: John Wiley & Sons, 2009, p. 367.
- [112] D. A. Porter, K. E. Easterling, and M. Y. Sherif, "Phase transformations in metals and alloys," 3rd ed. / David A. Porter, Kenneth E. Easterling, and Mohamed Y. Sherif. ed Boca Raton, Fla. ; London: CRC, 2009, p. 332.
- [113] G. Krauss, "Principles of heat treatment of steel," ed Metals Park, Ohio: American Society for Metals, 1980, p. 94.
- [114] W. D. Callister, Jr. / Rethwisch, David G., "Materials science and engineering: an introduction," 8th ed: John Wiley & Sons, 2009, pp. 367-369.
- [115] W. D. Callister, Jr. / Rethwisch, David G., "Materials science and engineering: an introduction," 8th ed: John Wiley & Sons, 2009, p. 370.
- [116] E. S. Davenport and E. C. Bain, "Transformation of austenite at constant subcritical temperatures," *Metallurgical Transactions*, vol. 1, pp. 3503-3530, 1970/12/01 1970.
- [117] N. Popescu, M. Cojocar, and V. Mihailov, "Experimental studies on bulk tempering of 34CrNiMo6 steel," *Surface Engineering and Applied Electrochemistry*, vol. 48, pp. 28-34, 2012.
- [118] H. E. McGannon, "The making, shaping and treating of steel," in *United States Steel Corporation*, 9th edition ed Pittsburgh, 1971, p. 1096.
- [119] <http://www.oyalmetal.com/tablolalar/339-vcnmo150.html>.



- [120] J. Nutting, Baker, and R. G. Baker, "The Microstructure of Metals," ed: London, 1965, p. 142.
- [121] J. Nutting, Baker, and R. G. Baker, "The Microstructure of Metals.," ed: London, 1965, p. 149.
- [122] H. Xue and T. N. Baker, "Mechanical properties of low carbon-vanadium microalloyed quenched and tempered steels with aluminium additions," *Materials Science and Technology*, vol. 11, pp. 883-892, 1995.
- [123] R. G. B. a. J. Nutting, "The Tempering of 2.25%Cr-1%Mo Steel after Quenching and Normalizing," *J. Iron Steel Inst*, vol. 192, pp. 257–268, 1959.
- [124] H. K. D. H. Bhadeshia, "Bainite in steels," 2nd ed: Institute of Materials, Minerals and Mining, 2001, p. 110.
- [125] T. Okuno, "Effect of microstructure on the toughness of hot work tool steels, AISI H13, H10, and H19," *Transactions ISIJ*, vol. 27, pp. 51-59, 1987.
- [126] G. Krauss, "Steels: Processing, Structure, And Performance," ed: ASM International, 2005, pp. 51-52.
- [127] L. A. Moiseeva and B. P. Moiseev, "Composition, structure, and sources of exogenous inclusions in steel," *Steel in Translation*, vol. 37, pp. 607-613, 2007.
- [128] L.-f. Zhang, "Inclusion and Bubble in Steel—A Review," *Journal of Iron and Steel Research, International*, vol. 13, pp. 1-8, 2006.
- [129] R. N. Kiessling, H., "publication No. 134," *Iron and Steel Institute*, pp. 179-185, 1972.
- [130] S. MATSUSHIMA, *Ironmaking and Steelmaking*, vol. 4, p. 29, 1977.
- [131] T. A. Engh, "Principles of metal refining," ed: Oxford University Press, 1992, pp. 19-38.
- [132] P. A. Thornton, "The influence of nonmetallic inclusions on the mechanical properties of steel: A review," *Journal of Materials Science*, vol. 6, pp. 347-356, 1971/04/01 1971.
- [133] Marie-Aline, "Formation and Morphology of non-Metallic Inclusions in Aluminium Killed Steels " PhD, Catholic University of Leuven, 2010.
- [134] B. B. R. Dekkers, P. Wollants, F. Haers, C. Vercruyssen, and B. Gommers, "Non-metallic inclusions in aluminium killed steels," *Ironmaking and Steelmaking* vol. 29, pp. 437-444, 2002.
- [135] G. P. a. B. Trentini, "Int. Conf. on Production and Application of Clean Steels," *The Iron and Steel Institute*, pp. 1-14, London 1970.
- [136] S. Omata, "Effects of Forged Grain Flow on Ultra-High-Cycle Fatigue Strength of Forged Crankshafts " *Journal of the JIME*, vol. 39, pp. 343-349, 2004.
- [137] R. B. Dekkers, B. ; Wollants, P. ; Haers, F. ; Gommers, B. ; Vercruyssen, C., "A Morphological Comparison between Inclusions in Aluminium Killed Steels and Deposits in Submerged Entry Nozzle," *Steel Research International*, vol. 74, pp. 351-355, 2003.
- [138] R. Dekkers, B. Blanpain, and P. Wollants, "Crystal growth in liquid steel during secondary metallurgy," *Metallurgical and Materials Transactions B*, vol. 34, pp. 161-171, 2003/04/01 2003.
- [139] G. Krauss, "Steels: Processing, Structure, And Performance," ed: ASM International, 2005, p. 157.
- [140] G. T., "Developments in inclusions control and their effects on steel properties," *Ironmaking and Steelmaking*, vol. 19, pp. 457-463, 1992.
- [141] C. M. Sellars and W. J. M. Tegart, "Hot Workability," *International Metallurgical Reviews*, vol. 17, pp. 1-24, 1972.

- [142] A. Ray, S. K. Paul, and S. Jha, "Effect of Inclusions and Microstructural Characteristics on the Mechanical Properties and Fracture Behavior of a High-Strength Low-Alloy Steel," *Journal of Materials Engineering and Performance*, vol. 4, pp. 679-688, 1995/12/01 1995.
- [143] A. M. J. Pacyna, "Relationship between the grain size and fracture toughness of tool steel," *Steel Research*, vol. 57 pp. 577-585, 1986.
- [144] H. V. Atkinson and G. Shi, "Characterization of inclusions in clean steels: a review including the statistics of extremes methods," *Progress in Materials Science*, vol. 48, pp. 457-520, 2003.
- [145] M. Ohring, "Solutions Manual to accompany Engineering Materials Science," ed, 1995, p. 131.
- [146] W. D. Callister, Jr. / Rethwisch, David G., "Materials science and engineering: an introduction," 8th ed: John Wiley & Sons, 2009, p. 180.
- [147] H. A. K. D. Medlin, "ASM handbook. Vol.8, Mechanical testing and evaluation," ed: Materials Park, OH : ASM International, 2000, p. 1344.
- [148] R. A. Higgins, "Materials for engineers and technicians," 4th ed Oxford: Newnes, 2006, p. 36.
- [149] W. D. Callister, Jr. / Rethwisch, David G., "Materials science and engineering: an introduction," 8th ed: John Wiley & Sons, 2009, p. 429.
- [150] W. D. Callister, Jr. / Rethwisch, David G., "Materials science and engineering: an introduction," 8th ed: John Wiley & Sons, 2009, p. 430.
- [151] D. Chakrabarti, M. Strangwood, and C. Davis, "Effect of Bimodal Grain Size Distribution on Scatter in Toughness," *Metallurgical and Materials Transactions A*, vol. 40, pp. 780-795, 2009/04/01 2009.
- [152] J. H. Chen, L. Zhu, and H. Ma, "On the scattering of the local fracture stress  $\sigma_f^*$ ," *Acta Metallurgica et Materialia*, vol. 38, pp. 2527-2535, 1990.
- [153] S. J. Wu and C. L. Davis, "Effect of duplex ferrite grain size distribution on local fracture stresses of Nb-microalloyed steels," *Materials Science and Engineering: A*, vol. 387-389, pp. 456-460, 2004.
- [154] W. Soboyejo, "Mechanical Properties of Engineered Materials," ed: Marcel Dekker, 2003, p. 51.
- [155] D. R. H. J. Michael Ashby, "Engineering Materials 2: an Introduction to Microstructures, Processing and Design." vol. 2, ed: Butterworth-Heinemann Ltd, 2005, p. 118.
- [156] K.-E. Thelning, "Steel and its heat treatment," 2nd ed London ; Boston: Butterworths, 1984, pp. 43-44.
- [157] J. A. B. LAMET, John Barsom, "Mechanical Testing and Evaluation." vol. 8, ed: ASM Handbook 2000, pp. 9-10.
- [158] M. W. Chunfang WANG, Jie SHI, Weijun HUI, Han DONG, "Effect of Microstructure Refinement on the Strength and Toughness of Low Alloy Martensitic Steel," *J. Mater. Sci. Technol.*, vol. 23 (05): 659-664, 2007.
- [159] C. Zhang, Q. Wang, J. Ren, R. Li, M. Wang, F. Zhang, and K. Sun, "Effect of martensitic morphology on mechanical properties of an as-quenched and tempered 25CrMo48V steel," *Materials Science and Engineering: A*, vol. 534, pp. 339-346, 2012.
- [160] C. Zhang, Q. Wang, J. Ren, R. Li, M. Wang, F. Zhang, and Z. Yan, "Effect of microstructure on the strength of 25CrMo48V martensitic steel tempered at different temperature and time," *Materials & Design*, vol. 36, pp. 220-226, 2012.
- [161] W. D. Callister, Jr. / Rethwisch, David G., "Materials science and engineering: an introduction," 8th ed: John Wiley & Sons, 2009, p. 376.

- [162] W. O. Soboyejo, "Mechanical properties of engineered materials," ed New York: Marcel Dekker, 2003, p. 369.
- [163] J. D. Verhoeven, "Steel metallurgy for the non-metallurgist," ed Materials Park, Ohio: ASM International, 2007, p. 26.
- [164] J. D. Verhoeven, "Steel metallurgy for the non-metallurgist," ed Materials Park, Ohio: ASM International, 2007, p. 48.
- [165] J. R. Davis, "Alloying : understanding the basics," ed Materials Park, OH: ASM International, 2001, pp. 150-156.
- [166] W. D. Callister, "Materials science and engineering : an introduction," 8th ed. New York ; Chichester: Wiley, 2009, p. 252.
- [167] M. A. Grossmann, Bain, and E. C. Bain, "Principles of Heat Treatment. Fifth edition.," ed Ohio: American Society for Metals, 1964, pp. 70-71.
- [168] M. A. Grossmann, Bain, and E. C. Bain, "Principles of Heat Treatment. Fifth edition.," ed Ohio: American Society for Metals, 1964, p. 71.
- [169] J. M. Hyzak and I. M. Bernstein, "The role of microstructure on the strength and toughness of fully pearlitic steels," *Metallurgical Transactions A*, vol. 7, pp. 1217-1224, 1976/08/01 1976.
- [170] N. J. Kim and A. H. Nakagawa, "Effective grain size of dual-phase steel," *Materials Science and Engineering*, vol. 83, pp. 145-149, 1986.
- [171] E. G. Nisbett, "Steel forgings : design, production, selection, testing, and application," ed West Conshohocken, PA: ASTM International, 2005, pp. 40-43.
- [172] <http://www.tunersgroup.com/forging.html>.
- [173] T. Altan, G. Ngaile, and G. Shen, *Cold and hot forging : fundamentals and applications* vol. 1: Materials Park, OH : ASM International, c2004 (2005 printing), 2005.
- [174] Y. Tanaka and T. Ishiguro, "Development of high-purity large-scale forgings for energy service," *Physica Status Solidi a-Applied Research*, vol. 160, pp. 305-320, Apr 16 1997.
- [175] G. E. Dieter and D. Bacon, "Mechanical metallurgy," SI metric ed. ed: McGraw-Hill, 1988, pp. 564-566.
- [176] S. L. S. Joseph R. Davis, "Forming and Forging," in *ASM Metals Handbook*. vol. 14, 9 ed: ASM International, 1989, p. 109.
- [177] N. T. Switzner, C. J. Van Tyne, and M. C. Mataya, "Effect of forging strain rate and deformation temperature on the mechanical properties of warm-worked 304L stainless steel," *Journal of Materials Processing Technology*, vol. 210, pp. 998-1007, 2010.
- [178] [http://www.scotforge.com/sf\\_facts\\_solution.htm](http://www.scotforge.com/sf_facts_solution.htm).
- [179] G. Krauss, "Steels: Processing, Structure, And Performance," ed: ASM International, 2005, p. 252.
- [180] K. H. Prabhudev, "Hand book of Heat Treatment of Steels," T. M.-H. Education, Ed., ed, 1988, pp. 43-44.
- [181] F. Klocke, "Manufacturing Processes 1: Cutting." vol. 1 ed, 2011, p. 257.
- [182] W. D. Callister, Jr. / Rethwisch, David G., "Materials science and engineering: an introduction," 8th ed: John Wiley & Sons, 2009, p. 423.
- [183] G. E. Totten, "Steel Heat Treatment Metallurgy and Technologies," in *Steel Heat Treatment Handbook*, Second Edition ed, 2006, pp. 334-335.
- [184] G. Krauss, "Steels: Processing, Structure, And Performance," ed: ASM International, 2005, p. 254.
- [185] G. E. Totten, "Steel Heat Treatment Metallurgy and Technologies," in *Steel Heat Treatment Handbook*, Second Edition ed, 2006, p. 336.

- [186] <http://www.substech.com/dokuwiki/doku.php?id=normalizing&DokuWiki=a123a387b09a094c3bf07a55f908f>.
- [187] G. Krauss, "Steels: Processing, Structure, And Performance," ed: ASM International, 2005, p. 253.
- [188] K. H. Prabhudev, "Hand book of Heat Treatment of Steels," T. M.-H. Education, Ed., ed, 1988, pp. 56-59.
- [189] R. E. Haimbaugh, "Practical induction heat treating," ed Materials Park, OH: ASM International, 2001, p. 87.
- [190] G. E. Totten, "Steel Heat Treatment Metallurgy and Technologies," in *Steel Heat Treatment Handbook*, Second Edition ed, 2006, p. 162.
- [191] H. E. Boyer, "Practical heat treating," ed Metals Park, OH: American Society for Metals, 1984, pp. 3-4.
- [192] R. E. Haimbaugh, "Practical induction heat treating," ed Materials Park, OH: ASM International, 2001, p. 137.
- [193] K.-E. Thelning, "Steel and its heat treatment," 2nd ed London ; Boston: Butterworths, 1984, p. 393.
- [194] K.-E. Thelning, "Steel and its heat treatment," 2nd ed London ; Boston: Butterworths, 1984, pp. 284-285.
- [195] K.-E. Thelning, "Steel and its heat treatment," 2nd ed London ; Boston: Butterworths, 1984, p. 286.
- [196] R. E. Haimbaugh, "Practical induction heat treating," ed Materials Park, OH: ASM International, 2001, p. 138.
- [197] J. H. Hollomon, and Jaffe, L. D. , "Time-Temperature Relations In Tempering Steel," *Trans. AIME*, vol. 162, pp. 223-249 1945.
- [198] H. Chandler, "Heat treater's guide : practices and procedures for irons and steels," 2nd ed. ed Materials Park, Ohio: ASM International, 1995, pp. 97-98.
- [199] H. Chandler, "Heat treater's guide : practices and procedures for irons and steels," 2nd ed. ed Materials Park, Ohio: ASM International, 1995, p. 99.
- [200] G. M. B. T Arai, "Heat Treating," in *ASM Handbook*. vol. 4, ed: ASM International, 1991, p. 128.
- [201] D. A. Porter, K. E. Easterling, and M. Y. Sherif, "Phase transformations in metals and alloys," 3rd ed. / David A. Porter, Kenneth E. Easterling, and Mohamed Y. Sherif. ed Boca Raton, Fla. ; London: CRC, 2009, p. 400.
- [202] D. A. Porter, K. E. Easterling, and M. Y. Sherif, "Phase transformations in metals and alloys," 3rd ed. / David A. Porter, Kenneth E. Easterling, and Mohamed Y. Sherif. ed Boca Raton, Fla. ; London: CRC, 2009, p. 399.
- [203] K.-E. Thelning, "Steel and its heat treatment," 2nd ed London ; Boston: Butterworths, 1984, pp. 21-22.
- [204] J. D. Verhoeven, "Steel metallurgy for the non-metallurgist," ed Materials Park, Ohio: ASM International, 2007, p. 100.
- [205] G. Krauss, "Steels : heat treatment and processing principles," ed Materials Park, Ohio: ASM International, 1990, pp. 218-219.
- [206] G. E. Totten, "Steel Heat Treatment Metallurgy and Technologies," in *Steel Heat Treatment Handbook*, Second Edition ed, 2006, pp. 107-108.
- [207] B. L. A. C.S. Roberts, and M. Cohen, "The Mechanism and Kinetics of the First Stage of Tempering," *Trans. ASM*, vol. 45, pp. 576-604, 1953.
- [208] G. K. George Roberts, Richard Kennedy, "Tool steels," 5th ed. Materials Park, OH: ASM International, 1998, p. 101.

- [209] H. K. D. H. Bhadeshia and R. W. K. Honeycombe, "Steels : microstructure and properties," 3rd ed. ed Amsterdam ; London: Butterworth-Heinemann, 2006, p. 186.
- [210] G. Krauss, "Steels : heat treatment and processing principles," ed Materials Park, Ohio: ASM International, 1990, p. 221.
- [211] D. L. Williamson, R. G. Schupmann, J. P. Materkowski, and G. Krauss, "Determination of small amounts of austenite and carbide in hardened medium carbon steels by Mössbauer spectroscopy," *Metallurgical Transactions A*, vol. 10, pp. 379-382, 1979.
- [212] G. Thomas, "Retained austenite and tempered martensite embrittlement," *Metallurgical Transactions A*, vol. 9, pp. 439-450, 1978.
- [213] G. Krauss, "Steels : heat treatment and processing principles," ed Materials Park, Ohio: ASM International, 1990, p. 224.
- [214] G. E. Totten, "Steel Heat Treatment Metallurgy and Technologies," in *Steel Heat Treatment Handbook*, Second Edition ed, 2006, p. 108.
- [215] M. Sarikaya, A. K. Jhingan, and G. Thomas, "Retained austenite and tempered martensite embrittlement in medium carbon steels," *Metallurgical Transactions A*, vol. 14, pp. 1121-1133, 1983.
- [216] S. Lee, D. Y. Lee, and R. J. Asaro, "Correlation of microstructure and tempered martensite embrittlement in two 4340 steels," *Metallurgical Transactions A*, vol. 20, pp. 1089-1103, 1989.
- [217] H. K. D. H. Bhadeshia and R. W. K. Honeycombe, "Steels : microstructure and properties," 3rd ed. ed Amsterdam ; London: Butterworth-Heinemann, 2006, p. 188.
- [218] <http://cml.postech.ac.kr/z/3750-004.pdf>.
- [219] H. K. D. H. Bhadeshia and R. W. K. Honeycombe, "Steels : microstructure and properties," 3rd ed. ed Amsterdam ; London: Butterworth-Heinemann, 2006, pp. 145-146.
- [220] [http://en.wikipedia.org/wiki/Tempering#cite\\_ref-16](http://en.wikipedia.org/wiki/Tempering#cite_ref-16).
- [221] H. K. D. H. Bhadeshia and R. W. K. Honeycombe, "Steels : microstructure and properties," 3rd ed. ed Amsterdam ; London: Butterworth-Heinemann, 2006, p. 253.
- [222] J. H. Bulloch, "Toughness losses in low alloy steels at high temperatures: an appraisal of certain factors concerning the small punch test," *International Journal of Pressure Vessels and Piping*, vol. 75, pp. 791-804, 1998.
- [223] M. Koutník, V. Landa, and V. Číhal, "The segregation of As, Sb and Bi in Cr-Ni steels and alloys with different Ni contents investigated using AES," *Microchimica Acta*, vol. 101, pp. 121-125, 1990/01/01 1990.
- [224] M. Guttman, P. Dumoulin, and M. Wayman, "The thermodynamics of interactive co-segregation of phosphorus and alloying elements in iron and temper-brittle steels," *Metallurgical Transactions A*, vol. 13, pp. 1693-1711, 1982/10/01 1982.
- [225] C. J. McMahon Jr, "Solute segregation and intergranular fracture in steels: a status report," *Materials Science and Engineering*, vol. 42, pp. 215-226, 1980.
- [226] P. Dumoulin, M. Guttman, M. Foucault, M. Palmier, M. Wayman, and M. Biscondi, "Role of molybdenum in phosphorus-induced temper embrittlement," *Metal Science*, vol. 14, pp. 1-15, 1980.
- [227] J. Yu and C. J. McMahon, "The effects of composition and carbide precipitation on temper embrittlement of 2.25 Cr-1 Mo steel: Part I. Effects of P and Sn," *Metallurgical Transactions A*, vol. 11, pp. 277-289, 1980.
- [228] K.-E. Thelning, "Steel and its heat treatment," 2nd ed London ; Boston: Butterworths, 1984, p. 300.
- [229] K.-E. Thelning, "Steel and its heat treatment," 2nd ed London ; Boston: Butterworths, 1984, pp. 132-138.

- [230] G. E. Totten, "Steel Heat Treatment Metallurgy and Technologies," in *Steel Heat Treatment Handbook*, Second Edition ed, 2006, p. 5.
- [231] R. A. Mulford, C. J. McMahon, D. P. Pope, and H. C. Feng, "Temper embrittlement of Ni-Cr Steels by phosphorus," *Metallurgical Transactions A*, vol. 7, pp. 1183-1195, 1976.
- [232] A. Nayar, "The Steel Handbook," ed: Tata McGraw-Hill Education, 2000, p. 27.
- [233] A. Polushin, S. Kamantsev, V. Gryzunov, and M. Minakov, "Heat treatment of steel rolls for cold rolling," *Metal Science and Heat Treatment*, vol. 53, pp. 225-229, 2011.
- [234] S. C. J. Y. W. KIM, "Effect of normalized microstructure in alloy steel on the performance of planetary gear set of automatic transmission " *SAE transactions* vol. 106, pp. 1786-1796 1997.
- [235] K. O. Lee, S. K. Hong, Y. K. Kang, H. J. Yoon, and S. S. Kang, "Grain refinement in bearing steels using a double-quenching heat-treatment process," *International Journal of Automotive Technology*, vol. 10, pp. 697-702, 2009/12/01 2009.
- [236] G. E. Totten, "Steel Heat Treatment Metallurgy and Technologies," in *Steel Heat Treatment Handbook*, Second Edition ed, 2006, p. 432.
- [237] E. G. Nisbett, "Steel forgings : design, production, selection, testing, and application," ed West Conshohocken, PA: ASTM International, 2005, p. 70.
- [238] G. Krauss, "Steels: Processing, Structure, And Performance," ed: ASM International, 2005, p. 555.
- [239] K.-E. Thelning, "Steel and its heat treatment," 2nd ed London ; Boston: Butterworths, 1984, pp. 294-296.
- [240] D. V. D. C.A. Siebert, and D.H. Breen, "The Hardenability of Steel," *American Society for Metals*, 1977.
- [241] H. K. D. H. Bhadeshia and R. W. K. Honeycombe, "Steels : microstructure and properties," 3rd ed. ed Amsterdam ; London: Butterworth-Heinemann, 2006, p. 167.
- [242] K.-E. Thelning, "Steel and its heat treatment," 2nd ed London ; Boston: Butterworths, 1984, p. 146.
- [243] G. K. George Roberts, Richard Kennedy, "Tool steels," 5th ed. Materials Park, OH: ASM International, 1998, p. 86.
- [244] K.-E. Thelning, "Steel and its heat treatment," 2nd ed London ; Boston: Butterworths, 1984, p. 145.
- [245] H. K. D. H. Bhadeshia and R. W. K. Honeycombe, "Steels : microstructure and properties," 3rd ed. ed Amsterdam ; London: Butterworth-Heinemann, 2006, p. 170.
- [246] M. A. Grossmann, Asimow, M., and Urban, S. F., "Hardenability of alloys steels," *ASM international*, Cleveland, Ohio, USA 1939.
- [247] G. E. Totten, "Steel Heat Treatment Metallurgy and Technologies," in *Steel Heat Treatment Handbook*, Second Edition ed, 2006, p. 217.
- [248] K.-E. Thelning, "Steel and its heat treatment," 2nd ed London ; Boston: Butterworths, 1984, p. 147.
- [249] G. E. Totten, "Steel Heat Treatment Metallurgy and Technologies," in *Steel Heat Treatment Handbook*, Second Edition ed, 2006, pp. 219-220.
- [250] G. M. B. T Arai, "Heat Treating," in *ASM Handbook*. vol. 4, ed, 1991, p. 20.
- [251] K.-E. Thelning, "Steel and its heat treatment," 2nd ed London ; Boston: Butterworths, 1984, p. 149.
- [252] K.-E. Thelning, "Steel and its heat treatment," 2nd ed London ; Boston: Butterworths, 1984, p. 150.
- [253] D. A. Porter, K. E. Easterling, and M. Y. Sherif, "Phase transformations in metals and alloys," 3rd ed. / David A. Porter, Kenneth E. Easterling, and Mohamed Y. Sherif. ed Boca Raton, Fla. ; London: CRC, 2009, pp. 327-331.

- [254] B. L. Bramfitt, "Major materials: carbon and alloy steels," ed Homer Research Laboratories, Bethlehem, Pennsylvania: Bethlehem Steel Corporation, p. 41.
- [255] D. A. Porter, K. E. Easterling, and M. Y. Sherif, "Phase transformations in metals and alloys," 3rd ed. / David A. Porter, Kenneth E. Easterling, and Mohamed Y. Sherif. ed Boca Raton, Fla. ; London: CRC, 2009, p. 329.
- [256] D. A. Porter, K. E. Easterling, and M. Y. Sherif, "Phase transformations in metals and alloys," 3rd ed. / David A. Porter, Kenneth E. Easterling, and Mohamed Y. Sherif. ed Boca Raton, Fla. ; London: CRC, 2009, p. 327.
- [257] D. A. Porter, K. E. Easterling, and M. Y. Sherif, "Phase transformations in metals and alloys," 3rd ed. / David A. Porter, Kenneth E. Easterling, and Mohamed Y. Sherif. ed Boca Raton, Fla. ; London: CRC, 2009, p. 330.
- [258] W. D. Callister, Jr. / Rethwisch, David G., "Materials science and engineering: an introduction," 8th ed: John Wiley & Sons, 2009, pp. 427-428.
- [259] W. D. Callister, Jr. / Rethwisch, David G., "Materials science and engineering: an introduction," 8th ed: John Wiley & Sons, 2009, p. 428.
- [260] W. L. Crafts, John L., "Effect of Some Elements on Hardenability," *Trans. AIME*, pp. 157-167, Metals Technology 1944.
- [261] C. A. Siebert, D. V. Doane, and D. H. Breen, "The hardenability of steels : concepts, metallurgical influences and industrial applications," ed Metals Park, Ohio: American Society for Metals, 1977, pp. 98-100.
- [262] O. Sandberg, P. Westerhult, and W. Roberts, "Vanadium-Modified alloy steels for quench-and-temper applications requiring high hardenability," *Journal of Heat Treating*, vol. 4, pp. 184-193, 1985/12/01 1985.
- [263] P. L. Mangonon, "The heat treatment of Vanadium-modified alloy steels," *Journal of Metals* vol. 33, pp. 18-24 1981.
- [264] Z. Patel and K. Khul'ka, "Niobium for Steelmaking," *Metallurgist*, vol. 45, pp. 477-480, 2001/11/01 2001.
- [265] C. R. Fossaert, G. Maurickx, T. Bhadeshia, H. K. D. H., "The effect of niobium on the hardenability of microalloyed austenite," *Metallurgical and Materials Transactions A*, vol. 26, pp. 21-30, 1995/01/01 1995.
- [266] D. T. H. Llewellyn, R. C., "Steels : metallurgy and applications," 3 ed Oxford: Butterworth-Heinemann, 1998, pp. 213-214.
- [267] G. E. Totten, "Steel Heat Treatment Metallurgy and Technologies," in *Steel Heat Treatment Handbook*, Second Edition ed, 2006, pp. 193-194.
- [268] T. Titova, N. Shulgan, and I. Malykhina, "Effect of boron microalloying on the structure and hardenability of building steel," *Metal Science and Heat Treatment*, vol. 49, pp. 39-44, 2007.
- [269] G. E. Totten, "Steel Heat Treatment Metallurgy and Technologies," in *Steel Heat Treatment Handbook*, Second Edition ed, 2006, p. 193.
- [270] Z. N. J. DŽUGAN, P. KONOPÍK, P. MOTYČKA, "Improvement of fatigue properties of 34CrNiMo6 steel by controlled thermomechanical treatment " *METAL* 2010.
- [271] C. A. Siebert, D. V. Doane, and D. H. Breen, *The hardenability of steels : concepts, metallurgical influences and industrial applications*. Metals Park, Ohio: American Society for Metals, 1977.
- [272] G. E. Hicho, C. H. Brady, L. C. Smith, and R. J. Fields, "Effects of heat treatment on the mechanical properties and microstructures of four different heats of a precipitation hardening HSLA steel," *Journal of Heat Treating*, vol. 5, pp. 7-19, 1987/03/01 1987.
- [273] M. Krzyzanowski, J. H. Beynon, and D. C. J. Farrugia, "Oxide scale behaviour in high temperature metal processing," ed Weinheim: Wiley-VCH, 2010, p. 12.

- [274] J. S. Hinton, "Laboratory Simulation of Microstructural Evolution in AISI 430 Ferritic Stainless Steel during the Steckel Mill Process," Ph D, Engineering Materials, The University of Sheffield, Sheffield, 2006.
- [275] <http://www.immpetus.group.shef.ac.uk/index.php/facilities-m/78-thermomechanical-compression-machine-tmc>.
- [276] K. Lee, S. Hong, Y. Kang, H. Yoon, and S. Kang, "Grain refinement in bearing steels using a double-quenching heat-treatment process," *International Journal of Automotive Technology*, vol. 10, pp. 697-702, 2009.
- [277] K.-E. Thelning, "Steel and its heat treatment," 2nd ed London ; Boston: Butterworths, 1984, p. 294.
- [278] R. L. Higginson and C. M. Sellars, "Worked examples in quantitative metallography," ed London: Maney, 2003, pp. 15-17.
- [279] M. Trull, "Modelling of Oxide Failure in Hot Metal Forming Operations," PhD, Department of Engineering Materials, The University of Sheffield, Sheffield, 2002.
- [280] P. Zhang, S. X. Li, and Z. F. Zhang, "General relationship between strength and hardness," *Materials Science and Engineering: A*, vol. 529, pp. 62-73, 2011.
- [281] W. D. Callister, Jr. / Rethwisch, David G., "Materials science and engineering: an introduction," 8th ed: John Wiley & Sons, 2009, p. 179.
- [282] M. G. G. Rosenberg, "Correlation between hardness and tensile properties in ultra-high strength dual phase steel-short communication " *Materials Engineering*, vol. 18, pp. 155-159, 2011.
- [283] C. Zener and J. H. Hollomon, "Effect of Strain Rate Upon Plastic Flow of Steel," *Journal of Applied Physics*, vol. 15, pp. 22-32, 1944.
- [284] H. J. McQueen and N. D. Ryan, "Constitutive analysis in hot working," *Materials Science and Engineering: A*, vol. 322, pp. 43-63, 2002.
- [285] N. J. S. S. B. Davenport, C. N. Sparks, and C. M. Sellars, "Development of constitutive equations for modelling of hot rolling," *Materials Science and Technology*, vol. 16, pp. 539-546, 2000.
- [286] H. Mirzadeh, A. Najafizadeh, and M. Moazeny, "Flow Curve Analysis of 17-4 PH Stainless Steel under Hot Compression Test," *Metallurgical and Materials Transactions A*, vol. 40, pp. 2950-2958, 2009.
- [287] R. Ebrahimi, S. H. Zahiri, and A. Najafizadeh, "Mathematical modelling of the stress-strain curves of Ti-IF steel at high temperature," *Journal of Materials Processing Technology*, vol. 171, pp. 301-305, 2006.
- [288] S.-I. Kim, Y. Lee, D.-L. Lee, and Y.-C. Yoo, "Modeling of AGS and recrystallized fraction of microalloyed medium carbon steel during hot deformation," *Materials Science and Engineering: A*, vol. 355, pp. 384-393, 2003.
- [289] J. S. Hinton, "Laboratory Simulation of Microstructural Evolution in AISI 430 Ferritic Stainless Steel during the Steckel Mill Process," Doctor of Philosophy, Department of Engineering Materials, The University of Sheffield, Sheffield, 2006.
- [290] R. Colás, "A model for the hot deformation of low-carbon steel," *Journal of Materials Processing Technology*, vol. 62, pp. 180-184, 1996.
- [291] C. M. Sellars, "The kinetics of softening processes during hot working of austenite," *Czechoslovak Journal of Physics*, vol. 35, pp. 239-248, 1985.
- [292] R. B. R. E. LINO, "Modeling Stress-Strain Curves of Hot Deformed Ti-Nb Interstitial Free Austenite," *ISIJ International*, vol. 45, pp. 1758-1760, 2005.
- [293] Y.-r. Xu, L.-s. Chen, D.-y. Wang, and L. Jin, "High temperature softening behaviors and flow stress model for a high molybdenum austenitic stainless steel," *Journal of Shanghai University (English Edition)*, vol. 4, pp. 254-259, 2000.



- [294] S. Srinivasulu and A. Jain, "A comparative analysis of training methods for artificial neural network rainfall–runoff models," *Applied Soft Computing*, vol. 6, pp. 295-306, 2006.
- [295] A. Jain and A. Kumar, "An evaluation of artificial neural network technique for the determination of infiltration model parameters," *Appl. Soft Comput.*, vol. 6, pp. 272-282, 2006.
- [296] S. Mandal, P. V. Sivaprasad, S. Venugopal, and K. P. N. Murthy, "Artificial neural network modeling to evaluate and predict the deformation behavior of stainless steel type AISI 304L during hot torsion," *Applied Soft Computing*, vol. 9, pp. 237-244, 2009.
- [297] H. A. J. Krawczyk, "The Kinetic of Austenite Grain Growth in Steel for Wind Power Plant Shafts," *Archives of Metallurgy and Materials*, vol. 55, 2010.
- [298] M. Militzer, E. B. Hawbolt, T. Ray Meadowcroft, and A. Giunelli, "Austenite grain growth kinetics in Al-killed plain carbon steels," *Metallurgical and Materials Transactions A*, vol. 27, pp. 3399-3409, 1996/11/01 1996.
- [299] J. Verhoeven, *Journal of Materials Engineering and Performance*, vol. 9, pp. 286-296, 2000.
- [300] F. G. Caballero, Garc, iacute, A. a-Junceda, C. Capdevila, A. a de, eacute, and C. s, *Materials Transactions*, vol. 47, pp. 2269-2276, 2006.
- [301] T. Majka, D. Matlock, and G. Krauss, "Development of microstructural banding in low-alloy steel with simulated Mn segregation," *Metallurgical and Materials Transactions A*, vol. 33, pp. 1627-1637, 2002/06/01 2002.
- [302] W. A. Spitzig, "Effect of sulfide inclusion morphology and pearlite banding on anisotropy of mechanical properties in normalized C-Mn steels," *Metallurgical Transactions A*, vol. 14, pp. 271-283, 1983/02/01 1983.
- [303] R. A. Grange, "Effect of microstructural banding in steel," *Metallurgical Transactions*, vol. 2, pp. 417-426, 1971/02/01 1971.
- [304] A. R. Marder, "Deformation characteristics of dual-phase steels," *Metallurgical Transactions A*, vol. 13, pp. 85-92, 1982/01/01 1982.
- [305] G. Krauss, "Steels: Processing, Structure, And Performance," ed: ASM International, 2005, pp. 172-174.
- [306] A. S. Bor, "Effect of Pearlite Banding on Mechanical Properties of Hot-rolled Steel Plates," *ISIJ International*, vol. 31, pp. 1445-1446, 1991.
- [307] S. V. Sajadifar, G. G. Yapici, M. Ketabchi, and B. Bemanizadeh, "High Temperature Deformation Behavior of 4340 Steel: Activation Energy Calculation and Modeling of Flow Response," *Journal of Iron and Steel Research, International*, vol. 20, pp. 133-139, 2013.
- [308] S. F. Medina and C. A. Hernandez, "General expression of the Zener-Hollomon parameter as a function of the chemical composition of low alloy and microalloyed steels," *Acta Materialia*, vol. 44, pp. 137-148, 1996.
- [309] P. Feltham, *Proc. Phys. Soc. B66*, pp. 865-883, 1953.
- [310] A. S. Hamada, L. P. Karjalainen, and M. C. Somani, "The influence of aluminum on hot deformation behavior and tensile properties of high-Mn TWIP steels," *Materials Science and Engineering: A*, vol. 467, pp. 114-124, 2007.
- [311] S.-I. Kim and Y.-C. Yoo, "Prediction of dynamic recrystallisation behaviour of AISI type 4140 medium carbon steel," *Materials Science and Technology*, vol. 18, pp. 160-164, 2002.
- [312] B. X. Wang, X. H. Liu, and G. D. Wang, "Dynamic recrystallization behavior and microstructural evolution in a Mn–Cr gear steel," *Materials Science and Engineering: A*, vol. 393, pp. 102-108, 2005.

- [313] Y. C. Lin, M.-S. Chen, and J. Zhong, "Effect of temperature and strain rate on the compressive deformation behavior of 42CrMo steel," *Journal of Materials Processing Technology*, vol. 205, pp. 308-315, 2008.
- [314] N. D. Ryan and H. J. McQueen, "Mean pass flow stresses and interpass softening in multistage processing of carbon-, HSLA-, tool- and  $\gamma$ -stainless steels," *Journal of Mechanical Working Technology*, vol. 12, pp. 323-349, 1986.
- [315] J. Luo, M. Q. Li, Y. G. Liu, and H. M. Sun, "The deformation behavior in isothermal compression of 300M ultrahigh-strength steel," *Materials Science and Engineering: A*, vol. 534, pp. 314-322, 2012.
- [316] S. F. Medina and C. A. Hernandez, "Modelling of the dynamic recrystallization of austenite in low alloy and microalloyed steels," *Acta Materialia*, vol. 44, pp. 165-171, 1996.
- [317] S. W. Thompson and P. R. Howell, "Factors influencing ferrite/pearlite banding and origin of large pearlite nodules in a hypoeutectoid plate steel," *Materials Science and Technology*, vol. 8, pp. 777-784, 1992.
- [318] C. Capdevila, García Caballero, Francisca, García de Andrés, Carlos, García-Junceda, A., "Evolution of microstructural banding during the manufacturing process of dual phase steels," *Materials Transactions*, vol. 47, pp. 2269-2276, 2006.
- [319] F. Basson and J. H. Driver, "Deformation banding mechanisms during plane strain compression of cube-oriented f.c.c. crystals," *Acta Materialia*, vol. 48, pp. 2101-2115, 2000.
- [320] K. C. Lee, Y. P. Zeng, and C. S. Lee, *Scripta Materialia*, vol. 40, pp. 197-202, 1998.
- [321] L. S. Van Houtte P., Seefeldt M. and Delannay L., *Int. J. Plasticity*, vol. 21, pp. 589-624, 2005.
- [322] L. K. Duggan B.J., Köhlhoff G. and Lee C.S., *Acta Metallurgica*, vol. 41, p. 1921, 1993.
- [323] A. J. Lacey, "Interaction of Testing Machine Characteristics and Specimen Geometry in Plane Strain Compression Testing," MPhil, Department of Engineering Materials, University of Sheffield, 2003.
- [324] L. J. Cuddy, "Microstructures developed during thermomechanical treatment of HSLA steels," *Metallurgical Transactions A*, vol. 12, pp. 1313-1320, 1981/07/01 1981.
- [325] Y. H. Li and C. M. Sellars, "Comparative investigations of interfacial heat transfer behaviour during hot forging and rolling of steel with oxide scale formation," *Journal of Materials Processing Technology*, vol. 80-81, pp. 282-286, 1998.
- [326] R. Matsumoto, Y. Osumi, and H. Utsunomiya, "Reduction of friction of steel covered with oxide scale in hot forging," *Journal of Materials Processing Technology*, vol. 214, pp. 651-659, 2014.
- [327] Y. Tomita, "Effect of continuous-cooling transformation structure on mechanical properties of 0.4C-Cr-Mo-Ni steel," *Journal of Materials Science*, vol. 29, pp. 1612-1616, 1994.
- [328] D. Lonsdale and P. E. J. Flewitt, "The role of grain size on the ductile-brittle transition of a 2.25 Pct Cr-1 Pct Mo steel," *Metallurgical Transactions A*, vol. 9, pp. 1619-1623, 1978.
- [329] R. Ritchie and R. M. Horn, "Further considerations on the inconsistency in toughness evaluation of AISI 4340 steel austenitized at increasing temperatures," *Metallurgical Transactions A*, vol. 9, pp. 331-341, 1978.
- [330] R. Ritchie, B. Francis, and W. Server, "Evaluation of toughness in AISI 4340 alloy steel austenitized at low and high temperatures," *Metallurgical Transactions A*, vol. 7, pp. 831-838, 1976.

- [331] D. Li, Y. Feng, Z. Yin, F. Shangguan, K. Wang, Q. Liu, and F. Hu, "Prediction of hot deformation behaviour of Fe–25Mn–3Si–3Al TWIP steel," *Materials Science and Engineering: A*, vol. 528, pp. 8084-8089, 2011.
- [332] M. A. Grossmann, Bain, and E. C. Bain, "Principles of Heat Treatment. Fifth edition.," ed Ohio: American Society for Metals, 1964, p. 68.
- [333] V. B. Ginzburg and R. Ballas, *Flat rolling fundamentals*. New York: Marcel Dekker, 2000.
- [334] M. S. Loveday, G. J. Mahon, B. Roebuck, A. J. Lacey, E. J. Palmiere, C. M. Sellars, and M. R. van der Winden, "Measurement of flow stress in hot plane strain compression tests," *Materials at High Temperatures*, vol. 23, pp. 85-118, 2006.
- [335] [http://www.steelnumber.com/en/steel\\_composition\\_eu.php?name\\_id=196](http://www.steelnumber.com/en/steel_composition_eu.php?name_id=196).
- [336] <http://www.metalravne.com/selector/steels/vcnmo150.html>.